Multiplexed Protein Analysis of Cellular Signal Transduction: Applications in Translational Research and Personalized Medicine

Dissertation

der Mathematisch-Naturwissenschaftlichen Fakultät

der Eberhard Karls Universität Tübingen

zur Erlangung des Grades eines

Doktors der Naturwissenschaften

(Dr. rer. nat.)

vorgelegt von

Aaron Stahl M.Sc.

aus Düsseldorf

Tübingen

2024

Gedruckt mit Genehmigung der Mathematisch-Naturwissenschaftlichen Fakultät der Eberhard Karls Universität Tübingen.

Tag der mündlichen Qualifikation:	30.01.2025
Dekan:	Prof. Dr. Thilo Stehle
1. Berichterstatter/-in:	Prof. Dr. Katja Schenke-Layland
2. Berichterstatter/-in:	Prof. Dr. Peter Loskill

“It is more important to know what kind of patient the disease has than to know what kind of disease the patient has”

Sir William Osler

Table of Contents

Abstract

Investigation of cellular signaling networks and their activation state is helpful for the study of diseases. Detailed proteomic analysis of signaling pathways can reveal how changes in protein expression patterns mediate the functional manifestation of disease-related (genetic) aberrations. A deepened understanding of proteomic alterations can help in the understanding and discovery of (novel) disease mechanisms for various conditions. Especially in the field of oncology, signaling proteins have become direct targets for drug intervention; thus, by providing accurate information on protein abundance and activation status, the analysis of cellular signaling presents a promising clinical tool for treatment evaluation in precision medicine. Likewise, in experimental clinical research, tangible information on individual proteins of interest and protein-mediated signaling as a whole can be used to evaluate action mechanisms of cell signaling-interfering drugs and aid to identify new target structures for future drug development.

DigiWest is a novel, antibody-based targeted protein analytics method which combines the robustness and specificity of traditional Western Blot with the high-throughput nature of bead-based parallelized assay systems. In a single analysis, the method provides information on 200 or more signaling proteins and/or their activation state. High flexibility in analyte selection makes it highly adaptable for various research questions.

Here, DigiWest was applied to evaluate efficacy and selectivity of tyrosine kinase inhibitors (TKI) as anti-cancer drugs in preclinical cellular models of FGFR2-fusion positive cholangiocarcinoma (iCCA). In a bedside to bench approach, analysis of signaling pathway modulation in treated cells carrying tumor driving FGFR2 fusions and resistance mutations was used to compare action mechanisms of different TKI. While FGFR2-selective and non-selective TKI showed similar effectiveness in treatment-sensitive cells, the non-selective TKI Lenvatinib proved superior in the presence of resistance mutations as was indicated by a conserved inhibition of key FGFR-related signaling pathways.

In a precision medicine approach, DigiWest was employed to define personalized protein profiles in gastrointestinal tumors and identify individualized treatment options. A retrospective DigiWest analysis of pancreatic and colorectal tumors, enabled tumor

stratification into subgroups within their respective entity based on pathway activity patterns, which were shown to match clinical patient characteristics. Methodological transfer of DigiWest into routine clinical setting was demonstrated through personalized characterization of 14 gastrointestinal tumors from patients presented to the molecular tumor board. Patient-specific protein/pathway activation profiles with drug-targetable alterations were revealed, which complemented genetic mutation analysis and provided additional information on treatment options. This highlights DigiWest as a suitable analytics tool for daily clinical precision oncology.

In an application for basic molecular research, DigiWest was employed to uncover disease-specific signatures in patient-derived iPSC models of Schizophrenia. Analysis of protein expression profiles in differentiated neuronal cells (NPC) highlighted disease-induced changes to developmental pathways and demonstrated impaired differentiation capabilities on the protein level. These NPC stage-specific aberrations affected cell cycle control and DNA damage response and were correlated to p53 expression and phosphorylation. Here, the potential of DigiWest to uncover novel, protein-based disease-mechanistic insights was demonstrated.

In this thesis, various applications of DigiWest were outlined. These evidently demonstrate the potential of this method for use in clinical, translational and basic research, e.g. in routine drug testing and disease mechanisms studies as well as in personalized medicine, specifically in clinical precision oncology settings.

Zusammenfassung

Die Untersuchung von zellulären Signalübertragungswegen ist für die Erforschung von Krankheiten unabdingbar. Detaillierte proteomische Analysen von Signalwegen können aufzeigen, wie Veränderungen in den Proteinexpressionsmustern die funktionelle Manifestation krankheitsbezogener (genetischer) Aberrationen vermitteln. Ein vertieftes Verständnis von proteomischen Veränderungen kann zum Verständnis und zur Entdeckung (neuartiger) Krankheitsmechanismen bei verschiedenen Erkrankungen beitragen. Gerade im Bereich der Onkologie haben sich Signalproteine zu direkten Zielen für medikamentöse Intervention entwickelt. Durch die Bereitstellung von akkuraten Informationen zu Proteinmenge und Aktivierungsstatus stellt die Analyse der zellulären Signalübertragung ein vielversprechendes Instrument für die klinische Behandlungsbewertung in der Präzisionsmedizin dar.

DigiWest ist eine neue, Antikörper-basierte zielgerichtete Proteinanalysemethode, welche die Robustheit von traditionellen Western Blots mit der Hochdurchsatz-Charakteristik von Bead-basierten parallelisierten Assay-Systemen kombiniert. In einer einzigen Analyse, liefert die Methode Daten zu 200 oder mehr Signalproteinen und/oder deren Aktivierungsstatus. Eine hohe Flexibilität bei der Auswahl der Analyten macht sie anpassungsfähig für verschiedenste wissenschaftliche Fragestellungen.

Hier wurde DigiWest angewendet, um die Wirksamkeit und Selektivität von Tyrosinkinase-Inhibitoren (TKI) als Krebsmedikamente in präklinischen Modellen des FGFR2-positiven Cholangiokarzinoms (iCCA) zu evaluieren. In einer bedside-to-bench Anwendung wurde die Analyse der Modulation von Signalübertragungswegen in behandelten Zellen, die tumortreibende FGFR2 Fusionen und resistenzinduzierende Mutationen tragen, zum Vergleich von Aktionsmechanismen verschiedener TKI verwendet. Während behandlungssensible Zellen ähnliche Hemmungsprofile für FGFR2-selektive und nichtselektive TKI aufweisen, erwies sich der nichtselektive TKI Lenvatinib bei Vorhandensein von Resistenzmutationen als überlegen, was durch eine erhaltene Inhibierung von zentralen FGFR-relevanten Signalwegen belegt wurde.

In einem präzisionsmedizinischen Ansatz wurde DigiWest auch verwendet, um personalisierte Proteinprofile in gastrointestinalen Tumoren zu bestimmen und individualisierte Behandlungsoptionen zu identifizieren. In einer retrospektiven Analyse

von primärem Bauchspeicheldrüsen- und Darmtumorgewebe konnten Tumoren anhand der Expressionsdaten innerhalb ihrer Entität basierend auf Signalweg-Aktivitätsmustern, die klinische Charakteristika widerspiegeln, stratifiziert werden. Der methodische Transfer von DigiWest in die klinische Routine wurde exemplarisch durch die personalisierte Charakterisierung von 14 gastrointestinalen Tumoren von Patienten gezeigt, die dem molekularen Tumorboard (MTB) vorgestellt wurden. In diesem Kontext wurden patientenspezifische Protein/Signalweg-Aktivierungsprofile mit medikamentös angreifbaren Veränderungen aufgezeigt. Diese ergänzten vorhandene genetische Mutationsanalysen und lieferten somit zusätzliche Informationen zu Behandlungsoptionen. Dies unterstreicht die Verwendbarkeit von DigiWest als analytische Methode in der täglichen klinischen Präzisionsonkologie.

In einer Anwendung für die molekulare Grundlagenforschung wurde DigiWest eingesetzt, um krankheitsspezifische Kennzeichen in patientenabgeleiteten iPSC-Modellen der Schizophrenie aufzudecken. Die Analyse von Proteinexpressionsmustern in differenzierten neuronalen Vorläuferzellenzellen (NPC) zeigte auf Proteinebene krankheitsbedingte Veränderungen von entwicklungsrelevanten Signalwegen sowie eine beeinträchtigte Differenzierungseffizienz. Die NPC-Stadium-spezifischen Veränderungen betrafen die Zellzykluskontrolle und die DNA-Schadens-Antwort und korrelierten mit der Expression und Phosphorylierung von p53. Hier wurde das Potenzial von DigiWest demonstriert, neue Protein-basierte Krankheitsmechanismen aufzudecken.

In dieser Thesis wurden verschieden Anwendungen des DigiWest gezeigt. Diese zeigen deutlich das Potenzial dieser Methode für den Einsatz in der klinischen, translationalen und Grundlagenforschung, beispielsweise bei routinemäßigen Arzneimitteltests und Studien zu Krankheitsmechanismen sowie in der personalisierten Medizin, insbesondere in der klinischen Präzisionsonkologie.

Abbreviations

4E-BP1 – eukaryotic translation initiation factor 4E-binding protein 1

ABL – tyrosine-protein kinase ABL1

AFI – accumulated fluorescent intensity

Akt – protein kinase B

ATR – ataxia telangiectasia and Rad3-related protein

CCA – cholangiocarcinoma

CD – cluster of differentiation

CDK – cyclin-dependent kinase

CDX2 – homeobox protein CDX-2

CEA – cancer embryonic antigen

CK1 – casein kinase 1

CK7 – cytokeratin-7

CK19 – cytokeratin-19

CTR – control

DDR – DNA damage response

DMSO – dimethyl sulfoxide

Dvl – segment polarity protein dishevelled homolog

eEF2 – eukaryotic elongation factor 2

eEF2K – eukaryotic elongation factor-2 kinase

EGFR – endothelial growth factor receptor

eIF2 – eukaryotic initiation factor 2

eIF4E – eukaryotic translation initiation factor 4E

ELISA – enzyme-linked immunosorbent assay

Erk – extracellular signal-regulated kinase

FACS – fluorescence-activated cell sorting

FDA – Food and Drug Administration

FGFR2 – fibroblast growth factor receptor 2

FGFR2-AHCYL2_p.V564F – cell line carrying FGFR2-AHCYL2 gene fusion and p.V564F mutation

FGFR2-AHCYL2_WT – cell line carrying FGFR2-AHCYL2 gene fusion

FRS2 – fibroblast growth factor receptor substrate 2

GI – gastrointestinal

GSK3 – glycogen synthase kinase 3

GWAS – genome-wide association study

IC50 – half maximal inhibitory concentration

ICC – immunocytochemical staining

iCCA – intrahepatic cholangiocarcinoma

iPSC – induced pluripotent stem cells

Jak – janus kinase

KIBRA – kidney and brain expressed protein

KIT – proto-oncogene c-KIT

KLF4 – Krüppel-like factor 4

LATS1 – large tumor suppressor kinase 1

LEF1 – lymphoid enhancer-binding factor 1

LRP6 – low-density lipoprotein receptor-related protein 6

MAP2 – microtubule-associated protein 2

MAPK – mitogen-activated protein kinase

MEK – dual specificity mitogen-activated protein kinase kinase

Mob1 – MOB kinase activator 1

MS – mass spectrometry

MSI – microsatellite instability

Mst1 – macrophage stimulating 1

MTB – molecular tumor board

mTOR – mammalian target of rapamycin

NCAM – neural cell adhesion molecule

NPC – neuronal progenitor cells

Oct4 – octamer-binding transcription factor 4

PAK1 – serine/threonine-protein kinase PAK 1

PAX6 – paired-box protein Pax-6

PDGFR – platelet-derived growth factor receptor

PDK1 – pyruvate dehydrogenase lipoamide kinase isozyme 1

PFS – progression-free survival

PI3K – phosphoinositide 3-kinase

PKC – protein kinase C

PLCγ – phospholipase C gamma

PM – personalized medicine

PTM – posttranslational modification

Raf – RAF proto-oncogene serine/threonine- protein kinase

Rb – retinoblastoma protein

RET – RET proto-oncogene

Rsk1 – ribosomal protein S6 kinase alpha-1

S6 RP – S6 ribosomal protein

SCZ – schizophrenia

SHP2 – Src homology region 2 domain-containing phosphatase-2

SIMOA – single molecule array

Sox1 – sex determining region Y-box 1

Sox2 – sex determining region Y-box 2

STAT – signal transducer and activator of transcription

SUFU – suppressor of fused homolog

TCF – T cell factor/lymphoid enhancer factor

TEAD – TEA domain family member

TGF – transforming growth factor

TIL – tumor-infiltrating lymphocytes

TKI – tyrosine kinase inhibitor

TSC2 – tuberous sclerosis complex 2

TTP – time to progression

VEGFR – vascular endothelial growth factor receptor

WB – Western Blotting

Wnt – proto-oncogene int-1 homolog

List of Figures

List of Publications

Publications as part of this thesis:

Accepted Manuscripts:

1. Spahn, S.*, Kleinhenz, F.*, Shevchenko, E., **Stahl, A**., Rasen, Y., Geisler, C., Ruhm, K., Klaumuenzer, M., Kronenberger, T., Laufer, S. A., Sundberg-Malek, H., Bui, K. C., Horger, M., Biskup, S., Schulze-Osthoff, K., Templin, M., Malek, N. P., Poso, A., Bitzer, M. (2024). The molecular interaction pattern of lenvatinib enables inhibition of wild-type or kinase-mutated FGFR2-driven cholangiocarcinoma. *Nature Communications, 15*(1). https://doi.org/10.1038/s41467-024-45247-6

*authors contributed equally

2. **Stahl A**., Heider J., Wüst, R., Fallgatter, A. J., Schenke-Layland, K., Volkmer, H., Templin, M. (2024). Patient iPSC-derived neural progenitor cells display aberrant cell cycle control, p53, and DNA damage response protein expression in schizophrenia. *BMC Psychiatry, 24*(1). https://doi.org/10.1186/s12888-024-06127-x

Manuscripts in revision:

3. **Stahl, A.,** Büringer, K., Missios, P., Hoffmann, T., Singer, S., Schäfer-Ruoff, F., Schenke-Layland, K., Malek, N. P., Bitzer, M., Templin, M. F. Personalized signaling pathway analysis of gastrointestinal tumors for patient stratification and drug target evaluation using clinically derived core biopsies.

Contributions of the candidate to these respective publications (in %) is outlined in the chapter “Contributions”.

Co-authored publications not part of this thesis:

Accepted manuscripts:

4. Fink, S.*, Ruoff, F.*, **Stahl, A**., Becker, M., Kaiser, P., Traenkle, B., Junker, D., Weise, F., Ruetalo, N., Hörber, S., Peter, A., Nelde, A., Walz, J., Krause, G., Baillot, A., Schenke-Layland, K., Joos, T. O., Rothbauer, U., Schneiderhan-Marra, N., Schindler, M., Templin, M. F. (2021). Multiplexed Serum Antibody Screening Platform Using Virus Extracts from Endemic Coronaviridae and SARS-CoV-2. *ACS Infectious Diseases, 7*(6), 1596–1606. https://doi.org/10.1021/acsinfecdis.0c00725

*authors contributed equally

5. Skoda, J., Dohnalova, K., Chalupsky, K., **Stahl, A**., Templin, M., Maixnerova, J., Micuda, S., Grøntved, L., Braeuning, A., & Pavek, P. (2022). Off-target lipid metabolism disruption by the mouse constitutive androstane receptor ligand TCPOBOP in humanized mice. *Biochemical Pharmacology, 197*, 114905. https://doi.org/10.1016/j.bcp.2021.114905

6. Ruoff, F., Kersten, N., Anderle, N., Jerbi, S., **Stahl, A**., Koch, A., Staebler, A., Hartkopf, A., Brucker, S. Y., Hahn, M., Schenke-Layland, K., Schmees, C., & Templin, M. F. (2022). Protein Profiling of Breast Carcinomas Reveals Expression of Immune-Suppressive Factors and Signatures Relevant for Patient Outcome. *Cancers, 14*(18), 4542. https://doi.org/10.3390/cancers14184542

7. Heider, J., **Stahl, A**., Sperlich, D., Hartmann, S. M., Vogel, S., Breitmeyer, R., Templin, M., & Volkmer, H. (2024). Defined co-cultures of glutamatergic and GABAergic neurons with a mutation in DISC1 reveal aberrant phenotypes in GABAergic neurons. *BMC Neuroscience, 25*(1). https://doi.org/10.1186/s12868-024-00858-z

8. Walter, B., Hirsch, S., Kuhlburger, L., **Stahl, A**., Schnabel, L., Wisser, S., Haeusser, L. A., Tsiami, F., Plöger, S., Aghaallaei, N., Dick, A. M., Skokowa, J., Schmees, C., Templin, M., Schenke-Layland, K., Tatagiba, M., Nahnsen, S., Merk, D. J., & Tabatabai, G. (2024). Functionally-instructed modifiers of response to ATR inhibition in experimental glioma. *Journal of Experimental & Clinical Cancer Research, 43*(1). https://doi.org/10.1186/s13046-024-02995-z

9. Wuerger, L. T. D., Sprenger, H., Krasikova, K., Templin, M., **Stahl, A**., Herfurth, U. M., Sieg, H., & Braeuning, A. (2024). A multi-omics approach to elucidate okadaic acid-induced changes in human HepaRG hepatocarcinoma cells. *Archives of Toxicology, 98*(9), 2919–2935. https://doi.org/10.1007/s00204-024-03796-1

10. Merk, D., Hirsch, S., Tsiami, F., Walter, B., Haeusser, L. A., Maile, J. D., **Stahl, A.**, Jarboui, M. A., Lechado-Terradas, A., Klose, F., Babaei, S., Admard, J., Casadei, N., Roggia, C., Spohn, M., Schittenhelm, J., Singer, S., Schüller, U., Piccioni, F., … Tabatabai, G. (2024). Functional screening reveals genetic dependencies and diverging cell cycle control in atypical teratoid rhabdoid tumors. *Genome Biology, 25*(1). https://doi.org/10.1186/s13059-024-03438-w

11. Kaldjob-Heinrich, L., Nuciforo, S., Lemke, S., **Stahl, A.**, Czemmel, S., Babaei, S., Blukacz, L., Meier, M.-A., Zhang, Y., Schürch, C. M., Gonzalez-Mendelez, I., Woelffing, P., Malek, N. P., Scheble, V., Nahnsen, S., Claassen, M., Templin, M., Bösmüller, H., Heim, M. H., … Bitzer, M. (2024). Adenosine receptor 3 in liver cancer: Expression variability, epigenetic modulation, and enhanced HDAC inhibitor effects. *Gastro Hep Advances*. https://doi.org/10.1016/j.gastha.2024.11.006

12. Haeusser, L. A., Becker, H., Kuhlburger, L., Zago, M., Walter, B., Tsiami, F., Erdmann, S., Trampert, J., Surender, S., **Stahl, A.**, Templin, M., Wegner, E., Schmidt, T., Schmees, C., Casadei, N., Sevenich, L., Claassen, M., Nahnsen, S., Beck, S., … Tabatabai, G. (2025). Genome-wide CRISPR-Cas 9 screens identify BCL family members as modulators of response to regorafenib in experimental glioma. *Neuro-Oncology*. https://doi.org/10.1093/neuonc/noae278

Contributions

Nr.	Accepted publication yes/no	List of authors	Position of candidate in list of authors	Scientific ideas by the candidate (%)	Data generation by the candidate (%)	Analysis and Interpretation by the candidate (%)	Paper writing done by the candidate (%)
1	yes	19	4	15	25	25	20
2	yes	7	1	35	65	65	60
3	no	10	1	40	60	80	60

1. Introduction

1.1. Why study proteins?

Despite significant scientific progress in recent decades, there is still a multitude of diseases where the detailed molecular mechanisms surrounding disease onset, progression and treatment evaluation remain unclear[1]. Given the fact that in many cases genetic underpinnings have known to contribute or underlie disease origins, a large number of studies have used genetics to characterize disease phenotypes in patients or patient-derived model systems[2]. However, in this context, focusing research efforts on proteins (proteomics) – thereby going beyond the genome level – is crucial[3], as the vast majority of biological processes is ultimately carried out by proteins. As the final step in the central dogma, proteins are the acting entity in any cell and thus are mechanistically most relevant, especially since the information transfer from genome to proteome can be restricted (genotype ≠ phenotype). Also, the genome can be regarded as static since the genetic sequence remains constant – in contrast, the proteome is much more dynamic temporally and spatially given its tight regulatory mechanisms through variable means of regulating protein expression and modification. Finally, information on RNA abundance from the transcriptomic level (e.g. RNA sequencing), only partially implies likewise protein expression[4], e.g. due to alternative splicing. Part of the proteome is organized as a complex network of signaling pathways governing central cellular functions[5]. In addition to changes in expression, proper regulation of this network is achieved by controlling protein activation through posttranslational modification (PTM), most notably phosphorylation[6]. Therefore, investigation of cellular signaling networks and activation states (PTMs) is vital for the study of any disease, as changes to protein expression patterns are frequently the presentation of underlying genetic aberrations. In light of this, (signaling) proteins have been singled out as primary molecular targets for therapeutic intervention, most notably in the field of oncology[7].

1.2. Application of proteomics in personalized/precision medicine

Personalized medicine (PM), also known as precision medicine, is an emerging medical approach focusing on and using information on the pathological characteristics of the individual to guide medical decisions[8,9]. Thus, in recent years, researchers and clinicians have strived to move away from generalized prevention, diagnostic and treatment strategies and advance towards tailoring them to the specific biological characteristics and thus the needs of the individual patient. However, requirements for implementation of such PM approaches are high. In order to gain sufficient insight, one has to rely on large sets of omics data[10-13]. Given significant technical and analytical advances in sequencing analyses, PM approaches have been heavily centered around genetics, but also proteomics presents a vital and meaningful area in PM research applications[14]. PM has specifically gained significant traction in cancer research[15,16]. In cancer, evaluating signaling pathway activity and disturbance is crucial as the underlying, acquired genetic mutations manifest as de-regulations in protein expression, activity and functionality[7,17,18]. The rapid development of a large number of new drugs with various cellular signaling targets have greatly propelled the field of cancer PM as more targeted intervention addressing dysregulated cellular signaling became possible[19]. Detailed proteomic analysis of individual tumor characteristics along with the interplay between signaling and specific drug agents presents a vital tool for drug testing and target identification as well as treatment evaluation[20]. Especially in a clinical context, gaining sufficient (beyond select classification/subtype markers) and meaningful (disease-relevant proteins/targets) information is key.

1.3. Which proteomic methods are available?

A variety of protein analytics methods with wide-ranging characteristics have been developed and could be considered for cellular signaling analysis in a PM/oncology setting. In the following, the most common will briefly be evaluated based on suitability.

The enzyme-linked immunosorbent assay (ELISA) is capable of detecting and quantifying antigens (proteins) in complex biological samples with excellent sensitivity[21,22]. It is accurate, easy to handle and suitable for automation and has proven as excellent for biomarker testing. For instance, gastrointestinal cancer serum biomarkers CA19-9 and CA125 are commonly assessed by ELISA in clinical practice[23].

However, throughput usually pertains to single or few analytes at a time, this making it unsuitable for broader analysis such as pathway activity studies or biomarker screenings.

Mass spectrometry (MS) presents another commonly used method for protein analysis[24,25]. It can give widespread information through global protein identification (shotgun proteomics). This broadness and generation of large datasets can however make data interpretation more difficult and cumbersome, which can be a hindrance for cellular signaling analysis in a clinical context. Most importantly, it also requires comparatively large amounts of sample material for extensive analysis. Finally, the detection of phosphorylation and thus activation of proteins can be more difficult in MS than in antibody-based methods.

Western Blotting (WB) still is the gold-standard method for protein analysis in most laboratories[26,27]. Its antibody-based nature gives great specificity. Although sensitivity is less in comparison to other methods such as ELISA or the high-end variation termed single molecule arrays (SIMOA), it is usually sufficient for detection of most cellular signaling proteins and extracellular receptors. It can easily detect protein phosphorylation by using antibodies specifically directed towards phosphorylated protein variants. Its main disadvantage is the requirement of high sample amounts, which in its current form makes it useful analysis of single effects, but not for broader insight into overall signaling events or the identification of new drug targets.

Another higher throughput Western Blot variation is the capillary-based Simple Western, also called ProteinSimple[28]. Here, protein separation is performed by capillary electrophoresis. Proteins are immobilized in the capillary and later probed with up to 25 different antibodies for detection.

A technique routinely used in clinical diagnostics for identification and classification of clinical specimen including tumor material is histology[29,30]. It allows for the visualization of cellular structures and tissues with labelled antibodies generating location/site-specific proteomic information, which can be highly advantageous in certain instances (e.g. highly intra-heterogeneous tissue samples). Like WB, it has good specificity (antibody-based) but is limited by its low throughput and high sample demands. Given these characteristics, only select tissue/tumor markers are routinely tested and thus suitability for detailed analysis of signaling is limited. Immunohistochemistry also exists

in a multiplexed form allowing assessment of multiple analytes on individual tissue sections[31,32]. However, limitations on throughput and sample amount equally apply.

1.4. DigiWest®: A method combining the advantages of others

The DigiWest is an alternative, powerful, but thus far relatively uncommon protein analytics tool. Methodologically, the developed concept transfers traditional WB onto a bead-based system (for details see Treindl et al. 2016[33]). An overview of DigiWest procedure is shown in Figure I.

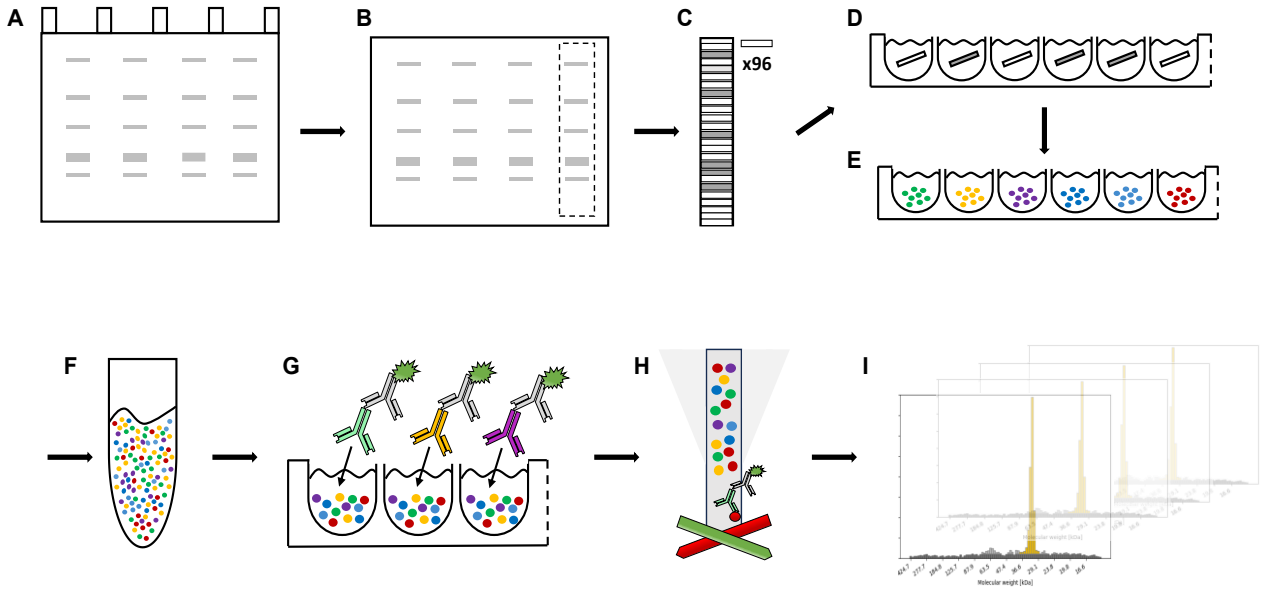

Figure I: DigiWest workflow. A-B: Western Blot. C: Cutting of each lane into 96 strips of defined molecular weight. D: Placement of strips into individual wells of a 96-well plate and elution of proteins. E: Coupling of protein fractions onto populations of color-coded beads. F: Pooling of all bead populations to reconstruct original sample lane. G: Incubation with primary and secondary (labelled) antibodies in direct immunoassay. H: Readout on flow cytometer. I: Integration of antigen-specific signals and data analysis.

In brief, size-separated proteins (WB) of distinct molecular weight fractions are immobilized on the surfaces of color-coded beads, which are then pooled reconstructing the original sample lane. In a series of subsequent direct immunoassays, analytes are detected via target-specific antibodies and can be quantified semi quantitatively through integration of bead-, size-, and thus antigen-specific signals. Crucially, the DigiWest combines the advantages of several proteomics methods discussed above. Its similarity to WB (antibody-based) allows for

very high specificity and the ability to easily detect phosphorylation and other PTMs, while retaining the sensitivity of traditional WB. In DigiWest, > 200 proteins can be measured in parallelized fashion using approximately 10 µg of cellular protein. Its multiplex nature drastically increases throughput, thus eliminating the issue of high sample consumption. This makes it extremely suitable for research questions requiring detailed cellular signaling analysis on precious material such as clinical specimens or other high-profile samples (e.g. specialized cell cultures). Moreover, upscaling and implementation into existing workflows is easily feasible to allow fast and accurate data processing and analysis. Also due to its large dynamic range (approximately 50 – 100 000 AFI = accumulated fluorescent intensity), DigiWest enables detection of all analytes relevant for cellular signaling ranging from low-abundance phosphorylated protein variants or transcription factors to high-abundance structural proteins. Specifically, measuring phosphorylation in addition to abundance gives vital additional information on protein (and thus pathway) activation status. By pre-selecting a panel of employed antibodies, DigiWest works in a targeted fashion, allowing for a focused analysis of proteins/analytes/targets in question, while limiting data amount, reducing complexity and aiding interpretation.

Overall, DigiWest combines the robustness and specificity of traditional WB with the high-throughput nature of bead-based parallelized assay systems. This “best of both worlds” scenario makes it an alternative, highly suitable method for analyzing cellular signaling pathways in the context of molecular disease mechanisms and to study interaction and manipulation of signaling proteins with drugs in disease and therapy in a PM clinical setting.

1.5. Analysis of cellular signal transduction via DigiWest

Detailed insights into activation and regulation of cell signaling pathways paves the way for a greater understanding of the manifestation of disease mechanisms on the protein level. For example, it is possible to evaluate the use and efficacy of drugs as therapeutic agents through analysis of their mechanisms of action through interaction with signaling proteins (e.g. tyrosine kinase receptors). Furthermore, it is possible to use DigiWest for individualized tumor activity profiling via signaling analysis in the context of clinical PM. Lastly, DigiWest can be applied for the identification of novel disease mechanisms and drug targets in psychiatric diseases. In this work, DigiWest was applied for these three separate research questions which are introduced separately in the following sections (1.5.1.-1.5.3).

1.5.1. Tyrosine kinase inhibitors in FGFR2-mutated cholangiocarcinoma

Tyrosine kinase inhibitors (TKI) are new anti-cancer drugs which are specifically directed against various growth factor receptors[34]. Certain TKI are either approved for or being experimentally evaluated as treatment for cholangiocarcinoma. Based on clinical observations made in patients, we aimed at comparing two TKI classes through analysis of cellular signaling.

1.5.1.1. FGFR2 fusions in intrahepatic cholangiocarcinoma

Cholangiocarcinoma (CCA) is an aggressive form of cancer affecting the bile ducts. Anatomically, clinicians group CCA into subtypes depending on the location of the tumor, distinguishing intrahepatic (liver parenchyma), perihilar (hepatic ducts) and distal (common bile duct) CCA[35]. CCA is generally diagnosed at advanced disease stages and thus associated with poor prognosis and a low survival rate. Despite a steady rise in CCA incidence over recent years, treatment options remain limited. From a clinical perspective, a combination of the classical chemotherapeutic agents Gemcitabine and Cisplatin has comprised the standard first line therapy for CCA at late disease stages[36]. Beyond this generalized treatment, there currently is no standardized second-line therapy concept for late stage CCA[37].

From a molecular standpoint, a subset (10-20 %) of intrahepatic CCAs (iCCA) carry a distinctive genetic alteration affecting the cell surface receptor fibroblast growth factor receptor 2 (FGFR2). Here, the FGFR2 gene is partly fused with another gene due to a chromosomal aberration[38,39]. This translocation leaves the extracellular and kinase domains of FGFR2 intact, with the fusion partner modulating the phosphorylation domain. A large variety of fusion partners are known; most common are BICC1, PPHLN1, TACC3, and MGEA5[40]. The resulting chimeric receptor protein is constitutively dimerized, thus inducing receptor phosphorylation and permanent activation of downstream signaling even in the absence of a ligand. Signaling pathways downstream of FGFR mainly include the MAPK/Erk, PI3K/Akt/mTOR and Jak/STAT cascades (Figure II)[41], which are also addressed by other tyrosine kinase receptors such as endothelial growth factor receptor (EGFR), vascular endothelial growth factor receptor (VEGFR) or platelet-derived growth factor receptor (PDGFR). Furthermore, FGFR activation also promotes PLCγ /PKC signaling.

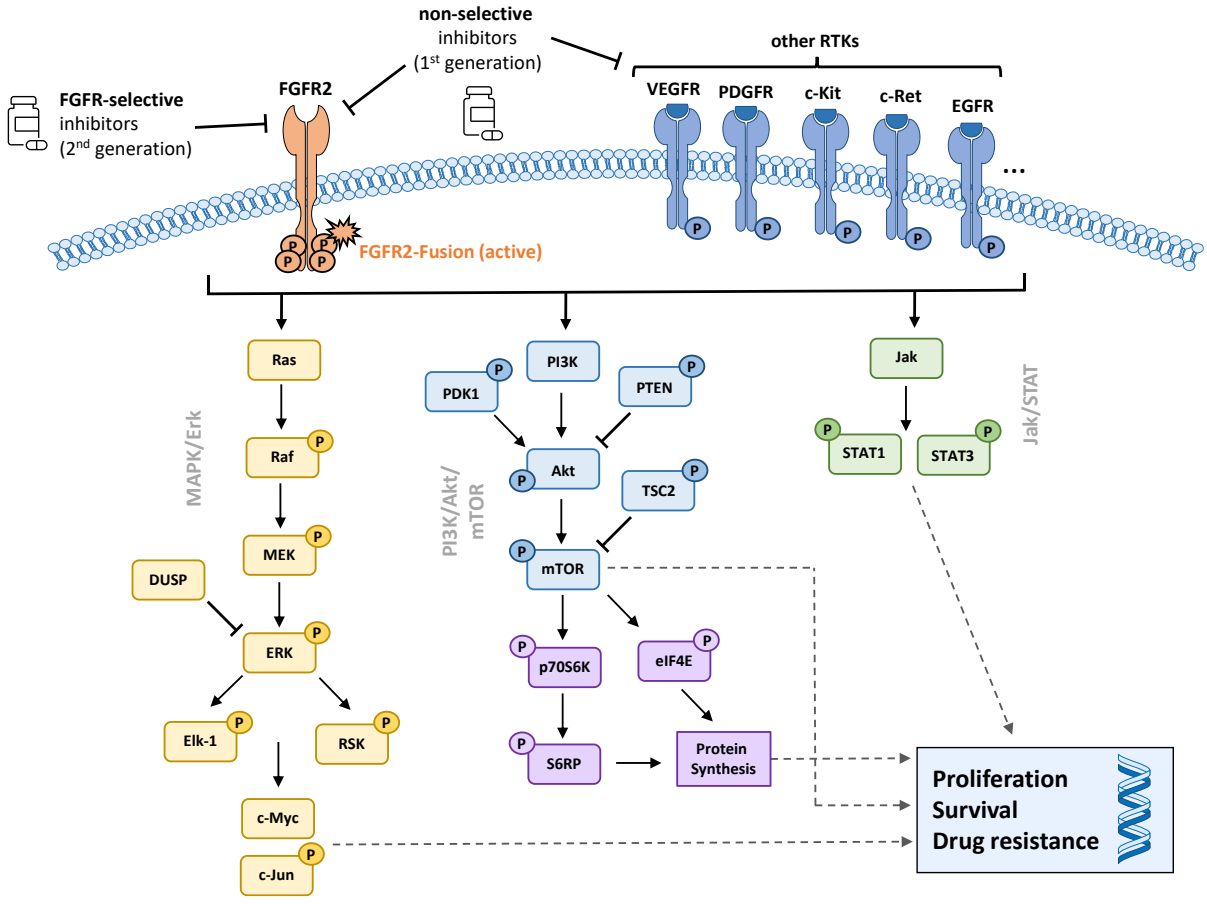

Figure II: TKI classes and FGFR-related signaling pathways in FGFR-fusion positive iCC. RTK = receptor tyrosine kinase.

Activated cellular signaling in turn leads to cancer-typical increase of proliferation, and de-regulation of the cell cycle and apoptosis, fueling tumor progression (Figure II). However, pathway activation patterns can vary depending on the individual tumor and type of FGFR-fusion gene.

1.5.1.2. TKI as therapeutic agents in FGFR2-fusion positive iCCA

In recent years, the FGFR signaling pathway has become a promising drug target in search of more personalized therapy approaches for iCCA[42,43]. This was enabled by the development of TKIs capable of specifically targeting and inhibiting members of the FGFR family. In this context, TKIs can generally be divided into two groups, namely FGFR-selective, and non-selective (multi-kinase) TKIs[44]. While the former such as Erdafitinib, Infigratinib (BGJ-398), Pemigatinib or Futibatinib (TAS-120) will exclusively target FGF receptors, the latter also inhibit other tyrosine kinase growth factor receptors aside from FGFR (Figure II). Non-selective TKI for instance include Ponatinib (inhibiting FGFR1-4, PDGFRα, ABL), Nintedanib (FGFR1-3, VEGFR1-3, PDGFRα/β) or Lenvatinib (FGFR1-4, VEGFR1-3, PDGFR, KIT, RET). Due to off-target effects of such 1st-generation TKIs[45], focus was shifted towards FGFR-selective TKIs (2nd generation) to enhance specificity. Thus far, only Infigratinib, Pemigatinib and Futibatinib[37], three FGFR-selective TKI, are FDA-approved for use in pre-treated iCCA tumors harboring FGFR2 fusions. Clinical trials involving these agents have shown varying response rates in patients, ranging from 23-45 %[46-49]. Non-selective TKI such as Lenvatinib are still used for a variety of tumor entities[50,51]. However, a detailed direct comparison of selective and non-selective TKI in FGFR2-mutated iCCA, especially containing high-throughput proteomic data on cellular signaling is yet to be reported.

1.5.1.3. Drug resistance to selective TKIs due to FGFR2 point mutations

A recurring problem upon treatment with selective TKI is that aside from experiencing significant side effects (e.g. hyperphosphatemia, retinal and dermatologic toxicities[52,53], patients often develop resistance to initially effective selective inhibitors and consequently experience disease progression. This is often attributed to the development of point mutations in the FGFR2 gene (in addition to the FGFR2-gene fusion) during treatment with e.g. Infigratinib or Pemigatinib (Figure III)[54,55]. One such frequently observed additional mutation in the FGFR2 domain affects the “gatekeeper”

residue at Valine (V) 564 (e.g. V564F or V564I), which is located in the ligand binding pocket of FGFR2 and thus is critical for drug-receptor interaction.

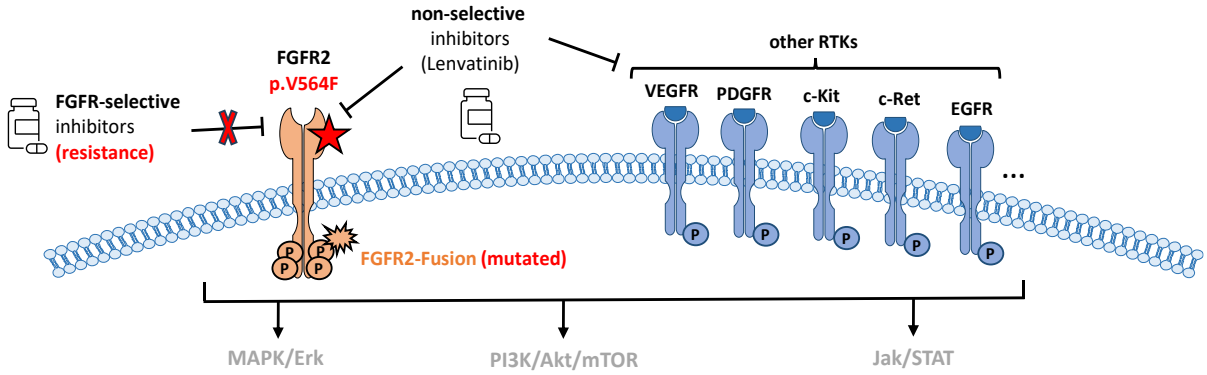

Figure III: Resistance to selective TKIs in the presence of FGFR2 point mutations. Secondary point mutations such as p.V564F can arise in the FGFR2 domain under treatment with selective TKIs such as Infigratinib or Pemigatinib and induce resistance to these drugs. The effect of unselective TKI such as Lenvatinib is unclear in this context.

Drug resistance due to gatekeeper mutations has also been described for other FGFR family members such as FGFR1 and FGFR3[56]. Another commonly altered section related to drug resistance in FGFR2 fusion proteins is the so-called molecular brake (NEK) triad. Comprising of residues N549, E565, and K641 (observed mutations are for example. N549K, N549D, E565A or E565G), it is essential for proper control of receptor activity via autoinhibition. However, the detailed molecular mechanisms underlying this resistance phenomenon remain poorly understood. It has been observed that select TKI such as Futibatinib can retain potency to some resistance mutations[57]. At the protein level, a direct comparison of selective and unselective TKI regarding treatment efficacy and resistance development is still missing. Here, DigiWest presents a viable tool given its simultaneous detection of proteins and protein variants. Especially its ability of measuring phosphorylation and in turn pathway activation/inhibition, makes it a suitable approach for such a mechanistic efficacy evaluation of inhibitory agents such as TKIs.

1.5.2. Personalized profiling of gastrointestinal tumors in clinical application

In cancer, acquired genetic alterations manifest as changes in activity of cellular signaling pathways on the protein level ultimately fueling tumor progression. This enhanced understanding of the effects of cancer-inherent mutations has greatly accelerated testing and development of new, protein-targeting drugs for clinical use[58]. Moreover, translational research has also been applied to identify specific treatment options for individual patients via personalized genetic tumor profiling in a precision oncology setting[59]. We aimed at uncovering the (clinical) potential of DigiWest for cell signaling analysis in a personalized protein profiling approach.

1.5.2.1. Cellular signal transduction and targeted therapies in cancer PM

De-regulation of cellular signaling pathways is considered a major driving factor in cancer, since these pathways innervate and regulate central cellular functions such as cell proliferation, survival or angiogenesis. Therefore, a large variety of signal-transducing proteins such as MAPK[60], PI3K/Akt[61] or cell cycle regulators[62] as well as tyrosine kinase receptors[63] (e.g. EGFR, FGFR, VEGFR, Her2) have emerged as primary therapeutic targets[64]. Moreover, several forms of immune therapies, including immune checkpoint inhibitors,[65,66] have been developed. Regulatory approval of target-specific drugs has thus greatly increased therapeutic options and paved the way for personalized/precision therapy approaches. This is demonstrated by the broad range of drugs available (including off-label therapies) for treatment in a particular patient case and by the emergence of precision oncology programs such as molecular tumor boards (MTBs)[67]. Moreover, the large inter- and intratumor heterogeneity frequently observed within and across tumor entities[68] has evoked a need for accurate and reliable PM approaches. Overall, there is clear evidence for a demand and also for the benefits of personalized cancer treatment. For instance, it has been reported that as much as 69 % of cancer patients did not respond to standard therapy[69], while others have demonstrated that progression-free survival (PFS) was significantly greater in patients receiving precision versus standard treatment[70]. Additionally, by increasing the chances of treatment success, a movement towards PM would also greatly reduce costs for patients and healthcare systems[71].

1.5.2.2. Gastrointestinal cancers and their characteristics

Gastrointestinal (GI) cancers are a class of malignancies of the gastrointestinal tract and include for instance cancers of the esophagus, stomach, liver, pancreas, colon, gallbladder or rectum. In particular, pancreatic and colorectal tumors are among the most common and lethal as diagnosis frequently occurs at advanced disease stages, severely limiting treatment options[72]. From a molecular genetics standpoint, pancreatic cancers frequently (> 90 %) present with mutations in the KRAS oncogene[73,74] as well as in TP53 (p53), CDKN2A (p16), SMAD4 (Smad4)[75] or receptor tyrosine kinases[76], whereas mutations affecting EGFR, KRAS (Ras), PIK3CA (PI3K alpha), PTEN and TGFBR1/2 (TGF beta receptor 1/2) are most common in colorectal cancers[77,78]. In line with this, several studies have pointed out regulatory alterations in a variety of downstream signaling pathways (MAPK/Erk, PI3K/Akt/mTOR, Jak/STAT, Wnt, TGF beta/Smad, Notch) to play a role in development and progression of pancreatic, colorectal and other GI cancers[79-81]. In addition, GI cancers are considered to be highly heterogeneous despite sharing certain genetic vulnerabilities. This high inter- and intratumor heterogeneity is reflected in the diverse clinical presentation of patients and the resulting variability regarding treatment response, resistance and therapeutic outcome[82]. For instance, colorectal carcinomas localized on the right or left side of the colon[83], or tumors diagnosed in young and old patients[84], are known to differ drastically from a molecular and clinical standpoint. Also, pancreatic cancers are clinically subdivided according to various classifications[85-87]. These aspects – in combination with its poor prognosis and high lethality – makes PM approaches especially suitable for application in GI cancer diagnosis and treatment evaluation[88]. Considering this, DigiWest presents a promising PM-applied protein analytics tool, for in-depth cellular signaling analysis. Detailed description of expression signatures and phosphorylation profiles in pancreatic, colorectal and other GI tumors would be greatly advantageous for patient stratification as well as for therapy response prediction and recommendation in individual cases. Especially when it comes to distinguishing between tumor driver mutations and identifying the most suitable drug targets, pathway activity-based information on the protein level would be heavily beneficial.

1.5.2.3. Proteomics versus genetics for personalized clinical oncology

As mentioned, a large variety of protein-directed therapeutic agents have been developed and gained regulatory approval as anti-cancer drugs in GI and other cancers. At the same time, significant progress in sequencing technology has greatly reduced costs of genetic mutation analysis, and thus genome profiling more accessible for application in clinical practice[89]. Therefore, precision oncology programs such as MTBs are frequently using sequencing data for personalized characterization of individual patients, establishing genetic mutation analysis as a cornerstone of PM approaches in clinical practice[90,91]. However, high heterogeneity of the genetic landscape and an increase of data amount have complicated clinical interpretation, making accurate treatment recommendation more challenging[92]. However, complementary proteomic methods (e.g. histochemistry, MS, reverse-phase protein arrays) examining cellular signaling in detail are still heavily underrepresented in clinical practice; mainly due to limitations associated with low throughput and high sample demands.

1.5.3. Signal transduction analysis for disease mechanism discovery in Schizophrenia

DigiWest and proteomic analyses in general not only hold great potential for PM applications, drug evaluation and drug testing studies in cancer research, but also in research fields concerning other diseases, for instance neurological disorders. One such example is schizophrenia (SCZ), which has been studied extensively at the molecular level[93,94]. However, crucially, there is still little proteomic evidence available in the SCZ research field, leaving a limited understanding of regulatory mechanisms surrounding SCZ pathology, onset and progression. We aimed to address this knowledge gap by performing DigiWest analysis of patient-derived neuronal cells.

1.5.3.1. Clinical presentation and risk factors of Schizophrenia

SCZ is a severe mental disorder with a worldwide prevalence of approximately 1 %. SCZ patients frequently present with impairments in cognitive, emotional, and social functioning[95,96]. From a clinical standpoint, symptoms are highly heterogeneous and can largely be grouped into three categories, namely positive (hallucinations, delusions), negative (social withdrawal, motivation loss) and cognitive (altered perception, attention, memory) symptoms[97]. Most patients start to experience symptoms in adolescence or early adulthood. Thus far, treatment options employing antipsychotic drugs are solely symptomatic and treatment efficacy can vary[98]. Aside from several environmental risk factors such as stress, toxin exposure or substance abuse, a large proportion of risk factors is attributed to heritability[99]. GWAS and sequencing studies have associated more than 100 risk loci and several risk variants such as DISC1[100] with the disease, thus strongly reflecting the large genetic component in SCZ development[101].

Crucially, SCZ is regarded as a neurodevelopmental disorder, thus linking alterations already occurring in the early phases of brain development to the disease[102]. Therefore, investigations at these early developmental stages are of particular interest to understand initial disease onset, progression and predisposition. However, the details of molecular mechanisms at play which underly SCZ pathology and onset remain elusive, which has also impeded the development of effective causal treatments for patients.

1.5.3.2. iPSC as a model system for schizophrenia

For multifaceted diseases such as SCZ with large genetic variability and proposed alterations in early development, one suitable approach for disease modeling is the use of induced pluripotent stem cells (iPSC)[103,104]. With this approach, cells directly obtained from the patient (e.g. fibroblasts, blood cells) can be reprogrammed through the addition of select transcription factors (Yamanaka factors: Oct4, Sox2, KLF4, c-myc) to become pluripotent[105]. These cells can then be differentiated into practically any cell type, while crucially retaining the genetic background of a patient[106,107]. In neuropsychiatric research, iPSC are frequently differentiated into neuronal progenitor cells (NPC), and eventually, neurons[108,109]. As mentioned above, early developmental stages can be of particular interest in SCZ; thus, NPC are regarded as a relevant cell type in SCZ research[110]. NPC, – in addition to iPSC-derived neurons as well as postmortem brain tissues – have been frequently used for analyses of phenotypic disease alterations[111,112].

Transcriptomic and proteomic evaluation of iPSC-derived cell types – including NPC – have been conducted and revealed SCZ-specific alterations in the expression of genes and proteins related to several key cellular processes, including neuronal differentiation, protein synthesis, cell adhesion, cytoskeletal remodeling or oxidative stress response[113-116]. With regards to cellular signaling, the alterations described in iPSC and or patient/postmortem studies prominently concern the Wnt, Akt/GSK3-beta and MAPK/Erk pathways[117-119]. It is worth noting that the majority of valuable insight that has been gained by these investigations have been gathered on the genome or transcriptome level, leaving many questions regarding the causal interplay of erroneous signaling pathway regulation and its manifestation in cellular patho-phenotypes unaddressed on the protein level. Thus here, DigiWest can present a viable tool to examine disease-specific alterations regarding cellular signal transduction in patient iPSC-derived neuronal cell types at different stages of the differentiation process, accurately mirroring early developmental failures in SCZ.

2. Objectives

Aim of the present thesis was to illustrate the suitability of DigiWest protein profiling for applications in personalized medicine, clinical research, and therapy. Specifically, it should be demonstrated that extensive analysis of cellular signal transduction via DigiWest can be used for mechanistic efficacy evaluation of anti-cancer drugs, personalized characterization and treatment evaluation of tumors as well as for the identification of new disease mechanisms and drug targets in psychiatric research (see Figure IV).

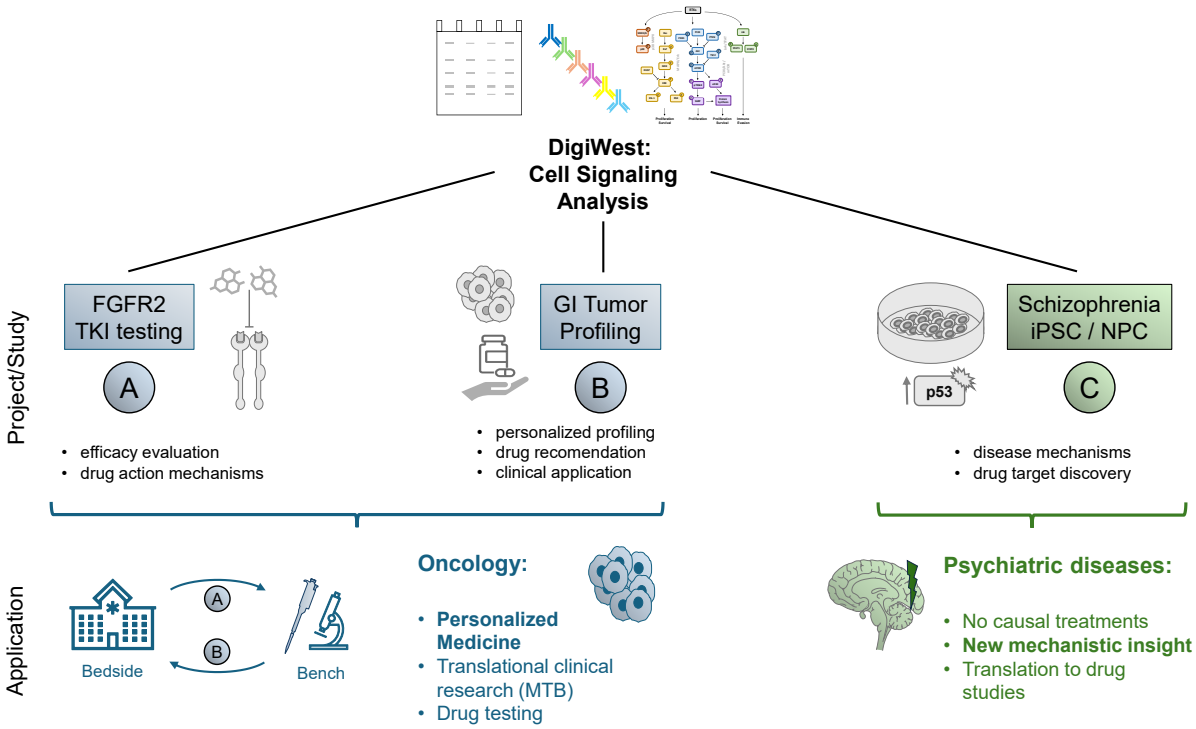

Figure IV: Overview of thesis objective and employed studies.

The first study aimed at comparing action mechanisms and performance of two tyrosine kinase inhibitor (TKI) classes using proteomic, in vitro and in silico data based on previous clinical observations made in a subclass of cholangiocarcinoma patients harboring FGFR2 gene rearrangements (A). In a bedside-to-bench approach, DigiWest should serve as an evaluator of drug efficacy via analysis of cellular signaling pathways in newly created patient-analogue cell lines. Specifically, comparative analysis of FGFR-selective and non-selective TKIs should be performed in treatment-sensitive cells and be expanded to cell lines carrying resistance-inducing FGFR2 point

mutations. Using DigiWest, special emphasis should be placed on the differential action mechanisms and molecular dynamics of the non-selective TKI Lenvatinib in comparison to its selective counterparts for application in future clinical cases.

Goal of the second study was to investigate cellular signaling in gastrointestinal (GI) tumors to identify personalized protein signatures and demonstrate clinical applicability of DigiWest and its suitability for integration into precision oncology programs (B). First, archived primary tumor tissues from pancreatic and colorectal carcinomas (along with patient-matched non-tumorous tissue) should be retrospectively analyzed via DigiWest to stratify samples based on proteomic and clinical data and to create personalized pathway activity profiles. In a subsequent direct clinical application (bench-to-bedside), we aimed at prospectively profiling 14 individual GI tumors from patients who underwent molecular tumor board (MTB) presentation. Identification of drug targets on a personalized basis and alignment of protein profiles with genetic mutation analysis and MTB drug recommendations should serve to evaluate the performance of DigiWest in a routine clinical setting and its potential for clinical precision oncology.

In the third study, DigiWest was aimed to be used for the extensive analysis of developing neuronal cells in a induced pluripotent stem cell (iPSC)-based model of schizophrenia (SCZ). In a field with little proteomic data available, the goal was to gain new insight into disease mechanisms underlying neuro-developmental aberrations associated with the disease on the protein level (C). Patient expression signatures should be compared to those of healthy controls in iPSC and differentiated neuronal progenitor cells (NPC) to pinpoint disease-relevant changes to signaling pathway regulation. DigiWest-based observations should be strengthened through immunohistochemistry and phenotypic assays (e.g. cell cycle dynamics) with the goal of uncovering disease mechanisms and its phenotypic manifestations to identify potential drug targets and aid future drug development in SCZ.

The overarching objective of this work was to highlight the power and flexibility of DigiWest by demonstrating its application for drug testing in clinical research (study A), for clinical personalized medicine approaches (study B) and for psychiatric research using iPSC-based systems (study C) and to encourage its use in future research endeavors.

3. Results

3.1. Mechanistic evaluation of TKIs in FGFR2-mutated cholangiocarcinoma

The contents of this chapter are based on:

Spahn, S.*, Kleinhenz, F.*, Shevchenko, E., **Stahl, A**., Rasen, Y., Geisler, C., Ruhm, K., Klaumuenzer, M., Kronenberger, T., Laufer, S. A., Sundberg-Malek, H., Bui, K. C., Horger, M., Biskup, S., Schulze-Osthoff, K., Templin, M., Malek, N. P., Poso, A., & Bitzer, M. (2024). *The molecular interaction pattern of lenvatinib enables inhibition of wild-type or kinase-mutated FGFR2-driven cholangiocarcinoma*. Nature communications, 15(1), 1287. https://doi.org/10.1038/s41467-024-45247-6

*authors contributed equally

Manuscript file is enclosed as **Appendix 1**.

Contribution:

In this work, I was responsible for all data relating to DigiWest and proteomic analyses. I prepared all samples and reagents required for DigiWest analysis and conducted all necessary experiments and assays for signaling pathway analysis independently. I generated and evaluated a suitable antibody panel for the expression analysis. I investigated and analyzed all the data independently. Finally, I also prepared all figures encompassing DigiWest data and wrote the manuscript portions relating to it together with Markus Templin.

3.1. Mechanistic evaluation of TKIs in FGFR2-mutated cholangiocarcinoma

Modulation of FGFR signaling through TKIs is employed as a therapeutic strategy in the treatment of several cancer types, including a subgroup of iCCA, which is defined by the frequent occurrence of FGFR2 gene rearrangements[39]. Among other TKIs, the non-selective TKI Lenvatinib presents an important therapeutic option for patients.

3.1.1. Clinical therapy responses to Lenvatinib in FGFR2-fusion iCCA

First, clinical therapy response to Lenvatinib was evaluated in a cohort consisting of seven iCCA patients harboring FGFR2 rearrangements. Given previously unsuccessful treatments and ineligibility to receive FGFR-specific inhibitors, patients were treated with Lenvatinib as per recommendation of the MTB at the University of Tübingen. Treatment with Lenvatinib achieved partial responses in 4/7 patients, and demonstrated superior clinical responses compared to patients´ previous and first-line treatments (Appendix 1 – Fig.1 a-b). Specifically, it significantly improved patient mPFS (median PFS) to 7 months in comparison to Gemcitabine/Cisplatin (2.1 months) as well as any other first-line therapies (2.5 months) received by patients in this cohort (Appendix 1 – Fig. 1c).

Within the cohort, one particular patient presented with a novel, so far unobserved FGFR2 fusion (FGFR2 with AHCYL2 gene), who had been sequentially treated with a variety of FGFR-inhibiting drugs (Ponatinib, Lenvatinib, Nintedanib, Infigratinib, Erdafinitb, Pemigatinib) over a time span of 30-35 months (Appendix 1 – Fig. 1d). Crucially, application of Lenvatinib yielded a partial response for 9 months, the longest of any TKI used. Furthermore, a subsequent liver biopsy analysis did not reveal any additional FGFR2 mutations aside from the gene fusion (e.g. resistance-inducing point mutations) occurring under treatment with Lenvatinib. At a later timepoint, the patient was treated with the FGFR-selective TKI Infigratinib in a clinical study. After initial treatment success and later withdrawal from the study for medical reasons, several FGFR2 resistance-inducing point mutations, among them p.V564F and p. E565A, were detected in a liquid biopsy (Appendix 1 – Fig. 1d). This striking patient history not only demonstrates the variability in effectiveness of FGFR-targeting drugs and notable treatment effect of Lenvatinib but also mirrors the major clinical concern of resistance

mutation development during treatment with selective FGFR inhibitors, in this case Infigratinib.

3.1.2. Bedside to bench approach of novel FGFR2-AHCYL2 fusion and subsequent cell line characterization

In a bedside to bench approach, NIH 3T3 cells were genetically modified to express this novel FGFR2-AHCYL2 fusion gene (termed FGFR2-AHCYL2_WT). Two additional cell lines, carrying the FGFR2-SH3GLB1 and the commonly observed FGFR2-BICC fusion, were also generated. All three cell lines showed expected increases in proliferation and anchorage independent growth (Appendix 1 – Fig. 2a-c) as compared to control (empty vector-transfected) cells. Furthermore, WB confirmed consistent expression of the fusion genes as well as activation (phosphorylation) of FGFR2-related downstream signal transducers FRS2, Erk1/2 and STAT3 (Appendix 1 – Fig. 2d) in all three cell lines. Thus, the new FGFR2-AHCYL2 fusion line showed a transformation potential comparable to other FGFR2-fusion-modelling cell lines and was used for further analyses.

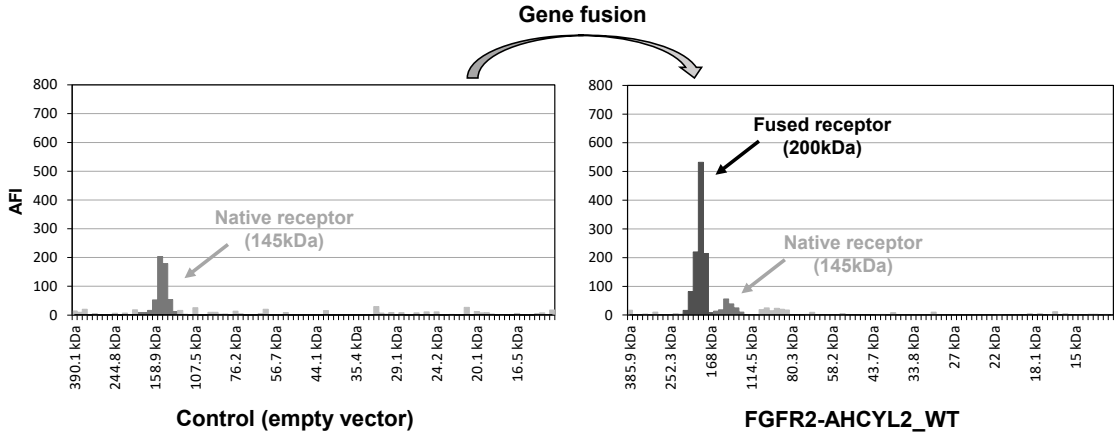

Figure V: Verification of presence of FGFR2 fusion via DigiWest in FGFR2-AHCYL2_WT and control (empty vector transfected) cells. DigiWest peak profiles using an FGFR2-directed antibody are shown. AFI = accumulated fluorescent intensity.

Presence of the fusion protein in the FGFR2-AHCYL2_WT line was also verified in advance via DigiWest (Figure V). The DigiWest profile of FGFR2 demonstrated a shift in molecular weight upon transfection. In empty vector-transfected cells, we only

observed a signal at 145 kDa, corresponding to the molecular weight of the native FGFR2 receptor form. In FGFR2-AHCYL2_WT cells, we found an additional signal (peak) at around 200 kDa, verifying the presence of the larger, fused receptor construct aside from an almost abolished signal of the native form.

3.1.3. Evaluating efficacy and action mechanisms of selective vs non-selective TKIs in FGFR2-AHYL2_WT cells

We next aimed at evaluating, characterizing and comparing FGFR-selective and non-selective TKIs with regards to efficacy and mechanism of action in FGFR2-AHCYL2_WT cells. The chosen non-selective TKIs were Lenvatinib, Ponatinib and Nintedanib, with Infigratinib and Futibatinib serving as selective TKIs. Cell viability assays revealed comparable dose-dependent efficacy in growth reduction of FGFR2-AHCYL2_WT cells between all FGFR2-inhibiting drugs compared to controls (Appendix 1 – Fig. 3a), indicating little difference in inhibitory capability between the two TKI classes. Of all tested TKI, the FGFR2-AHCYL2_WT cell line was least responsive to Nintedanib, which interestingly also proved ineffective in treatment of the analogue patient carrying the FGFR2-AHCYL2 fusion gene (see 3.1.1.). Cabozantinib, a TKI which does not target FGFR, was used as a negative control and expectedly did not show any growth-inhibitory effect on any of the tested cell lines. Overall, both FGFR-selective and non-selective TKIs proved equally suitable to inhibit cell growth of the FGFR2-AHCYL2_WT line in vitro.

To study the molecular mechanisms of action of these drugs in more detail, we evaluated intracellular signaling in FGFR2-AHCYL2 cells treated with either selective or non-selective TKIs using DigiWest protein profiling. To gain insight into activity patterns of affected signaling pathways downstream of FGFR2, an antibody panel comprising of 77 antibodies predominantly covering MAPK, PI3K/Akt/mTOR and Jak/STAT signaling was established. Notably, 35 of those antibodies were specifically directed to phosphorylated protein variants governing protein activation. Lenvatinib/Ponatinib treatment was applied to represent non-selective TKIs, and Infigratinib/Futibatinib treatment represented FGFR-selective TKIs. Notably, all four tested drugs were shown to be capable of significantly inhibiting FGFR2 phosphorylation (activation) to a similar extent (Appendix 1 – Fig. 3C). No phospho-FGFR2 signal was detected in empty-vector cells.

For more detailed analysis of differential downstream target activation, expression patterns of cells treated with agents of the respective TKI classes were each compared to solvent (DMSO) controls. Upon exposure of cells to FGFR-selective TKIs, we observed significant inhibition of exclusively MAPK proteins, as indicated by reductions in levels of phosphorylated Erk1/2 (T202/Y204), Rsk1 (T573) and the downstream target c-Myc (T58/62) along with total c-Myc levels (Appendix 1 – Fig. 3d). Phosphorylation of SHP-2 (Y542), a receptor-interacting protein critical for carrying signals downstream to the MAPK/Erk cascade, was similarly affected. In contrast, non-selective TKI were able to additionally reduce phosphorylation and thus inhibit activation of proteins unrelated to MAPK/Erk signaling (Appendix 1 – Fig. 4d, Supplementary Fig. 5), namely p70S6 Kinase (T389) and S6 ribosomal protein (S235/236), both downstream effectors of the mTOR pathway. Furthermore, non-selective TKI affected a broader spectrum of MAPK proteins which included phosphorylated c-Raf (S289/296/301), MEK1 (S298) and MEK1/2 (S217/221) aside from Erk1/2 (T202/Y204) and SHP2 (Y542).

Overall, DigiWest data shows that the FGFR2-AHCYL2 fusion appears to be addicted to the FGFR2-MAPK/Erk signaling axis which is sensitive to either class of inhibitors. However, non-selective TKI generally possess a broader inhibitory spectrum and can additionally target further signaling pathways such as the mTOR cascade. This observation could be crucial regarding the development of treatment resistance, given that these downstream pathways are shared among several tyrosine kinase receptors (see Figure II, Figure III, sections 1.5.1.2. - 1.5.1.3.).

3.1.4. Evaluating selective and non-selective TKI in FGFR2-AHCYL2 cells carrying resistance mutations

As stated above, the patient carrying the FGFR2-AHCYL2 mutation developed drug resistance due to the acquisition of several resistance-inducing point mutations in the FGFR2 domain (including p.V564F and p.E565A) under treatment with Infigratinib (section 3.1.1.). Crucially, these mutations were not yet present after previous treatment with the non-selective TKI Lenvatinib (Appendix 1 – Fig. 1d). This resistance phenomenon is well described and a major clinical concern for the use of FGFR2-selective TKIs. We therefore generated two further cell lines carrying the FGFR2-AHCYL2 fusion construct together with either the p.V564F (“gatekeeper”) and p.E565A

(“brake”) mutations (termed FGFR2-AHCYL2_p.V564F and FGFR2-AHCYL2_p.E565A) and again treated them with Infigratinib/Futibatinib (selective TKIs) or Lenvatinib/Ponatinib (unselective TKIs). As expected, both mutated cell lines were insensitive to Infigratinib, with pronounced resistance for the p.V564F mutated cell line (Appendix 1 – Fig. 4a). Treatment with Futibatinib still reduced cell growth to some extent in both cell lines, but the required does (IC50) were roughly 20-30 times higher compared to FGFR2-AHCYL2_WT cells (Appendix 1 – Fig. 4b). On the other hand, Lenvatinib was able to inhibit cell growth in both mutated cell lines with similar effectiveness as in the FGFR2-AHCYL2_WT line, especially at low concentrations (Appendix 1 – Fig. 4a-b). This indicates that Lenvatinib is able to retain its inhibitory potential in the presence of either mutation.

We again followed up our phenotypic observations with DigiWest analysis to disentangle molecular mechanisms of action of various TKIs and compare their inhibitory effects on FGFR signaling. Focus of the proteomic analysis was placed on the p.V564F mutated cell line, as this specific mutation is most crucial for drug-receptor interaction. DigiWest analysis revealed a strong reduction in FGFR2 phosphorylation upon treatment with the non-selective TKIs Lenvatinib and Ponatinib, as well as with Futibatinib, which binds irreversibly to FGFR1-4. In clear contrast, FGFR2 phosphorylation was not inhibited by Infigratinib (Appendix 1 – Fig. 4c).

For analysis of downstream signaling, we focused on the differential response of Infigratinib (selective) and Lenvatinib (non-selective TKI), serving as representatives for their respective TKI class. Infigratinib only showed very little inhibitory effects on downstream protein phosphorylations (Appendix 1 – Fig. 4d). And despite being significant, the magnitude of reduction of Erk2 (T202/Y204) and Rsk1 (T573) was lower compared to WT cells (Appendix 1 – Supplementary Fig. 5). In contrast, treatment with Lenvatinib inhibited the phosphorylation of a greater number of proteins (Appendix 1 – Fig. 4e). The compound not only retained its capacity to inhibit the FGFR2-MAPK/Erk axis, but also targeted phosphorylation of key PI3K/Akt/mTOR pathway players such as Akt (S473), mTOR (S2481), p70S6 Kinase (T389) and eIF4E (S209, Appendix 1 – Supplementary Fig. 5). The differential effect of Lenvatinib and Infigratinib became even more evident upon direct comparison of the two TKIs, highlighting the persistent effect of Lenvatinib on FGFR2 phosphorylation and its additional inhibition of mTOR signaling (Appendix 1 – Fig. 4f), both aspects contributing to its superior effectiveness in the presence of the p.V564F mutation.

It is interesting to note that, we observed generally higher expression of a multitude of analytes in the p.V564F cell line compared to the unmutated (WT) cell line independent of treatment (Figure VI). For instance, phosphorylation of FGFR2 was drastically increased. Moreover, aside from key MAPK analytes, phosphorylated protein variants from other key pathways such as Akt (S473), AMPK (T172), MKK (S257/T261), STAT3 (S727), p70S6 Kinase (T389) and GSK3α (S21) were also affected. This already points at increased baseline FGFR2 phosphorylation and pathway activity induced by the p.V564F mutation.

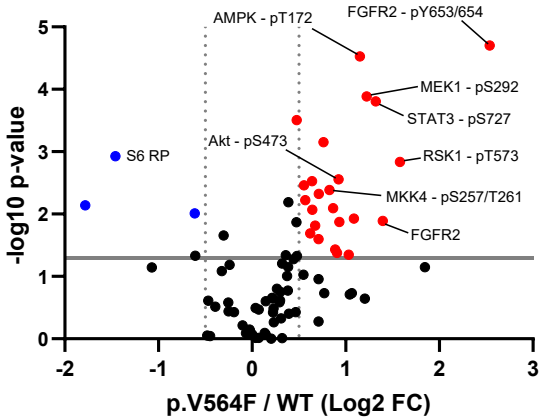

Figure VI: Treatment-independent comparison of p.V564F and WT cells as assessed via DigiWest. Volcano plot indicates significant changes in expression levels of relevant proteins and phosphorylated protein variants (Wilcoxon Test, p < 0.05). Median Log2 Fold Change was calculated for FGFR2-AHCYL2_p.V564F/ FGFR2-AHCYL2_WT signal ratio across all samples. Red dots indicate higher expression in p.V564F and blue dots in WT cells, respectively. Non-significant or analytes with FC < |0.5| are colored black.

3.1.5. In silico profiling of Lenvatinib and selective TKIs in resistance-mutated FGFR2

Furthermore, we performed in silico modeling to investigate the molecular interaction pattern of select TKI including Lenvatinib with resistance-mutated FGFR2 in greater detail. The binding and interaction profiles of Lenvatinib were compared to those of Infigratinib and Pemigatinib for selected FGFR2 resistance mutations V564F, E565A, and N549K (Appendix 1 – Fig. 5a-b), all of which have a previously demonstrated clinical relevance of inducing drug resistance.

Detailed interaction analysis of Lenvatinib, Infigratinib and Pemigatinib with the mutated FGFR2 residues, revealed a superior engagement of Lenvatinib compared to

Infigratinib and Pemigatinib in any of the tested scenarios (Appendix 1 – Fig. 5c). This illustrates the ability of Lenvatinib to flexibly adapt its interaction pattern to amino acid substitutions and retain its inhibitory capabilities. This is in line with our above described in vitro and proteomic data where Lenvatinib also remained potently active in FGFR2-mutant settings, specifically under the p.V564F mutation. For further tested resistance-inducing or gain-of-function FGFR2 point mutations (N549D, V562L, V564I and E565G), Lenvatinib also showed superior engagement compared to Infigratinib and Pemigatinib. Crucially, rotation profile analysis of Lenvatinib highlighted a greater steric flexibility. Overall, our in silico data show that Lenvatinib surpasses selective TKIs in the presence of FGFR2 resistance mutations due to its greater adaptational ability.

3.1.6. Application of Lenvatinib in a representative clinical case

Finally, our findings were used to select Lenvatinib for treatment in a representative clinical case. A patient with a FGFR2-BICC fusion experienced strong side effects (hyperphosphatemia, hair loss, nail bed infections, hepatic calcification = liver tissue scarring) during treatment with Pemigatinib. Upon disease progression after 13 months, an additional N549K brake mutation had occurred under Pemigatinib. The patient was then treated with Lenvatinib inducing a striking clinical response. Tumor manifestations were greatly reduced; consistent shrinkage of liver lesions observed in subsequent CT (computer tomography) scans (Appendix 1 – Fig. 6) was accompanied by a considerable mitigation of side effects. Overall, this clinical case underlines the suitability and potential of Lenvatinib as a therapeutic option in FGFR2-fusion positive CCA even in the presence of resistance mutations.

3.2. Personalized profiling of gastrointestinal tumors in clinical application

The contents of this chapter are based on:

Stahl, A., Büringer, K., Missios, P., Hoffmann, T., Singer, S., Schäfer-Ruoff, F., Schenke-Layland, K., Malek, N. P., Bitzer, M., Templin, M. F. (2024). *Personalized signaling pathway analysis of gastrointestinal tumors for patient stratification and drug target evaluation using clinically derived core biopsies.* npj Precision Oncology.

Manuscript file is enclosed as **Appendix 2**.

Contributions:

In this work, I conceptualized the project together with Markus Templin and Michael Bitzer. I planned and conducted all DigiWest experiments. I investigated and analyzed all DigiWest data independently. I also generated and evaluated the DigiWest antibody panel. I prepared all figures and tables shown in the manuscript. Finally, I also wrote the initial manuscript draft independently and formulated the final manuscript together with Markus Templin and Michael Bitzer.

3.2. Personalized profiling of gastrointestinal tumors in clinical application

Profiling of individual tumors through analysis of cellular signaling holds great potential for accelerating personalized proteomics approaches in a clinical setting. In the present study, DigiWest was used to analyze protein expression patterns in clinical GI tumor samples from both a retrospective cohort of pancreatic and colorectal carcinomas as well as a prospective case series of MTB patients.

3.2.1. Expression signatures distinguishing pancreatic and colorectal tumors

In the retrospective analysis, expression of 137 proteins and protein variants was assessed in archived primary tumor tissue of pancreatic (n = 10) and colorectal (n = 10) tumors. Direct comparison of tumor tissues (pancreas versus colon) revealed a clear separation according to the respective tissue type (Appendix 2 – Suppl. Fig. S2a). DigiWest analysis highlighted consistent differences between the tumor entities (Appendix 2 – Fig. 1a-b, Suppl. Fig. S2b-c) for tissue markers such as CK7 (pancreas) and CDX2 (colon), cell cycle- (pancreas), mTOR-, and Wnt- (colon) regulating proteins, as well as immune cell markers (pancreas). Since we also had patient-matched, non-tumorous control tissues available for all 20 tumors, we compared all tumor tissues with their respective non-tumorous control tissues in a paired fashion. Expectedly, upregulation of general tumor markers including cancer embryonic antigen (CEA) was observed (Appendix 2 – Suppl. Fig. S3a-b) in all tumors.

In the following, all DigiWest expression data from any tumor sample was solely evaluated in relation to its matched normal tissue (as Log2 Fold Change). Thus, all following data analyses are based upon a relative change in expression occurring from normal to cancerous tissue for a given analyte. Up- or downregulations of specific analytes or groups of analytes would infer changes in activity of signaling pathways. A comparison based on tumor entity analogue to the one described above yielded different results (Appendix 2 – Fig. 1c). As expected, more diverse expression patterns were revealed (Appendix 2 – Suppl. Fig. S4) and absolute (background) expression of tissue-specific markers such as CDX2 was excluded (no differential expression, Appendix 2 – Suppl. Fig. S5a). In this setting, we did observe significant differences between the tumor entities with regards to expression changes of proteins from key proto-oncogenes and tumor suppressors (Appendix 2 – Fig. 1c-d), despite notable

variability within a sample set. For instance, pancreatic carcinomas on average showed elevations of Ras (KRAS), c-myc (MYC), Ha-Ras (HRAS) or PI3K alpha (PIK3CA) expression as well as drastic downregulations of p53 (TP53), whereas colorectal carcinomas displayed strong reductions in p27 (CDKN1A) and PTEN levels. Thus, inclusion of patient-matched non tumorous tissue as a reference allowed selective analysis and distinction of pancreatic and colorectal tumors based on relative expression changes of key genetic vulnerabilities in the respective entity.

3.2.2. Molecular and clinical stratification of pancreatic and colorectal tumors via DigiWest

Next, we stratified each of the two cohorts separately using relative, normal tissue matched DigiWest data. Within the pancreas cohort, tumors (n = 10) were clearly separable into two groups with distinct expression signatures (Appendix 2 – Fig. 2a-b). The first group (n = 5) was characterized by upregulations of cytokeratins, downregulation of p53 levels, stimulated activity in the mTOR and NF-kappaB pathways along with increased modification of histones, indicating altered epigenetic regulation (Appendix 2 – Fig. 2c-e, Suppl. Fig. S6b-c). Expression levels of all these analytes were unchanged or reduced in the other group (n = 5) of pancreatic tumors, which in contrast were defined by increased expression of immune cell markers and elevated Smad signaling (Appendix 2 – Fig. 2c-e, Suppl. Fig. S6d). Overall, we were able to stratify pancreatic tumors based on activity changes to cellular signaling inherent to and distinctive for the respective tumor subgroup.

Given the available clinical data, the colorectal tumors (n = 10) were more heterogenous with regards to patient age, tumor localization (left/right sided) and the receival of previous treatment (Appendix 2 – Table 1). Accordingly, expression patterns were more diverse compared to the pancreas cohort, thereby separating the colorectal tumors into four subgroups (Appendix 2 – Fig. 3a, suppl. Fig. S7b). A classification and comparison of colorectal tumors based on patient age and tumor localization was sensible to show expression differences between clinically relevant subgroups. One tumor sample (hepatoid carcinoma) was excluded from this analysis due to its divergent clinical nature. Notably, we observed a downregulation of mTOR and cell-cycle proteins exclusively in younger patients (< 55 y, n = 3), while the signals were on average unchanged in the older patient group (n = 6, Appendix 2 – Fig. 3b).

Furthermore, based on tumor location, left-sided colon carcinomas (n = 4) displayed upregulations of EGFR, mTOR-, and MAPK proteins (Appendix 2 – Fig. 3c), with an opposing trend in right-sided tumors (n = 5). In this fashion, we were able to link relative changes in protein expression to clinically and treatment-relevant subgroups.

A summary of the retrospective study design and DigiWest expression profiles relating to pancreatic and colorectal cancer stratification according to entity, subgroup defining-pathway activity and -clinical data is outlined in Figure VII. Finally, protein expression profiles were evaluated separately for each tumor.

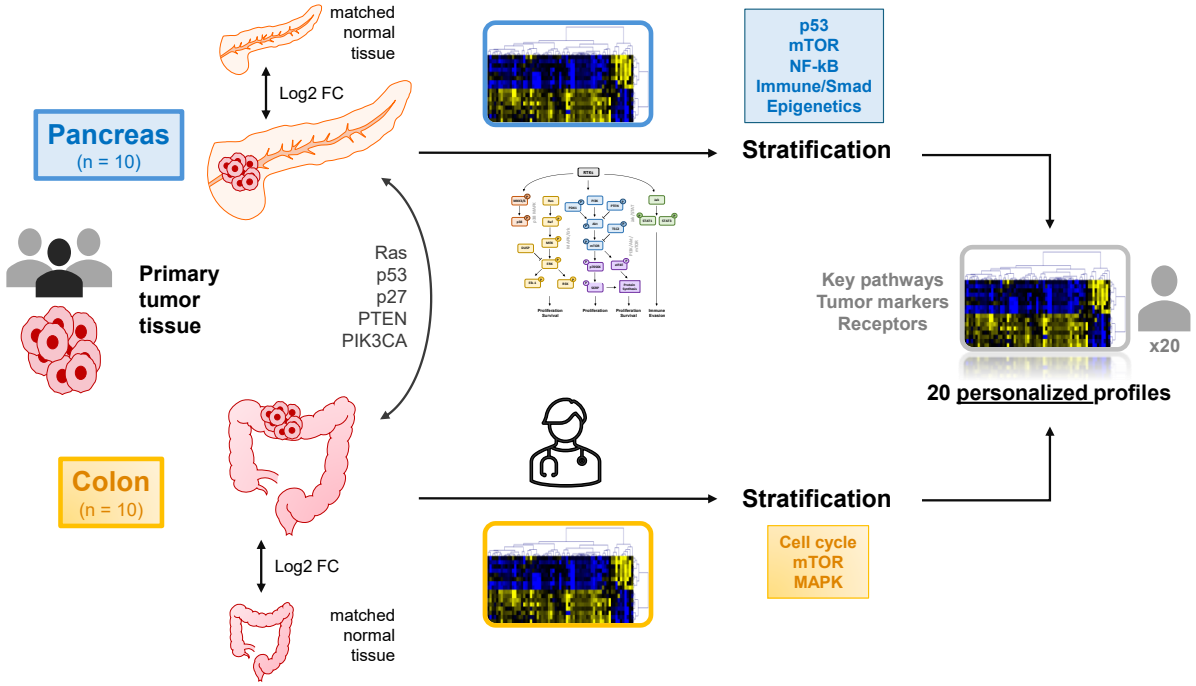

Figure VII: Summary of retrospective DigiWest study – stratification of pancreatic and colorectal carcinomas based on cellular signaling and clinical characteristics as well as personalized profiling of individual tumors (see section 3.2.3).

3.2.3. Personalized pathway activity profiles in individual GI tumors

Individual analysis of protein expression for each tumor (in relation to matched non-tumorous tissue) yielded 20 personalized, patient (tumor)-specific protein profiles. In 15 cases (75 %), one or more signaling pathways and/or tyrosine kinase receptors could be retrospectively identified as potentially tumor-driving based on DigiWest data alone. Since several of the measured and individually identified proteins are known targets for FDA-approved drugs, we also established a list of potentially applicable

drug targets in each individual case. The high level of inter-patient heterogeneity intrinsic to GI tumors (see section 1.5.2.2.) was also evident in our personalized data sets, as various marker patterns, pathways and receptors were identified across samples (Appendix 2 – Table 1, Suppl. Figs. S8-S23).

Expectedly, almost all tumors (19/20) presented with an increase in CEA levels compared to its matched normal tissue. Moreover, most pancreatic tumors showed increases in CK7 and CK19 expression. Two colorectal cancers with distinct clinical characteristics – a rare hepatoid carcinoma and a microsatellite instability (MSI)-high tumor – were clearly distinguishable from the rest of the colon cohort based on the sole and notable expression of CK7 and CDX2, respectively (Appendix 2 – Table 1). Two individual exemplary cases are outlined in detail below.

In one pancreatic cancer case, we observed strong upregulations of expression and phosphorylation of several mTOR-pathway proteins (mTOR, PDK1, Raptor) as well as relevant downstream targets such as S6 RP or eIF4E (Appendix 2 – Fig. 4a-b). Moreover, a strong reduction of p53 and upregulations of Cyclins D2, D3 and E1 hinted at impairments in cell cycle control. Aside from this, we noted elevated Wnt and NF-kappaB signaling. All in all, our data allowed us to identify mTOR signaling and the cell cycle as the most relevant druggable pathways in this particular case.

In the second example, a colorectal tumor displayed elevated activity in the MAPK/Erk and Jak/STAT pathways, as indicated by coherent upregulations of phosphorylated variants of Erk1, Erk2, MEK1/2, b-Raf, Rsk1 as well as STAT3 (Appendix 2 – Fig. 4a+d). Furthermore, expression levels of EGFR and PDGFR were increased, which led us to identify these upstream receptors as key drug targets. In several other cases (mostly pancreatic cancers), MAPK/Erk activity was accompanied by increases in Ras (KRAS) expression (e.g. Appendix 2 – Fig. 4c), highlighting this key oncogene as a potential drug target.

Interestingly, upregulations of several immune cell markers (CD4, CD8, CD11c, CD25, CD68, CD56, CD163) were apparent in 9/20 examined tumors, which is generally indicative of immune cell infiltration (“hot” tumors) and further stratified and functionally grouped our retrospective sample cohort. For select cases (e.g. Appendix 2 – Fig. 4e), this was accompanied by increased Smad signaling, whereas activity in other common oncogenic pathways (e.g. MAPK, mTOR, Wnt) was not apparent; this drew attention to immune therapy as a form of (hypothetical) treatment.

Overall, by creating personalized expression patterns using relative DigiWest data, we were able to individually characterize each tumor while capturing the intrinsic clinical and molecular heterogeneity of this representative patient cohort and highlighting treatment-relevant aberrations and drug targets on a personalized level.

3.2.4. Individual characterization of MTB cases and alignment with genetic profiling

In light of the promising results obtained in the retrospective part of the study (sections 3.2.1. - 3.2.3.), we aimed to uncover the potential of DigiWest protein profiling for integration into precision oncology programs and clinical routine. In order to test its performance in an exploratory direct clinical application, we examined and profiled 14 GI tumor samples in similar fashion using primary patient material in the form of clinically derived core biopsies. These were taken from patients as a routine diagnostic step during presentation to the MTB of Tübingen University. A schematic overview of DigiWest in clinical application as demonstrated here is shown in Figure VIII.

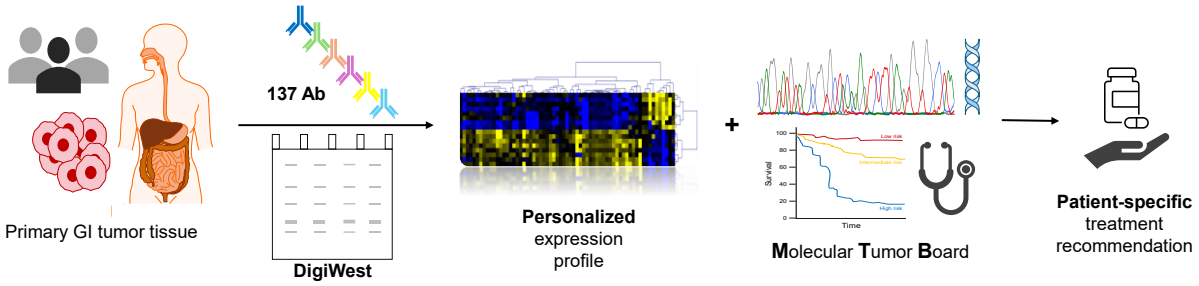

Figure VIII: Overview of clinical application of DigiWest. Primary tumor tissue was obtained from GI tumor patients as needle biopsies and subjected to DigiWest analysis. Information on pathway activity and potential drug targets from personalized DigiWest expression profile was combined with patient-specific genetic (sequencing) and clinical data to yield individualized treatment recommendations. Ab = antibody.

Notably, this GI cancer patient cohort displayed extraordinary clinical heterogeneity with regards to tumor entity and included pancreatic, gallbladder, colorectal, cholangio, gastric, esophageal and rectal carcinomas (Appendix 2 – Table 2). Furthermore, several patients had been extensively pre-treated before sampling. Notably, non-tumorous control samples were unavailable for this cohort due to routine procedures, as sampling via needle biopsies usually does not provide sufficient non-tumorous

tissue. Thus, protein expression levels of a particular analyte were here compared to its average expression level across the cohort.

Upon individual DigiWest profiling of each tumor, we were able to identify coherent expression and activation patterns in key oncogenic signaling pathways for 12/14 patients (85 %) and pinpointed several potential drug targets in each individual case (Appendix 2 – Table 2, Suppl. Figs. S25-S36). Since all patients were included into the MTB, all tumors had been previously subjected to genome sequencing analysis. In order to evaluate the meaningfulness of our proteomics-based characterization, we compared DigiWest data with key mutations identified via genetic analysis and with the ultimate treatment recommendations suggested by the MTB for each patient. Crucially, in 8/12 applicable cases, information on protein/pathway/receptor activation and expression gained via DigiWest matched with genetic MTB observations and treatment decisions.

For instance, the protein profile of a colorectal tumor revealed coherently elevated activity (phosphorylation) in the MAPK/Erk (Erk1, Erk2, Rsk1) and Jak/STAT (STAT1, STAT3) pathways, as well as exceptionally high expression of FGFR2 (Appendix 2 – Fig. 5a-d). In line with this, genetic profiling had revealed an amplification of the FGFR2 gene and thus treatment with an FGFR inhibitor was recommended by the MTB (Appendix 2 – Table 2). Here, DigiWest data was clearly able to confirm this observation on the protein level by indicating both the genetic aberration to the upstream receptor (FGFR2) as well as the resulting activity in downstream pathways (MAPK and Jak/STAT). In a second exemplary case (hepatocellular carcinoma), DNA sequencing had identified a deletion in the mTOR-regulating tumor suppressor TSC2 and subsequently recommended treatment with an mTOR inhibitor in combination with an immune checkpoint inhibitor (Appendix 2 – Table 2). In line with this, DigiWest analysis revealed an exceptionally high expression and activity of mTOR as well as other related key analytes such as Raptor, Rictor, PI3K alpha, PI3K beta and S6 RP (Appendix 2 – Fig. 5e-g). Furthermore, high expression levels of CD4, CD8 and CD163 indicated immune cell infiltration and thus an immunologically “hot” tumor.

Overall, in this exploratory clinical application of DigiWest, we were able to showcase its potential in this setting, as unique, personalized expression profiled were created, which aligned significantly with existing mutation analysis and drug recommendations made by the MTB.

3.3. Signal transduction analysis for disease mechanism discovery in schizophrenia

The contents of this chapter are based on:

Stahl A., Heider J., Wüst, R., Fallgatter, A. J., Schenke-Layland, K., Volkmer, H., Templin, M. (2024). *Patient iPSC-derived neural progenitor cells display aberrant cell cycle control, p53, and DNA damage response protein expression in schizophrenia.* BMC Psychiatry, 24, 757. https://doi.org/10.1186/s12888-024-06127-x

Manuscript file is enclosed as **Appendix 3**.

Contributions:

In this work, I conceptualized the project and planned the experimental designs together with Johanna Heider. I was responsible for all data relating to DigiWest and Western Blot experiments. For both, I prepared all required samples and reagents, conducted all necessary and investigated and analyzed all data independently. I also generated and evaluated the DigiWest antibody panel. Johanna Heider performed and analyzed all immunohistochemical and FACS analyses. I prepared all figures encompassing DigiWest, Western Blot and ICC-related data. Finally, I also wrote the initial manuscript together with Johanna Heider and edited the final manuscript together with Hansjürgen Volkmer and Markus Templin.

3.3. Signal transduction analysis for disease mechanism discovery in schizophrenia

The molecular mechanisms surrounding schizophrenia (SCZ) pathology and onset largely remain elusive, especially with regards to protein expression and signaling pathway activity. Thus, we examined cellular signaling via DigiWest in SCZ patient-derived iPSC and developing neuronal progenitors (NPC) to compare the respective cell stages and highlight disease-specific protein expression signatures in comparison to healthy controls (Figure IX).

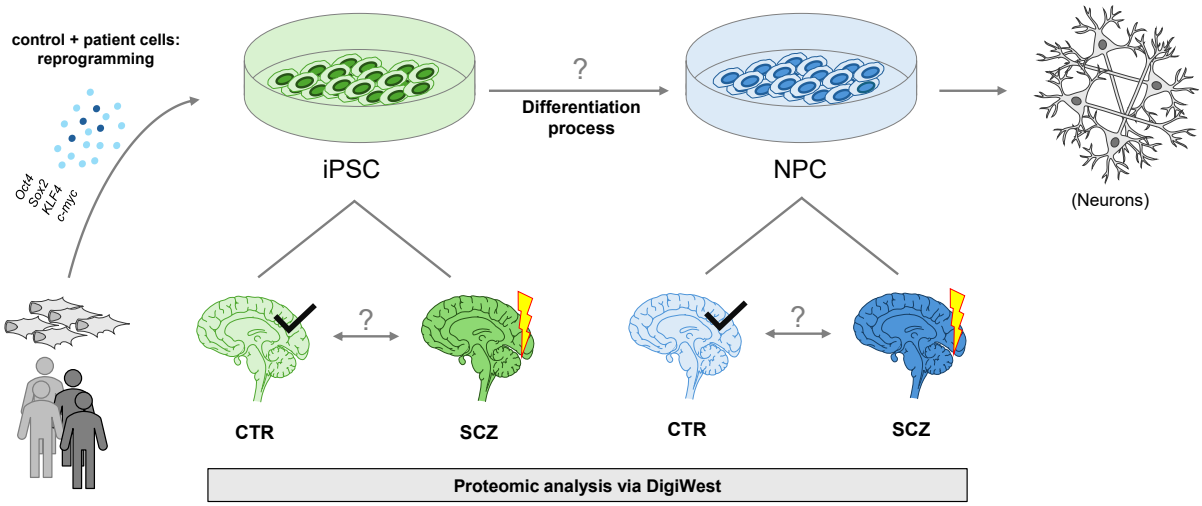

Figure IX: Overview of DigiWest analysis of patient-derived iPSC and NPC in comparison to healthy controls. Fibroblasts from SCZ patients and healthy controls were obtained and reprogrammed to iPSC and then differentiated into neuronal progenitors (NPC). Expression signatures of controls (CTR) and patients (SCZ) were compared via DigiWest at the iPSC and NPC stage, respectively. Furthermore, the iPSC and NPC stages were compared independently of disease allocation to examine protein expression patterns during the differentiation process.

3.3.1. Marker expression and pathway activity changes during differentiation from iPSC into NPC

In the entire protein dataset, we observed a consistent grouping of all samples according to their respective cell stages (iPSC or NPC, Appendix 3 – Fig. S1) across three independently performed neuronal differentiations. Accordingly, we first analyzed expression differences between the cell stages independent of disease status and observed strong changes in key differentiation markers. Despite expression levels varying across clones, as expected, NPC generally present with lower levels of Oct4

(indicator for pluripotency) and higher expression of MAP2, Sox1, Sox2, Nestin, Pax6, Vimentin, and NCAM, all markers for differentiated neuronal progenitor cells (Appendix 3 – Fig. 1A/B). We exemplarily confirmed our observations by performing immunocytochemical (ICC) staining for some of these eight proteins with matching results (Appendix 3 – Fig. 1C, Fig. S4).

Crucially, we also found strong expression differences between the iPSC and NPC stages beyond these characteristic markers. A total of 85/137 measured analytes showed differential expression between iPSC and NPC (Appendix 3 – Fig. 2A). Among the many proteins significantly upregulated in NPC were key members of the Wnt (active/total beta-catenin, Wnt3/7, LRP6, Dvl2/3, LEF1, TCF1/7), Hippo (LATS1, Mob1, Mst1, TEAD, KIBRA) and Hedgehog (Gli2/3, SUFU) pathways (Appendix 3 – Fig. 2B). Importantly, these signaling pathway are all known to play a crucial role in neurodevelopment. Several cell cycle proteins (CDK1/2/4/6, Cyclins D1/2, p21, Rb) also showed notably higher expression in NPC (Appendix 3 – Fig. 2B). For select key analytes – namely the vital Wnt proteins beta-catenin and LEF1 as well as the cell cycle regulator p21 – we again validated the higher expression levels in NPC via ICC staining (Appendix 3 – Fig. 2C-D). Overall, all iPSC and NPC can clearly be distinguished based on the expression of key differentiation markers as well as the activation of neurodevelopmental signaling pathways, as highlighted by DigiWest.

Next, we investigated changes in protein expression occurring during differentiation from iPSC to NPC for patient- (SCZ) and healthy control-derived cells (CTR) independently. Given the consistent expression differences across all samples, effects concerning a total of 62 analytes were expectedly shared between the two conditions (CTR and SCZ, Appendix 3 – Fig. S5). Moreover, a large proportion of analytes (approximately 90 %) was upregulated in both CTR and SCZ NPC compared to the respective iPSC.

However, there were also several analytes which displayed varying or opposing trends in expression during differentiation from iPSC into NPC for SCZ and CTR-derived cells. For instance, LEF1, phosphorylated CDK1 (Y15), p21, phosphorylated Erk1/2 (T202/Y204) and Smurf1 are upregulated to a greater extent during differentiation of SCZ iPSC into NPC compared to CTR cells (Appendix 3 – Fig. 2E/F, Fig. S6). This indicates disease-specific alterations in protein expression occurring during development of early-stage neuronal cells in SCZ.

Overall, these data demonstrate that DigiWest can characterize iPSC-derived neuronal cells at different developmental stages regarding the expression of key marker proteins and beyond. Moreover, we demonstrate the ability of the methodology to track both consistent as well as SCZ-specific changes to protein expression signatures occurring during the differentiation process from iPSC into NPC.

3.3.2. SCZ-specific protein alterations in iPSC and reduced differentiation efficiency

In the following, we evaluated expression between SCZ and CTR samples at the iPSC and NPC stage separately, in order to highlight disease-relevant proteomic alterations at the respective developmental stages. When comparing CTR and SCZ iPSC, a total of 11 proteins (8 %) were differentially expressed between the two conditions, with 6 down- and 5 upregulations in SCZ (Appendix 3 – Fig. 3A/B, Table S4). Among these, changes to levels of p53 and its phosphorylated variant p53 – pS15 were by far the strongest with 3- and 10-fold upregulations in SCZ iPSC, respectively (Appendix 3 – Fig. 3C). This notable up-regulation of p53 was also confirmed through ICC analysis (Appendix 3 – Fig. 3D-E). In contrast, the other observed differences were, despite statistically significant, unpronounced in magnitude. Overall, there were little apparent SCZ-specific proteomic alterations detected in iPSC. However, a drastic increase in expression and more so in phosphorylation (S15) of p53 is of note at the innate iPSC stage.

Comparison of CTR and SCZ samples at the NPC stage revealed a much larger number of differentially expressed analytes with 33 (24 %) (Appendix 3 – Fig. 4A+B), with 23 proteins/protein variants being up- and only 7 downregulated in SCZ. This is almost triple the amount compared to iPSC, underscoring the greater significance of our findings in NPC, given that they are the more representative cell type due to their neuro-specific lineage. Interestingly, several of the previously discussed differentiation markers (see section 3.3.1.) were among these SCZ-associated de-regulations (Appendix 3 – Fig. 4C). Although differences in absolute expression levels do persist across individual clones (Appendix 3 – Fig. S8), SCZ NPC overall presented with higher levels of the pluripotency marker Oct4 and lower levels of the NPC markers MAP2, NCAM and Sox1 which is generally indicative of a lower grade of differentiation, thus less mature neuronal cells. Similar trends can also be observed in exemplary ICC

images (Appendix 3 – Fig. 1D). In line with this, we performed neurite outgrowth assays and also observed a greater reduction of neurite length in SCZ NPC over time (Appendix 3 – Fig. S9). This demonstrates that the reduced differentiation efficiency of SCZ iPSC into NPC not only manifests as changes in marker expression but also in phenotypic aberrations potentially affecting neurodevelopment in NPC, which have been previously reported in and linked to SCZ.

3.3.3. Aberrant signaling pathway activity as SCZ-relevant proteomic alterations in NPC

The majority (27/33) of analytes showing SCZ-specific differential expression in NPC only did so at this more relevant developmental stage but did not in iPSC (Appendix 3 – Fig. 4D). Four analytes consistently showed alterations in both cell types. These included small changes to CDK4 and ATM and, crucially, strongly increased levels of p53 phosphorylation (S15) and total p53 levels (Appendix 3 – Fig. 4E, Fig. S10A) – with even greater changes in magnitude (20-fold/6-fold in NPC) compared to the iPSC stage. We observed similarly pronounced effects via WB and also confirmed p53 upregulation via ICC (Appendix 3 – Fig. 4F-I).

The 27 SCZ NPC-exclusive de-regulated analytes specifically addressed phosphorylated variants of key signaling proteins, suggesting changes to their direct activation and thus to cellular signaling. Therefore, alterations were evaluated based on their pathway allocation and involvement in cellular functions. For instance, SCZ-derived NPC displayed roughly 2-fold elevated expression of phosphorylated CDK1 (Y15), Cyclin B1, Aurora kinase A and Histone H3 (S10) as well as total CDK1, Aurora kinase B and Cyclin E1 (Appendix 3 – Fig. 5A, Fig. S10B). Notably, all these proteins are involved in regulating the transition from G2 to M phase in the cell cycle. Moreover, several analytes in the DNA-damage response (DDR) cascade were affected, including phosphorylated ATR (S428 and S1989), Chk1 (S296) as well as Histone H2A.X (S139) (Appendix 3 – Fig. 5B), which indicates an implication of DNA damage. DigiWest analysis also revealed coherent alterations to expression and phosphorylation of translation-regulating proteins including eEF2 (T56), eIF2 alpha, S6 RP, eIF4E (S209), total eEF2, eEF2K (S366) and 4E-BP1 (T37/46) (Appendix 3 – Fig. 5C, Fig. S10B). We also identified dysregulations of key Wnt pathway regulators. These included a decrease in non-phosphorylated, active beta-catenin (non-

pS33/41/45), phosphorylated (T197) and total PKA C as well as increases to LEF1 and CK1 alpha levels (Appendix 3 – Fig. 5D, Fig. S10B). Lastly, we were able to identify changes to the MAPK/Erk cascade, as patient-derived cells (SCZ) presented with upregulated phosphorylation of c-Raf (S289/296/301), Erk1 (T202/Y204), Erk2 (T202/Y104) and Rsk1 (T573) (Appendix 3 – Fig. 5E). Overall, as highlighted by DigiWest, the observed protein expression patterns indicate higher translational activity, increased DNA damage and DDR, altered Wnt and MAPK/Erk signaling as well as elevated levels of G2M-phase specific proteins in SCZ-derived NPC in comparison to healthy controls.

3.3.4. G2/M stage-specific changes to cell cycle control in SCZ NPC

Some of the pathways outlined above such as Wnt and MAPK signaling have previously been associated with SCZ and were also shown to be affected in iPSC-based neuronal cell types like NPC. However, an upregulation of cell cycle regulators specific to a particular stage is yet to be reported. First, we confirmed observations on altered cell cycle regulation made with DigiWest (see section 3.3.3.) via ICC staining for G2/M-specific proteins. Again, SCZ NPC, but not iPSC, presented with higher expression of Cyclin B1 and Aurora A (Appendix 3 – Fig. 6A+B). Wanting to investigate this matter further on a phenotypic level, we also performed FACS-based experiments to investigate cell-phase distribution of NPC. Crucially, we found a significantly larger proportion of cells in G2/M phase in patient-derived NPC in comparison to controls, whereas no significant differences were detected for the S and G0/G1 phases (Appendix 3 – Fig. 6C-D, Fig. S9). As a positive control, we also treated cells with Nocodazole, an agent which knowingly arrests cells in the G2/M phase.

3.3.5. Correlation of differentiation markers and G2M-phase proteins with p53

As mentioned (see section 3.3.3.), expression and phosphorylation of p53 was upregulated in SCZ NPC to an even greater extent than SCZ iPSC. Given the drastic nature of this increase, we aimed to further investigate its relevance for and relation to the observed cellular phenotypes of SCZ-derived cells (differentiation efficiency and cell cycle alterations). Thus, we correlated p53 expression and phosphorylation levels (S15) to the affected differentiation markers (Oct4, MAP2, NCAM, Sox1) as well as to

G2/M-regulating proteins by using DigiWest data across all employed clones (Appendix 3 – Fig. S12). Levels of phosphorylated p53 correlated strongly (Spearman´s r = 0.9671) with total p53 levels (Appendix 3 – Fig. 6E), suggesting a dependence of p53 phosphorylation to p53 abundance. Moreover, p53 showed a positive correlation with Oct4 (r = 0.8007) and negative correlations with MAP2 (r = -0.6272), NCAM (r = -0.8289) and Sox1 (r = -0.6763) (Appendix 3 – Fig. 6F); therefore, the observed reduction in differentiation efficiency in diseased cells also appears to be related to p53 (phosphorylation) levels. Finally, we found strong or moderate correlations with Aurora A (r = 0.8958), Cyclin B1 (r = 0.8614) and CDK1 – pY15 (r = 0.5869), respectively (Appendix 3 – Fig. 6G). Overall, based on the proteomic data, we were able to establish a potential link between changes to p53 expression and phosphorylation with phenotypic alterations of SCZ-derived cells, namely hampered differentiation capacity and altered cell-cycle dynamics.

All observations made through DigiWest protein profiling regarding iPSC differentiation and SCZ-specific expression signatures at the respective cell stages are summarized in Figure X.

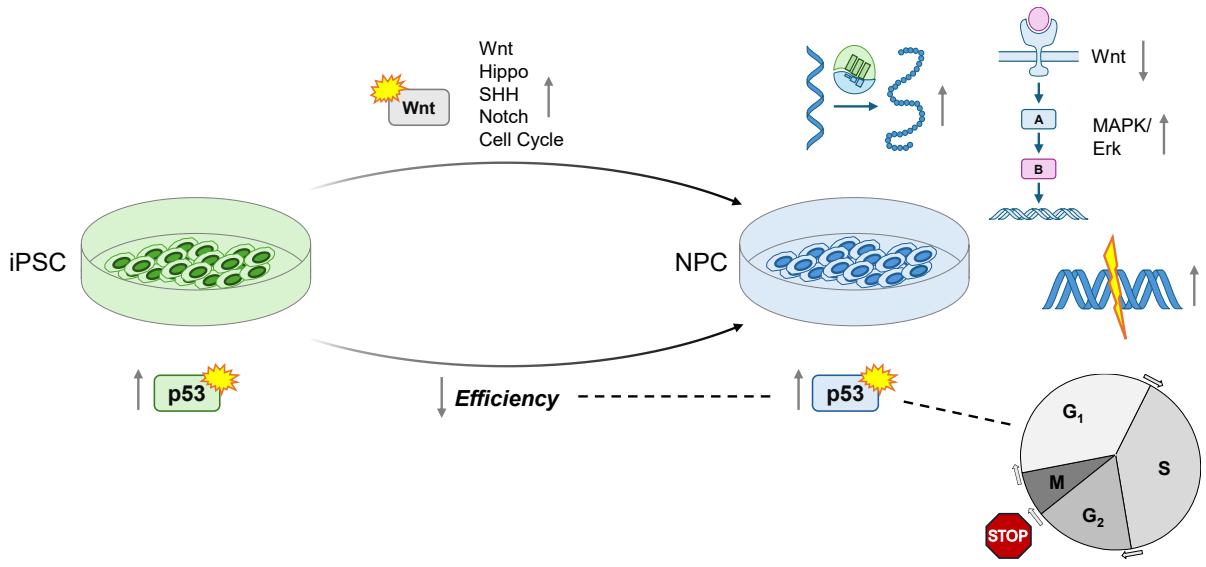

Figure X: Summary of observed differentiation effects and SCZ-specific alterations based on DigiWest data in iPSC-derived neuronal cells. Activation of neurodevelopmental pathways and is observed upon differentiation. SCZ iPSC and NPC present with high levels of p53 and show decreased differentiation efficiency. SCZ NPC are characterized by altered Wnt and MAPK signaling, DDR, and cell cycle control inducing G2/M phase accumulation. SHH = sonic hedgehog.

4. Discussion

Alterations in cellular signal transduction present disease-specific phenotypes and mechanistic drivers in a variety of disorders, while equally holding a high potential for therapeutic intervention. In this thesis, at the example of DigiWest, the suitability of protein-based signaling pathway analysis as an analytical tool for various clinical, basic and personalized research applications was scrutinized. Specifically, DigiWest protein profiling was used to study expression patterns upon TKI treatment in preclinical models of FGFR2-fusion positive iCCA, to identify personalized protein profiles in primary GI tumor tissue and to uncover disease-specific expression signatures in patient-derived iPSC models of SCZ.

4.1. Efficacy evaluation of TKI in clinical cell models of iCCA

After observing clinically meaningful responses of the non-selective TKI Lenvatinib in iCCA patients with tumors harboring FGFR2 rearrangements, we created and characterized patient-analogue cell lines, including one carrying the novel FGFR2-AHCYL2 fusion. We investigated this cell line upon treatment with either selective or non-selective TKI including Lenvatinib. TKI action mechanisms were compared based on cellular signaling analysis (DigiWest), which revealed a similar inhibition profile for the two TKI classes. Analogue evaluations in a cell line additionally carrying the resistance-inducing p.V564F mutation indicated superior effectiveness of Lenvatinib compared to selective TKI and a broader inhibitory effect on signaling proteins, including FGFR2 and mTOR. Finally, we supported our findings with in silico data highlighting a more favorable interaction pattern of Lenvatinib with mutated FGFR2.

4.1.1. Clinical benefit of Lenvatinib and novel FGFR2-AHCYL2 fusion

Here we describe a cohort of seven patients who had received Lenvatinib as their first targeted treatment. The growth modulation index (GMI) serves as a tool for intra-patient treatment comparison. It assumes progression-free intervals in advanced

cancers get shorter with each subsequent treatment and relates the time to progression (TTP) of a respective treatment to the TTP of previous treatments. A GMI > 1.3 is considered clinically meaningful[70,120]. Lenvatinib treatment achieved a GMI > 1.3 in 6/7 patients in comparison to previous treatment regimens and included a patient carrying the novel FGFR2-AHCYL2 fusion. This particular gene fusion has not yet been reported, although a structurally similar one (FGFR2-AHCYL1) has been described[40]. The cell line we newly created carrying the novel fusion gene showed comparable characteristics to other lines with more common alterations (e.g. FGFR2-BICC1), including growth enhancement and activation of related downstream targets (Erk1/2, FRS2, STAT3).

Moreover, in vitro testing of TKI in the patient-analogue cell line (FGFR2-AHCYL2_WT) generally mirrored clinical observations on treatment response. For instance, clinical treatment with the non-selective TKI Nintedanib was unsuccessful; likewise, our matching cell line model proved insensitive to Nintedanib. In contrast, the patient did respond to Lenvatinib and Infigratinib and accordingly, our cell viability assays and IC50 values revealed an increased sensitivity of the FGFR2-AHCYL2_WT line to these two agents. DigiWest cellular signaling analysis revealed similar effects of both TKI classes on receptor phosphorylation and downstream signaling, which was mainly centered around MAPK/Erk signaling, with FGFR-selective TKIs even exclusively inhibiting MAPK-related proteins. This demonstrates a reliance of the FGFR fusion gene on the MAPK/Erk cascade, which has been identified as a necessary and sufficient driver of iCCA[121]. Moreover, mutations in MAPK proteins were shown to induce resistance to FGFR inhibition[122].

Importantly, this patient did not develop resistance mutations under treatment with Lenvatinib (unlike under Infigratinib). However, disease progression still occurred, indicating the involvement of other promoting factors. In line with this, regulatory feedback via the EGFR-PAK1-Erk5 signaling cascade has been hypothesized as a potential resistance mechanism for Lenvatinib in hepatocellular carcinoma[123].

4.1.2. Investigation of resistance mechanisms in cellular models carrying the p.V564F mutation

Our in vitro data demonstrated that Lenvatinib, unlike selective TKI, is still capable of inhibiting growth in cells carrying mutations at the gatekeeper- (V564F) and brake-

(E565A) residues of FGFR2, even at low concentrations. DigiWest analysis of the FGFR2-AHCYL2_WT cell line had indicated a reliance on the FGFR-MAPK/Erk axis and the capability of Lenvatinib to inhibit non-MAPK proteins such as p70S6K, S6 and STAT3. Especially the p.V564F mutation and has been frequently detected in patients developing resistance to selective TKIs such as Infigratinib[124,125]. In the presence of this mutation, DigiWest profiling revealed a persistent ability of Lenvatinib to inhibit FGFR2 phosphorylation. The broader inhibitory profile of Lenvatinib extending beyond the MAPK cascade towards key mTOR proteins (mTOR, Akt, p70S6K, eIF4E) likely contributes to the superior performance of Lenvatinib in this setting. A direct comparison with Infigratinib further highlighted this aspect and points out mTOR as a potential player in the development of treatment resistance. This role of mTOR appeared to be specific to the action of Lenvatinib in the mutated condition, as it was not significantly different between TKI classes in WT cells. In line with this, other groups have suggested combination therapies of FGFR- and mTOR-inhibitors for treatment for resistance-mutated FGFR-fusion CCA[55,126]. We also detected higher baseline FGFR2, MAPK, mTOR and other pathway activity in both treated and untreated p.V564F cells compared to WT. This could possibly be explained by FGFR2 re-activation and/or the simultaneous activation of other tyrosine kinase receptors via feedback mechanisms upon development of this mutation, which itself could be implicated in resistance development of selective TKI. This presents an additional benefit of the unselective nature of Lenvatinib due to its broader inhibition profile. Accordingly, bypass-activation of alternative signaling pathways and enhanced downstream signaling or TKIs sequestration have been proposed as possible explanations for resistance development[127].

Our in silico modeling data suggest that Lenvatinib surpasses selective TKIs in the presence of FGFR2 resistance mutations due to its greater adaptational ability. As the compound carries a terminal cyclopropyl group instead of the larger terminal dimethoxyphenyl group of Infigratinib and Pemigatinib (Figure XI), it exhibits a greater steric flexibility, which supports binding/interaction with mutated FGFR2. This could also help explain the strong resistance capabilities of p.V564F mutated cells towards other TKI. Through the introduction of a large phenyl group in phenylalanine (F), the bulky residue induces steric hindrance preventing drug access to the binding site, which likely mediates resistance to the selective TKIs Infigratinib and Futibatinib[124]. Notably, Futibatinib proved retained inhibitory activity against the p.V564I mutation[128]

but not against p.V564F, likely due to the smaller Isoleucine (I) residue causing less steric hindrance.

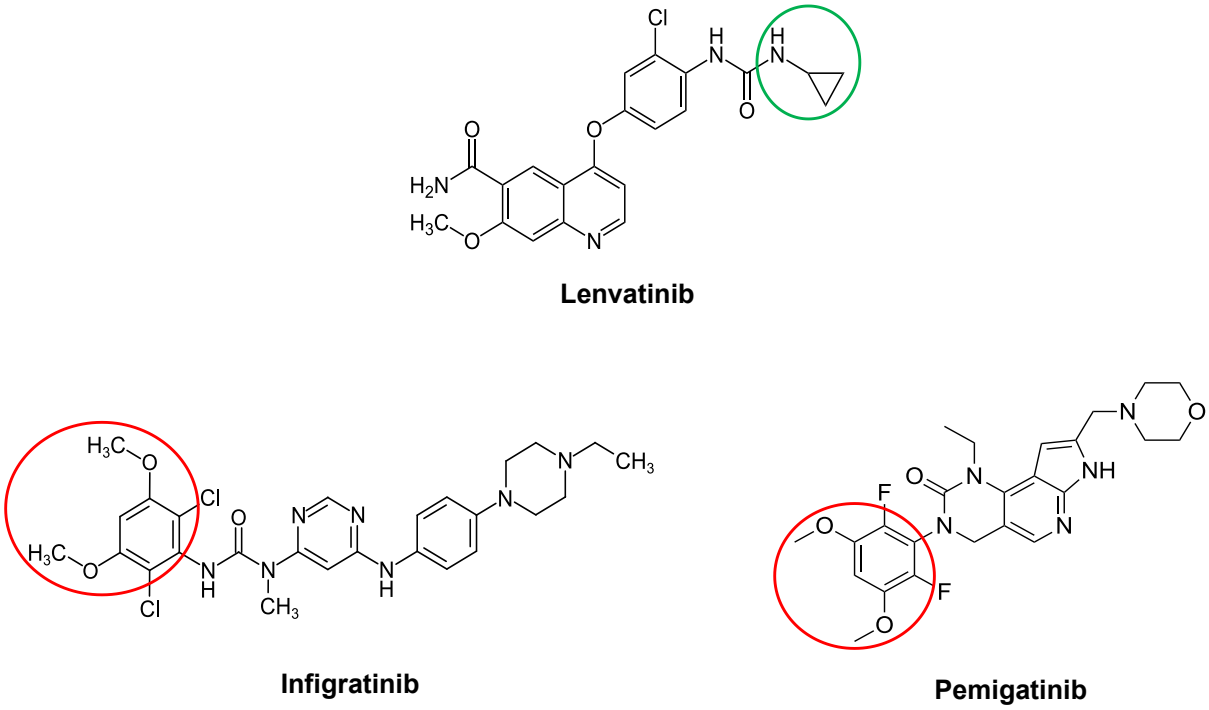

Figure XI: Chemical structures of tested TKIs (adapted from Spahn et al. 2024). The smaller cyclopropyl group of Lenvatinib is indicated in green, the larger dimethoxyphenyl group of Infigratinib and Pemigatinib in red.

4.1.3. Future considerations for Lenvatinib as a therapeutic option in FGFR-fusion positive iCCA

The results have several implications for application of Lenvatinib as a therapeutic option in iCCA and its role in clinical treatment algorithms for patients with FGFR2 fusions/rearrangements/mutations. In an exemplary patient case, we have already demonstrated its suitability, given the clinically meaningful and durable response to Lenvatinib observed in a patient (as of time of publication – February 2024) who previously progressed under treatment with the selective TKI Pemigatinib and presented with a p.N549K resistance mutation. Moreover, side-effects observed under Pemigatinib were no longer present with Lenvatinib, potentially due to its greater selectivity towards FGFR2 versus FGFR1 compared to Pemigatinib or Infigratinib (data not shown). In future, it would be worth investigating treatment responses and adverse

effects of Lenvatinib treatment in more patients carrying various mutations, especially the p.V564F gatekeeper variant. For optimal inclusion into clinical treatment regimens[129], it would be helpful to continuously monitor the possible appearance of point mutations through repeated liquid biopsies under treatment with Lenvatinib or other, selective TKI[130]. Overall, given the broader inhibitory profile on cellular signaling and its increased steric flexibility, Lenvatinib presents a viable treatment option for iCCA, especially in the presence of resistance mutations.

Our data also stimulates future exploratory studies to aim at evaluating action mechanisms and investigate (proteomic) inhibition patterns of other TKI, which are being developed and/or experimentally evaluated for use in iCCA. A recent study demonstrated profound anti-tumor effects of the FGFR-selective inhibitor Tasurgratinib in preclinical models carrying FGFR2 fusion genes[131]. In this study, the novel drug was capable of inhibiting FGFR signaling and also proved potent against several resistance mutations (including N549K), however, not against the bulky V564F residue. A similar recent report[132] has characterized the action of a next-generation, irreversible FGFR-selective inhibitor, KIN3248. Crucially, the authors report a conserved effect in V564F-mutated cells, and also highlight combination treatment with EGFR and MEK inhibitors as beneficial. Analyzing the effects of KIN3248 in presence of the V564F mutation via DigiWest and comparing protein expression profiles to those of Lenvatinib would be of great interest to deepen the understanding of resistance development and how it can be overcome most effectively to advance iCCA therapy and benefit patients.

4.2. Personalized profiling of GI tumors

Here, we employed DigiWest for the characterization of cellular signaling in a retrospective cohort of pancreatic and colorectal carcinomas. Using data relating protein expression signals from primary tumor tissues to those of patient-matched normal tissues, we distinguished samples based on tumor origin and stratified tumors into subgroups within their respective entity based on pathway activity patterns and clinical characteristics. Moreover, we characterized all tumors individually, highlighting unique patient-specific, protein expression signatures. In a direct clinical application, we prospectively profiled tumors from a series of MTB patients. DigiWest analysis revealed personalized protein/pathway activation profiles with drug-targetable alterations, which complemented genetic mutation analysis and eventual treatment recommendation.

4.2.1. Retrospective distinction of pancreatic and colorectal carcinomas via DigiWest

For our retrospective analysis, we selected pancreatic and colorectal carcinomas as representative tumor subtypes for highly invasive and heterogeneous GI tumors with known clinical and molecular-genomic characteristics. Our initial comparison of pancreatic and colorectal tumor tissues (without factoring in non-tumorous tissue as reference), was analogue to previous evaluations of primary patient material using DigiWest and other proteomic methods[133-136]. Using absolute protein expression data, one cannot distinguish whether differential effects between entities were due to tissue origin (e.g. tissue markers) or inherent to the nature of the tumors themselves. By using patient-matched, non-tumorous reference tissue, we were able to provide more precise data, as relative changes in pathway activity and protein expression can be detected instead of mere abundance-indicating values. The inclusion of patient-matched normal tissues also greatly reduced variability within the data set, given the high inter-patient variability inherent to these tumor entities. With this approach, we were able to distinguish pancreatic and colorectal carcinomas largely on expression changes of key tumor-suppressive and oncogenic proteins, as mutations affecting these are frequently implicated in carcinogenesis. Moreover, differences between the entities mirrored the genetic landscape characteristic for the respective tumor type. Among others, TP53 and KRAS were affected in pancreatic carcinomas, whereas PTEN and p27 (CDKN1B)

were altered colorectal carcinomas. As this is in line with a multitude of genetic studies[137-142], it was demonstrated that DigiWest is able to recapitulate distinctions present on the genome level with matching proteomic data.

4.2.2. Proteomic-based subgrouping of pancreatic and colorectal carcinomas

Using this dataset, we also stratified pancreas tumors within their entity, revealing two pathway activity-based subgroupings. Various previous studies have phenotypically stratified pancreatic carcinomas[86,87,143-145]. The molecular characteristics defined by one particular classification[86] – distinguishing among others the squamous and immunogenic subtypes – are in line with those described here. The squamous subtype is defined by frequent alterations of TP53 and changes in autophagy and metabolism regulation. In accordance with this, we observed a strong reduction of p53 levels (mutation/loss) in one subgroup, as well as elevated mTOR signaling, which is a key hub for downstream regulation of several cell functions, including autophagic and metabolism pathways[146,147]. The other subgroup was mainly characterized by high immune cell marker expression and Smad signaling, indicating the presence of tumor-infiltrating lymphocytes (TILs) and activity of immunogenic signaling pathways (e.g. Smad). Accordingly, pancreatic tumors of the immunogenic subtypes are regarded as immune-infiltrated (“hot”).

The molecularly far more heterogenous colorectal carcinoma cohort was stratified based on clinical classifications, i.e. tumor localization and patient age. There is a clear distinction between left- and right-sided colon carcinomas as two subgroups with different molecular profiles, clinical characteristics and treatment responses[83,148]. Our data highlights correlating expression changes between them; for instance, DigiWest data showed a downregulation of EGFR expression in right-sided tumors only. In line with this, treatment regimens do not recommend EGFR-directed first-line therapy for right sided tumors[149].

There is growing clinical concern of increasing incidence of colorectal tumors in younger patients. Comparisons of late- and early onset carcinomas have been conducted on the genetic level[150,151], with only little transcriptomic or proteomic information available[152]. Our data addresses this by highlighting differences related to cell cycle control and mTOR signaling between the two groups.

Overall, we identified tumor subtypes within the respective cohorts based on DigiWest data. These distinctive changes in cellular signaling can be indicators of the different molecular features and treatment responses observed in these clinically relevant subgroups. Future studies should aim to explore and verify these observations in larger patient cohorts using similar methodologies for more expansive insight and to improve treatment strategies for patients within these respective subgroups.

4.2.3. DigiWest protein profiling on the personalized level

Using patient-matched, normal-tissue relative expression data, we were also able to highlight personalized expression signatures for all 20 individual tumors. Doing so, we identified druggable alterations of key signaling proteins, and thus address pathway activity in a personalized fashion. This not only underscores the relevance of the analysis for this approach given the suitability of our antibody panel for generating clinically meaningful data (druggable targets), but also points out the potential of the method for therapeutic use applying individual protein expression data to yield patient benefit. Despite highlighting unique protein expression signatures (e.g. distinctive tissue markers in the MSI-high and hepatoid carcinoma samples), we were able to identify similar patterns across groups of tumors (see section 3.2.3.). For instance, we were able to decipher infiltrated (“hot”) from non-infiltrated (“cold”) tumors independent of entity, analogue to results reported in a previous DigiWest study[134]. This enabled the attribution of individual tumors into specific functional groups with implications for selective treatment. In these cases, immunotherapeutic approaches likely present an (additional) viable treatment option. Overall, this demonstrates that DigiWest is capable of providing treatment-relevant data on an individualized level in tumors with a highly heterogeneous clinical and molecular-genomic presentation. Moreover, only 15 µg of protein (equivalent of a single tissue section) are required for analysis; usually, this amount is easily obtained in clinical routine from tumorous as well as non-tumorous adjacent tissue or through individual needle biopsies.

4.2.4. Clinical application of personalized DigiWest profiling in a precision oncology setting

Our retrospective analysis demonstrated that DigiWest has the potential for a clinical application on a personalized level. Thus, we explored its use in a prospective, proof-of concept study analyzing single needle biopsies from MTB patients with various GI tumors. For clinical practice surrounding precision oncology programs such as MTB, there is still heavy reliance on genetic data and the meaningfulness of mutation analyses. In light of this, we evaluated DigiWest methodologically as a source of additional information to examine its applicability for use in confirmatory fashion to other data available to the MTB, most importantly sequencing analysis, histological staining and treatment history. DigiWest data on protein activity and expression is useful as complementary to genetic alterations, because it allows to distinguish pathologically active (“true”) driver mutations which have manifested on the protein level, from the many merely potential tumor-driving alterations identified through genetic sequencing. Despite high heterogeneity within the patient cohort (mix of entities, heavily pre-treated patients) and no external reference tissue (unlike in the retrospective study, see previous sections), we were able to identify altered pathway activity in 12/14 individual cases. In 8/12 applicable cases, our data showed coherent overlap with key genetic mutations, as for instance shown in the two example cases described in section 3.2.4. In other examples KRAS or TP53 mutations inferred elevated MAPK and cell cycle activity, ultimately leading to the recommendation of KRAS/MEK- and CDK4/6- directed therapies, respectively. Thus, in this context, the accurate detection of changes in activity (phosphorylation) of druggable proteins in a key strength of DigiWest. Importantly, DigiWest should not be regarded as a sole measure for treatment decision but should be regarded as an additional tool in unison with other analyses. These could be subsequently employed for validation, for instance (further) histological analyses to confirm activation of targets identified by DigiWest.

In a similar study[153], the reverse-phase protein array technology was employed to analyze expression of 27 proteins in MTB patients to retrospectively evaluate proteomic-based treatment options and to compare these to previously made genetics-based treatment recommendations. The authors noted an inconsistent overlap (10-57 %) between the respective recommendations. Yet, they underscored the suitability for and importance of integrating proteomics into precision oncology practice. Notably,

using DigiWest we achieved a greater overlap (67 %) while generating higher-throughput data covering more relevant analytes/pathways (e.g. immune cell markers).

In two cases where no overlap between gene and protein data was detected, we were unable to identify any coherently activated pathway via DigiWest. This might be due to a comparatively high percentage of non-tumorous cells (e.g. stroma) in the obtained sample (needle biopsy). This issue was further complicated by a lack of suitable reference, as in this part of the study, antigen-specific signals were only compared to other tumors within the cohort using absolute expression values. Having non-tumorous patient-matched tissue available would have been greatly advantageous as shown in the retrospective part of the study (see section 4.2.1.). However, this was not possible for the prospective cohort, as needle biopsies for adjacent tissues are not routinely performed for MTB presentation. In future, data quality and meaningfulness could be improved significantly by obtaining patient-matched reference tissue in each case. Given the extremely low amount of material required for DigiWest, this is feasible and could easily be integrated into standard MTB procedures.

Given that our study followed an exploratory proof-of concept approach, we only included a small number of patients, who had presented to the MTB over a period of 11 months. The approach exemplarily demonstrated here should in future be expanded to a larger patient cohort to verify its application potential for routine clinical use. Moreover, treatment effectiveness of DigiWest-based treatment recommendations would have to be evaluated in comparison to other recommendations (genomic, transcriptomic, MS) in a large-scale clinical study.

In summary, both our retrospective study and the transfer into a prospective clinical case series demonstrated applicability, suitability and potential for integration of DigiWest into clinical algorithms/practice for PM approaches. Especially if patient-matched normal tissues can be obtained, personalized DigiWest activity profiles incorporate vital complementary information to serve as an additional tool in the hands of oncologists in a clinical PM setting to help make better, individually tailored treatment decisions to improve success and benefit patients.

4.3. Uncovering of disease mechanisms in Schizophrenia

Employing DigiWest in a targeted proteomics approach, we analyzed cellular signal transduction in iPSC-derived neuronal cells in order to identify SCZ-related expression signatures and investigate alterations occurring during early neurodevelopment. Furthermore, we highlighted changes to developmental pathways in patient-derived cells and demonstrate impaired differentiation capabilities on the protein level and in phenotypic assays. The detected disease-related aberrations were NPC-stage specific and affected among others cell cycle control and DNA damage response. Finally, we were able to link these aspects quantitatively to p53 expression and phosphorylation.

4.3.1. Monitoring of iPSC differentiation into NPC via DigiWest

Given the composition of the employed antibody panel, we were able to measure expression and modification of key signaling proteins from pathways implicated in neuronal development (e.g. Wnt[154], Hippo[155], Hedgehog[156]). This gives an indication of the status of developmental process and also could be regarded as an indicator of “differentiation efficiency”, in this case being indicative of the condition of the resulting differentiated cells (NPCs). Usually, differentiation is monitored using only select pluripotency and (neuronal) differentiation markers which are commonly assessed via ICC[157]. Our data shows that DigiWest analysis can not only recapitulate marker expression with identical trends and sensitivity to ICC but can also provide information and monitor changes on a broader pathway level. This tracking ability allows the method to serve as an extensive quality control analysis; not only for neuronal differentiation but for iPSC and iPSC-derived systems in general, which would present an additional, novel application for DigiWest.

Other studies have previously related phenotypic changes such as decreased differentiation capacity[158,159] and reduced neurite outgrowth to SCZ[110,113]. In our patient-derived models, we were able to recapitulate these phenotypes as indicated by altered marker expression (DigiWest and ICC) and outgrowth assays. Furthermore, we could identify changes in pathway activity (Wnt, MAPK, cell cycle) of SCZ-derived cells during differentiation into NPC. Thus, with DigiWest we expanded on these shortcomings by highlighting potential underlying changes in pathway activity which are not necessarily visible through the assessment of marker proteins alone.

4.3.2. DNA damage response and cell cycle regulation in SCZ

Among the most consistent disease-specific effects uncovered by DigiWest on the NPC level were changes to DDR protein expression and alterations in cell-cycle dynamics, specifically affecting G2/M transition.

Our proteomic data confirmed previously made associations of DNA damage and DDR with the disease[160,161]. For instance, one particular postmortem study using transcriptomic analysis reported increase of DDR in SCZ patients[162]. Several other reports have linked mitochondrial dysfunction[163] and the generation of reactive oxygen species (ROS)[113,164,165] to SCZ in stem cell-derived systems, which are both indicators of DNA damage.

Additionally, (de-)regulation of the cell cycle has been shown to be relevant for neuronal development [166] and has been implicated in SCZ[163,167,168]. However, no indications have been made about a specific cell phase, let alone G2/M, which is considered the central DNA damage-related checkpoint. With our DigiWest data we do not only provide further evidence for cell cycle and DNA damage implications in SCZ but also focus the attention on G2/M transition, which could serve as a starting point for future studies seeking validation in larger patient cohorts.

4.3.3. Uncovering new implications of p53 in SCZ

Using DigiWest data, we have demonstrated an association of p53 expression and phosphorylation levels with SCZ in iPSC and more prevalently in NPC. p53 (TP53) is most commonly associated with tumorigenesis and holds a tumor-suppressive function due to coordinating responses of cell proliferation apoptosis and DNA repair. p53 has also been associated with a variety of CNS diseases including SCZ such as Parkinson´s disease, Alzheimer´s disease or epilepsy as well as with neuronal development[169,170], but the direct implication in SCZ remains unclear. However, it is considered a susceptibility risk gene in SCZ[171] and has been associated with SCZ previously[169,172]. Also, a negative correlation of SCZ and cancer has been reported in several studies[173,174] further underscores an involvement of p53 in SCZ, given its tumor suppressive function. Finally, p53 has been shown to be implicated in stem cell development[175], as upregulation of p53 due to genotoxic stress can lead to unspecific, unwanted differentiation. Crucially, we observed notable disease-relevant changes on

both the iPSC and NPC level only for p53 expression and phosphorylation (among all detected analytes). This further underscores the notion of p53 potentially occupying a special role in the developmental process of developing (SCZ) cells.

We were able to quantitatively correlate p53 expression with the observed phenotypes of altered cell cycle dynamics and reduced differentiation. Thus, we for the first time provide a link between these aspects based on proteomic data, which have all individually been shown to be implicated in SCZ but have not yet previously been linked mechanistically. This allowed us to formulate a hypothesis of a potential delay in cell cycle progression of developing neuronal cells due to the acquisition of damage and subsequent p53 upregulation. A setting which results in less mature cells is likely responsible for the decreased differentiation phenotype and neurodevelopmental failure observed in SCZ. To confirm our observations, future studies should thrive to instigate these results in larger patient cohorts.

4.3.4. DigiWest as an application in SCZ research

Here, DigiWest is presented as an application in a field with little proteomic-based knowledge, as most studies in SCZ and other psychiatric research fields have been performed on the genetic and/or transcriptomic levels, leaving an incomplete picture of mechanisms surrounding disease onset with regards to proteomics and specifically cellular signaling.

Previous studies investigating the proteome in SCZ have mainly been based on MS and followed a non-targeted (shotgun) approach[176-178]. Therefore, such studies have mainly focused on the implication of entire pathways, leaving more in-depth regulatory alterations to individual or groups of proteins within a cascade unaddressed. Hence, the DigiWest antibody panel which was developed for this study was partially based and expanded upon this previous knowledge. In this study, we have confirmed what has been demonstrated via other omics approaches, such as implications of Wnt, MAPK/Erk signaling and protein synthesis. With DigiWest being a targeted approach, we were able to focus on uncovering mechanistic changes in greater detail and selecting antibodies accordingly. The detection of several phosphorylated protein variants incorporated an additional layer of information; with the advantage of more accurate insight into activation of key regulatory proteins to infer superiorly accurate disease-related pathway activity changes. For instance, we have deepened the

understanding of the role cell cycle control, DDR, differentiation efficiency in SCZ by demonstrating altered regulation affecting a specific cell cycle phase (G2/M) while also have underscoring it with phenotypic FACS analysis.

Overall, we have proven the potential of DigiWest for the characterization and disease-specific evaluation of iPSC-based model systems in SCZ for other psychiatric diseases. Our data expands the existing knowledge by deepening the understanding mechanistic insight into disease mechanisms of SCZ. Crucially, our patho-mechanistic findings are also helpful in the search for potential drug targets[179]. Especially if our findings can be replicated in future studies using larger patient cohort and/or employing more complex model systems (e.g. brain organoids, organ-on chip), they could accelerate the formulation and development of urgently needed novel treatment options to ultimately benefit patients.

4.4. Methodological implications of DigiWest

This thesis has outlined the suitability and applicability of DigiWest protein profiling for a variety of research settings as well as in a clinical context. Despite still possessing developmental potential from a methodological standpoint, DigiWest holds several key advantages in comparison to other proteomic methods available. Its broad application potential elevates it to an especially fitting, sensible-to-use analytics tool to use including and beyond the applications discussed here.

Foremost, the possibility to accurately measure PTMs, specifically phosphorylation, presents a major advantage of DigiWest over alternative proteomic methods, most notably MS, without compromising data quality. Despite being notably different methods, we have demonstrated good comparability of DigiWest and MS in a recent publication[180]. Phosphorylation can be difficult to accurately detect via MS; even if, the large number of phosphorylation sites detected equally transmits to a large number of non-relevant phosphorylation events being analyzed. As mentioned previously, the additional layer of information gained by PTM analysis is vital for clinical applications and drug testing. Through this, DigiWest yields more accurate, meaningful data and elevates itself from transcriptomic and genomic techniques, especially for treatment-related approaches aiming at clinical benefit.

As mentioned before (section 1.4.), the capacity for automation is inherent to the method by its setup and would in theory allow for high sample throughput. If streamlined with regards to time and throughput, DigiWest data can be provided within 5 days of sample collection, which is highly advantageous in a diagnostic or therapeutic setting. This would make analyzing MTB patient material or the testing of drug effectiveness faster than most sequencing analyses (2 weeks). Currently, the amount of hands-on work required presents a bottleneck. Especially the handling and cutting of WB membrane fractions is challenging to automate. Despite the procedure being technically demanding and requiring training, its similarity to WB is helpful as materials for and knowledge of this standard method are present in most research and clinical laboratories aiding fast implementation into clinical routine. In its current form, DigiWest relies on a specific flow cytometer for readout (Luminex), which is not considered a conventional instrument. However, despite considerable costs for beads and antibodies, implementation would not be more expensive than a standard MS

instrument. Also, costs for individual DigiWest analytes are in a similar range compared to MS.

The advancement of high throughput analysis goes hand in hand with a reduction in required sample amount, which presents a major advantage of DigiWest compared to other proteomic methods including MS and reverse-phase protein arrays. This is especially crucial when analyzing precious, irretrievable samples such as clinical patient material or pure immune-cell cultures (e.g. macrophages) as well as samples which are cumbersome and/or expensive to produce (e.g. differentiated iPSC, neurons, CAR-T cells). Accordingly, we showed that the protein amount obtained from the equivalent of a single tissue section or needle biopsy is sufficient for clinical analysis (see section 4.2.3.). Further improvements to reduce the sample amount required per analyte can be made by transferring the DigiWest assay to the novel Luminex INTELLIFLEX system. It encompasses a second reporter channel to allow concomitant detection of two analytes on the surface of the same bead (e.g. parent protein and its phosphorylated variant or two entirely different antigens). Ultimately, this could cut sample consumption in half, thus doubling throughput and analyte number making DigiWest even more appealing for use in any setting. Especially for clinical use greater proteome coverage would also enhance the overlap with usually much larger genetic panels to be run on the same patient in personalized fashion. In DigiWest, signal generation relies on interaction of the antigen with antibodies and the similarity to standard WB grants use of any commercially available WB antibodies possible. Despite the potential of lot-to-lot variations or poorly performing (cross-reacting) antibodies, this allows extraordinary flexibility, as any targets and protein modifications for which antibodies are commercially available can be included. One can adapt the analyte panel to the research question at hand; for instance, in a clinical setting, the panel can be fine-tuned to fit a specific tumor entity or be aligned with a list of available drugs to investigate activity surrounding relevant targets. Additionally, as demonstrated here in our study on SCZ (see section 4.3.4), one can customize analyte selection building on previous molecular studies (e.g. MS shotgun proteomics) to focus on the parts of the proteome most relevant to the question at hand (targeted proteomics). Most importantly, using a targeted approach greatly reduces complexity and eases data interpretation as one is not encountering what has been referred to as a data “tsunami”[181].

The large dynamic range of DigiWest allows detection of both high and low-abundance proteins, accurately representing the range observed in a common cell lysate. However, sensitivity of the system partially remains as a limitation. As mentioned, it is less sensitive compared ELISA or SIMOA. Certain analytes can fall short of the detection limit including select transcription factors, low-abundance protein modifications or frequently catalyzed products. Thus, further improvements to sensitivity (e.g. by reducing assay background) would enable even more widespread analysis.

One further aspect that needs to be considered is that observations on cellular signaling represent the status of the system at the time of sampling (“snapshot”), thus not fully capturing the dynamic nature of the proteome over time. However, the overarching picture of pathway activity (and thus the respective DigiWest signals) is consistent over time, especially in scenarios where addiction to certain pathways (e.g. FGFR2-MAPK/Erk axis) or the manifestation of genetic (constant) mutations (e.g. TP53 loss) is considered. Finally, DigiWest signals are representative of the average expression of a given analyte across the entire sample, as all cells (including different cell types such as immune and tumor cells) become “mixed”. This loss of spatial resolution is also inherent to MS or standard WB and presents an advantage of histological methods, which however are at a crucial disadvantage given their comparatively low throughput.

5. Outlook

General implications of this thesis for future applications

In this work, DigiWest was demonstrated to be a suitable and applicable tool for three different research questions. The discussed studies on FGFR2 and GI tumor profiling were centered around signaling pathway activity in cancer and its interplay with treatment-relevant protein-targeting drugs. In both these studies, the results obtained have direct clinical relevance since the material used was either primary patient material or a cellular patient-analogue cellular model. Moreover, the direct clinical applicability was clearly demonstrated.

Here, a clinical observation (Lenvatinib) was exemplarily underscored via DigiWest (bedside to bench). In future, DigiWest could be employed to mechanistically support bedside observations on treatment response for clinical re-application. This would entail the extensive comparative testing of available drugs to anticipate drug response, evaluate risk of resistance, or recommend novel therapeutic approaches (e.g. combination therapies) to predict treatment success. Moreover, novel therapeutic approaches such as RNA interference where small interference (si)-RNAs bind to mRNAs to induce translational repression of (pathogenic) proteins[182,183], could be explored. Here, DigiWest would not only monitor the effect of RNA treatment on the target protein (silencing) but also detect subsequent effects on downstream signaling regulators. Drug testing approaches using DigiWest could be extended from simple cellular patient models to more complex, 3D-organoid[184-186] and/or organ-on chip systems, which have been frequently used to recapitulate patient phenotypes and physiology in various cancer types[187-190].

Furthermore, DigiWest was for the first time applied on a personalized, individual patient level and data was directly contributory to patient treatment (bench to bedside). Integration into clinical practice in the context of precision medicine is feasible and sensible (e.g. see sections 4.2.4., 4.4.) and if more extensive validation (greater patient numbers, normal tissue as reference) is achieved it could be established as a standard methodology employed by MTBs. It is worth noting that the information gained should be viewed in unison (and comparison) to genetic, transcriptomic and histological analyses to broaden individual tumor characterization in a targeted manner. In future,

overlap with other omics data (especially genetic sequencing) could be performed using bioinformatics or artificial intelligence algorithms. Especially given the rising cancer rates in the population, combining these with an automated, higher-sample throughput version of DigiWest would leave clinical decision-making in the hands of the oncologists but enable them to evaluate more cases in the same timeframe without compromising treatment quality.

The study on SCZ disease mechanisms demonstrates the applicability of DigiWest in basic research to help understand complex diseases. As this was the first time it was employed in an iPSC-based system, we also demonstrate the suitability of DigiWest in the analysis, testing and quality control of iPSC and differentiated cells. In comparison to oncology, knowledge on SCZ pathology is “one step behind” as efficient causal treatments are yet to be established. Here, the translation to drug studies and testing of the observations made (e.g. p53 knockdown, cell cycle disruption) will be key. Again, translating our findings into further differentiated cells, i.e. iPSC-derived neurons and more complex 3D systems such as brain organoids[191,192] would be another logical step. Finally, a transition into more complex and accurate disease models should also incorporate DigiWest into the analysis of organ-on chip technologies, which are more accurate pathology models for a variety of diseases, including neurological disorders[193-195].

6. Conclusion

All in all, this thesis investigated the suitability and application potential of DigiWest as a method in clinical, and basic research as well as personalized medicine. Its status as an innovative tool for extensive proteomic analysis across various domains of biomedical research and clinical practice was highlighted comprehensively. Its inherent high-throughput nature combined with the specificity of Western Blotting enables accurate investigation of signaling proteins and their activation states facilitating a deeper understanding of molecular drug action patterns, tumor-driving events and respective treatment responses as well as general disease mechanisms. DigiWest demonstrates outstanding adaptability to personalized medicine, as it allows accurate patient-specific tumor profiling enhancing patient stratification along with individually tailored treatment decision-making, which could heavily benefit the advancement of this method in the field of clinical precision oncology. Furthermore, its application in basic research, here in studying schizophrenia using iPSC-based model systems, not only revealed novel critical insights into disease-specific alterations on a mechanistic level but also underscored the importance of proteomic analysis in psychiatric research.

There is an urgent need for a continued advancement of proteomic analysis into clinical routine and clinically applied research to further enhance treatment decision making. DigiWest stands out as a pivotal tool to serve as a transition platform between laboratory research and patient care, also when regarded as complementary to other proteomic approaches and genetics. This thesis specifically calls for the integration of this unique method into precision oncology programs, routine drug testing approaches and disease mechanism studies, to ultimately lead the way towards more effective therapeutic strategies as well as more precise and impactful biomedical, translational research.

References

1 Keenan, S. E. & Shvartsman, S. Y. Mechanisms and causality in molecular diseases. *Hist Philos Life Sci* **39**, 35, doi:10.1007/s40656-017-0162-1 (2017).

2 Brittain, H. K., Scott, R. & Thomas, E. The rise of the genome and personalised medicine. *Clin Med (Lond)* **17**, 545-551, doi:10.7861/clinmedicine.17-6-545 (2017).

3 Duarte, T. T. & Spencer, C. T. Personalized Proteomics: The Future of Precision Medicine. *Proteomes* **4**, doi:10.3390/proteomes4040029 (2016).

4 Jia, X. *et al.* Protein translation: biological processes and therapeutic strategies for human diseases. *Signal Transduct Target Ther* **9**, 44, doi:10.1038/s41392-024-01749-9 (2024).

5 Jordan, J. D., Landau, E. M. & Iyengar, R. Signaling networks: the origins of cellular multitasking. *Cell* **103**, 193-200, doi:10.1016/s0092-8674(00)00112-4 (2000).

6 Casado, P., Hijazi, M., Gerdes, H. & Cutillas, P. R. Implementation of Clinical Phosphoproteomics and Proteomics for Personalized Medicine. *Methods Mol Biol* **2420**, 87-106, doi:10.1007/978-1-0716-1936-0_8 (2022).

7 Yip, H. Y. K. & Papa, A. Signaling Pathways in Cancer: Therapeutic Targets, Combinatorial Treatments, and New Developments. *Cells* **10**, doi:10.3390/cells10030659 (2021).

8 Denny, J. C. & Collins, F. S. Precision medicine in 2030-seven ways to transform healthcare. *Cell* **184**, 1415-1419, doi:10.1016/j.cell.2021.01.015 (2021).

9 Stenzinger, A. *et al.* Implementation of precision medicine in healthcare-A European perspective. *J Intern Med* **294**, 437-454, doi:10.1111/joim.13698 (2023).

10 Zilocchi, M., Wang, C., Babu, M. & Li, J. A panoramic view of proteomics and multiomics in precision health. *iScience* **24**, 102925, doi:10.1016/j.isci.2021.102925 (2021).

11 Babu, M. & Snyder, M. Multi-Omics Profiling for Health. *Mol Cell Proteomics* **22**, 100561, doi:10.1016/j.mcpro.2023.100561 (2023).

12 Zhao, J., Feng, Q. & Wei, W. Q. Integration of Omics and Phenotypic Data for Precision Medicine. *Methods Mol Biol* **2486**, 19-35, doi:10.1007/978-1-0716-2265-0_2 (2022).

13 Chen, C. *et al.* Applications of multi-omics analysis in human diseases. *MedComm (2020)* **4**, e315, doi:10.1002/mco2.315 (2023).

14 Kowalczyk, T., Ciborowski, M., Kisluk, J., Kretowski, A. & Barbas, C. Mass spectrometry based proteomics and metabolomics in personalized oncology. *Biochim Biophys Acta Mol Basis Dis* **1866**, 165690, doi:10.1016/j.bbadis.2020.165690 (2020).

15 Missios, P., Beha, J., Bitzer, M. & Malek, N. P. [The molecular tumor board]. *Chirurg* **92**, 1011-1015, doi:10.1007/s00104-021-01487-6 (2021).

16 Stenzinger, A. *et al.* Trailblazing precision medicine in Europe: A joint view by Genomic Medicine Sweden and the Centers for Personalized Medicine, ZPM, in Germany. *Semin Cancer Biol* **84**, 242-254, doi:10.1016/j.semcancer.2021.05.026 (2022).

17 Zhang, S. *et al.* Tumor initiation and early tumorigenesis: molecular mechanisms and interventional targets. *Signal Transduct Target Ther* **9**, 149, doi:10.1038/s41392-024-01848-7 (2024).

18 Backwell, L. & Marsh, J. A. Diverse Molecular Mechanisms Underlying Pathogenic Protein Mutations: Beyond the Loss-of-Function Paradigm. *Annu Rev Genomics Hum Genet* **23**, 475-498, doi:10.1146/annurev-genom-111221-103208 (2022).

19 Riedl, J. M. *et al.* Molecular diagnostics tailoring personalized cancer therapy-an oncologist's view. *Virchows Arch* **484**, 169-179, doi:10.1007/s00428-023-03702-7 (2024).

20 Su, M. *et al.* Proteomics, Personalized Medicine and Cancer. *Cancers (Basel)* **13**, doi:10.3390/cancers13112512 (2021).

21 Konstantinou, G. N. Enzyme-Linked Immunosorbent Assay (ELISA). *Methods Mol Biol* **1592**, 79-94, doi:10.1007/978-1-4939-6925-8_7 (2017).

22 Hayrapetyan, H., Tran, T., Tellez-Corrales, E. & Madiraju, C. Enzyme-Linked Immunosorbent Assay: Types and Applications. *Methods Mol Biol* **2612**, 1-17, doi:10.1007/978-1-0716-2903-1_1 (2023).

23 Lertkhachonsuk, A. A. *et al.* Serum CA19-9, CA-125 and CEA as tumor markers for mucinous ovarian tumors. *J Obstet Gynaecol Res* **46**, 2287-2291, doi:10.1111/jog.14427 (2020).

24 Macklin, A., Khan, S. & Kislinger, T. Recent advances in mass spectrometry based clinical proteomics: applications to cancer research. *Clin Proteomics* **17**, 17, doi:10.1186/s12014-020-09283-w (2020).

25 Birhanu, A. G. Mass spectrometry-based proteomics as an emerging tool in clinical laboratories. *Clin Proteomics* **20**, 32, doi:10.1186/s12014-023-09424-x (2023).
26 Pillai-Kastoori, L., Schutz-Geschwender, A. R. & Harford, J. A. A systematic approach to quantitative Western blot analysis. *Anal Biochem* **593**, 113608, doi:10.1016/j.ab.2020.113608 (2020).
27 Owen, C., Fader, K. A. & Hassanein, M. Western blotting: evolution of an old analytical method to a new quantitative tool for biomarker measurements. *Bioanalysis* **16**, 319-328, doi:10.4155/bio-2023-0212 (2024).
28 Harris, V. M. Protein detection by Simple Western analysis. *Methods Mol Biol* **1312**, 465-468, doi:10.1007/978-1-4939-2694-7_47 (2015).
29 Ramos-Vara, J. A. Principles and Methods of Immunohistochemistry. *Methods Mol Biol* **1641**, 115-128, doi:10.1007/978-1-4939-7172-5_5 (2017).
30 Magaki, S., Hojat, S. A., Wei, B., So, A. & Yong, W. H. An Introduction to the Performance of Immunohistochemistry. *Methods Mol Biol* **1897**, 289-298, doi:10.1007/978-1-4939-8935-5_25 (2019).
31 Gerdes, M. J. *et al.* Highly multiplexed single-cell analysis of formalin-fixed, paraffin-embedded cancer tissue. *Proc Natl Acad Sci U S A* **110**, 11982-11987, doi:10.1073/pnas.1300136110 (2013).
32 Tan, W. C. C. *et al.* Overview of multiplex immunohistochemistry/immunofluorescence techniques in the era of cancer immunotherapy. *Cancer Commun (Lond)* **40**, 135-153, doi:10.1002/cac2.12023 (2020).
33 Treindl, F. *et al.* A bead-based western for high-throughput cellular signal transduction analyses. *Nat Commun* **7**, 12852, doi:10.1038/ncomms12852 (2016).
34 Pottier, C. *et al.* Tyrosine Kinase Inhibitors in Cancer: Breakthrough and Challenges of Targeted Therapy. *Cancers (Basel)* **12**, doi:10.3390/cancers12030731 (2020).
35 Brindley, P. J. *et al.* Cholangiocarcinoma. *Nat Rev Dis Primers* **7**, 65, doi:10.1038/s41572-021-00300-2 (2021).
36 Elvevi, A. *et al.* Clinical treatment of cholangiocarcinoma: an updated comprehensive review. *Ann Hepatol* **27**, 100737, doi:10.1016/j.aohep.2022.100737 (2022).
37 Saborowski, A., Lehmann, U. & Vogel, A. FGFR inhibitors in cholangiocarcinoma: what's now and what's next? *Ther Adv Med Oncol* **12**, 1758835920953293, doi:10.1177/1758835920953293 (2020).
38 Neumann, O. *et al.* Genomic architecture of FGFR2 fusions in cholangiocarcinoma and its implication for molecular testing. *Br J Cancer* **127**, 1540-1549, doi:10.1038/s41416-022-01908-1 (2022).
39 Brandi, G. *et al.* Activated FGFR2 signalling as a biomarker for selection of intrahepatic cholangiocarcinoma patients candidate to FGFR targeted therapies. *Sci Rep* **14**, 3136, doi:10.1038/s41598-024-52991-8 (2024).
40 Arai, Y. *et al.* Fibroblast growth factor receptor 2 tyrosine kinase fusions define a unique molecular subtype of cholangiocarcinoma. *Hepatology* **59**, 1427-1434, doi:10.1002/hep.26890 (2014).
41 Xie, Y. *et al.* FGF/FGFR signaling in health and disease. *Signal Transduct Target Ther* **5**, 181, doi:10.1038/s41392-020-00222-7 (2020).
42 Bitzer, M. *et al.* Targeting extracellular and juxtamembrane FGFR2 mutations in chemotherapy-refractory cholangiocarcinoma. *NPJ Precis Oncol* **5**, 80, doi:10.1038/s41698-021-00220-0 (2021).
43 Zugman, M., Botrus, G., Pestana, R. C. & Uson Junior, P. L. S. Precision Medicine Targeting FGFR2 Genomic Alterations in Advanced Cholangiocarcinoma: Current State and Future Perspectives. *Front Oncol* **12**, 860453, doi:10.3389/fonc.2022.860453 (2022).
44 Pacini, L., Jenks, A. D., Lima, N. C. & Huang, P. H. Targeting the Fibroblast Growth Factor Receptor (FGFR) Family in Lung Cancer. *Cells* **10**, doi:10.3390/cells10051154 (2021).
45 Katoh, M. Fibroblast growth factor receptors as treatment targets in clinical oncology. *Nat Rev Clin Oncol* **16**, 105-122, doi:10.1038/s41571-018-0115-y (2019).
46 Javle, M. *et al.* Infigratinib (BGJ398) in previously treated patients with advanced or metastatic cholangiocarcinoma with FGFR2 fusions or rearrangements: mature results from a multicentre, open-label, single-arm, phase 2 study. *Lancet Gastroenterol Hepatol* **6**, 803-815, doi:10.1016/S2468-1253(21)00196-5 (2021).
47 Abou-Alfa, G. K. *et al.* Pemigatinib for previously treated, locally advanced or metastatic cholangiocarcinoma: a multicentre, open-label, phase 2 study. *Lancet Oncol* **21**, 671-684, doi:10.1016/S1470-2045(20)30109-1 (2020).

48 Goyal, L. *et al.* Futibatinib for FGFR2-Rearranged Intrahepatic Cholangiocarcinoma. *N Engl J Med* **388**, 228-239, doi:10.1056/NEJMoa2206834 (2023).
49 Parisi, A. *et al.* Pemigatinib for patients with previously treated, locally advanced or metastatic cholangiocarcinoma harboring FGFR2 fusions or rearrangements: A joint analysis of the French PEMI-BIL and Italian PEMI-REAL cohort studies. *Eur J Cancer* **200**, 113587, doi:10.1016/j.ejca.2024.113587 (2024).
50 Yamashita, T. *et al.* REFLECT-a phase 3 trial comparing efficacy and safety of lenvatinib to sorafenib for the treatment of unresectable hepatocellular carcinoma: an analysis of Japanese subset. *J Gastroenterol* **55**, 113-122, doi:10.1007/s00535-019-01642-1 (2020).
51 Choueiri, T. K. *et al.* Lenvatinib plus pembrolizumab versus sunitinib as first-line treatment of patients with advanced renal cell carcinoma (CLEAR): extended follow-up from the phase 3, randomised, open-label study. *Lancet Oncol* **24**, 228-238, doi:10.1016/S1470-2045(23)00049-9 (2023).
52 King, G. & Javle, M. FGFR Inhibitors: Clinical Activity and Development in the Treatment of Cholangiocarcinoma. *Curr Oncol Rep* **23**, 108, doi:10.1007/s11912-021-01100-3 (2021).
53 Mahipal, A., Tella, S. H., Kommalapati, A., Yu, J. & Kim, R. Prevention and treatment of FGFR inhibitor-associated toxicities. *Crit Rev Oncol Hematol* **155**, 103091, doi:10.1016/j.critrevonc.2020.103091 (2020).
54 Silverman, I. M. *et al.* Clinicogenomic Analysis of FGFR2-Rearranged Cholangiocarcinoma Identifies Correlates of Response and Mechanisms of Resistance to Pemigatinib. *Cancer Discov* **11**, 326-339, doi:10.1158/2159-8290.CD-20-0766 (2021).
55 Krook, M. A. *et al.* Efficacy of FGFR Inhibitors and Combination Therapies for Acquired Resistance in FGFR2-Fusion Cholangiocarcinoma. *Mol Cancer Ther* **19**, 847-857, doi:10.1158/1535-7163.MCT-19-0631 (2020).
56 Lin, Q. *et al.* Characterization of the cholangiocarcinoma drug pemigatinib against FGFR gatekeeper mutants. *Commun Chem* **5**, 100, doi:10.1038/s42004-022-00718-z (2022).
57 Goyal, L. *et al.* TAS-120 Overcomes Resistance to ATP-Competitive FGFR Inhibitors in Patients with FGFR2 Fusion-Positive Intrahepatic Cholangiocarcinoma. *Cancer Discov* **9**, 1064-1079, doi:10.1158/2159-8290.CD-19-0182 (2019).
58 Cohen, P., Cross, D. & Janne, P. A. Kinase drug discovery 20 years after imatinib: progress and future directions. *Nat Rev Drug Discov* **20**, 551-569, doi:10.1038/s41573-021-00195-4 (2021).
59 Rulten, S. L., Grose, R. P., Gatz, S. A., Jones, J. L. & Cameron, A. J. M. The Future of Precision Oncology. *Int J Mol Sci* **24**, doi:10.3390/ijms241612613 (2023).
60 Braicu, C. *et al.* A Comprehensive Review on MAPK: A Promising Therapeutic Target in Cancer. *Cancers (Basel)* **11**, doi:10.3390/cancers11101618 (2019).
61 Yang, J. *et al.* Targeting PI3K in cancer: mechanisms and advances in clinical trials. *Mol Cancer* **18**, 26, doi:10.1186/s12943-019-0954-x (2019).
62 Beaver, J. A. *et al.* FDA Approval: Palbociclib for the Treatment of Postmenopausal Patients with Estrogen Receptor-Positive, HER2-Negative Metastatic Breast Cancer. *Clin Cancer Res* **21**, 4760-4766, doi:10.1158/1078-0432.CCR-15-1185 (2015).
63 Tomuleasa, C. *et al.* Therapeutic advances of targeting receptor tyrosine kinases in cancer. *Signal Transduct Target Ther* **9**, 201, doi:10.1038/s41392-024-01899-w (2024).
64 Waarts, M. R., Stonestrom, A. J., Park, Y. C. & Levine, R. L. Targeting mutations in cancer. *J Clin Invest* **132**, doi:10.1172/JCI154943 (2022).
65 Kiyotani, K., Toyoshima, Y. & Nakamura, Y. Personalized immunotherapy in cancer precision medicine. *Cancer Biol Med* **18**, 955-965, doi:10.20892/j.issn.2095-3941.2021.0032 (2021).
66 DeCarli, K., Strosberg, J. & Almhanna, K. Immune Checkpoint Inhibitors for Gastrointestinal Malignancies: An Update. *Cancers (Basel)* **14**, doi:10.3390/cancers14174201 (2022).
67 Tsimberidou, A. M. *et al.* Molecular tumour boards - current and future considerations for precision oncology. *Nat Rev Clin Oncol* **20**, 843-863, doi:10.1038/s41571-023-00824-4 (2023).
68 Liu, J., Dang, H. & Wang, X. W. The significance of intertumor and intratumor heterogeneity in liver cancer. *Exp Mol Med* **50**, e416, doi:10.1038/emm.2017.165 (2018).
69 Maldonado, E. B., Parsons, S., Chen, E. Y., Haslam, A. & Prasad, V. Estimation of US patients with cancer who may respond to cytotoxic chemotherapy. *Future Sci OA* **6**, FSO600, doi:10.2144/fsoa-2020-0024 (2020).
70 Miller, R. W. *et al.* Molecular Tumor Board-Assisted Care in an Advanced Cancer Population: Results of a Phase II Clinical Trial. *JCO Precis Oncol* **6**, e2100524, doi:10.1200/PO.21.00524 (2022).
71 Kasztura, M., Richard, A., Bempong, N. E., Loncar, D. & Flahault, A. Cost-effectiveness of precision medicine: a scoping review. *Int J Public Health* **64**, 1261-1271, doi:10.1007/s00038-019-01298-x (2019).

72 Wang, S. *et al.* Global, regional, and national lifetime risks of developing and dying from gastrointestinal cancers in 185 countries: a population-based systematic analysis of GLOBOCAN. *Lancet Gastroenterol Hepatol* **9**, 229-237, doi:10.1016/S2468-1253(23)00366-7 (2024).
73 Polireddy, K. & Chen, Q. Cancer of the Pancreas: Molecular Pathways and Current Advancement in Treatment. *J Cancer* **7**, 1497-1514, doi:10.7150/jca.14922 (2016).
74 Linehan, A., O'Reilly, M., McDermott, R. & O'Kane, G. M. Targeting KRAS mutations in pancreatic cancer: opportunities for future strategies. *Front Med (Lausanne)* **11**, 1369136, doi:10.3389/fmed.2024.1369136 (2024).
75 Hu, H. F. *et al.* Mutations in key driver genes of pancreatic cancer: molecularly targeted therapies and other clinical implications. *Acta Pharmacol Sin* **42**, 1725-1741, doi:10.1038/s41401-020-00584-2 (2021).
76 Troiani, T. *et al.* Targeting EGFR in pancreatic cancer treatment. *Curr Drug Targets* **13**, 802-810, doi:10.2174/138945012800564158 (2012).
77 Nunes, L. *et al.* Prognostic genome and transcriptome signatures in colorectal cancers. *Nature*, doi:10.1038/s41586-024-07769-3 (2024).
78 Koveitypour, Z. *et al.* Signaling pathways involved in colorectal cancer progression. *Cell Biosci* **9**, 97, doi:10.1186/s13578-019-0361-4 (2019).
79 Stefani, C. *et al.* Growth Factors, PI3K/AKT/mTOR and MAPK Signaling Pathways in Colorectal Cancer Pathogenesis: Where Are We Now? *Int J Mol Sci* **22**, doi:10.3390/ijms221910260 (2021).
80 Javadrashid, D. *et al.* Pancreatic Cancer Signaling Pathways, Genetic Alterations, and Tumor Microenvironment: The Barriers Affecting the Method of Treatment. *Biomedicines* **9**, doi:10.3390/biomedicines9040373 (2021).
81 Ahmad, R. *et al.* Emerging trends in colorectal cancer: Dysregulated signaling pathways (Review). *Int J Mol Med* **47**, doi:10.3892/ijmm.2021.4847 (2021).
82 Li, M. M., Yuan, J., Guan, X. Y., Ma, N. F. & Liu, M. Molecular subclassification of gastrointestinal cancers based on cancer stem cell traits. *Exp Hematol Oncol* **10**, 53, doi:10.1186/s40164-021-00246-x (2021).
83 Mukund, K., Syulyukina, N., Ramamoorthy, S. & Subramaniam, S. Right and left-sided colon cancers - specificity of molecular mechanisms in tumorigenesis and progression. *BMC Cancer* **20**, 317, doi:10.1186/s12885-020-06784-7 (2020).
84 Collaborative, R. *et al.* Characteristics of Early-Onset vs Late-Onset Colorectal Cancer: A Review. *JAMA Surg* **156**, 865-874, doi:10.1001/jamasurg.2021.2380 (2021).
85 Gullo, I., Carneiro, F., Oliveira, C. & Almeida, G. M. Heterogeneity in Gastric Cancer: From Pure Morphology to Molecular Classifications. *Pathobiology* **85**, 50-63, doi:10.1159/000473881 (2018).
86 Bailey, P. *et al.* Genomic analyses identify molecular subtypes of pancreatic cancer. *Nature* **531**, 47-52, doi:10.1038/nature16965 (2016).
87 Collisson, E. A., Bailey, P., Chang, D. K. & Biankin, A. V. Molecular subtypes of pancreatic cancer. *Nat Rev Gastroenterol Hepatol* **16**, 207-220, doi:10.1038/s41575-019-0109-y (2019).
88 Matsuoka, T. & Yashiro, M. Precision medicine for gastrointestinal cancer: Recent progress and future perspective. *World J Gastrointest Oncol* **12**, 1-20, doi:10.4251/wjgo.v12.i1.1 (2020).
89 Dalton, W. B. *et al.* Personalized Medicine in the Oncology Clinic: Implementation and Outcomes of the Johns Hopkins Molecular Tumor Board. *JCO Precis Oncol* **2017**, doi:10.1200/PO.16.00046 (2017).
90 Ballatore, Z. *et al.* Molecular Tumour Board (MTB): From Standard Therapy to Precision Medicine. *J Clin Med* **12**, doi:10.3390/jcm12206666 (2023).
91 Thiery, J. & Fahrner, M. Integration of proteomics in the molecular tumor board. *Proteomics* **24**, e2300002, doi:10.1002/pmic.202300002 (2024).
92 Leichsenring, J. *et al.* Variant classification in precision oncology. *Int J Cancer* **145**, 2996-3010, doi:10.1002/ijc.32358 (2019).
93 Lang, U. E., Puls, I., Muller, D. J., Strutz-Seebohm, N. & Gallinat, J. Molecular mechanisms of schizophrenia. *Cell Physiol Biochem* **20**, 687-702, doi:10.1159/000110430 (2007).
94 Nakamura, T. & Takata, A. The molecular pathology of schizophrenia: an overview of existing knowledge and new directions for future research. *Mol Psychiatry* **28**, 1868-1889, doi:10.1038/s41380-023-02005-2 (2023).
95 McCutcheon, R. A., Reis Marques, T. & Howes, O. D. Schizophrenia-An Overview. *JAMA Psychiatry* **77**, 201-210, doi:10.1001/jamapsychiatry.2019.3360 (2020).
96 Jauhar, S., Johnstone, M. & McKenna, P. J. Schizophrenia. *Lancet* **399**, 473-486, doi:10.1016/S0140-6736(21)01730-X (2022).

97 Patel, K. R., Cherian, J., Gohil, K. & Atkinson, D. Schizophrenia: overview and treatment options. *P T* **39**, 638-645 (2014).
98 Correll, C. U. *et al.* Systematic literature review of schizophrenia clinical practice guidelines on acute and maintenance management with antipsychotics. *Schizophrenia (Heidelb)* **8**, 5, doi:10.1038/s41537-021-00192-x (2022).
99 Howes, O. D. *et al.* Pathways to schizophrenia: the impact of environmental factors. *Int J Neuropsychopharmacol* **7 Suppl 1**, S7-S13, doi:10.1017/S1461145704004122 (2004).
100 Heider, J. *et al.* Defined co-cultures of glutamatergic and GABAergic neurons with a mutation in DISC1 reveal aberrant phenotypes in GABAergic neurons. *BMC Neurosci* **25**, 12, doi:10.1186/s12868-024-00858-z (2024).
101 He, D. *et al.* Prioritization of schizophrenia risk genes from GWAS results by integrating multi-omics data. *Transl Psychiatry* **11**, 175, doi:10.1038/s41398-021-01294-x (2021).
102 Birnbaum, R. & Weinberger, D. R. The Genesis of Schizophrenia: An Origin Story. *Am J Psychiatry* **181**, 482-492, doi:10.1176/appi.ajp.20240305 (2024).
103 Doss, M. X. & Sachinidis, A. Current Challenges of iPSC-Based Disease Modeling and Therapeutic Implications. *Cells* **8**, doi:10.3390/cells8050403 (2019).
104 Heider, J., Vogel, S., Volkmer, H. & Breitmeyer, R. Human iPSC-Derived Glia as a Tool for Neuropsychiatric Research and Drug Development. *Int J Mol Sci* **22**, doi:10.3390/ijms221910254 (2021).
105 Takahashi, K. & Yamanaka, S. A decade of transcription factor-mediated reprogramming to pluripotency. *Nat Rev Mol Cell Biol* **17**, 183-193, doi:10.1038/nrm.2016.8 (2016).
106 Paik, D. T., Chandy, M. & Wu, J. C. Patient and Disease-Specific Induced Pluripotent Stem Cells for Discovery of Personalized Cardiovascular Drugs and Therapeutics. *Pharmacol Rev* **72**, 320-342, doi:10.1124/pr.116.013003 (2020).
107 Cerneckis, J., Cai, H. & Shi, Y. Induced pluripotent stem cells (iPSCs): molecular mechanisms of induction and applications. *Signal Transduct Target Ther* **9**, 112, doi:10.1038/s41392-024-01809-0 (2024).
108 Stock, R. *et al.* The potential of induced pluripotent stem cells for discriminating neurodevelopmental disorders. *Stem Cells Transl Med* **10**, 50-56, doi:10.1002/sctm.20-0206 (2021).
109 Hong, Y., Yang, Q., Song, H. & Ming, G. L. Opportunities and limitations for studying neuropsychiatric disorders using patient-derived induced pluripotent stem cells. *Mol Psychiatry* **28**, 1430-1439, doi:10.1038/s41380-023-01990-8 (2023).
110 Grunwald, L. M. *et al.* Comparative characterization of human induced pluripotent stem cells (hiPSC) derived from patients with schizophrenia and autism. *Transl Psychiatry* **9**, 179, doi:10.1038/s41398-019-0517-3 (2019).
111 Brennand, K. J. *et al.* Modelling schizophrenia using human induced pluripotent stem cells. *Nature* **473**, 221-225, doi:10.1038/nature09915 (2011).
112 Ruzicka, W. B. *et al.* Single-cell multi-cohort dissection of the schizophrenia transcriptome. *Science* **384**, eadg5136, doi:10.1126/science.adg5136 (2024).
113 Brennand, K. *et al.* Phenotypic differences in hiPSC NPCs derived from patients with schizophrenia. *Mol Psychiatry* **20**, 361-368, doi:10.1038/mp.2014.22 (2015).
114 Hoffman, G. E. *et al.* Transcriptional signatures of schizophrenia in hiPSC-derived NPCs and neurons are concordant with post-mortem adult brains. *Nat Commun* **8**, 2225, doi:10.1038/s41467-017-02330-5 (2017).
115 Chandrasekaran, A. *et al.* A protein-centric view of in vitro biological model systems for schizophrenia. *Stem Cells* **39**, 1569-1578, doi:10.1002/stem.3447 (2021).
116 Nascimento, J. M. *et al.* Proteomic signatures of schizophrenia-sourced iPSC-derived neural cells and brain organoids are similar to patients' postmortem brains. *Cell Biosci* **12**, 189, doi:10.1186/s13578-022-00928-x (2022).
117 Freyberg, Z., Ferrando, S. J. & Javitch, J. A. Roles of the Akt/GSK-3 and Wnt signaling pathways in schizophrenia and antipsychotic drug action. *Am J Psychiatry* **167**, 388-396, doi:10.1176/appi.ajp.2009.08121873 (2010).
118 Funk, A. J., McCullumsmith, R. E., Haroutunian, V. & Meador-Woodruff, J. H. Abnormal activity of the MAPK- and cAMP-associated signaling pathways in frontal cortical areas in postmortem brain in schizophrenia. *Neuropsychopharmacology* **37**, 896-905, doi:10.1038/npp.2011.267 (2012).
119 Hoseth, E. Z. *et al.* Exploring the Wnt signaling pathway in schizophrenia and bipolar disorder. *Transl Psychiatry* **8**, 55, doi:10.1038/s41398-018-0102-1 (2018).

120 Penel, N. *et al.* Growth modulation index as metric of clinical benefit assessment among advanced soft tissue sarcoma patients receiving trabectedin as a salvage therapy. *Ann Oncol* **24**, 537-542, doi:10.1093/annonc/mds470 (2013).
121 Vogel, A., Segatto, O., Stenzinger, A. & Saborowski, A. FGFR2 Inhibition in Cholangiocarcinoma. *Annu Rev Med* **74**, 293-306, doi:10.1146/annurev-med-042921-024707 (2023).
122 DiPeri, T. P. *et al.* Convergent MAPK pathway alterations mediate acquired resistance to FGFR inhibitors in FGFR2 fusion-positive cholangiocarcinoma. *J Hepatol* **80**, 322-334, doi:10.1016/j.jhep.2023.10.041 (2024).
123 Jin, H. *et al.* EGFR activation limits the response of liver cancer to lenvatinib. *Nature* **595**, 730-734, doi:10.1038/s41586-021-03741-7 (2021).
124 Goyal, L. *et al.* Polyclonal Secondary FGFR2 Mutations Drive Acquired Resistance to FGFR Inhibition in Patients with FGFR2 Fusion-Positive Cholangiocarcinoma. *Cancer Discov* **7**, 252-263, doi:10.1158/2159-8290.CD-16-1000 (2017).
125 Varghese, A. M. *et al.* Noninvasive Detection of Polyclonal Acquired Resistance to FGFR Inhibition in Patients With Cholangiocarcinoma Harboring FGFR2 Alterations. *JCO Precis Oncol* **5**, doi:10.1200/PO.20.00178 (2021).
126 Mahaamnad, N. *et al.* Dual blockage of PI3K-mTOR and FGFR induced autophagic cell death in cholangiocarcinoma cells. *Heliyon* **10**, e31112, doi:10.1016/j.heliyon.2024.e31112 (2024).
127 Yue, S. *et al.* FGFR-TKI resistance in cancer: current status and perspectives. *J Hematol Oncol* **14**, 23, doi:10.1186/s13045-021-01040-2 (2021).
128 Sootome, H. *et al.* Futibatinib Is a Novel Irreversible FGFR 1-4 Inhibitor That Shows Selective Antitumor Activity against FGFR-Deregulated Tumors. *Cancer Res* **80**, 4986-4997, doi:10.1158/0008-5472.CAN-19-2568 (2020).
129 Banales, J. M. *et al.* Cholangiocarcinoma 2020: the next horizon in mechanisms and management. *Nat Rev Gastroenterol Hepatol* **17**, 557-588, doi:10.1038/s41575-020-0310-z (2020).
130 Stenzinger, A. *et al.* Molecular profiling in cholangiocarcinoma: A practical guide to next-generation sequencing. *Cancer Treat Rev* **122**, 102649, doi:10.1016/j.ctrv.2023.102649 (2024).
131 Kawano, S. *et al.* Antitumor Activity of Tasurgratinib as an Orally Available FGFR1-3 Inhibitor in Cholangiocarcinoma Models With FGFR2-fusion. *Anticancer Res* **44**, 2393-2406, doi:10.21873/anticanres.17046 (2024).
132 Balasooriya, E. R. *et al.* The Irreversible FGFR Inhibitor KIN-3248 Overcomes FGFR2 Kinase Domain Mutations. *Clin Cancer Res* **30**, 2181-2192, doi:10.1158/1078-0432.CCR-23-3588 (2024).
133 Bockmayr, T. *et al.* Multiclass cancer classification in fresh frozen and formalin-fixed paraffin-embedded tissue by DigiWest multiplex protein analysis. *Lab Invest* **100**, 1288-1299, doi:10.1038/s41374-020-0455-y (2020).
134 Ruoff, F. *et al.* Protein Profiling of Breast Carcinomas Reveals Expression of Immune-Suppressive Factors and Signatures Relevant for Patient Outcome. *Cancers (Basel)* **14**, doi:10.3390/cancers14184542 (2022).
135 Zhou, Y. *et al.* Proteomic signatures of 16 major types of human cancer reveal universal and cancer-type-specific proteins for the identification of potential therapeutic targets. *J Hematol Oncol* **13**, 170, doi:10.1186/s13045-020-01013-x (2020).
136 Asleh, K. *et al.* Proteomic analysis of archival breast cancer clinical specimens identifies biological subtypes with distinct survival outcomes. *Nat Commun* **13**, 896, doi:10.1038/s41467-022-28524-0 (2022).
137 Zhang, Z., Zhang, H., Liao, X. & Tsai, H. I. KRAS mutation: The booster of pancreatic ductal adenocarcinoma transformation and progression. *Front Cell Dev Biol* **11**, 1147676, doi:10.3389/fcell.2023.1147676 (2023).
138 Voutsadakis, I. A. Mutations of p53 associated with pancreatic cancer and therapeutic implications. *Ann Hepatobiliary Pancreat Surg* **25**, 315-327, doi:10.14701/ahbps.2021.25.3.315 (2021).
139 Day, F. L. *et al.* PIK3CA and PTEN gene and exon mutation-specific clinicopathologic and molecular associations in colorectal cancer. *Clin Cancer Res* **19**, 3285-3296, doi:10.1158/1078-0432.CCR-12-3614 (2013).
140 Salvatore, L. *et al.* PTEN in Colorectal Cancer: Shedding Light on Its Role as Predictor and Target. *Cancers (Basel)* **11**, doi:10.3390/cancers11111765 (2019).
141 Sawai, H. *et al.* Loss of PTEN expression is associated with colorectal cancer liver metastasis and poor patient survival. *BMC Gastroenterol* **8**, 56, doi:10.1186/1471-230X-8-56 (2008).

142 Ogino, S. *et al.* Cytoplasmic localization of p27 (cyclin-dependent kinase inhibitor 1B/KIP1) in colorectal cancer: inverse correlations with nuclear p27 loss, microsatellite instability, and CpG island methylator phenotype. *Hum Pathol* **38**, 585-592, doi:10.1016/j.humpath.2006.09.014 (2007).
143 Collisson, E. A. *et al.* Subtypes of pancreatic ductal adenocarcinoma and their differing responses to therapy. *Nat Med* **17**, 500-503, doi:10.1038/nm.2344 (2011).
144 Moffitt, R. A. *et al.* Virtual microdissection identifies distinct tumor- and stroma-specific subtypes of pancreatic ductal adenocarcinoma. *Nat Genet* **47**, 1168-1178, doi:10.1038/ng.3398 (2015).
145 Elebo, N., Abdel-Shafy, E. A., Cacciatore, S. & Nweke, E. E. Exploiting the molecular subtypes and genetic landscape in pancreatic cancer: the quest to find effective drugs. *Front Genet* **14**, 1170571, doi:10.3389/fgene.2023.1170571 (2023).
146 Deleyto-Seldas, N. & Efeyan, A. The mTOR-Autophagy Axis and the Control of Metabolism. *Front Cell Dev Biol* **9**, 655731, doi:10.3389/fcell.2021.655731 (2021).
147 Saxton, R. A. & Sabatini, D. M. mTOR Signaling in Growth, Metabolism, and Disease. *Cell* **168**, 960-976, doi:10.1016/j.cell.2017.02.004 (2017).
148 Baran, B. *et al.* Difference Between Left-Sided and Right-Sided Colorectal Cancer: A Focused Review of Literature. *Gastroenterology Res* **11**, 264-273, doi:10.14740/gr1062w (2018).
149 Salem, M. E. *et al.* Comparative molecular analyses of left-sided colon, right-sided colon, and rectal cancers. *Oncotarget* **8**, 86356-86368, doi:10.18632/oncotarget.21169 (2017).
150 Lieu, C. H. *et al.* Comprehensive Genomic Landscapes in Early and Later Onset Colorectal Cancer. *Clin Cancer Res* **25**, 5852-5858, doi:10.1158/1078-0432.CCR-19-0899 (2019).
151 Cercek, A. *et al.* A Comprehensive Comparison of Early-Onset and Average-Onset Colorectal Cancers. *J Natl Cancer Inst* **113**, 1683-1692, doi:10.1093/jnci/djab124 (2021).
152 Lu, C. *et al.* Molecular characteristics of microsatellite stable early-onset colorectal cancer as predictors of prognosis and immunotherapeutic response. *NPJ Precis Oncol* **7**, 63, doi:10.1038/s41698-023-00414-8 (2023).
153 Wahjudi, L. W. *et al.* Integrating proteomics into precision oncology. *Int J Cancer* **148**, 1438-1451, doi:10.1002/ijc.33301 (2021).
154 Mulligan, K. A. & Cheyette, B. N. Wnt signaling in vertebrate neural development and function. *J Neuroimmune Pharmacol* **7**, 774-787, doi:10.1007/s11481-012-9404-x (2012).
155 Sahu, M. R. & Mondal, A. C. Neuronal Hippo signaling: From development to diseases. *Dev Neurobiol* **81**, 92-109, doi:10.1002/dneu.22796 (2021).
156 Yang, C., Qi, Y. & Sun, Z. The Role of Sonic Hedgehog Pathway in the Development of the Central Nervous System and Aging-Related Neurodegenerative Diseases. *Front Mol Biosci* **8**, 711710, doi:10.3389/fmolb.2021.711710 (2021).
157 Rust, R. *et al.* Xeno-free induced pluripotent stem cell-derived neural progenitor cells for in vivo applications. *J Transl Med* **20**, 421, doi:10.1186/s12967-022-03610-5 (2022).
158 Robicsek, O. *et al.* Abnormal neuronal differentiation and mitochondrial dysfunction in hair follicle-derived induced pluripotent stem cells of schizophrenia patients. *Mol Psychiatry* **18**, 1067-1076, doi:10.1038/mp.2013.67 (2013).
159 Toyoshima, M. *et al.* Analysis of induced pluripotent stem cells carrying 22q11.2 deletion. *Transl Psychiatry* **6**, e934, doi:10.1038/tp.2016.206 (2016).
160 Markkanen, E., Meyer, U. & Dianov, G. L. DNA Damage and Repair in Schizophrenia and Autism: Implications for Cancer Comorbidity and Beyond. *Int J Mol Sci* **17**, doi:10.3390/ijms17060856 (2016).
161 Catts, V. S. *et al.* Evidence of aberrant DNA damage response signalling but normal rates of DNA repair in dividing lymphoblasts from patients with schizophrenia. *World J Biol Psychiatry* **13**, 114-125, doi:10.3109/15622975.2011.565073 (2012).
162 Shishido, R. *et al.* Evidence for increased DNA damage repair in the postmortem brain of the high stress-response group of schizophrenia. *Front Psychiatry* **14**, 1183696, doi:10.3389/fpsyt.2023.1183696 (2023).
163 Zuccoli, G. S., Nascimento, J. M., Moraes-Vieira, P. M., Rehen, S. K. & Martins-de-Souza, D. Mitochondrial, cell cycle control and neuritogenesis alterations in an iPSC-based neurodevelopmental model for schizophrenia. *Eur Arch Psychiatry Clin Neurosci* **273**, 1649-1664, doi:10.1007/s00406-023-01605-x (2023).
164 Paulsen Bda, S. *et al.* Altered oxygen metabolism associated to neurogenesis of induced pluripotent stem cells derived from a schizophrenic patient. *Cell Transplant* **21**, 1547-1559, doi:10.3727/096368911X600957 (2012).
165 Cabungcal, J. H. *et al.* Juvenile antioxidant treatment prevents adult deficits in a developmental model of schizophrenia. *Neuron* **83**, 1073-1084, doi:10.1016/j.neuron.2014.07.028 (2014).

166 Cremisi, F., Philpott, A. & Ohnuma, S. Cell cycle and cell fate interactions in neural development. *Curr Opin Neurobiol* **13**, 26-33, doi:10.1016/s0959-4388(03)00005-9 (2003).
167 Fan, Y., Abrahamsen, G., McGrath, J. J. & Mackay-Sim, A. Altered cell cycle dynamics in schizophrenia. *Biol Psychiatry* **71**, 129-135, doi:10.1016/j.biopsych.2011.10.004 (2012).
168 Okazaki, S. *et al.* The cell cycle-related genes as biomarkers for schizophrenia. *Prog Neuropsychopharmacol Biol Psychiatry* **70**, 85-91, doi:10.1016/j.pnpbp.2016.05.005 (2016).
169 Li, H., Zhang, Z., Li, H., Pan, X. & Wang, Y. New Insights into the Roles of p53 in Central Nervous System Diseases. *Int J Neuropsychopharmacol* **26**, 465-473, doi:10.1093/ijnp/pyad030 (2023).
170 Xiong, Y., Zhang, Y., Xiong, S. & Williams-Villalobo, A. E. A Glance of p53 Functions in Brain Development, Neural Stem Cells, and Brain Cancer. *Biology (Basel)* **9**, doi:10.3390/biology9090285 (2020).
171 Catts, V. S. & Catts, S. V. Apoptosis and schizophrenia: is the tumour suppressor gene, p53, a candidate susceptibility gene? *Schizophr Res* **41**, 405-415, doi:10.1016/s0920-9964(99)00077-8 (2000).
172 Zhuo, C. *et al.* Double-Edged Sword of Tumour Suppressor Genes in Schizophrenia. *Front Mol Neurosci* **12**, 1, doi:10.3389/fnmol.2019.00001 (2019).
173 Gal, G. *et al.* Cancer in parents of persons with schizophrenia: is there a genetic protection? *Schizophr Res* **139**, 189-193, doi:10.1016/j.schres.2012.04.018 (2012).
174 Cohen, M., Dembling, B. & Schorling, J. The association between schizophrenia and cancer: a population-based mortality study. *Schizophr Res* **57**, 139-146, doi:10.1016/s0920-9964(01)00308-5 (2002).
175 Fu, X., Wu, S., Li, B., Xu, Y. & Liu, J. Functions of p53 in pluripotent stem cells. *Protein Cell* **11**, 71-78, doi:10.1007/s13238-019-00665-x (2020).
176 Rodrigues, J. E. *et al.* Systematic Review and Meta-Analysis of Mass Spectrometry Proteomics Applied to Human Peripheral Fluids to Assess Potential Biomarkers of Schizophrenia. *Int J Mol Sci* **23**, doi:10.3390/ijms23094917 (2022).
177 English, J. A. *et al.* Reduced protein synthesis in schizophrenia patient-derived olfactory cells. *Transl Psychiatry* **5**, e663, doi:10.1038/tp.2015.119 (2015).
178 Topol, A. *et al.* Increased abundance of translation machinery in stem cell-derived neural progenitor cells from four schizophrenia patients. *Transl Psychiatry* **5**, e662, doi:10.1038/tp.2015.118 (2015).
179 Fernandes, B. S., Dai, Y., Jia, P. & Zhao, Z. Charting the proteome landscape in major psychiatric disorders: From biomarkers to biological pathways towards drug discovery. *Eur Neuropsychopharmacol* **61**, 43-59, doi:10.1016/j.euroneuro.2022.06.001 (2022).
180 Kling, S. *et al.* Characterization of hepatic zonation in mice by mass-spectrometric and antibody-based proteomics approaches. *Biol Chem* **403**, 331-343, doi:10.1515/hsz-2021-0314 (2022).
181 Aldea, M. *et al.* Precision medicine in the era of multi-omics: can the data tsunami guide rational treatment decision? *ESMO Open* **8**, 101642, doi:10.1016/j.esmoop.2023.101642 (2023).
182 Friedrich, M. & Aigner, A. Therapeutic siRNA: State-of-the-Art and Future Perspectives. *BioDrugs* **36**, 549-571, doi:10.1007/s40259-022-00549-3 (2022).
183 Zhang, J. *et al.* A Comprehensive Review of Small Interfering RNAs (siRNAs): Mechanism, Therapeutic Targets, and Delivery Strategies for Cancer Therapy. *Int J Nanomedicine* **18**, 7605-7635, doi:10.2147/IJN.S436038 (2023).
184 LeSavage, B. L., Suhar, R. A., Broguiere, N., Lutolf, M. P. & Heilshorn, S. C. Next-generation cancer organoids. *Nat Mater* **21**, 143-159, doi:10.1038/s41563-021-01057-5 (2022).
185 Ma, X. *et al.* Cancer organoids: A platform in basic and translational research. *Genes Dis* **11**, 614-632, doi:10.1016/j.gendis.2023.02.052 (2024).
186 Kondo, J. & Inoue, M. Application of Cancer Organoid Model for Drug Screening and Personalized Therapy. *Cells* **8**, doi:10.3390/cells8050470 (2019).
187 Liu, X. *et al.* Tumor-on-a-chip: from bioinspired design to biomedical application. *Microsyst Nanoeng* **7**, 50, doi:10.1038/s41378-021-00277-8 (2021).
188 Kromidas, E. *et al.* Immunocompetent PDMS-Free Organ-on-Chip Model of Cervical Cancer Integrating Patient-Specific Cervical Fibroblasts and Neutrophils. *Adv Healthc Mater* **13**, e2302714, doi:10.1002/adhm.202302714 (2024).
189 Regmi, S., Poudel, C., Adhikari, R. & Luo, K. Q. Applications of Microfluidics and Organ-on-a-Chip in Cancer Research. *Biosensors (Basel)* **12**, doi:10.3390/bios12070459 (2022).
190 Maulana, T. I. *et al.* Breast cancer-on-chip for patient-specific efficacy and safety testing of CAR-T cells. *Cell Stem Cell* **31**, 989-1002 e1009, doi:10.1016/j.stem.2024.04.018 (2024).
191 Villanueva, R. Advances in the knowledge and therapeutics of schizophrenia, major depression disorder, and bipolar disorder from human brain organoid research. *Front Psychiatry* **14**, 1178494, doi:10.3389/fpsyt.2023.1178494 (2023).

192 Notaras, M., Lodhi, A., Fang, H., Greening, D. & Colak, D. The proteomic architecture of schizophrenia iPSC-derived cerebral organoids reveals alterations in GWAS and neuronal development factors. *Transl Psychiatry* **11**, 541, doi:10.1038/s41398-021-01664-5 (2021).
193 Amirifar, L. *et al.* Brain-on-a-chip: Recent advances in design and techniques for microfluidic models of the brain in health and disease. *Biomaterials* **285**, 121531, doi:10.1016/j.biomaterials.2022.121531 (2022).
194 Amartumur, S. *et al.* Neuropathogenesis-on-chips for neurodegenerative diseases. *Nat Commun* **15**, 2219, doi:10.1038/s41467-024-46554-8 (2024).
195 van der Moolen, M. *et al.* Cancer-mediated axonal guidance of sensory neurons in a microelectrode-based innervation MPS. *Biofabrication* **16**, doi:10.1088/1758-5090/ad218a (2024).

Acknowledgements

Ein herzlicher Dank gilt meiner Erstgutachterin Frau Prof. Dr. Katja Schenke-Layland für die ausgezeichnete Betreuung meiner Promotion und die Begleitung meiner Zeit als Doktorand mit fachlichem Rat und Expertise. Außerdem ein besonderes Dankeschön an Prof. Dr. Peter Loskill für die Zweitbegutachtung meiner Arbeit und die wertvollen Einschätzungen und wissenschaftlichen Diskussionen.

Ein außerordentlicher Dank gilt meinem Betreuer Dr. Markus Templin, der mich auf meinem Weg stets begleitet und diese Dissertation mit vielen Ratschlägen, produktiven Gesprächen und wissenschaftlichen Ideen mitgeprägt hat. Danke, dass Du mich immer unterstützt und hinter mir gestanden hast.

Ein weiterer Dank gilt allen Kollaboratoren, die zum wissenschaftlichen Inhalt dieser Arbeit beigetragen haben, insbesondere Prof. Dr. Michael Bitzer, Dr. Stephan Spahn und Prof. Dr. Hansjürgen Volkmer. Unsere wissenschaftliche Zusammenarbeit hat mir große Freude bereitet und meine Arbeit exzellent unterstützt.

Ein besonderer Dank gilt zudem Johanna Heider. Danke nicht nur für Deine Mitarbeit an unserem gemeinsam organisierten Projekt, das Teil dieser Arbeit geworden ist.

Nicht zuletzt muss ich allen aktuellen und ehemaligen Mitarbeitenden der Arbeitsgruppe Assay Entwicklung sowie meinen Kollegen vom gesamten 4. Stock während meiner Zeit am NMI danken. Besonders zu erwähnen sind hier Simon Fink, Dr. Felix Schäfer-Ruoff, Sandra Jerbi, Marius Kolodziej und Anette Döttinger. Danke für die tolle Arbeitsatmosphäre, Kollegialität und stetige Unterstützung im (Labor-) Alltag.

Zuletzt möchte ich ausdrücklich meinen Eltern, meiner Familie und meinen Freunden für ihre Geduld, Zuneigung und Ermutigungen während der Arbeit an dieser Dissertation danken. Danke, dass Ihr immer an mich geglaubt habt.

Declaration

Ich erkläre hiermit, dass ich die zur Promotion eingereichte Arbeit mit dem Titel “Multiplexed Protein Analysis of Cellular Signal Transduction: Applications in Translational Research and Personalized Medicine” selbstständig verfasst, nur die angegebenen Quellen und Hilfsmittel benutzt und wörtlich oder inhaltlich übernommene Zitate als solche gekennzeichnet habe. Ich erkläre, dass die Richtlinien zur Sicherung guter wissenschaftlicher Praxis der Universität Tübingen beachtet wurden. Ich versichere an Eides statt, dass diese Angaben wahr sind und dass ich nichts verschwiegen habe. Mir ist bekannt, dass die falsche Angabe einer Versicherung an Eides statt mit Freiheitsstrafe bis zu drei Jahren oder mit Geldstrafe bestraft wird.

Aaron Stahl

Appendix

Appendix 1

Spahn, S.*, Kleinhenz, F.*, Shevchenko, E., **Stahl, A**., Rasen, Y., Geisler, C., Ruhm, K., Klaumuenzer, M., Kronenberger, T., Laufer, S. A., Sundberg-Malek, H., Bui, K. C., Horger, M., Biskup, S., Schulze-Osthoff, K., Templin, M., Malek, N. P., Poso, A., & Bitzer, M. (2024). The molecular interaction pattern of lenvatinib enables inhibition of wild-type or kinase-mutated FGFR2-driven cholangiocarcinoma. *Nature Communications, 15*(1). https://doi.org/10.1038/s41467-024-45247-6

*authors contributed equally

nature communications

Article

https://doi.org/10.1038/s41467-024-45247-6

The molecular interaction pattern of lenvatinib enables inhibition of wild-type or kinase-mutated FGFR2-driven cholangiocarcinoma

Received: 6 February 2023

Accepted: 18 January 2024

Published online: 12 February 2024

Check for updates

Stephan Spahn[1,13] ✉, Fabian Kleinhenz[1,13], Ekaterina Shevchenko[2,3], Aaron Stahl[4], Yvonne Rasen[1], Christine Geisler[1], Kristina Ruhm[5], Marion Klaumuenzer[6], Thales Kronenberger[2,3], Stefan A. Laufer[2,3,7], Holly Sundberg-Malek[5], Khac Cuong Bui[1], Marius Horger[8], Saskia Biskup[6], Klaus Schulze-Osthoff[7,9,10], Markus Templin[4], Nisar P. Malek[1,5,7,10,11], Antti Poso[2,3,7,12] & Michael Bitzer[1,5,7,11] ✉

Fibroblast growth factor receptor (FGFR)−2 can be inhibited by FGFR-selective or non-selective tyrosine kinase inhibitors (TKIs). Selective TKIs are approved for cholangiocarcinoma (CCA) with FGFR2 fusions; however, their application is limited by a characteristic pattern of adverse events or evocation of kinase domain mutations. A comprehensive characterization of a patient cohort treated with the non-selective TKI lenvatinib reveals promising efficacy in FGFR2-driven CCA. In a bed-to-bench approach, we investigate FGFR2 fusion proteins bearing critical tumor-relevant point mutations. These mutations confer growth advantage of tumor cells and increased resistance to selective TKIs but remain intriguingly sensitive to lenvatinib. In line with clinical observations, in-silico analyses reveal a more favorable interaction pattern of lenvatinib with FGFR2, including an increased flexibility and ligand efficacy, compared to FGFR-selective TKIs. Finally, the treatment of a patient with progressive disease and a newly developed kinase mutation during therapy with a selective inhibitor results in a striking response to lenvatinib. Our in vitro, in silico, and clinical data suggest that lenvatinib is a promising treatment option for FGFR2-driven CCA, especially when insurmountable adverse reactions of selective TKIs or acquired kinase mutations occur.

Cholangiocarcinoma (CCA) is a rare yet highly aggressive and deadly cancer with rising worldwide incidence and mortality[1]. CCA comprises a heterogeneous group of tumors with different histological and molecular subtypes[2,3]. For over a decade, a combination of gemcitabine and cisplatin has been the recommended first-line systemic treatment for advanced disease stages[4]. However, during the last few years, CCAs have become an attractive candidate for personalized medicine approaches due to the discovery that they harbor several druggable molecular targets[5–10].

One such target is the fibroblast growth factor receptor (FGFR) 2 signaling pathway. Up to 16% of intrahepatic cholangiocarcinomas (iCCAs) harbor an *FGFR2* gene fusion that induces constitutive receptor dimerization and ligand-independent pathway activation[5,11–15]. Three drugs, pemigatinib, infigratinib, and futibatinib have been

A full list of affiliations appears at the end of the paper. ✉e-mail: stephan.spahn@med.uni-tuebingen.de; michael.bitzer@uni-tuebingen.de

recently approved by the FDA for previously treated iCCA tumors with FGFR2 fusions or rearrangements[16–18]. In the pivotal phase II trials that led to the approval of these drugs, independent reviews found objective response rates between 23 and 42% of all treated patients[19–21]. In addition to CCAs addicted to *FGFR2* fusion genes, activating mutations and in-frame deletions in *FGFR2* define a further group of treatment-sensitive CCAs[18,22–24]. However, these latter alterations are not yet included in the approved labels for treatment.

FGFR-targeting tyrosine kinase inhibitors (TKI) can be classified into first-generation non-selective multikinase- and second-generation selective FGFR inhibitors[25]. Most non-selective inhibitors were initially designed for other kinases but proved to harbor potent inhibitory activity towards FGFRs[26], such as ponatinib, pazopanib, nintedanib, or lenvatinib[25,27–29]. Subsequently, second-generation TKIs were developed to increase anti-FGFR activity and reduce the well-known off-target effects of multikinase TKIs[22,26]. Besides pemigatinib, futibatinib and infigratinib, further compounds are under clinical investigation for CCA, for example, erdafitinib or derazantinib[30,31]. However, by introducing these new drugs, a substantial fraction of patients develop a unique spectrum of clinically significant adverse events due to FGFR targeting. The most remarkable events are hyperphosphatemia, ocular toxicities ranging from dry eyes to severe retinal damage, and dermatologic toxicities with stomatitis, onycholysis, nail bed infections, alopecia, or calcinosis cutis[32,33]. Furthermore, several reports describe the development of acquired FGFR2 kinase domain resistances during the treatment with selective inhibitors due to multiple recurrent and polyclonal point mutations[34–37].

Much work currently focuses on the further improvement of FGFR-targeting drugs. Despite the recent development in the field of second-generation FGFR-specific inhibitors, we and others observed several profound treatment responses in FGFR2-driven CCA with non-selective TKIs, even with reduced treatment doses compared to different tumor entities[24,28,31]. In a comprehensively characterized patient cohort with CCA, we found a promising efficacy for lenvatinib in FGFR2-driven CCA. In a bedside-to-bench approach, we compared the effect of first- and second-generation FGFR-inhibiting drugs on tumor cells with patient-derived *FGFR2* alterations, including resistance-mediating point mutations. Cellular reaction patterns, proteomic and in-silico analysis demonstrate a superior activity of lenvatinib even in the presence of resistance-mediating *FGFR2* mutations. As a proof-of-principle, lenvatinib led to a long-lasting partial response in a patient with CCA who developed a kinase mutation and progressive disease during treatment with pemigatinib.

Results

Clinical responses of FGFR2-driven iCCA to the non-selective TKI lenvatinib

Before the approval of pemigatinib by the European Commission in 03/2021, seven iCCA patients with FGFR2 alterations were treated with the multi tyrosine kinase inhibitor lenvatinib according to a recommendation of the Molecular Tumor Board (MTB) at Tuebingen University. Notably, due to a lack of approval or fitting clinical studies, these patients could not receive a selective, second-generation FGFR-inhibiting TKI. The *FGFR2* alterations of these heavily pretreated patients are shown in Fig. 1a. One patient (370_371delinsCys & Del) of this cohort has been reported in detail previously[24]. Of note, lenvatinib led to a partial response (PR) in four of the seven patients (Fig. 1a). Two representative [^{18}F]fluorodeoxyglucose (FDG)−positron emission tomography (PET) scans prior to and eight weeks after the start of lenvatinib treatment documented apparent metabolic responses (Fig. 1b). Median progression-free survival (mPFS) in this small cohort was 7.0 months, nearly three times as long as the mPFS of 2.5 months for these patients' first-line therapies (Suppl. Figure 1). Interestingly, the PFS during treatment with the established gemcitabine/cisplatin (Gem/Cis) therapy in any prior line of treatment was significantly lower than the treatment with lenvatinib after Gem/Cis (7 vs. 2.1 months, $p \leq 0.001$) (Fig. 1c). In this context, the Von Hoff model uses patients as their own control by comparing the PFS of a selected treatment with PFS values from previous lines of therapy[38]. A ratio of PFS from the investigated drug to PFS of a previous treatment of >1.3–1.5 is thereby regarded as clinically meaningful[39–41]. Of note, the PFS ratio was favorable compared to both previous and first-line therapies in 6 of 7 patients (Fig. 1a). Together with the observation of a median overall survival (OS) of more than 12 months in this heavily pretreated cohort since the start of lenvatinib therapy (Fig. 1c), these data suggest a clinically meaningful response to the treatment with lenvatinib in FGFR2-driven iCCA, even with daily doses of 12 mg or less (Fig. 1a, b).

Therapy responses for an iCCA with a *FGFR2-AHCYL2* fusion to different TKIs

A so far unknown *FGFR2* fusion, *FGFR2-AHCYL2*, was detected in the tumor of a young female patient with an exceptional clinical course (Fig. 1d). The patient was treated with several different FGFR-inhibiting drugs. In brief, after progression on Gem/Cis and identification of the fusion, she was treated with the non-selective TKI ponatinib based on a case report[28]. However, progressive disease (PD) was already detected after 45 days. Subsequent chemotherapy was not tolerated, and lenvatinib was started as a second option to inhibit FGFR2 signaling. Intriguingly, MRI scanning revealed a partial response with normalization of initially elevated levels of the tumor marker CA19-9 six weeks later. The treatment continued until PD occurred after 9 months. A sequential liver biopsy of the progressive lesion did not find any *FGFR2* mutations as a potential explanation for tumor progression.

After an unsuccessful further treatment approach with chemotherapy and another non-selective TKI, the patient was subsequently included in a then available clinical study with infigratinib, which again led to a partial response (Fig. 1d). Of note, this observation shows that despite progression under a previous FGFR-inhibiting drug, the tumor was still addicted to FGFR signaling. However, prolonged therapy interruptions due to recurrent cholangitis led to the patient's formal study exclusion without tumor progression. A further liver biopsy was performed, which again showed the *FGFR2-AHCYL2* fusion. However, no further responses could be achieved afterward with either erdafitinib (5th line TKI; PFS: 0.8 months) or pemigatinib (6th line TKI; PFS: 0.8 months). In the meantime, further molecular diagnostics of the liver biopsy revealed the previously described *FGFR2* resistance mutation p.N549H, and a liquid biopsy additionally detected several further resistance sub- and polyclonal mutations, including a p.V564F gatekeeper and p.E565A molecular brake mutation (Fig. 1d). The patient passed away 31 months after the initiation of the treatment with lenvatinib. Taken together, this patient history demonstrates that FGFR-addicted iCCAs can show a prolonged time window for FGFR-targeted drugs; but not all selected TKIs with a preclinically known FGFR-inhibitory function could achieve a clinical response.

Bedside to bench: generation and characterization of *FGFR2* fusion-expressing cell lines

Stable transfection of NIH3T3 cells has been used previously in several studies to investigate the transforming potential of FGFR2-fusion proteins or in-frame deletions and their sensitivity to FGFR-inhibiting drugs[11,13,18]. To investigate the effects of the newly discovered *FGFR2* fusion, we generated NIH3T3 cells to stably express the patient-specific *FGFR2-AHCYL2* fusion gene. In addition, we generated cell lines that stably expressed a second observed fusion gene from the patient cohort, *FGFR2-SH3GLB1*, and the most prevalently reported fusion in iCCA, *FGFR2-BICC1*. Characterization of these cell lines demonstrated that the expression of all three fusion genes induced a comparably increased proliferation (Fig. 2a) and anchorage-independent growth (Fig. 2b, c). Western blot analyses verified the stable expression of FGFR2 fusion proteins in the cell lines. Analysis of the downstream

 https://doi.org/10.1038/s41467-024-45247-6

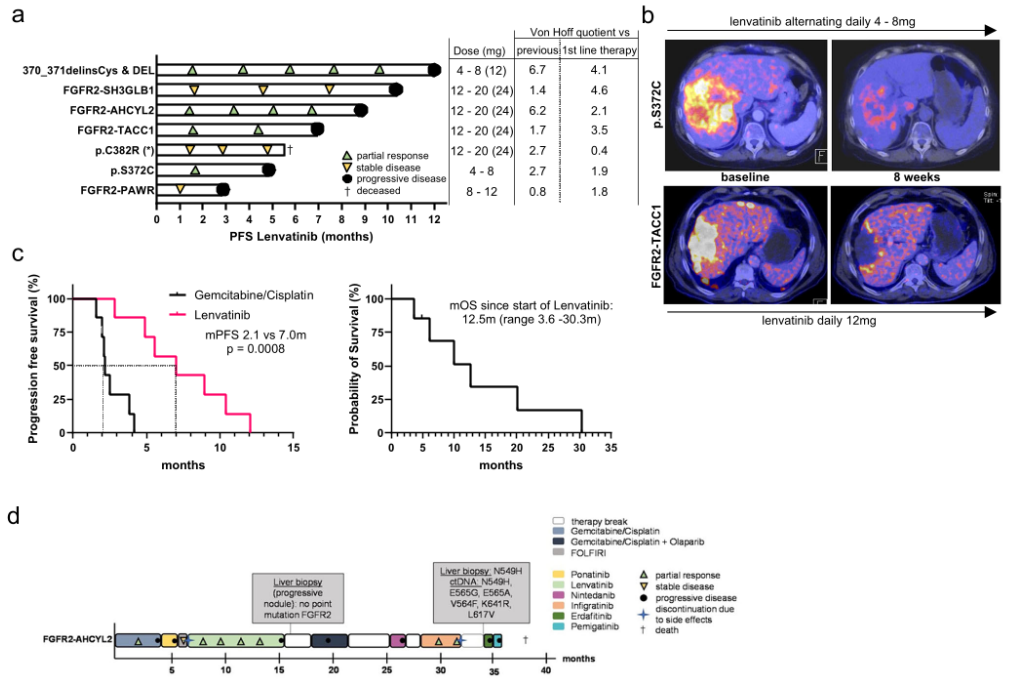

Fig. 1 | Lenvatinib leads to clinically meaningful responses in FGFR2-driven iCCA. a Swimmer plots illustrating the duration of individual therapy responses after the start of lenvatinib treatment. Detected molecular alterations from tumor biopsies, the applied lenvatinib dose that was used most of the treatment course with the maximal dose in brackets, and the Von Hoff quotient of lenvatinib vs. 1st line and previous therapies are shown. First-line therapies were Gem/Cis (Gemcitabine/Cisplatin) in all patients but one, who was treated with FOLFIRINOX (*). The first patient (370_371delinsCys & Del) has been reported in detail previously[24]. **b** PET-CT scans after 8 weeks of lenvatinib treatment in two patients harboring a *FGFR2* p.S372C point mutation and a *FGFR2-TACC1* fusion. The lenvatinib dose during the treatment period is shown for each patient. **c** Kaplan–Meier-survival curves demonstrating PFS of lenvatinib compared to prior Gem/Cis therapy (left panel) and the OS since the start of lenvatinib treatment (right panel). **d** Individual treatment course of a young female patient with a *FGFR2-AHCYL2* fusion undergoing treatment with different FGFR-specific and multi-targeted TKI compounds. Time points and results of *FGFR2* sequencing of liver and liquid biopsies are included. Infigratinib therapy had to be discontinued according to the clinical study protocol despite treatment response due to relapsing episodes of cholangitis. Progression was documented 43 days after end of that treatment. Two further FGFR inhibitors, erdafitinib and pemigatinib, did not reach a further response. Retrospective analysis of a liver biopsy and circulating tumor DNA (ctDNA) prior to erdafitinib revealed multiple resistance-associated point mutations.

pathways revealed that the *FGFR2* fusions predominantly led to phosphorylation and, thereby, activation of FGFR substrate 2 (FRS2), the kinases p44/42 ERK1/2, and transcription factor STAT3 (Fig. 2e). Phosphorylation of pFGF, ERK1/2 and STAT3 could be reversed through treatment inhibition with infigratinib, confirming the specificity of the phospho-specific-antibodies (Supplementary Fig. 2) Overall, these results suggest a transformation potential of the so far unknown *FGFR2-AHCYL2* fusion, comparable to the two previously described fusions, thereby qualifying these cell lines as in-vitro models for further mechanistic studies.

Characterization of drugs with different TKI activity profiles in cells with *FGFR2*-fusions

A direct comparison of specific and multitargeted TKIs with FGFR2-inhibitory activity in the presence of different patient-derived *FGFR2* fusion genes has not been reported in detail yet. Besides lenvatinib (targeting: VEGFR1-3, FGFR1-4, PDGFRA, KIT and RET), we selected ponatinib (targeting: ABL, PDGFRA, VEGFR2, FGFR1-2, SRC) and nintedanib (targeting: VEGFR1-3, FGFR1-3, PDGFRA/B) as multitargeted TKIs, infigratinib (targeting FGFR1-3) and futibatinib (targeting: FGFR1-4) as FGFR-selective TKIs and cabozantinib (targeting: VEGFR2, MET, RET, KIT, FLT1,3,4, TIE2, AXL) as a multitargeted TKI without relevant FGFR-inhibitory activity as a negative control. Of note, all FGFR2-inhibiting drugs reduced cell growth in the cell line overexpressing *FGFR2-AHCYL2* (Fig. 3a). In contrast, cabozantinib, a drug without FGFR-inhibitory activity, reduced cellular proliferation stronger in the empty vector control cells than in cells transfected with *FGFR2-AHCYL2* (Fig. 3a). Treatment of the *FGFR2-SH3GLB1* and *FGFR2-BICC1* expressing cells led to similar results (Fig. 3b). Expression of *FGFR2-SH3GLB1* and *FGFR2-BICC1* led to a strong sensitization of NIH3T3 cells to the selective FGFR inhibitors futibatinib and infigratinib, resulting in an apparent strong reduction of the IC_{50} values (1.8% and 7.3% compared to control transfected cells). A similar in vitro efficiency was found for the non-selective FGFR2 inhibitors lenvatinib and ponatinib, which reduced the IC_{50} values of both drugs to 18.7% and 16.9%, respectively, compared to control cells. Nintedanib, which was ineffective in the above-described patient history (Fig. 1e), induced only weak responses in cells with *BICC1* and *AHCYL2*

Article https://doi.org/10.1038/s41467-024-45247-6

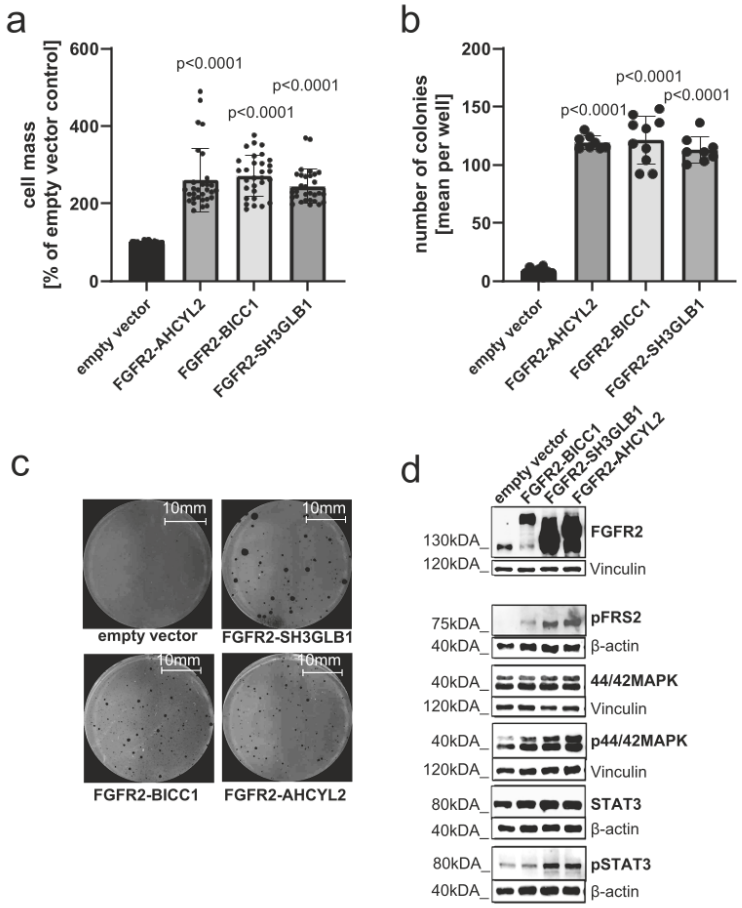

Fig. 2 | Malignant transformation by patient-specific FGFR2-fusion proteins. **a** Proliferation analyses of FGFR2-fusion expressing cell lines using SRB assays after 7 days in culture, $^{****}P \leq 0.0001$ compared to control transduced NIH3T3 cells with one-way ANOVA with Dunnett's multiple comparison test. Bars represent mean ± SD ($n = 30$ vials examined over 10 independent experiments). **b** Quantification of soft agar colony formation after 21 days with *FGFR2*-fusion-expressing cell lines and a control cell line transfected with the empty vector, $^{****}P \leq 0.0001$ compared to control transfected NIH3T3 cells with one-way ANOVA with Dunetts's multiple comparison test. Bars represent mean ± SD ($n = 8$ vials (empty vector, FGFR2-AHCYL2, FGFR2-SH3GLB1), $n = 10$ vials (FGFR2-BICC)) examined over 3 independent experiments. **c** Representative images of soft agar assays with the indicated cell lines after 21 days. **d** Representative Western blot analysis of FGFR2 downstream signals in NIH3T3 cell lines stably transfected with patient-derived *FGFR2* gene fusions (*FGFR2-BICC1*, *FGFR2-SH3GLB1*, *FGFR2-AHCYL2*) or control transfected NIH3T3 cells ($n = 3$ biologically independent samples).

fusions and no response in the *FGFR2-SH3GLB1*-expressing cell line (Fig. 3b). Besides inhibiting proliferation, colony formation assays showed comparable inhibitory activity of selective and non-selective FGFR inhibiting TKIs in *FGFR2-AHCYL2* transfected cells (Supplementary Fig. 3A, B).

So far, the clinical and in vitro results suggest that both FGFR2-selective and multi-target TKIs could be employed to inhibit the cell growth of *FGFR2*-fusion-positive tumors. To dissect the molecular mechanism of selective and non-selective TKIs for FGFR signaling in more detail, we characterized the *FGFR2-AHCYL2* expressing cell line via DigiWest, a high-throughput proteomic approach to analyze cellular signaling pathways[42] (Supplementary Fig. 4). To allow comparison, concentrations of TKIs were selected leading to approximately 50% cell mass reduction in the SRB assays. First, we looked at phosphorylated FGFR2 (p-FGFR2) and found a similar inhibition of FGFR2 phosphorylation for all drugs (Fig. 3c). Of note, no p-FGFR2 signal was detected in control transfected NIH3T3 cells. Further study of downstream targets revealed that FGFR-selective TKIs exclusively inhibited members of the MAPK pathway, such as ERK1/2 (p- Thr202/Tyr204) and RSK1 (p90RSK, p-Thr573), SHP2 (p-Tyr542), and the downstream target c-Myc (p-)Thr58/Ser62 in *FGFR2-AHCYL2* transfected cells (Fig. 3d, Supplementary Data 1). In contrast, the non-selective TKIs additionally inhibited MAPK-unrelated proteins, such as p70S6 kinase (Thr389)) and S6 ribosomal protein (Ser235/236), which are involved in Jak/STAT or PI3K/AKT/mTOR pathways and inhibited a broader spectrum of MAPK-related

Article https://doi.org/10.1038/s41467-024-45247-6

a

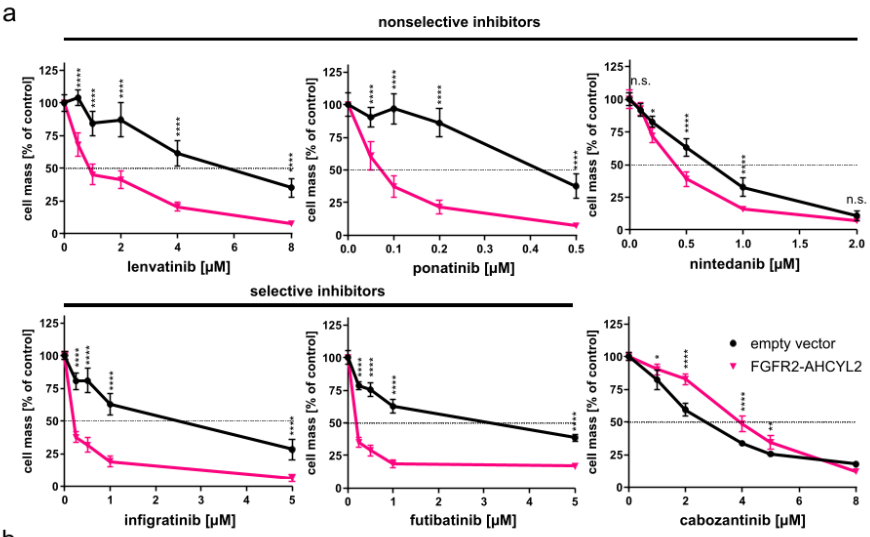

b

	lenvatinib		ponatinib		nintedanib		infigratinib		futibatinib		cabozantinib	
	IC_{50} in nmol/L SD (n)	% of IC_{50} empty vector	IC_{50} in nmol/L SD (n)	% of IC_{50} empty vector	IC_{50} in nmol/L SD (n)	% of IC_{50} empty vector	IC_{50} in nmol/L SD (n)	% of IC_{50} empty vector	IC_{50} in nmol/L SD (n)	% of IC_{50} empty vector	IC_{50} in nmol/L SD (n)	% of IC_{50} empty vector
empty vector	5456 405 (6)	100,0	408 26 (6)	100,0	634 26 (6)	100,0	1815 184 (6)	100,0	2389 203 (6)	100,0	2594 66 (6)	100,0
FGFR2-BICC1	1620 236 (6)	29,7	156 7 (6)	38,2	428 24 (6)	67,5	229 9 (6)	12,6	33 22 (6)	1,4	2670 62 (6)	102,9
FGFR2-SH3GLB1	1260 63 (6)	23,1	159 12 (6)	39,0	707 43 (6)	111,5	171 31 (6)	9,4	29 35 (6)	1,2	3229 104 (6)	124,5
FGFR2-AHCYL2	1021 69 (6)	18,7	69 4 (6)	16,9	376 13 (6)	59,3	133 19 (6)	7,3	42 14 (6)	1,8	3893 84 (6)	150,1

c

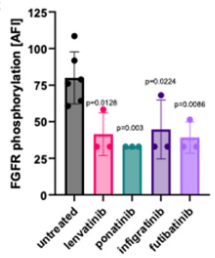

d

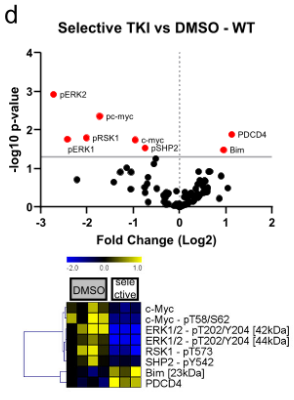

e

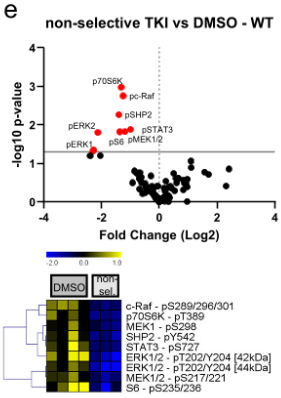

proteins, such as MEK1/2 (p-Ser217/Ser221) and c-RAF (p-Ser289/296/301) (Fig. 3e, Supplementary Fig. 5a, Supplementary Data 1). Interestingly, this broader inhibition of additional signaling pathways by the non-selective TKIs was particularly prominent in the *FGFR2*-fusion expressing cell line, which might be important in the context of treatment responses and the acquisition of therapy resistance. No significant difference was observed in the phosphorylation status of mTOR or p38 (Supplementary Data 1).

Fig. 3 | FGFR-selective and non-selective TKIs in FGFR2-fusion positive cells. **a** Proliferation analyses in NIH3T3 cells with the *FGFR2-AHCYL2* fusion employing SRB assays after 7 days of treatment. Applied drugs included the non-selective TKIs lenvatinib, ponatinib and nintedanib; the selective FGFR inhibitors infigratinib and futibatinib; and cabozantinib, a TKI without FGFR2-inhibitory activity as a negative control. *$P \leq 0.05$, **$P \leq 0.01$, ****$P \leq 0.0001$ compared to control transduced NIH3T3 cells with one-way ANOVA with Dunnett's multiple comparison test. Data are presented as mean ± SD ($n = 6$ independent experiments). **b** IC_{50} values of different drugs for NIH3T3 cells expressing the indicated construct in nmol/L ± SD and the respective percentage of the value for empty vector-transfected cells. Cell background gradient: green = lower, red = higher IC_{50} compared to empty vector. **c**–**e** DigiWest protein profiling analysis of *FGFR2-AHCYL2* fusion cell line treated with selective and non-selective TKIs. **c** Phosphorylation status (accumulated fluorescent intensity) of FGFR2 (Y653/654) in *FGFR2-AHCYL2* samples. Bars represent mean ± SD ($n = 6$ (untreated) and $n = 3$ (TKI-treated) biologically independent samples), One-Way-ANOVA with Dunnett's multiple comparison test. Volcano plot and hierarchical cluster (HCL) analysis of proteins and phosphoproteins significantly different between (**d**) selective inhibitors (infigratinib and futibatinib, $n = 3$ biologically independent samples) and (**e**) non-selective inhibitors (lenvatinib and ponatinib, $n = 3$ biologically independent samples) compared to control (DMSO, $n = 4$ biologically independent samples) in samples from *FGFR2-AHCYL2* cells (two-sided T-test, Welch, $P \leq 0.05$). Expression values were normalized to total protein signals across all samples for a given analyte, median-centered and Log-2 transformed. Shown are selected signaling proteins, the full DigiWest data set is included in the Supplementary Data file 1. Hierarchical cluster analysis was performed using Pearson correlation and complete linkage.

Generation and characterization of cell lines expressing resistance mutations within the *FGFR2* kinase domain

The selection of resistant subclones during the treatment with a selective FGFR2 inhibitor is a well-described mechanism and a major clinical concern[34–36,43]. The patient with the *FGFR2-AHCYL2* fusion finally developed polyclonal resistances after the treatment with infigratinib (Fig. 1d). In the preceding treatment with lenvatinib over 9 months, no resistance mutation was found. As our proteomics analysis revealed different inhibitory patterns of FGFR-specific and multitargeted TKIs, we speculated that resistance-mediating point mutations in *FGFR2* might be a predominant problem that arises during the treatment with FGFR-specific TKIs. Hence, we generated two additional cell lines that expressed either the *FGFR2-AHCYL2* construct with the previously described p.V564F "gatekeeper-mutation" (hereafter called *FGFR2-AHCYL2 plus* p.V564F) or p.E565A "brake-mutation" (*FGFR2-AHCYL2 plus* p.E565A). No differences in proliferation or expression levels of (mutated) FGFR2-fusion protein were noted between cells transfected with *FGFR2-AHCYL2 plus* p.V564 or plus p.E565A or *FGFR2-AHCYL2* without these mutations (Supplementary Fig. 6).

Employing different FGFR-inhibitory drugs, cell viability assays showed that the *FGFR2-AHCYL2 plus* p.V564F and the *FGFR2-AHCYL2 plus* p.E565A mutations, as expected, caused resistance to infigratinib and, to a lesser extent, to futibatinib (Fig. 4a). Nevertheless, IC_{50} values for futibatinib were up to 28.5 higher in the cell lines expressing the *FGFR2-AHCYL2* plus point mutations compared to the cells transfected with *FGFR2-AHCYL2* (Fig. 4b). In contrast, only slight effects on IC_{50} (1.9-fold change for FGFR2-*AHCYL2* plus p.V564F; 2.7-fold change for FGFR2-*AHCYL2* plus p.E565A compared to *FGFR-AHCYL2*) were noted for lenvatinib, with a clear inhibition of cell growth, especially at low concentrations. Ponatinib was still active in the presence of the p.V564F "gatekeeper-mutation" in our model, yet did not show an impact on the proliferation of cells with the *FGFR2-AHCYL2* plus p.E565A "brake-mutation" (Fig. 4a).

To further characterize the different response patterns of selective and multitargeted TKIs in the presence of resistance mutations, we performed a proteomic analysis of the *FGFR2-AHCYL2* plus p.V564F "gatekeeper mutation" harboring cell line. Interestingly, treatment with the multitargeted TKIs lenvatinib and ponatinib, as well as with the irreversible pan-FGFR inhibitor futibatinib, led to reduced phosphorylation of FGFR2 (Fig. 4c). In clear contrast, the p.V564F mutation prevented dephosphorylation of FGFR2 after infigratinib treatment (Fig. 4c). DigiWest analysis of downstream signaling pathways in infigratinib- or lenvatinib-treated cells demonstrated that lenvatinib could still inhibit the phosphorylation of non-MAPK signaling proteins, such as AKT (Ser473), mTOR (Ser2481 und Ser2448), p70S6K (Thr389), and eIF4E (Ser209), which are mainly involved in PI3K/AKT/mTOR signaling (Fig. 4d, e, Supplementary Fig. 5b, Supplementary Data 1). This was underlined by directly comparing the two treatments to each other. Lenvatinib exhibited a conserved inhibitory differential effect for phosphorylation of FGFR2 (Tyr653/Tyr654), mTOR (Ser2481), eIF4E (Ser209) as well as total mTOR (Fig. 4f, Supplementary Data 1). This not only underscores the differential effect on FGFR2 phosphorylation (see Fig. 4c) but also highlights the persistent inhibition of downstream pathways of lenvatinib, suggesting that the sustained activity of lenvatinib is likely due to conserved direct FGFR2 inhibition even in the presence of the p.V564F mutation.

In-silico modeling demonstrates a favorable interaction pattern of lenvatinib within the ATP-binding pocket of FGFR2

To gain more insight into the molecular interaction of lenvatinib with wild-type and mutated FGFR2, we performed in-silico modeling applying long time-scale (in total 48 µs) molecular dynamics (MD) simulations for wild-type FGFR2 and the three exemplarily selected mutations E565A, V564F, and N549K (Fig. 5a, b). Resulting trajectories were subjected to interaction analysis (Fig. 5c, Supplementary Tables 1–3), evaluation of binding free energy and its components with molecular mechanics energies combined with the generalized Born and surface area continuum solvation (MM-GBSA) (Supplementary Figs. 7–12), and TKIs study of torsional profiles (Supplementary Figs. 13–15).

First, we conducted an interaction analysis of the FGFR2 molecular brake, a regulatory element comprising a molecular triad of residues N549, E565, and K641, governing autoinhibition[44–48]. Despite previous indications of its significance in drug resistance, our investigation did not reveal notable differences in the interactions involving the molecular brake across selected TKIs (chemical structures are shown in Supplementary Figs. 13–15) and mutations (Supplementary Table 1). Hence, we observed that the molecular brake changes do not play a prominent role in our studied mutation-inhibitor combinations and omitted them from further investigation into this aspect.

Further analysis highlighted lenvatinib's prominent interaction engagement, excelling infigratinib and pemigatinib in both WT and mutant FGFR2 settings (Fig. 5c, Supplementary Table 2A and Suppl. Discussion). These observations suggest that lenvatinib possesses a dynamic ability to alter its interaction pattern in response to mutations, thus fine-tuning its binding to the evolving protein binding pocket. We extended these analyses to four further mutations that have been described in the context of therapy resistance to FGFR2-specific TKIs[21,35,44] or gain of function[44], namely N549D, V562L, V564I, and E565G (24 µs), which showed similar results (Supplementary Table 2B). This adaptability was further reflected in the prevalence of hydrophobic interactions, with lenvatinib displaying superior hydrophobic engagement compared to the other two TKIs (Supplementary Table 3). This observation was further supported by lenvatinib's leading ligand efficacy (Supplementary Fig. 7) and the MM-GBSA binding free energy components (Supplementary Figs. 8–12, Supplementary Discussion).

To unravel the basis of Lenvatinib's adaptability, we delved into the torsional profiles of the TKIs within the gate area and back cleft of

Article https://doi.org/10.1038/s41467-024-45247-6

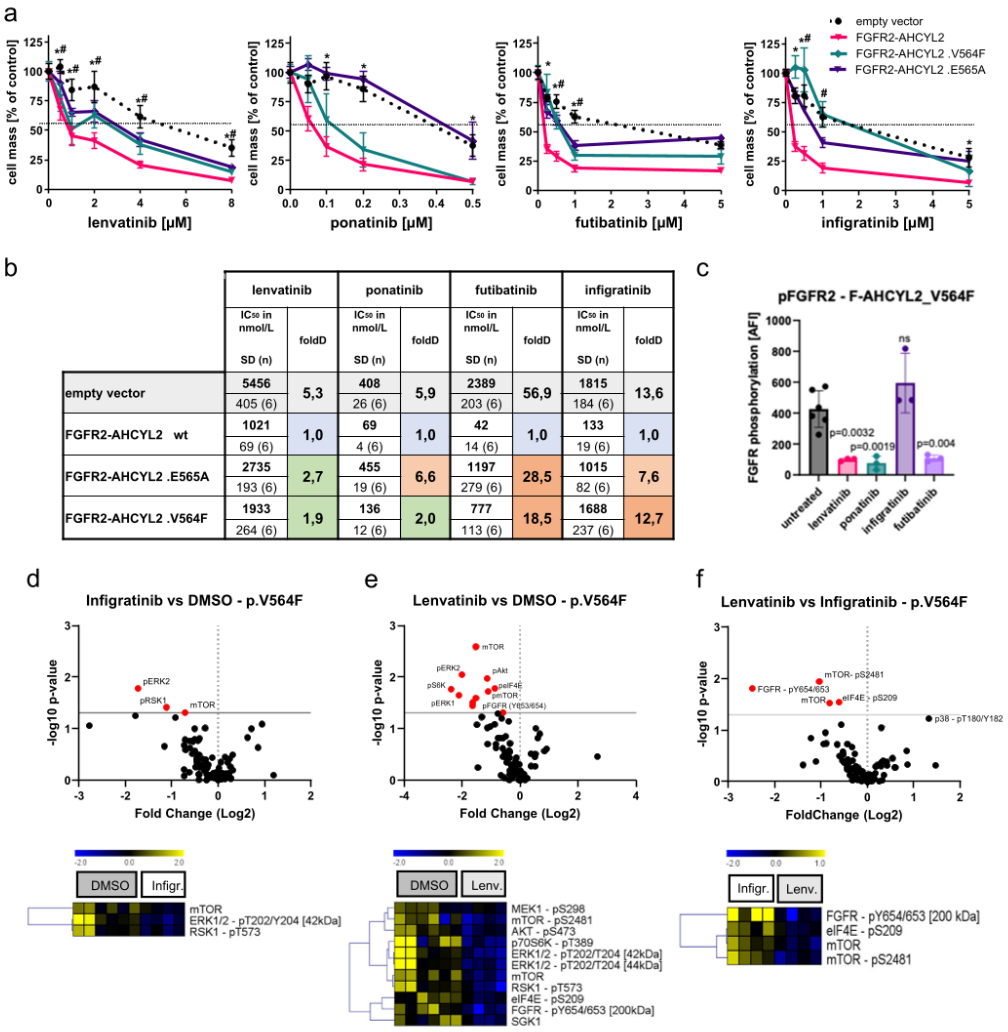

	lenvatinib		ponatinib		futibatinib		infigratinib	
	IC50 in nmol/L SD (n)	foldD	IC50 in nmol/L SD (n)	foldD	IC50 in nmol/L SD (n)	foldD	IC50 in nmol/L SD (n)	foldD
empty vector	5456 405 (6)	5,3	408 26 (6)	5,9	2389 203 (6)	56,9	1815 184 (6)	13,6
FGFR2-AHCYL2 wt	1021 69 (6)	1,0	69 4 (6)	1,0	42 14 (6)	1,0	133 19 (6)	1,0
FGFR2-AHCYL2 .E565A	2735 193 (6)	2,7	455 19 (6)	6,6	1197 279 (6)	28,5	1015 82 (6)	7,6
FGFR2-AHCYL2 .V564F	1933 264 (6)	1,9	136 12 (6)	2,0	777 113 (6)	18,5	1688 237 (6)	12,7

Fig. 4 | Non-selective and selective TKIs with FGFR2-inhibitory activity in the presence of resistance-mediating mutations. a Proliferation analyses using SRB assays in the NIH3T3 cell lines harboring *FGFR2-AHCYL2* fusions with either wild-type (WT), p.E565A, or p.V564F mutations in the kinase domain of the *FGFR2-AHCYL2* fusion. Cell lines were analyzed after 7 days of treatment with the indicated non-selective TKIs lenvatinib and ponatinib or the FGFR-selective TKIs infigratinib and futibatinib, $^{*}P \leq 0.05$ for FGFR2-AHCYL2 plus p.E565A vs empty vector control at the indicated drug dose, $\#P \leq 0.05$ for FGFR2-AHCYL2 plus p.V564F vs empty control at the indicated drug dose using two-way ANOVA with Tukey's multiple comparison test. Data are presented as mean ± SD ($n = 6$ independent experiments). **b** IC_{50} values and fold difference (foldD) of different drugs for NIH3T3 cells expressing the indicated construct in nmol/L ± SD and their respective percentage of the value for empty vector-transfected cells. Cell background gradient: green = lower foldD, red = higher foldD of IC_{50} compared to FGFR2-AHCYL2 wildtype cells. **c**–**e** DigiWest protein profiling of NIH3T3 cells expressing the p.V564F_*FGFR2-AHCYL2* fusion gene after treatment with selective or non-selective TKIs. The full DigiWest data set is included in the Supplementary Date file 1. **c** Phosphorylation status (accumulated fluorescence intensity) of FGFR (Y653/654) in p.V564F *FGFR2-AHCYL2* samples. Bars represent mean ± SD ($n = 6$ (untreated) and $n = 3$ (TKI-treated) biologically independent samples), One-Way-ANOVA with Dunnett's multiple comparison test. Volcano Plot and hierarchical cluster (HCL) analysis of proteins and phosphoproteins that significantly differed between (**d**) infigratinib-treated ($n = 4$ biologically independent samples), (**e**) lenvatinib-treated ($n = 4$ biologically independent samples) compared to control (DMSO, $n = 6$ biologically independent samples) or (**f**) lenvatinib- vs. infigratinib-treated ($n = 4$ biologically independent samples) p.V564F *FGFR2-AHCYL2* samples (two-sided T-test, Welch, $P \leq 0.05$).

 https://doi.org/10.1038/s41467-024-45247-6

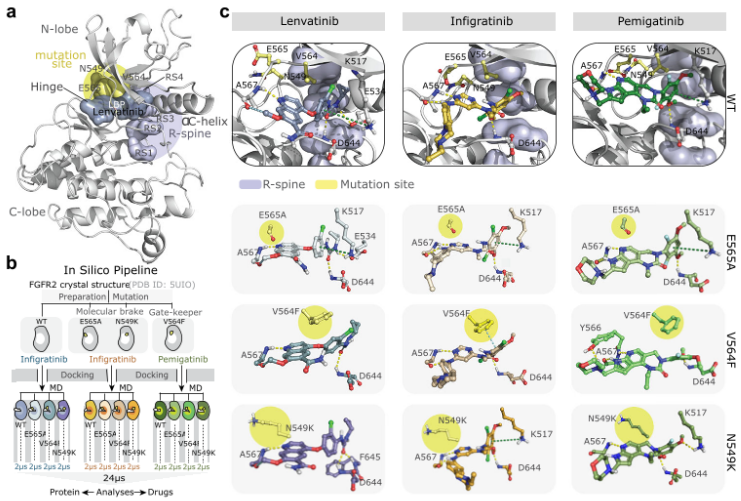

Fig. 5 | In-silico modeling suggests that lenvatinib adapts better to FGFR2 kinase mutations than infigratinib or pemigatinib. a Structure of wild-type FGFR2 kinase domain bound to lenvatinib in the ATP-binding cleft. The location of the mutations E565A, V564F, and N549K is shown in the yellow circle, lenvatinib is shown in blue and, the regulatory R-spine residues R1-R4 in violet; the R-spine is shown in assembled (active) conformation. **b** In-silico pipeline for analyses of the FGFR2 mutation impact on drug effectiveness. **c** Lenvatinib, infigratinib and pemigatinib interactions with wild-type FGFR2 and different mutants. The pictures show representative snapshots from Molecular Dynamics trajectories with contacts occurring in more than 20% of the simulation time (full data is available in Supplementary Table 2). Ligands are represented with stick models, colors of carbon atoms are as in **b**, and colors of the structural elements are as in **a**. Studied mutations are highlighted with yellow circles. A light blue dashed line represents π−π stacking, a green line represents π-cation, a yellow line represents H-bond, and a dark blue line represents aromatic H-bond.

FGFR2. Our analysis highlighted a dynamic flexibility of the lenvatinib terminal flexible cyclopropyl moiety in contrast to the more rigid terminal dimethoxyphenyl moiety of infigratinib and pemigatinib, which suggests that lenvatinib is sterically more flexible in the presence of FGFR2 mutations (Supplementary Figs. 13–15).

A more detailed description of the in-silico work is given in Supplementary Material, Results and Discussion. Taken together, these observations and the in vitro data reveal that lenvatinib can adapt better to FGFR2 mutations than the investigated FGFR-specific TKIs.

Lenvatinib overcomes resistance to pemigatinib in a patient with *FGFR2-BICC* N549K resistance mutation

Intrigued by these results, we treated a female patient with lenvatinib after development of progressive disease during a previous treatment with pemigatinib. Initially, the patient had a partial response to pemigatinib but developed hyperphosphatemia and additional side effects, such as complete hair loss and recurrent nailbed inflammations. Of note, during treatment with pemigatinib, also increased hepatic calcification (Supplementary Fig. 16) appeared as a phenomenon that had been previously described in a patient treated with infigratinib[27]. Unfortunately, the patient developed progressive disease after a PFS of 13 months during pemigatinib therapy.

A further biopsy of a liver lesion was then performed that revealed a *FGFR2* N549K brake mutation. We therefore started therapy with lenvatinib. Strikingly, a follow-up CT scan taken 29 days later showed a consistent shrinkage of all liver lesions accompanied by a considerable reduction of the rim enhancement (Fig. 6). Besides mild hypertension, no phosphate elevation occurred, the nailbed inflammations disappeared, and hair growth returned. Up to date, four further follow-up scans confirmed the ongoing effective partial response, showing an even more profound reduction of tumor manifestations, with some completely disappearing (Fig. 6).

Discussion

Protein kinase inhibitors have emerged as essential tools in the armamentarium to treat cancer, resulting in the approval of more than 70 new drugs since the first approval of imatinib in 2001[49]. Each drug has different pharmacological properties and individual kinase-inhibitory profiles that might be utilized to personalize TKI selection. Here, we describe a cohort of 7 patients with FGFR2-driven CCA that have been treated with the multikinase TKI lenvatinib as first line FGFR2 targeted therapy and one additional patient that was treated with lenvatinib after developing resistance to the treatment with the selective FGFR2 inhibitor pemigatinib.

In the 7 patients, the growth modulation index (GMI), which is based on the assumption that the time to progression tends to be shorter in each subsequent treatment line in advanced cancers[38,40,50–52], was analyzed as an intra-patient comparison of different treatment regimens. Of note, six of the seven patients treated with lenvatinib had a GMI value > 1.3 regarding the previous and even compared to the first-line therapy (Fig. 1a), suggesting lenvatinib to be efficient in this treatment setting. This observation was further supported by (i) PET-CT scans documenting metabolic responses during the first weeks of treatment and (ii) the comparison of the median PFS of 7.0 months for the treatment with lenvatinib to 2.1 months for the first-line treatment with Gem/Cis in this cohort.

One of the patients had an *FGFR2-AHCYL2* fusion, which to our knowledge has not been described so far, although *FGFR2-AHCYL1*, a structurally related fusion gene, was reported previously[13]. To characterize the fusion protein on the cellular level, we generated NIH3T3 cell lines to stably overexpress *FGFR2-AHCYL2*, *FGFR2-SH3GLB1*, or *FGFR2-BICC1*. All three fusions conferred enhanced proliferation, colony formation, or activation of the downstream targets FRS2, ERK1/2, and STAT3.

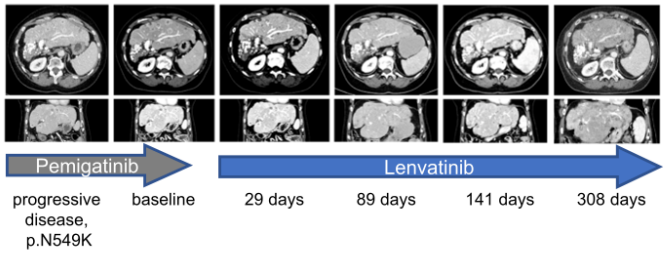

Fig. 6 | Lenvatinib leads to a partial response after progression to pemigatinib in the presence of the N549K resistance-mediating mutation. Axial contrast-enhanced CT of the liver in the portal-venous phase after progressive disease to pemigatinib in the presence of an N549K kinase mutation detected in a liver biopsy of a progressive lesion. From left to right: progressive disease during therapy with pemigatinib; baseline CT scan prior to lenvatinib; first follow-up scan 29 days later with consistent shrinkage of all liver lesions, accompanied by considerable reductions of the rim enhancement; second follow-up 89 days after the start of lenvatinib, showing a confirmation of the treatment responses with even more efficient reduction of tumor manifestations, some of them having completely disappeared; further confirmation of the ongoing response at days 141 and 308.

Interestingly, the clinical case with *FGFR2-AHCYL2* showed treatment responses to lenvatinib and infigratinib, but not to ponatinib or nintedanib (Fig. 1d). A comparison of the IC_{50} values of different FGFR-inhibitory drugs revealed an increased sensitivity for lenvatinib, ponatinib, infigratinib, and futibatinib in cells transfected with the fusion gene compared to control cells. In contrast, nintedanib showed only minor effects in fusion-positive cells. Whereas the cellular response to nintedanib might mirror the missing response during our patient's treatment, it cannot explain the absent response to ponatinib. Of note, this case illustrates several important features of FGFR2-addicted CCAs. First, FGFR2 can remain a relevant drug target despite progression during treatment. It is tempting to speculate that at the end of the patient's treatment, a FGFR inhibitor targeting most of the polyclonal resistance mutations would have led to a further clinical benefit. Second, no kinase mutation was detected after progression despite the treatment with lenvatinib for more than nine months. For lenvatinib, feedback activation of the EGFR-PAK2-ERK5 signaling axis has been described as a resistance mechanism in hepatocellular carcinoma[53]. Thus, other factors than kinase mutations might have to be considered after the progression of FGFR2-driven CCAs during therapy with lenvatinib.

One of our initial hypotheses was that the influence of resistance-mediating kinase mutations might be different between FGFR-selective and multikinase TKIs. To investigate this possibility, we selected two previously described point mutations in *FGFR2*: p.V564F and p.E565A. The valine residue in the drug-binding pocket of the kinase domain is conserved in FGFR1-4[25]. Amino acid substitutions at this gatekeeper position alter the mode of drug-FGFR interactions and are called gatekeeper mutations[22]. An autoinhibitory brake that is made up of three main residues, an asparagine (N), a glutamate (E), and a lysine (K), is called the NEK or molecular brake triad. Within FGFR2, this conformation is located at p.N549, p.E565, and p.K641[25]. As molecular brake residues mediate the autoinhibition of FGFR kinases, mutations in this region lead to constitutive kinase activation[22].

Cell viability assays surprisingly revealed that despite the presence of the p.V564F gatekeeper or the p.E565A mutations, lenvatinib significantly inhibited cell growth, even at low concentrations. Moreover, lenvatinib conferred inhibition of downstream targets in protein profiling analyses, besides typical FGFR2 downstream signaling pathways, which might be important in the context of treatment responses or acquisition of resistance and might be a beneficial additive consequence of the more unselective nature of lenvatinib. To gain further insights into mutation impact on drug binding, we applied an in-silico pipeline to model lenvatinib-, infigratinib-, and pemigatinib-FGFR2 bound systems, encompassing WT, N549K, N549D, E565A, E565G, V562L, V564F, and V564I mutations, followed by classical all-atom MD simulations. FGFR2 MD studies were previously reported in work by Sangeetha et al.[54]; however, with a total timescale of 48 μs in our work, we go far beyond the reported data. Our results suggest that lenvatinib's superior inhibitory performance occurs not only due to a more favorable interaction pattern but to a set of additional factors such as hydrophobic stabilization, increased flexibility of the lenvatinib in the gate area and back cleft and superior free energy ligand efficiency (for additional information see Supplementary Methods, Results and Discussion).

As an outcome of our work, we treated a patient after progression to the selective inhibitor pemigatinib and the development of a resistance mutation with lenvatinib, which revealed an impressive and, so far, durable response. Furthermore, as an additional clinically relevant observation, the class-specific side effects of pemigatinib, which limited the quality of life in that patient, subsided after the end of pemigatinib treatment and did not return during the treatment with lenvatinib. In contrast to the selective FGFR inhibitors infigratinib and pemigatinib, lenvatinib has a higher inhibition efficiency of FGFR2 than FGFR1 (see Supplementary Table 4). We hypothesize that this could be one reason for the different spectrum of adverse effects.

Our results stimulate hypotheses for exploratory studies that could guide the optimal inclusion of lenvatinib in the treatment algorithm of FGFR2-driven CCA, such as to compare the appearance of kinase resistance mutations during the treatment with lenvatinib or specific-FGFR inhibiting TKIs by repeated liquid biopsies or therapy responses despite the presence of resistance-mediating mutations.

In conclusion, we demonstrate the potential of the unspecific TKI lenvatinib, even at low doses, to treat CCA addicted to FGFR2 signaling even in the presence of resistance mutations. Our observations have several clinical implications. First, in the case of insurmountable characteristic adverse reactions of FGFR-specific TKIs, lenvatinib seems to be an efficient alternative. Second, our data suggest that due to its broader activity on intracellular signaling events and increased flexibility in the kinase pocket, lenvatinib can overcome and might prevent or delay the development of resistance-mediating FGFR2 mutations.

Methods

Patients

All presented patients were referred to the Molecular Tumor Board (MTB) at the University Hospital Tuebingen. The translational study was reviewed and approved by the local ethics committee of the medical faculty (714/2019BO2). Off-label treatments were recommended by the MTB, which consists of an interdisciplinary team including experts in clinical and translational oncology, pathology, bioinformatics, molecular biology, radiology, and human genetics[6]. All

patients gave written informed consent before treatment with lenvatinib. Before genetic tumor analysis, patients were consulted by a specialist in clinical genetics. Tumor genetic analysis [liquid biopsy, next generation sequencing (NGS), transcriptome or whole-exome sequencing (WES)] were performed by CeGaT GmbH, Tuebingen, the Institute of Medical Genetics and Applied Genomics, Tuebingen, or inside the Molecularly Aided Stratification for Tumor Eradication Research (MASTER) precision oncology program at the National Center for Tumor Diseases/German Cancer Consortium (NCT/DKTK), as previously described[6,55]. To assess treatment efficacy, CT or MRI scans were reviewed for complete (CR) and partial response (PR), stable disease (SD) or progressive disease (PD) by an experienced radiologist based on principles of RECIST version 1.1. criteria. Staging examinations were performed every 4–12 weeks.

Cell culture and chemicals

The NIH3T3 cell line was a kind gift by Wolfgang Neubert (Max Planck Institute for Biochemistry, Martinsried, Germany) and authenticated by ATCC using Short Tandem Repeats (STR). Cells were grown in a humidified atmosphere at 37 °C in 5% CO_2 in Dulbecco's Modified Eagle's Medium (DMEM)—high glucose (Sigma-Aldrich, Taufkirchen, Germany) complemented with 10% FBS and 1% penicillin-streptomycin (Thermo Fisher Scientific, Schwerte, Germany) and routinely tested for mycoplasma with a DAPI test. Futibatinib was purchased from Cayman Chemicals (Ann Arbor, MI, USA); all other TKIs and gemcitabine were purchased from Selleckchem (Houston, TX, USA).

Cloning strategy and stable transfection

The *FGFR2-AHCYL2*, *FGFR2-SH3GLB1*, and *FGFR2-BICC1* fusion genes were generated and cloned into the pcDNA3.1(+)P2A-eGFP vector by GenScript (New Jersey, U.S). GenScript used site-directed mutagenesis to introduce the p.V564F and p.E565A SNVs into the *FGFR2-AHCYL2* fusion. NIH3T3 cells were stably transfected with 2 μg of the linearized vectors using Effectene® transfection reagent (Qiagen, Hilden, Germany). Single clones were selected using Geneticin (G418 disulfate salt; Biochrom, Berlin, Germany). Empty pcDNA3.1(+)P2A-eGFP transfected NIH3T3 were used as control.

Western blot analysis

Primary antibodies are specified in Supplementary Table 5. To determine the relative protein abundance, densitometry of the total surface area of the respective bands was performed and normalized to the respective band of β-actin or vinculin using ImageJ. Preparation of cells and technical details are shown in Supplementary Methods.

Cell viability assay

For proliferation and IC_{50} measurements using different compounds, sulforhodamine B-assays (SRB) were performed as described in Supplementary Methods.

Soft agar colony formation assays

2000 cells were suspended in DMEM with 20% FBS and 0.35% Difco™ Noble Agar (BD Biosciences, Heidelberg, Germany) and the indicated substances. Subsequently, the cells were seeded in six-well plates plated with DMEM with 20% FBS with 0.7% Difco™ Noble Agar (BD Biosciences). After 21 days in culture, colonies were stained overnight using Iodonitrotetrazolium chloride (violet) (Sigma-Aldrich). Colonies were counted using Image J.

DigiWest multiplex protein analysis

DigiWest was performed as described previously[42] using 10–12 μg of cell lysate per sample. A detailed description of the DigiWest procedure is included in the Supplementary Methods. A scheme outlining the DigiWest workflow can be found in Supplementary Fig. 4, the employed antibodies are described in the Supplementary Data 1and the complete data set of all DigiWest investigations is included in the Supplementary Data 1. Signal quantification and analysis were performed using an Excel-based analysis tool. MEV 4.9.0 was used for heatmap generation and respective statistics (Welch´s T-Test, group comparison). For DigiWest Supplementary Figs. 4A/B, after correction for experimental variation, groups were compared to DMSO controls using Welch´s ANOVA with Dunnett´s Multiple Comparisons Test.

In-silico modeling

Preparation of FGFR2 WT, N549K, N549D, E565A, E565G, V562L, V564F, and V564I systems. At the time of the analysis 47 FGFR2 structures were available in the RCSB Protein Data Bank with 31 containing the kinase domain (https://www.rcsb.org, accessed 13/07/2022). The crystal structure used for the modeling was FGFR2 harboring an E565A/K659M double mutation (PDB ID: 5UIO[56]) with the resolution of 2.05 Å, comprising 324 amino acids. As E565A was of interest, we reversed the K659M mutation using Maestro (2021.3) with further hydrogen bond assignment and energy minimization with Protein Preparation Wizard[57] (Maestro 2021.3, Schrödinger LLC, New York, NY, USA). The rotamer position of the reversed K659 residue was checked from the wild-type FGFR2 crystal structure (PDB ID: 2PVF[44]). To maintain the consistency in system preparation and annihilate potential artificial errors in further system comparisons, we subsequently reversed the E565A mutation. In the obtained wild-type FGFR2 we introduced separately N549K, N549D, E565A, E565G, V562L, V564F, and V564I mutations, followed by hydrogen bonds and energy minimization with the same protocol as above. The rotamer position of gatekeeper V564F mutation was comparable to those in the corresponding crystal (PDB ID: 7KIA[58]), the FGFR2 N549K, N549D, V564I crystal structure has not been solved to date.

Docking of lenvatinib, infigratinib and pemigatinib in prepared FGFR2 systems. To generate the grid for further docking, we aligned the FGFR1–lenvatinib crystal structure (PDB ID: 5ZV2[59]) with our newly generated WT model. FGFR1 and FGFR2 share 87% sequence similarity in the kinase domain, which refers to comparable ligand position inside the ligand-binding pocket. After superimposing, the FGFR1 structure was deleted and the remaining lenvatinib in the binding pocket was used for SiteMap[60,61] binding site evaluation. 5 Å buffer distance from lenvatinib with more restrictive definition of hydrophobicity was used for evaluation. The output from SiteMap was used for the receptor grid generation with Glide[62–64].

Lenvatinib, infigratinib and pemigatinib were prepared using LigPrep (Schrödinger Release 2021-3: LigPrep, Schrödinger, LLC, New York, NY, 2021; default settings) to generate the 3D conformation of the compounds, their ionization states to pH 7.0 ± 1.0, and calculate their charges. Subsequently, prepared ligands were docked into the FGFR2 WT, N549K, N549D, E565A, E565G, V562L, V564F, and V564I model using Glide[62,64] (default settings, XP-accuracy). To validate model precision, post-docking validation of infigratinib pose was made by comparison to the co-crystallized FGFR1–infigratinib complex (PDB ID: 3TT0[65]); crystal structures encompassing pemigatinib have not been solved to date.

Detailed information on Molecular Dynamics Simulations, interaction analysis and MM-GBSA energy calculations are given in the Supplementary Methods section (Supplementary Methods, Results and Discussion).

FGFR2-binding site residues definition. Definitions of FGFR2-binding site regions were obtained from the KLIFS database[66].

Data visualization. Results were plotted with Seaborn library for Python[67]. Protein structures were visualized with PyMOL (PyMOL Molecular Graphics System, Version 2.5.2 Schrödinger, LLC.) Graphical representations of figures were arranged using Adobe Illustrator©.

Statistical analysis

Data were analyzed using GraphPad Prism 7 and 9 (GraphPad Software Inc, CA, US) and are shown as mean ± standard deviation (SD). Statistical analysis was performed using unpaired, two-tailed Student's *t* test and one-way ANOVA as appropriate, unless stated otherwise. IC_{50} values were generated using nonlinear regression analysis (dose-response inhibition) by comparing the inhibitor with a normalized response assuming a variable slope. All experiments were independently performed at least three times, and $P < 0.05$ was accepted for statistical significance.

Reporting summary

Further information on research design is available in the Nature Portfolio Reporting Summary linked to this article.

Data availability

The in-silico data generated in this study have been deposited in the Zenodo database (https://zenodo.org/records/7456830) The authors declare that all data supporting the findings of this study are available within the Article, Supplementary Information, or Source Data file. Source data are provided with this paper. Our ethical approval does not allow the complete upload of the results from patient DNA sequencing. All relevant information from the DNA sequencing are included in the manuscript. Source data are provided with this paper.

References

1. Banales, J. M. et al. Cholangiocarcinoma 2020: the next horizon in mechanisms and management. *Nat. Rev. Gastroenterol. Hepatol.* **17**, 557–588 (2020).
2. Rizvi, S., Khan, S. A., Hallemeier, C. L., Kelley, R. K. & Gores, G. J. Cholangiocarcinoma—evolving concepts and therapeutic strategies. *Nat. Rev. Clin. Oncol.* **15**, 95–111 (2018).
3. Valle, J. W., Kelley, R. K., Nervi, B., Oh, D. Y. & Zhu, A. X. Biliary tract cancer. *Lancet* **397**, 428–444 (2021).
4. Valle, J. et al. Cisplatin plus gemcitabine versus gemcitabine for biliary tract cancer. *N. Engl. J. Med.* **362**, 1273–1281 (2010).
5. Valle, J. W., Lamarca, A., Goyal, L., Barriuso, J. & Zhu, A. X. New Horizons for Precision Medicine in Biliary Tract Cancers. *Cancer Discov.* **7**, 943–962 (2017).
6. Bitzer, M., et al. Next-Generation Sequencing of Advanced GI Tumors Reveals Individual Treatment Options. *JCO Precis. Oncol.*, **4**, 258–271 (2020).
7. O'Rourke, C. J., Munoz-Garrido, P. & Andersen, J. B. Molecular Targets in Cholangiocarcinoma. *Hepatology* **73**, 62–74 (2021).
8. Personeni, N. et al. Biliary Tract Cancers: Molecular Heterogeneity and New Treatment Options. *Cancers* **12**, 3370 (2020).
9. Malenica, I., Donadon, M. & Lleo, A. Molecular and Immunological Characterization of Biliary Tract Cancers: A Paradigm Shift Towards a Personalized Medicine. *Cancers* **12**, 2190 (2020).
10. Kam, A. E., Masood, A. & Shroff, R. T. Current and emerging therapies for advanced biliary tract cancers. *Lancet Gastroenterol. Hepatol.* **6**, 956–969 (2021).
11. Sia, D. et al. Massive parallel sequencing uncovers actionable FGFR2-PPHLN1 fusion and ARAF mutations in intrahepatic cholangiocarcinoma. *Nat. Commun.* **6**, 6087 (2015).
12. Banales, J. M. et al. Expert consensus document: Cholangiocarcinoma: current knowledge and future perspectives consensus statement from the European Network for the Study of Cholangiocarcinoma (ENS-CCA). *Nat. Rev. Gastroenterol. Hepatol.* **13**, 261–280 (2016).
13. Arai, Y. et al. Fibroblast growth factor receptor 2 tyrosine kinase fusions define a unique molecular subtype of cholangiocarcinoma. *Hepatology* **59**, 1427–1434 (2014).
14. Lowery, M. A. et al. Comprehensive Molecular Profiling of Intrahepatic and Extrahepatic Cholangiocarcinomas: Potential Targets for Intervention. *Clin. Cancer Res.* **24**, 4154–4161 (2018).
15. Graham, R. P. et al. Fibroblast growth factor receptor 2 translocations in intrahepatic cholangiocarcinoma. *Hum. Pathol.* **45**, 1630–1638 (2014).
16. Hoy, S. M. Pemigatinib: First Approval. *Drugs* **80**, 923–929 (2020).
17. Kang, C. Infigratinib: First Approval. *Drugs* **81**, 1355–1360 (2021).
18. Cleary, J. M. et al. FGFR2 Extracellular Domain In-Frame Deletions are Therapeutically Targetable Genomic Alterations that Function as Oncogenic Drivers in Cholangiocarcinoma. *Cancer Discov.* **11**, 2488–2505 (2021).
19. Abou-Alfa, G. K. et al. Pemigatinib for previously treated, locally advanced or metastatic cholangiocarcinoma: a multicentre, open-label, phase 2 study. *Lancet Oncol.* **21**, 671–684 (2020).
20. Javle, M. et al. Infigratinib (BGJ398) in previously treated patients with advanced or metastatic cholangiocarcinoma with FGFR2 fusions or rearrangements: mature results from a multicentre, open-label, single-arm, phase 2 study. *Lancet Gastroenterol. Hepatol.* **6**, 803–815 (2021).
21. Goyal, L. et al. Futibatinib for FGFR2-Rearranged Intrahepatic Cholangiocarcinoma. *N. Engl. J. Med.* **388**, 228–239 (2023).
22. Katoh M. Fibroblast growth factor receptors as treatment targets in clinical oncology. *Nat. Rev. Clin. Oncol.* **16**, 105–122 (2018).
23. Farrell, B. & Breeze, A. L. Structure, activation and dysregulation of fibroblast growth factor receptor kinases: perspectives for clinical targeting. *Biochem Soc. Trans.* **46**, 1753–1770 (2018).
24. Bitzer, M. et al. Targeting extracellular and juxtamembrane FGFR2 mutations in chemotherapy-refractory cholangiocarcinoma. *npj Precis. Oncol.* **5**, 80 (2021).
25. Roskoski, R. Jr. The role of fibroblast growth factor receptor (FGFR) protein-tyrosine kinase inhibitors in the treatment of cancers including those of the urinary bladder. *Pharm. Res.* **151**, 104567 (2020).
26. Dai, S., Zhou, Z., Chen, Z., Xu, G. & Chen, Y. Fibroblast Growth Factor Receptors (FGFRs): Structures and Small Molecule Inhibitors. *Cells* **8**, 614 (2019).
27. King, G. & Javle, M. FGFR Inhibitors: Clinical Activity and Development in the Treatment of Cholangiocarcinoma. *Curr. Oncol. Rep.* **23**, 108 (2021).
28. Borad, M. J. et al. Integrated genomic characterization reveals novel, therapeutically relevant drug targets in FGFR and EGFR pathways in sporadic intrahepatic cholangiocarcinoma. *PLoS Genet* **10**, e1004135 (2014).
29. Yamamoto, Y. et al. Lenvatinib, an angiogenesis inhibitor targeting VEGFR/FGFR, shows broad antitumor activity in human tumor xenograft models associated with microvessel density and pericyte coverage. *Vasc. Cell* **6**, 18 (2014).
30. Bahleda, R. et al. Multicenter Phase I Study of Erdafitinib (JNJ-42756493), Oral Pan-Fibroblast Growth Factor Receptor Inhibitor, in Patients with Advanced or Refractory Solid Tumors. *Clin. Cancer Res.* **25**, 4888–4897 (2019).
31. Mazzaferro, V. et al. Derazantinib (ARQ 087) in advanced or inoperable FGFR2 gene fusion-positive intrahepatic cholangiocarcinoma. *Br. J. Cancer* **120**, 165–171 (2019).
32. Kommalapati, A., Tella, S. H., Borad, M., Javle, M. & Mahipal, A. FGFR Inhibitors in Oncology: Insight on the Management of Toxicities in Clinical Practice. *Cancers* **13**, 2968 (2021).
33. Mahipal, A., Tella, S. H., Kommalapati, A., Yu, J. & Kim, R. Prevention and treatment of FGFR inhibitor-associated toxicities. *Crit. Rev. Oncol. Hematol.* **155**, 103091 (2020).
34. Goyal, L. et al. Polyclonal Secondary FGFR2 Mutations Drive Acquired Resistance to FGFR Inhibition in Patients with FGFR2 Fusion-Positive Cholangiocarcinoma. *Cancer Discov.* **7**, 252–263 (2017).

35. Goyal, L. et al. TAS-120 Overcomes Resistance to ATP-Competitive FGFR Inhibitors in Patients with FGFR2 Fusion-Positive Intrahepatic Cholangiocarcinoma. *Cancer Discov.* **9**, 1064–1079 (2019).
36. Silverman, I. M. et al. Clinicogenomic Analysis of FGFR2-Rearranged Cholangiocarcinoma Identifies Correlates of Response and Mechanisms of Resistance to Pemigatinib. *Cancer Discov.* **11**, 326–339 (2021).
37. Krook, M. A. et al. Efficacy of FGFR Inhibitors and Combination Therapies for Acquired Resistance in FGFR2-Fusion Cholangiocarcinoma. *Mol. Cancer Ther.* **19**, 847–857 (2020).
38. Von Hoff, D. D. There are no bad anticancer agents, only bad clinical trial designs-twenty-first Richard and Hinda Rosenthal Foundation Award Lecture. *Clin. Cancer Res.* **4**, 1079–1086 (1998).
39. Rodon, J. et al. Genomic and transcriptomic profiling expands precision cancer medicine: the WINTHER trial. *Nat. Med.* **25**, 751–758 (2019).
40. Von Hoff, D. D. et al. Pilot study using molecular profiling of patients' tumors to find potential targets and select treatments for their refractory cancers. *J. Clin. Oncol.* **28**, 4877–4883 (2010).
41. Sicklick, J. K. et al. Molecular profiling of cancer patients enables personalized combination therapy: the I-PREDICT study. *Nat. Med.* **25**, 744–750 (2019).
42. Treindl, F. et al. A bead-based western for high-throughput cellular signal transduction analyses. *Nat. Commun.* **7**, 12852 (2016).
43. Krook, M. A. et al. Fibroblast growth factor receptors in cancer: genetic alterations, diagnostics, therapeutic targets and mechanisms of resistance. *Br. J. Cancer* **124**, 880–892 (2021).
44. Chen, H. et al. A molecular brake in the kinase hinge region regulates the activity of receptor tyrosine kinases. *Mol. Cell* **27**, 717–730 (2007).
45. Hu, J. et al. Kinase regulation by hydrophobic spine assembly in cancer. *Mol. Cell Biol.* **35**, 264–276 (2015).
46. Kornev, A. P., Taylor, S. S. & Ten Eyck, L. F. A helix scaffold for the assembly of active protein kinases. *Proc. Natl Acad. Sci. USA* **105**, 14377–14382 (2008).
47. Taylor, S. S. & Kornev, A. P. Protein kinases: evolution of dynamic regulatory proteins. *Trends Biochem Sci.* **36**, 65–77 (2011).
48. Meharena, H. S. et al. Deciphering the structural basis of eukaryotic protein kinase regulation. *PLoS Biol.* **11**, e1001680 (2013).
49. Cohen, P., Cross, D. & Janne, P. A. Kinase drug discovery 20 years after imatinib: progress and future directions. *Nat. Rev. Drug Discov.* **20**, 551–569 (2021).
50. Bailey, C. H. et al. Progression-free Survival Decreases with Each Subsequent Therapy in Patients Presenting for Phase I Clinical Trials. *J. Cancer* **3**, 7–13 (2012).
51. Cousin, S. et al. Correlation between overall survival and growth modulation index in pre-treated sarcoma patients: a study from the French Sarcoma Group. *Ann. Oncol.* **24**, 2681–2685 (2013).
52. Massard, C. et al. High-Throughput Genomics and Clinical Outcome in Hard-to-Treat Advanced Cancers: Results of the MOSCATO 01 Trial. *Cancer Discov.* **7**, 586–595 (2017).
53. Jin, H. et al. EGFR activation limits the response of liver cancer to lenvatinib. *Nature* **595**, 730–734 (2021).
54. Sangeetha, R., Arockia Jeya Yasmi Prabha, E., Lakshmi, A., Sangavi, P. & Langeswaran, K. Molecular docking and dynamic simulations of Ocimum basilicum compounds against HCC and structural, vibrational, quantum, and chemical investigation of campesterol. *J. Biomol. Struct. Dyn.* **40**, 13997–14012 (2022).
55. Horak, P. et al. Comprehensive Genomic and Transcriptomic Analysis for Guiding Therapeutic Decisions in Patients with Rare Cancers. *Cancer Discov.* **11**, 2780–2795 (2021).
56. Chen, H. et al. Elucidation of a four-site allosteric network in fibroblast growth factor receptor tyrosine kinases. *Elife* **6**, e21137 (2017).
57. Sastry, G. M., Adzhigirey, M., Day, T., Annabhimoju, R. & Sherman, W. Protein and ligand preparation: parameters, protocols, and influence on virtual screening enrichments. *J. Comput Aided Mol. Des.* **27**, 221–234 (2013).
58. Brawn, R. A. et al. Discovery of Aminopyrazole Derivatives as Potent Inhibitors of Wild-Type and Gatekeeper Mutant FGFR2 and 3. *ACS Med Chem. Lett.* **12**, 93–98 (2021).
59. Matsuki, M. et al. Lenvatinib inhibits angiogenesis and tumor fibroblast growth factor signaling pathways in human hepatocellular carcinoma models. *Cancer Med.* **7**, 2641–2653 (2018).
60. Halgren, T. A. Identifying and characterizing binding sites and assessing druggability. *J. Chem. Inf. Model* **49**, 377–389 (2009).
61. Halgren, T. New method for fast and accurate binding-site identification and analysis. *Chem. Biol. Drug Des.* **69**, 146–148 (2007).
62. Friesner, R. A. et al. Extra precision glide: docking and scoring incorporating a model of hydrophobic enclosure for protein-ligand complexes. *J. Med Chem.* **49**, 6177–6196 (2006).
63. Friesner, R. A. et al. Glide: a new approach for rapid, accurate docking and scoring. 1. Method and assessment of docking accuracy. *J. Med Chem.* **47**, 1739–1749 (2004).
64. Halgren, T. A. et al. Glide: a new approach for rapid, accurate docking and scoring. 2. Enrichment factors in database screening. *J. Med Chem.* **47**, 1750–1759 (2004).
65. Guagnano, V. et al. Discovery of 3-(2,6-dichloro-3,5-dimethoxy-phenyl)–1-{6-[4-(4-ethyl-piperazin-1-yl)-phenylamin o]-pyrimidin-4-yl}–1-methyl-urea (NVP-BGJ398), a potent and selective inhibitor of the fibroblast growth factor receptor family of receptor tyrosine kinase. *J. Med. Chem.* **54**, 7066–7083 (2011).
66. Kanev, G. K., de Graaf, C., Westerman, B. A., de Esch, I. J. P. & Kooistra, A. J. KLIFS: an overhaul after the first 5 years of supporting kinase research. *Nucleic Acids Res.* **49**, D562–D569 (2021).
67. Waskom M. seaborn: statistical data visualization. *J. Open Source Softw.* **6**, 3021 (2021).

Acknowledgements

Authors were supported by the German Research Foundation (DFG) grant SFB/TR 209 (M.B, K.S.O. and N.P.M.), Else Kröner-Fresenius Foundation (Else Kröner Forschungskolleg Tubingen (2015_Kolleg_14), S.S. and M.B), German Cancer Aid (70114571, S.S.), the Forum Gesundheitsforschung of the Baden-Württemberg State Ministry of Science, Research and Arts (32-5400/58/2, M.B. and K.S.O.), the Ministry of Baden-Württemberg for Economic Affairs, Labor and Tourism (3-4332.62-HSG/84, A.S. and M.T.) and the German Ministry for Education and Research (eMed, Multiscale HCC (FKZ 01ZX1601G) to M.B. and N.P.M.). We acknowledge support from the Open Access Publication Fund of the University of Tübingen.

Author contributions

S.S. and M.B. conceived and designed the study. S.S., F.K., Y.R., C.G. and K.C.B. conducted in vitro experiments. S.S. F.K. and M.B. analyzed data and performed statistical analyses. A.S. and M.T. performed and analyzed DigiWest experiments. K.R., M.K., H.S-M. and S.B. conducted patient data and sample collection as well as medical evaluation and analysis. M.H. evaluated the radiologic responses. E.S., T.K., S.A.L. and A.P. performed and analyzed the in-silico modeling. S.S. and M.B. wrote the first draft of the manuscript. E.S., K.S-O., N.P.M. and A.P. contributed to data interpretation and manuscript edit. All authors critically reviewed and approved the manuscript.

Funding

Open Access funding enabled and organized by Projekt DEAL.

Competing interests

M.B. reports that he received compensations as a member of scientific advisory boards of Roche Pharma AG, Incyte Biosciences Germany

GmbH, Bayer Vital GmbH, Bristol-Myers Squibb, MSD Sharp & Dome, Taiho oncology Europe, outside the submitted work. The remaining authors declare no potential conflicts of interest.

Additional information

Supplementary information The online version contains supplementary material available at https://doi.org/10.1038/s41467-024-45247-6.

Correspondence and requests for materials should be addressed to Stephan Spahn or Michael Bitzer.

Peer review information *Nature Communications* thanks the anonymous reviewers for their contribution to the peer review of this work. A peer review file is available.

Reprints and permissions information is available at http://www.nature.com/reprints

Publisher's note Springer Nature remains neutral with regard to jurisdictional claims in published maps and institutional affiliations.

[1]Department of Internal Medicine I, University Hospital Tuebingen, 72076 Tuebingen, Germany. [2]Department of Pharmaceutical and Medicinal Chemistry, Institute of Pharmaceutical Sciences, Eberhard-Karls-University, 72076 Tuebingen, Germany. [3]Tuebingen Center for Academic Drug Discovery & Development (TüCAD2), 72076 Tuebingen, Germany. [4]NMI Natural and Medical Sciences Institute at the University of Tuebingen, 72770 Reutlingen, Germany. [5]Center for Personalized Medicine, Eberhard-Karls University, 72076 Tuebingen, Germany. [6]CeGaT GmbH and Praxis für Humangenetik, 72076 Tuebingen, Germany. [7]Cluster of Excellence, Image Guided and Functionally Instructed Tumor Therapies, Eberhard-Karls University, 72076 Tuebingen, Germany. [8]Department of Diagnostic and Interventional Radiology, Eberhard-Karls University, 72076 Tuebingen, Germany. [9]Department of Molecular Medicine, Interfaculty Institute for Biochemistry, Eberhard-Karls University, 72076 Tuebingen, Germany. [10]German Cancer Consortium (DKTK) and German Cancer Research Center (DKFZ), 69120 Heidelberg, Germany. [11]M3-Research Center for Malignome, Metabolome and Microbiome, Eberhard-Karls University, 72076 Tuebingen, Germany. [12]School of Pharmacy, University of Eastern Finland, 70210 Kuopio, Finland. [13]These authors contributed equally: Stephan Spahn, Fabian Kleinhenz. ✉e-mail: stephan.spahn@med.uni-tuebingen.de; michael.bitzer@uni-tuebingen.de

Supplementary Information

Here, only the Supplementary Information related to this manuscript which is discussed in this thesis is presented (Supplementary Figure 5).

The entire Supplementary Information is available at Nature Communications (https://doi.org/10.1038/s41467-024-45247-6).

Supplementary Figure 5

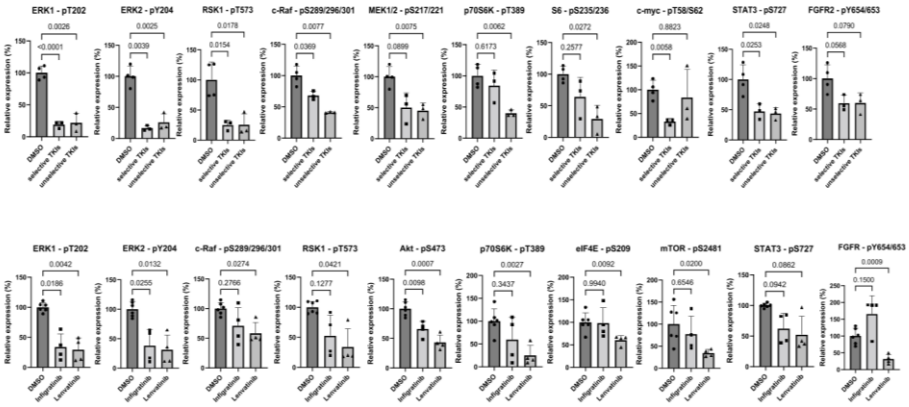

Effect of selective and unselective FGFR2 inhibiting TKIs on selected downstream targets on key downstream phosphorylation events: DigiWest analysis of selected downstream targets in (A) F-AHCYL2 WT and (B) F-AHCYL2_p.V564F cells. Data are shown relative to their respective control and each condition was compared to DMSO using Welch´s ANOVA with Dunnett´s Multiple Comparisons. Bars represent mean ± SD, n = 4 (DMSO) and n =3 (selective and unselective TKIs) biologically independent samples for F-AHCYL2 WT cells and n = 6 (DMSO) and n = 4 (infigratinib and lenvatinib) biologically independent samples for F-AHCYL2_p.V564F cells

Appendix 2

Stahl, A., Büringer, K., Missios, P., Hoffmann, T., Singer, S., Schäfer-Ruoff, F., Schenke-Layland, K., Malek, N. P., Bitzer, M., Templin, M. F. Personalized signaling pathway analysis of gastrointestinal tumors for patient stratification and drug target evaluation using clinically derived core biopsies.

This manuscript is currently in revision at npj Precision Oncology.

Personalized signaling pathway analysis of gastrointestinal tumors for patient stratification and drug target evaluation using clinically derived core biopsies

Aaron Stahl[1,2], Karsten Büringer[3], Pavlos Missios[3,4], Tatjana Hoffmann[3], Stephan Singer[5], Felix Schäfer-Ruoff[1], Katja Schenke-Layland[1,2], Nisar P. Malek[3,4,6], Michael Bitzer[3,4,6]*, Markus F. Templin[1]*

1 NMI Natural and Medical Sciences Institute at the University of Tübingen, Reutlingen, Germany

2 Institute of Biomedical Engineering, Department for Medical Technologies and Regenerative Medicine, University of Tübingen, Tübingen, Germany

3 Department of Internal Medicine I, University Hospital Tübingen, Tübingen, Germany

4 Center for Personalized Medicine, Eberhard-Karls University, Tübingen, Germany

5 Department of Pathology and Neuropathology, University Hospital Tübingen, Tübingen, Germany

6 Cluster of Excellence, Image Guided and Functionally Instructed Tumor Therapies, Eberhard-Karls University, Tübingen, Germany

*Shared Senior Authorship / Correspondence

Keywords: DigiWest, cellular signal transduction, gastrointestinal tumors, personalized medicine, drug targets

Contact:

Dr. Markus F. Templin

Head Assay Development

NMI Natural and Medical Sciences Institute at the University of Tübingen

Markwiesenstraße 55

72770 Reutlingen, Germany

Phone +49 7121 51530-828

Fax +49 7121 51530-816

markus.templin@nmi.de

Prof. Dr. med. Michael Bitzer

Department of Internal Medicine I

Eberhard-Karls University

Otfried-Müller-Str. 10

34 72076 Tübingen, Germany
35 Phone +49 7071 2985415
36 Fax +49 7071 29 4402
37 m.bitzer@med.uni-tuebingen.de

1. Abstract

Aberrant cellular signaling is a major driving factor in cancer development and progression. Therefore, precisely characterizing regulatory alterations in signal transduction pathways in individual tumors provides critical insights on a personalized basis. Clinically, detailed understanding of the activation status of signaling proteins and pathways can complement genetic and histological analyses, enhancing the evaluation of therapeutic options. In this study, we employed the high-throughput Western Blot system DigiWest for the proteomic characterization of gastrointestinal tumors, both in a retrospective study and in a proof-of concept, direct clinical application.

Retrospective analysis of primary pancreatic and colorectal carcinoma tissues, compared to matched normal tissues, revealed protein expression and activation patterns corresponding to clinically relevant subgroups. The pathway analysis enabled (i) the differentiation between squamous and immunogenic subtypes of pancreatic tumors, (ii) early/late-onset of disease and (iii) right/left-sided colorectal carcinomas. Protein profiles generated for individual tumors indicated drug-targetable alterations in cellular signaling pathways, demonstrating DigiWest's capability to accurately analyze tumor tissue with high clinical and molecular heterogeneity.

In the proof-of-concept direct clinical application, we analyzed single core needle biopsies from 14 patients with various gastrointestinal tumors who underwent Molecular Tumor Board presentation. The proteomic data enabled the identification of treatment-relevant, personalized pathway activity patterns, and overlaps with existing genetic mutation analyses and drug recommendations were evaluated. Our findings highlight the value of personalized signaling pathway analysis as a complementary confirmatory tool to sequencing analyses, demonstrating its suitability as a method for personalized protein analytics in clinical diagnostics and treatment evaluation within precision oncology settings.

2. Introduction

Our mechanistic understanding of cancer is heavily reliant on the identification of aberrantly regulated signaling pathways, as tumor-acquired genetic aberrations (e.g. point mutations, deletions, amplifications, gene fusions or CNVs) manifest as changes in pathway activity on the protein level. In light of this, signal-transducing proteins have become a primary target for therapeutic intervention [1]. Especially in the age of personalized medicine, the identification of pathway-based activity patterns can not only serve as a basis for patient stratification within and across various tumor entities but also opens opportunities for individualized tumor characterization and personalized treatment evaluation. In recent decades, a large variety of drugs have been developed targeting various pathways such as MAPK [2], PI3K/Akt/mTOR [3, 4], or cell cycle regulation [5] as well as upstream tyrosine kinase receptors including EGFR [6], FGFR [7, 8], VEGFR [9] or Her2 [10]. With regulatory approval of such drugs (as mono- or combination therapies) along with immunotherapeutic approaches [11-13] for use across tumor entities [14], clinical oncologists now have a vast array of treatment options available, including the potential of off-label therapies. At the same time, significant progress in sequencing technologies and genome profiling [15, 16] has made genetic mutation analyses a key tool for translational oncology programs (e.g. molecular tumor boards). However, with increasing complexity in genome profiling, clinical interpretation and thus identification of potential tumor drivers has also become more challenging [17]. Selecting the most suitable therapeutic option in each individual case is crucial, especially for patients with recurring tumor or diagnoses at advanced disease stages. In recent years, the transfer of personalized approaches into clinical application have mainly focused on genetic mutation analyses. However, pathway activity changes ultimately manifest on the proteome level rendering the implementation of personalized proteomic approaches especially crucial. To do so – and given the complexity of signaling networks – insight into protein expression and posttranslational modification (e.g. phosphorylation, methylation, acetylation) is required at a large scale. Many protein analytics methods such as standard and multiplexed immunohistochemistry [18, 19], Reverse-Phase Protein Arrays (RPPA) [20] and Mass Spectrometry either lack the throughput required for extensive

signaling pathway analysis and/or demand high sample amounts [21]. These crucial drawbacks leave proteomic methods still heavily underrepresented in clinical practice. Thus, proteomic analysis of molecular drug targets and cellular signaling entails a promising approach for individualized tumor profiling and subsequent treatment evaluation.

Gastrointestinal (GI) cancers encompass some of the most common and lethal forms of cancer including pancreatic and colorectal carcinomas. Alike other GI tumors (e.g. esophagus, liver, stomach, gallbladder) they are often diagnosed at advances stages and treatment options remain limited [22], thus leaving an urgent need for novel, personalized therapy approaches. Commonly altered signaling pathways in pancreatic, colorectal and other GI cancers for instance include MAPK/Erk, PI3K/mTOR/Akt, TGF beta/Smad, Wnt/beta-catenin, Notch or Jak/STAT signaling [23, 24]. At the genome level, most pancreatic carcinomas (> 90 %) harbor mutations in the KRAS oncogene [25]; other commonly mutated genes are the tumor-suppressors TP53, SMAD4 and CDKN2A [26] as well as various tyrosine kinase receptors [27]. Common mutations in colon tumors include EGFR, KRAS, PIK3CA, PTEN and TGFBR1/2 [28]. Loss of the Wnt regulator APC is also observed in 80 % of cases [29]. Despite several of these genetic traits being shared among tumors of the same tissue, both pancreatic and colorectal cancers (as well as other GI tumors) are highly heterogenous. This substantial inter-tumor and inter-patient variability brings about wide-spread tumor behaviors and characteristics affecting therapy response, treatment resistance and patient outcome [22, 30], thus making personalized medicine approaches especially suitable for this class of malignancies. Given the complexity of signaling networks and the fact that their activation status distinguishes true from potential tumor drivers, this calls for the integration of intracellular signal transduction analysis as it may define individualized treatment options and stratify patients beyond the capabilities of genetic and transcriptomic analysis. The DigiWest is a high-throughput Western Blot variation, which allows concomitant detection of up to 200 proteins and phosphorylated protein variants from minimal amount of sample while retaining the sensitivity of classical Western Blotting [31]. It has previously been employed for signal transduction analysis of both cellular *in vitro* cancer models and primary tumor tissue [32-36], for instance for the

expression-based stratification of mamma carcinomas based on immune-cell-related protein signatures [37].

Here, we have developed an antibody panel tailored to the analysis of gastrointestinal tumors encompassing > 130 proteins and phospho-proteins (**Supplementary Table 1**) for extensive signaling pathway analysis. In a first step, we use this panel consisting of major drug targets, key signaling proteins, tyrosine kinase receptors, tumor markers, and immune cell markers to retrospectively characterize archived primary tumor tissue from pancreatic and colorectal carcinomas. Using patient-specific, normal tissue-matched expression data, we conceptually show the suitability of the panel and methodology by stratifying these tumors based on cellular signaling and clinical data. We also create individualized protein profiles for each tumor. Secondly, in an exploratory direct clinical application based on patient-derived tissue core biopsies, we transfer this personalized proteomics approach to a prospective case series of molecular tumor board cases highlighting the potential of DigiWest to suggest individual treatment options.

3. Materials and Methods

3.1. Retrospective Patient Cohort

A total of 20 tumors (10 pancreatic and 10 colorectal carcinomas each) was utilized and available samples were selected from the tumor bank of the University Hospital Tübingen. The study was reviewed and approved by the local ethics committee at the medical faculty of the University of Tübingen (364/2023BO2). In addition, only tumors for which non-tumorous, normal tissue from the same patient was available, were included. All tumor (n = 20) and normal tissues (n = 20) were obtained as fresh-frozen samples. At the time of surgery, none of the patients with pancreatic tumors had previously received any systemic anticancer treatment, whereas four of the colon carcinoma patients did (see **Table 1**). From the tissue blocks, layered cuts of 10 µM each were prepared for each sample (pancreas tissues: 20 curls/sample, colon tissues: 15 curls/sample).

3.2. Prospective analysis of biopsy samples (MTB patient cohort)

Tumor samples for DigiWest analysis were obtained from patients that received a core needle biopsy to perform NGS analysis for the MTB (n = 14). The patients gave written informed consent, and the study was reviewed and approved by the local ethics committee at the medical faculty of the University of Tübingen (341/2021BO2). Details on tumor tissue origin, patient age and previous therapy are shown in **Table 2**. Samples were stored at -80°C until lysis.

3.3. Sample Preparation for DigiWest

Before protein profiling analysis, tissue sections (curls) were lysed using 50 µl of lysis buffer (LDS Lysis Buffer (Life Technologies, Carlsbad, CA, USA), supplemented with 10% reducing agent (Thermo Fisher Scientific), 4% Protease-Inhibitor (Roche, Basel, Switzerland) and 10% Phosphatase-Inhibitor (Roche)). Proteins were denatured by heating to 95°C for 10 min. Fresh frozen biopsy samples were lysed with 50-100 µl of lysis buffer and homogenized using a pistil during heating.

For all utilized samples, protein quantification was performed using in-gel staining. 1 µl of each original lysate per sample were loaded onto a NuPAGE 4-12% Bis-Tris precast gel (Thermo Fisher

Scientific) and run according to the manufacturer´s instructions. The gel was washed with water and proteins were stained with BlueBandit (VWR, Radnor, PA, USA) for 1 h. The gel was de-stained over night with ddH2O before detection on a LI-COR Odyssey instrument. Analysis and protein quantification was performed using ImageStudio and signals were compared to reference samples of known protein amounts.

3.4. DigiWest Protein Profiling

DigiWest was performed as published [31] using 15 µg of cellular protein. In brief, the NuPAGE system (Life Technologies) was used for gel electrophoresis and blotting onto PVDF membranes. Proteins were biotinylated on the membrane using NHS-PEG12-Biotin (50 µM) in PBST for 1 h. Sample lanes were cut into 96 strips (0.5 mm each) and placed in one well of a 96-well plate before adding 10 µl elution buffer (8 M urea, 1% Triton-X100 in 100 mM Tris-HCl pH 9.5). Each strip/protein fraction was incubated with 1 distinct Neutravidin-coated MagPlex bead population (Luminex, Austin, TX, USA). Coupling was performed over-night and non-bound binding sites were blocked with 500 µM deactivated NHS-PEG12-Biotin for 1 h. By pooling all 96 protein-loaded bead populations, the original sample lane was reconstituted.

5 µl aliquots of bead mix were added to 96-well plates containing 50 µl assay buffer (Blocking Reagent for ELISA (Roche) supplemented with 0.2% milk powder, 0.05% Tween-20 and 0.02% sodium azide). Upon discarding of the assay buffer, 30 µl of primary antibody (diluted in assay buffer) was added per well. After overnight incubation at 15°C, the bead-mixes were washed twice with PBST and species-specific PE-labelled (Phycoerythrin) secondary antibodies (Dianova, Hamburg, Germany) were added for 1 h at 23°C. Beads were washed twice with PBST before readout on a Luminex FlexMAP 3D instrument.

136 (retrospective analysis of pancreas and colon carcinomas) or 132 (non-retrospective analysis of GI tumors) primary antibodies (**Suppl. Table 1**) were selected from a collection of > 1 500 available antibodies, all of which are performance-evaluated and routinely used in DigiWest. Pathway

allocation of analytes was mapped based on the Kyoto Encyclopedia of Genes and Genomes (KEGG) database [38, 39].

Peak identification and integration were performed using an Excel-based analysis tool. For the retrospective analysis, a total of 150 peaks were identified, with 137 (91.3 %) generating reliable and non-weak signals (AFI > 50). For the prospective analysis, good signal was detected for 135 / 142 identified peaks (95.1%). For all samples, signal intensity was normalized to total protein amount loaded onto the beads. The software package MeV 4.9.0 was used for heatmap generation and differential expression analysis [40]. Hierarchical clustering (HCL) was performed using Euclidian Distance and complete linkage. For heatmaps using absolute expression data (**Fig. 1 + Fig. 5**), fluorescent signals were median centered across samples for a given analyte and Log2-transformed. For relative data, (**Fig. 2- Fig. 4**) Log2 Fold Changes of expression signals against the respective matched normal tissue were calculated for each analyte and directly used for heatmap generation. The entire DigiWest dataset is shown in **Suppl. Fig.1** and all raw and normalized DigiWest data can be found in **Suppl. Tables 2-3.**

3.5. Genetic Analysis of prospective MTB patient cohort

All tumors from patients of the prospective MTB-cohort received next generation panel sequencing by CeGaT GmbH, Tübingen or the Institute of Medical Genetics and Applied Genomics, Tübingen as previously described [41]. The identified therapy-relevant alterations and the drug recommendations of the MTB for each patient is shown in **Table 2**.

3.6 Statistical Analysis

Statistical analysis was performed using GraphPad Prism 9 and 10 (Graphpad Software, San Diego, CA, USA). Data was tested for normality using the Shapiro-Wilk test. Only if groups were normally distributed, they were compared via unpaired, two-tailed t-test. If normality was not met, the two-tailed Mann-Whitney-U Test was used. The Wilcoxon Rank-Sum test was used for differential expression analysis (heatmaps). N numbers and further statistical details for each experiment can be

found in the respective figure legend. In all cases, a p-value < 0.05 was considered significant unless stated otherwise and all exact p-values are stated in the respective figures.

4. Results

Absolute and relative expression differences between pancreatic and colorectal tumor tissues

In the first part of our study, we use our developed antibody panel to characterize the retrospective sample cohort in detail. As an initial analysis, pancreatic (n = 10) and colorectal (n = 10) tumors were compared using absolute DigiWest expression data, thus without factoring in normal tissue. Hierarchical cluster (HCL) analysis indicated an almost ideal separation of tumor samples according to their origin tissue (**Suppl. Fig. S2a**). Of the 137 measured analytes, 39 (28.4%) were differentially expressed between the two tumor types, (**Fig. 1a**). Expectedly, we observed high, consistent expression differences for tissue markers such as Cytokeratin 7 (pancreas) and CDX2 (colon, **Fig. 1b, Suppl. Fig. S2b-c**). Pancreas carcinomas generally showed greater expression of cell cycle-regulating proteins, immune cell markers or PDGFR beta while expression of Wnt and mTOR-signaling proteins was higher in colon carcinomas (**Fig. 1a-b, Suppl. Fig. S2b-c**). However, when using expression data from tumors only, it is difficult to distinguish between tissue-specific markers and expression differences inherent to the tumors themselves. Next, we compared all tumor tissues (n = 20) to their patient-matched normal tissue (n = 20, **Suppl. Fig. S3a**). Here, we observed consistently elevated expression of the tumor marker cancer embryonic antigen (CEA) and several other tumor-associated proteins (e.g. BcL-xL, CDK2, beta-Actin, FN1) for both tumor types (**Suppl. Fig. S3b**).

Based on this, all data from tumor tissues were now solely regarded in relation to its respective normal tissue (as Log2 Foldchange). Thus, each individual datapoint indicates a relative expression change occurring from non-cancerous to cancerous tissue stemming from the same patient. When comparing the two tumor entities in this fashion, 28 analytes (20.4%) were significantly different between them (**Fig. 1c**), only 7 of which were also found when comparing tumor tissues directly (see **Fig. 1a**). Furthermore, tumors no longer clustered according to their tissue origin (**Suppl. Fig. S4**) and tissue-specific analytes such as CDX2 now expectedly showed no differential expression (**Suppl. Fig. S5a**). Crucially, the pancreas carcinomas on average showed upregulations of several proto-oncogenic

proteins such as Ras (KRAS), c-myc (MYC), Ha-Ras (HRAS) or PI3K alpha (PIK3CA), among others (**Fig. 1d, Suppl. Fig. S5b**). Moreover, strong downregulation (5-fold) of the tumor suppressor protein p53 (TP53) was observed to a greater extent (**Fig. 1d**). Lastly, CK7 was drastically upregulated (up to 10-fold) in some pancreatic tumors. On the other hand, colon carcinomas for instance displayed strongly reduced levels of the tumor suppressors p27 (CDKN1B) and PTEN (**Fig. 1d**). However, substantial variability within the cohorts is generally worth noting (e.g. see p53, Ras). Thus, when including normal tissue as a reference, the tumor entities could be distinguished largely based on protein expression changes of key tumor suppressors and oncogenes, placing emphasis on a pathway-activity based distinction. Next – again using relative data – we stratified tumors within their respective cohorts.

Relative expression changes distinguish samples within the pancreas carcinoma cohort

Cluster analysis clearly separated the 10 pancreatic tumors into two subsets of five (**Fig. 2a**), indicating differential pathway activity in the two groups. In contrast to the colon cohort, none of the pancreatic carcinoma patients had received systemic anticancer treatment before sampling (**Table 1**). Our data revealed that tumor-induced changes to a striking 40.1% (55/137) of analytes were significantly different between the two subgroups (**Fig. 2b**), with 42 of those showing higher changes in magnitude for group/cluster 1 (light blue) and only 13 for group/cluster 2 (dark blue). Notably, group 1 generally showed strong upregulation (ca. 5-fold) of Cytokeratins (**Fig. 2c, Suppl. Fig. S6a**), whereas CK levels were not changed in group 2. Downregulation of p53 was another feature of group 1 carcinomas (**Fig. 2d**). In addition, group 1 showed an upregulation of several mTOR-pathway-proteins, its downstream targets (**Fig. 2e**) and several others (**Suppl. Fig. S6b**). They also showed highly increased amounts of modified Histone H3 (**Fig. 2e**) as well as strong up-regulatory effects on NF-kappaB signaling (**Fig. 2e**, **Suppl. Fig. S6c**). On average, expression levels of all these analytes were downregulated or unchanged compared to normal tissue in group 2. Conversely, these pancreatic tumors were characterized by higher signals for immune cell markers (**Fig. 2e**) along with key Smad signaling proteins (**Fig. 2e, Suppl.**

Fig. S6d). Overall, pancreatic carcinomas showed a clear separation into two groups with different expression signatures emerging for either subgroup upon comparison to normal tissue.

Clinical data can be linked to relative expression changes within the colorectal carcinoma cohort

In the colorectal carcinoma cohort, there was more variation with regards to patient age (**Suppl. Fig. S7a**), tumor localization (left vs right sided) and previous treatment, given the available clinical data (**Table 1**). This comparatively high level of heterogeneity was also evident in the protein expression data, as the ten colon tumors separated into four subgroups upon clustering (**Fig. 3a, Suppl. Fig. S7b**). Therefore, we aimed at stratifying and comparing samples based on patient age and tumor localization, rather than on signaling alone. Due to its unusual clinical nature, we excluded the hepatoid adenocarcinoma sample (#18). Notably, we observed that tumors of young and old patients differed significantly regarding their expression change of cell-cycle-and mTOR-regulating proteins (**Fig. 3b**). In younger patients (<55 y, n = 3), their expression was downregulated, whereas upregulations or no changes compared to normal tissue were observed in older patients (n = 6). Likewise, right-sided colon tumors (n = 5) generally showed downregulations of EGFR, mTOR, MAPK proteins (MEK1/2 and phospho-b-Raf) as well as ATM (**Fig. 3c**). On the other hand, an upregulation of expression was detected in left-sided (n = 4) tumors for these analytes. Overall, we were able to show differences in the clinically relevant subgroups of right- and left-sided cancers as well as in the subgroups of early-onset or late-onset colorectal cancers.

DigiWest highlights distinct expression and pathway activity profiles in individual tumors

Next, we investigated each tumor individually by creating personalized profiles according to dysregulated analytes and analyte groups that infer abnormal signaling pathway activity or impaired cell function. In 15/20 (75%) of cases, based on DigiWest data alone, we were able to assign one or several key pathways and/or tyrosine kinase receptors which could be (substantially) contributing to

tumor progression (**Table 1**). Crucially, of all measured analytes, 37 are direct FDA-approved drug targets (https://www.proteinatlas.org/search/protein_class:FDA+approved+drug+targets), with a further 47 indirectly indicating a target response (e.g. Erk for MEK inhibition). Four exemplary cases are shown in detail in **Fig. 4**. Analogue protein profiles of all other tumors are shown in **Suppl. Figs S8-S23**. For each individual tumor, a list of relevant analytes/pathways including potential drug targets is given.

Individual analysis of pancreas carcinoma #3 revealed a variety of expression changes (**Fig. 4a**). Among the strongest were upregulations of the tumor marker CEA as well as the markers CK7 and 19 (**Fig. 4b**). Upregulations of several mTOR signaling proteins (e.g. mTOR, PDK1, Rictor), as well as its downstream targets p70S6K, S6 RP and eIF4E (including phospho-variants), indicated substantial activity in this pathway (**Fig. 4b**). Increased Histone modification, EGFR, Her2 and c-Met expression as well as elevated Wnt (beta-catenin, Dvl2, GSK3 beta, Wnt3) and NF-kappaB signaling (IkappaB, NF-kappaB, IKK alpha) were also noted. Moreover, a strong downregulation (> 4-fold) of p53 along with upregulated Cyclins E1, D2 and D3 levels drew attention to potentially impaired cell cycle regulation. Pancreas carcinoma #7 exhibited a similar marker expression pattern and displayed coherent activation (phosphorylation) of key MAPK proteins (p38, RSK1, Erk2, MEK1/2, b-Raf), along with elevated Ras, EGFR and PDGFR (**Fig. 4a+c**). In similar fashion, colon carcinoma #13 showed increased CEA, EGFR and PDGFR levels along with upregulated MAPK/Erk and STAT3 phosphorylation (**Fig. 4a+d**). Interestingly, Ras expression was slightly reduced in this case. We were also able to clearly differentiate the MSI-high tumor (#16) and the hepatoid carcinoma sample (#18,) from the others based on marker expression; they were either the only colon tumor with CK7 upregulation (**Suppl. Fig. S19**) or the one with the highest increase in CK19 (11-fold) and CDX2 (6-fold) (**Suppl. Fig. S21**), respectively.

Finally, we opted to investigate immune cell markers (CDs, for details see **Suppl. Table S1**) as their expression is often indicative of immune cell infiltration into the tumor (so called “hot” versus “cold” tumors). Across all 20 tumors, groups of CD proteins were consistently upregulated in nine cases (**Table 1**) in some of which their higher expression being among the most prevalent key changes, potentially indicating an immunologically “hot” tumor. One such example (colon #12) is shown in **Fig. 4a+e**.

Notably, CD16, CD4, CD25 and CD11c expression is elevated along with TGF beta, phospho-Smad1/5 and phospho-Smad 2/3, which can play a role in immunogenic signaling. In contrast, expression of proteins from other common signaling pathways (e.g. mTOR, Wnt) was reduced.

In summary, we were able to profile each tumor individually on the protein level based on potential treatment-relevant aberrations in pathway activity, detect divergent expression patterns in special cases and functionally group tumors, e.g. based on immune cell infiltration.

Personalized expression signatures and treatment recommendations for a prospective MTB case series

In contrast to the analyses discussed above, where archived biobank samples were retrospectively selected, we next aimed at a potential integration of DigiWest into clinical algorithms by investigating tissues gained by a core needle biopsy of tumor tissue. As a proof-of-principle, we included 14 patients who got needle biopsies of their tumors taken as a diagnostic step for the Molecular Tumor Board (MTB) at Tuebingen University. This approach usually does not provide sufficient non-malignant tissue, which was so far used in our investigations to identify tumor-specific up or downregulations. Thus, expression levels from a specific tumor were compared to the “baseline” (median) expression value of a given analyte across all other tumors. The patient cohort of the MTB displayed substantial heterogeneity; it encompassed a variety of gastrointestinal tumor entities, including cholangio-, colon, gallbladder, hepatocellular, pancreatic, gastric, rectal and esophageal carcinomas (**Table 2**). Furthermore, several patients were heavily pre-treated, in some cases also with targeted therapies. We performed DigiWest analysis using a slightly modified antibody panel of 135 analytes on this small cohort (**Suppl. Fig. S24**). For 12 of the 14 patients, we were able to identify coherent abnormalities regarding the activation of key tumor-related signaling pathways (**Table 2**), even without normal tissue being available as a reference. Based on our proteomic data, we also identified potential drug targets for each patient (**Table 2**). Since all patients were included into the MTB, genetic (sequencing) data and

respective MTB interpretation was available for each case. Thus, we scrutinized the additional information to this data that could be gained by DigiWest. Upon comparison of proteomic data and MTB treatment recommendation, we observed confirmative pathway alterations to key tumor-driving mutations in 8/12 applicable cases. Two cases are shown in greater detail in **Fig. 5**. Individual profiles of all other patients are shown in **Suppl. Fig. S25-36**. In the first case of a colon tumor, DigiWest analysis showed elevated expression levels (> 2-fold) for a multitude of analytes, most notably FGFR2, the phosphorylated variants of STAT1, STAT3, Erk1, and Erk2 along with several cell cycle proteins (**Fig. 5a-b**). Absolute levels of phospho-Erk and phospho-STAT were the highest among the entire cohort (**Fig. 5c**) and FGFR2 showed an exceptional DigiWest peak profile (**Fig. 5d**). Accordingly, the genetic data had identified an amplification of the FGFR2 gene (**Table 2**). Thus, we were able to prove this observation on the proteomic level, given the notable FGFR2 expression signal well as the activation of downstream pathways MAPK/Erk and Jak/STAT. In the second case, a hepatocellular carcinoma with a peculiar expression signature (**Fig. 5e**) displayed strongly elevated signals for mTOR-related protein expression and phosphorylation (mTOR, PI3KA, PI3KB, S6 RP, **Fig. 5f**). Again, signals were substantially higher than in the rest of the cohort (**Fig. 5g**). On the genetic side, a deletion of the mTOR-regulating tumor suppressor TSC2 was identified (**Table 2**) confirming the proteomic observations. Furthermore, DigiWest revealed the presence of tumor infiltrating lymphocytes (“hot” tumor) given strong expression levels of CD8 alpha, CD163 and CD4 (**Fig. 5f**).

Thereby, we were able to detect personalized protein signatures in a direct clinical application of DigiWest. For 12/14 cases we identified coherent and treatment-relevant patterns of pathway activation and were able to link protein expression data with genetic mutation analysis and MTB drug recommendations.

5. Discussion

Using ultrasound-guided tissue core biopsies of gastrointestinal tumors, we successfully generated profiles of signal transduction pathway signatures for direct clinical evaluation through high-throughput Western Blotting (DigiWest). Initially, we performed a retrospective analysis of archived primary pancreatic and colorectal tumor tissues to demonstrate the capabilities of DigiWest for tumor stratification and personalized profiling. This involved comparing protein expression data from tumors with matched normal tissues. We identified tumor subgroups within the cohorts based on pathway activity, and we further characterized individual tumors, highlighting unique, treatment-relevant expression signatures. Building on this foundation, we then applied the DigiWest system to profile biopsy-derived tumor samples from current Molecular Tumor Board (MTB) patients in a proof-of-principle approach, testing whether the integration of proteomic data enhances the interpretation of genetic data to provide a more comprehensive molecular understanding of each tumor.

Earlier retrospective analyses of primary tumor tissues of various entities [32, 37, 42, 43] have classified and stratified sample groups according to protein expression signatures. For our retrospective analysis, we chose two highly invasive GI carcinomas (colorectal and pancreatic). A direct comparison analogue to these previous studies using tumor tissue only, revealed tissue-specific markers and entity-relevant pathway activity (e.g. Wnt signaling in colon) as described in the literature [44-46]. The introduction of patient matching normal tissue as an internal reference allowed us to generate relative expression data, thus solely highlighting tumor-specific changes in protein expression signatures while at the same time reducing inter-patient variability. In line with this, our data distinguished colon and pancreatic tumors largely based on the expression of tumor suppressors and oncogenes. For pancreatic carcinomas, these included Ras (KRAS) and p53 (TP53), which are commonly described as a frequent mutations in this tumor entity [47, 48]. Likewise, colorectal carcinomas more frequently presented with PTEN and p27 (CDKN1B), which has been described previously in genetic analyses [49-52]. Thus, our proteomic data comparison mirrors genetic mutations that are different between colon and pancreatic carcinomas.

Closer evaluation of the pancreas cohort revealed a division into two subgroups, characterized by differences in relative expression changes of p53, Cytokeratins, mTOR signaling and immune markers. There has been extensive evidence of a sub-division of pancreatic carcinoma regarding molecular and clinical phenotypes [53-57]. One particular classification into subtypes [53] identifies a squamous and immunogenic type, among others. The expression signatures identified by DigiWest match the characteristics of these two specific groups: Squamous subtype pancreatic carcinomas are for instance characterized by mutations and alterations in TP53 as well as in genes regulating metabolism and autophagy, which is in line with our Group 1 subtype (p53 reduction, mTOR-related signaling). Group 2 in our cohort clearly showed upregulation of immune cell markers and Smad signaling, which has been associated with immune responses [58, 59]. This matches the characteristics of immunogenic pancreas carcinomas, which are often regarded as immune-infiltrated.

Regarding clinical parameters, the colon carcinoma cohort was more heterogeneous. This was reflected in our proteomic data, as we – unlike in pancreatic carcinomas – did not observe a clear separation into expression-based subgroups. In clinical practice, right- and left-sided colon carcinomas are differentiated [60, 61] as these subgroups strongly differ with regards to molecular characteristics and treatment responses. For instance, EGFR-directed therapy (EGFR-Ab) is not recommended as a first-line treatment for right-sided colon carcinomas [62]. In line with this, we observed an EGFR downregulation in right-sided carcinomas and an upregulation in left-sided carcinomas.

Moreover, there is a general concern among clinical oncologists, that the age of onset for colon carcinomas is decreasing and that early- and late onset tumors greatly differ regarding aggressiveness, treatment options and therapy response [63-65]. We observed consistent differences in expression of key cell-cycle and mTOR proteins, when separating our cohort based on age. Although studies have previously characterized the genetic mutation signatures of early onset colon tumors [66, 67], detailed transcriptional let alone proteomic features remained elusive [68].

Overall, these potential signaling indicators for patient age and/or tumor localization might reflect the different clinical behavior of these subgroups and could add important details to improve treatment recommendations, if these observations could be confirmed in larger cohorts.

Using DigiWest we were also able to create personalized protein profiles for each individual tumor and identify drug-targetable activity changes in pathway regulation. These personalized characterizations were achieved via the DigiWest approach using only 15 µg of protein, roughly corresponding to a single tissue section. In this specific retrospective study, having matched non-tumorous control tissue was advantageous. Despite the protein-expression based groupings that were observed across samples (see above), the diversity among samples on an individual level was still evident. Our analytical method was able to accurately depict this thus suggesting a suitability of DigiWest for the analysis of tumors with high clinical and molecular heterogeneity (e.g. #16, #18).

Overall, our retrospective analysis did not only prove DigiWest as suitable for tumor stratification, but also points out a use for direct clinical application, as protein expression and activation on directly druggable targets is achievable on a personalized level with equal sensitivity and high throughput compared to other proteomic methods.

Currently, personalized medicine approaches in clinical oncology still primarily rely on genetic profiling and histological staining, with limited use of high-throughput protein analytics. As a proof-of concept, we analyzed single core needle biopsies from 14 patients with various GI tumors. The protein data obtained, reflecting the expression and activation of key signal transducers, tumor markers, and receptors from a panel of 135 analytes that included a high number of druggable targets, was assessed as complementary to the next-generation sequencing data available to the Molecular Tumor Board. DigiWest profiling data generation proved feasible in this setting, thus adding protein analytics for clinical evaluation and application. We observed substantial overlap between pathway de-regulations identified by DigiWest and corresponding genetic mutations (e.g. cell cycle activity and *TP53* mutations). This underscores the importance of accurately detecting treatment-relevant expression

signatures and phosphorylation states of druggable signaling proteins and receptors for accurate information transfer on the manifestation of tumor-driving mutations from the genome to the proteome. In a similar approach using RPPA technology, Wahjudi et al. analyzed 27 proteins to retrospectively recommended treatment options for tumor board patients and compared these to genetic information [69]. They noted an inconsistent partial overlap (10-57%) between genetic and proteomic-based recommendations yet emphasized the prognostic value of proteomic data as a readout for tumor physiology and its suitability for integration into precision oncology programs. By the same token, DigiWest is a powerful potential tool to be used complementary and confirmatory to standard sequencing analyses in a clinical setting, with even greater throughput and substantially higher coverage of relevant signaling pathways. This equally holds true for the comparison of DigiWest to multiplexed immunohistochemistry, while also having the advantage of generating semi quantitative data. Furthermore, in a recent publication [70] we demonstrated good comparability of DigiWest and Mass Spectrometry, however emphasizing a superiority of DigiWest in detecting phosphorylated variants, which is especially important for the question at hand. It can meet the demands of daily clinical routine as it only requires a minimal amount of material (one core needle biopsy obtained during a standard diagnostic procedure) and DigiWest analysis (including data evaluation) can be completed within five days. Moreover, the ability to customize the antibody panel based on specific tumor types or to align with particular drug targets is highly advantageous. DigiWest can provide additional insights into treatment options and facilitate appropriate drug selection on a personalized level, thereby expanding the basis of information available to the oncologist. Methodologically, it aids in distinguishing relevant tumor drivers and selecting the most suitable treatment for individual patients, enhancing the success rate of targeted therapies and ultimately improving treatment outcome. Notably, both our retrospective and prospective datasets demonstrate the potential of the method. However, it is worth noting that the accuracy of DigiWest data is improved even more by including patient-matched normal tissue. These findings suggest incorporating DigiWest profiling into

454 future clinical studies to evaluate the potential of this technology to further improve response
455 prediction.

6. Data Availability

All DigiWest-related raw and normalized data generated or analyzed during this study are included within the article (see **Suppl. Tables 2-3**).

Our ethical approval does not allow the complete upload of the results from patient DNA sequencing. All relevant information from the DNA sequencing are included in the manuscript.

All other datasets used and/or analyzed during the study are available from the corresponding author on reasonable request.

7. References

1. Waarts, M.R., et al., *Targeting mutations in cancer.* J Clin Invest, 2022. **132**(8).
2. Braicu, C., et al., *A Comprehensive Review on MAPK: A Promising Therapeutic Target in Cancer.* Cancers (Basel), 2019. **11**(10).
3. Yang, J., et al., *Targeting PI3K in cancer: mechanisms and advances in clinical trials.* Mol Cancer, 2019. **18**(1): p. 26.
4. He, Y., et al., *Targeting PI3K/Akt signal transduction for cancer therapy.* Signal Transduct Target Ther, 2021. **6**(1): p. 425.
5. Beaver, J.A., et al., *FDA Approval: Palbociclib for the Treatment of Postmenopausal Patients with Estrogen Receptor-Positive, HER2-Negative Metastatic Breast Cancer.* Clin Cancer Res, 2015. **21**(21): p. 4760-6.
6. Zubair, T. and D. Bandyopadhyay, *Small Molecule EGFR Inhibitors as Anti-Cancer Agents: Discovery, Mechanisms of Action, and Opportunities.* Int J Mol Sci, 2023. **24**(3).
7. Krook, M.A., et al., *Fibroblast growth factor receptors in cancer: genetic alterations, diagnostics, therapeutic targets and mechanisms of resistance.* Br J Cancer, 2021. **124**(5): p. 880-892.
8. Nair, A., et al., *FDA Supplemental Approval Summary: Lenvatinib for the Treatment of Unresectable Hepatocellular Carcinoma.* Oncologist, 2021. **26**(3): p. e484-e491.
9. Strickler, J.H. and H.I. Hurwitz, *Bevacizumab-based therapies in the first-line treatment of metastatic colorectal cancer.* Oncologist, 2012. **17**(4): p. 513-24.
10. Slamon, D., et al., *Adjuvant trastuzumab in HER2-positive breast cancer.* N Engl J Med, 2011. **365**(14): p. 1273-83.
11. Wang, D.K., et al., *Targeted Immunotherapies in Gastrointestinal Cancer: From Molecular Mechanisms to Implications.* Front Immunol, 2021. **12**: p. 705999.
12. DeCarli, K., J. Strosberg, and K. Almhanna, *Immune Checkpoint Inhibitors for Gastrointestinal Malignancies: An Update.* Cancers (Basel), 2022. **14**(17).
13. Le, D.T., et al., *PD-1 Blockade in Tumors with Mismatch-Repair Deficiency.* N Engl J Med, 2015. **372**(26): p. 2509-20.
14. Sochacka-Cwikla, A., M. Maczynski, and A. Regiec, *FDA-Approved Small Molecule Compounds as Drugs for Solid Cancers from Early 2011 to the End of 2021.* Molecules, 2022. **27**(7).
15. Gambardella, V., et al., *Personalized Medicine: Recent Progress in Cancer Therapy.* Cancers (Basel), 2020. **12**(4).
16. Matsuoka, T. and M. Yashiro, *Precision medicine for gastrointestinal cancer: Recent progress and future perspective.* World J Gastrointest Oncol, 2020. **12**(1): p. 1-20.
17. Leichsenring, J., et al., *Variant classification in precision oncology.* Int J Cancer, 2019. **145**(11): p. 2996-3010.
18. Tan, W.C.C., et al., *Overview of multiplex immunohistochemistry/immunofluorescence techniques in the era of cancer immunotherapy.* Cancer Commun (Lond), 2020. **40**(4): p. 135-153.
19. Birkman, E.M., et al., *Gastric cancer: immunohistochemical classification of molecular subtypes and their association with clinicopathological characteristics.* Virchows Arch, 2018. **472**(3): p. 369-382.
20. Espina, V., et al., *Reverse phase protein microarrays for theranostics and patient-tailored therapy.* Methods Mol Biol, 2008. **441**: p. 113-28.
21. Duarte, T.T. and C.T. Spencer, *Personalized Proteomics: The Future of Precision Medicine.* Proteomes, 2016. **4**(4).
22. Nobili, S. and E. Mini, *Special Issue: "Gastrointestinal Cancers and Personalized Medicine".* J Pers Med, 2022. **12**(3).
23. Javadrashid, D., et al., *Pancreatic Cancer Signaling Pathways, Genetic Alterations, and Tumor Microenvironment: The Barriers Affecting the Method of Treatment.* Biomedicines, 2021. **9**(4).

24. Ahmad, R., et al., *Emerging trends in colorectal cancer: Dysregulated signaling pathways (Review).* Int J Mol Med, 2021. **47**(3).
25. Polireddy, K. and Q. Chen, *Cancer of the Pancreas: Molecular Pathways and Current Advancement in Treatment.* J Cancer, 2016. **7**(11): p. 1497-514.
26. Hu, H.F., et al., *Mutations in key driver genes of pancreatic cancer: molecularly targeted therapies and other clinical implications.* Acta Pharmacol Sin, 2021. **42**(11): p. 1725-1741.
27. Troiani, T., et al., *Targeting EGFR in pancreatic cancer treatment.* Curr Drug Targets, 2012. **13**(6): p. 802-10.
28. Koveitypour, Z., et al., *Signaling pathways involved in colorectal cancer progression.* Cell Biosci, 2019. **9**: p. 97.
29. Inamura, K., *Colorectal Cancers: An Update on Their Molecular Pathology.* Cancers (Basel), 2018. **10**(1).
30. Li, M.M., et al., *Molecular subclassification of gastrointestinal cancers based on cancer stem cell traits.* Exp Hematol Oncol, 2021. **10**(1): p. 53.
31. Treindl, F., et al., *A bead-based western for high-throughput cellular signal transduction analyses.* Nat Commun, 2016. **7**: p. 12852.
32. Bockmayr, T., et al., *Multiclass cancer classification in fresh frozen and formalin-fixed paraffin-embedded tissue by DigiWest multiplex protein analysis.* Lab Invest, 2020. **100**(10): p. 1288-1299.
33. Spahn, S., et al., *The molecular interaction pattern of lenvatinib enables inhibition of wild-type or kinase-mutated FGFR2-driven cholangiocarcinoma.* Nat Commun, 2024. **15**(1): p. 1287.
34. Walter, B., et al., *Functionally-instructed modifiers of response to ATR inhibition in experimental glioma.* J Exp Clin Cancer Res, 2024. **43**(1): p. 77.
35. Inder, S., et al., *Multiplex profiling identifies clinically relevant signalling proteins in an isogenic prostate cancer model of radioresistance.* Sci Rep, 2019. **9**(1): p. 17325.
36. Naskou, J., et al., *EZH2 Loss Drives Resistance to Carboplatin and Paclitaxel in Serous Ovarian Cancers Expressing ATM.* Mol Cancer Res, 2020. **18**(2): p. 278-286.
37. Ruoff, F., et al., *Protein Profiling of Breast Carcinomas Reveals Expression of Immune-Suppressive Factors and Signatures Relevant for Patient Outcome.* Cancers (Basel), 2022. **14**(18).
38. Kanehisa, M. and S. Goto, *KEGG: kyoto encyclopedia of genes and genomes.* Nucleic Acids Res, 2000. **28**(1): p. 27-30.
39. Kanehisa, M. and Y. Sato, *KEGG Mapper for inferring cellular functions from protein sequences.* Protein Sci, 2020. **29**(1): p. 28-35.
40. Saeed, A.I., et al., *TM4: a free, open-source system for microarray data management and analysis.* Biotechniques, 2003. **34**(2): p. 374-8.
41. Bitzer, M., et al., *Next-Generation Sequencing of Advanced GI Tumors Reveals Individual Treatment Options.* JCO Precis Oncol, 2020. **4**.
42. Zhou, Y., et al., *Proteomic signatures of 16 major types of human cancer reveal universal and cancer-type-specific proteins for the identification of potential therapeutic targets.* J Hematol Oncol, 2020. **13**(1): p. 170.
43. Asleh, K., et al., *Proteomic analysis of archival breast cancer clinical specimens identifies biological subtypes with distinct survival outcomes.* Nat Commun, 2022. **13**(1): p. 896.
44. Li, T., et al., *Platelet-derived growth factor-BB mediates pancreatic cancer malignancy via regulation of the Hippo/Yes-associated protein signaling pathway.* Oncol Rep, 2021. **45**(1): p. 83-94.
45. Cheng, X., et al., *Therapeutic potential of targeting the Wnt/beta-catenin signaling pathway in colorectal cancer.* Biomed Pharmacother, 2019. **110**: p. 473-481.
46. Zhong, J., et al., *To Investigate the Occurrence and Development of Colorectal Cancer Based on the PI3K/AKT/mTOR Signaling Pathway.* Front Biosci (Landmark Ed), 2023. **28**(2): p. 37.
47. Zhang, Z., et al., *KRAS mutation: The booster of pancreatic ductal adenocarcinoma transformation and progression.* Front Cell Dev Biol, 2023. **11**: p. 1147676.

48. Voutsadakis, I.A., *Mutations of p53 associated with pancreatic cancer and therapeutic implications.* Ann Hepatobiliary Pancreat Surg, 2021. **25**(3): p. 315-327.
49. Day, F.L., et al., *PIK3CA and PTEN gene and exon mutation-specific clinicopathologic and molecular associations in colorectal cancer.* Clin Cancer Res, 2013. **19**(12): p. 3285-96.
50. Salvatore, L., et al., *PTEN in Colorectal Cancer: Shedding Light on Its Role as Predictor and Target.* Cancers (Basel), 2019. **11**(11).
51. Sawai, H., et al., *Loss of PTEN expression is associated with colorectal cancer liver metastasis and poor patient survival.* BMC Gastroenterol, 2008. **8**: p. 56.
52. Ogino, S., et al., *Cytoplasmic localization of p27 (cyclin-dependent kinase inhibitor 1B/KIP1) in colorectal cancer: inverse correlations with nuclear p27 loss, microsatellite instability, and CpG island methylator phenotype.* Hum Pathol, 2007. **38**(4): p. 585-92.
53. Bailey, P., et al., *Genomic analyses identify molecular subtypes of pancreatic cancer.* Nature, 2016. **531**(7592): p. 47-52.
54. Collisson, E.A., et al., *Subtypes of pancreatic ductal adenocarcinoma and their differing responses to therapy.* Nat Med, 2011. **17**(4): p. 500-3.
55. Moffitt, R.A., et al., *Virtual microdissection identifies distinct tumor- and stroma-specific subtypes of pancreatic ductal adenocarcinoma.* Nat Genet, 2015. **47**(10): p. 1168-78.
56. Elebo, N., et al., *Exploiting the molecular subtypes and genetic landscape in pancreatic cancer: the quest to find effective drugs.* Front Genet, 2023. **14**: p. 1170571.
57. Collisson, E.A., et al., *Molecular subtypes of pancreatic cancer.* Nat Rev Gastroenterol Hepatol, 2019. **16**(4): p. 207-220.
58. Batlle, E. and J. Massague, *Transforming Growth Factor-beta Signaling in Immunity and Cancer.* Immunity, 2019. **50**(4): p. 924-940.
59. Chandiran, K. and L.S. Cauley, *The diverse effects of transforming growth factor-beta and SMAD signaling pathways during the CTL response.* Front Immunol, 2023. **14**: p. 1199671.
60. Baran, B., et al., *Difference Between Left-Sided and Right-Sided Colorectal Cancer: A Focused Review of Literature.* Gastroenterology Res, 2018. **11**(4): p. 264-273.
61. Mukund, K., et al., *Right and left-sided colon cancers - specificity of molecular mechanisms in tumorigenesis and progression.* BMC Cancer, 2020. **20**(1): p. 317.
62. Salem, M.E., et al., *Comparative molecular analyses of left-sided colon, right-sided colon, and rectal cancers.* Oncotarget, 2017. **8**(49): p. 86356-86368.
63. Collaborative, R., et al., *Characteristics of Early-Onset vs Late-Onset Colorectal Cancer: A Review.* JAMA Surg, 2021. **156**(9): p. 865-874.
64. Ren, B., et al., *Survival outcome and prognostic factors for early-onset and late-onset metastatic colorectal cancer: a population based study from SEER database.* Sci Rep, 2024. **14**(1): p. 4377.
65. Foppa, C., et al., *Different Oncologic Outcomes in Early-Onset and Late-Onset Sporadic Colorectal Cancer: A Regression Analysis on 2073 Patients.* Cancers (Basel), 2022. **14**(24).
66. Lieu, C.H., et al., *Comprehensive Genomic Landscapes in Early and Later Onset Colorectal Cancer.* Clin Cancer Res, 2019. **25**(19): p. 5852-5858.
67. Cercek, A., et al., *A Comprehensive Comparison of Early-Onset and Average-Onset Colorectal Cancers.* J Natl Cancer Inst, 2021. **113**(12): p. 1683-1692.
68. Lu, C., et al., *Molecular characteristics of microsatellite stable early-onset colorectal cancer as predictors of prognosis and immunotherapeutic response.* NPJ Precis Oncol, 2023. **7**(1): p. 63.
69. Wahjudi, L.W., et al., *Integrating proteomics into precision oncology.* Int J Cancer, 2021. **148**(6): p. 1438-1451.
70. Kling, S., et al., *Characterization of hepatic zonation in mice by mass-spectrometric and antibody-based proteomics approaches.* Biol Chem, 2022. **403**(3): p. 331-343.

8. Author Contributions

Conceptualization: AS, MB and MFT; methodology: AS, MFT; DigiWest experiments: AS, FS-R; DigiWest investigation and analysis: AS; clinical patient and data evaluation: KB, TH, PM, MB; writing—original draft preparation: AS, MB and MFT; writing—review and editing: KS-L, SS, PM, FS-R, NPM; material support: MB, KB, TH; supervision: MT, KS-L, NPM; project administration: MFT and MB. All authors read and approved the final manuscript.

9. Acknowledgements

None.

10. Competing Interests

All authors declare no financial or non-financial competing interests.

11. Figures

Figure 1

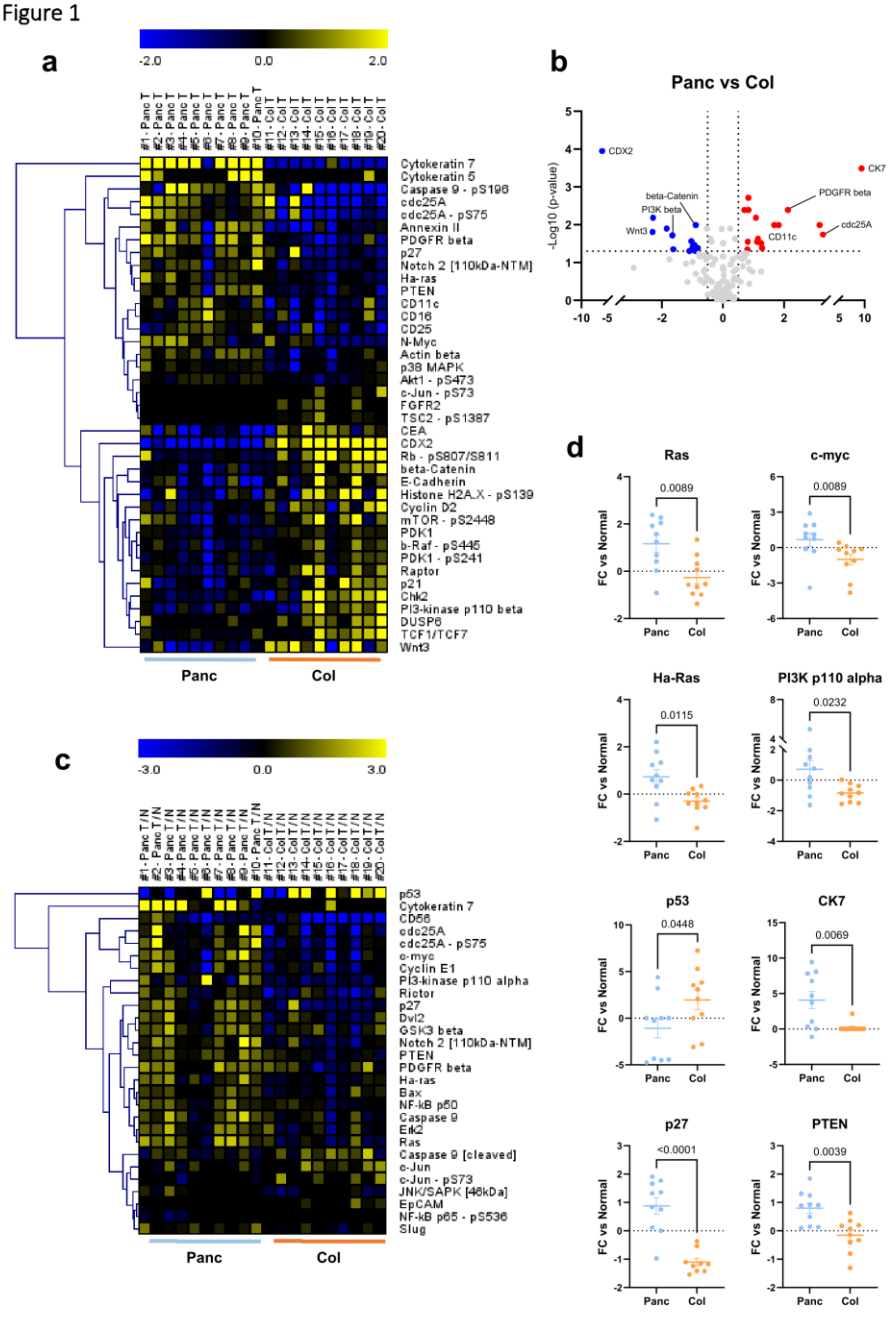

Figure 1: Comparison of pancreas and colorectal carcinomas. a: Heatmap and Hierarchical Cluster analysis of analytes significantly different between pancreas (n=10) and colon (n=10) tumor tissues using AFI (accumulated fluorescent intensity) signals; Wilcoxon test, $p < 0.05$. **b:** Volcano plot of comparison shown in A. Significantly upregulated proteins are shown in red, downregulated proteins in blue. Analytes with FCs < I0.5I are excluded. **c:** Heatmap and Hierarchical Cluster analysis of analytes significantly different between pancreas (n=10) and colon (n=10) samples based on expression changes relative to matched normal tissue (as Log2 FC tumor/normal); Wilcoxon test, $p < 0.05$. **d:** Tumor/normal relative DigiWest data (Log2 FCs) for selected differentially expressed analytes; Mann-Whitney test, $p < 0.05$. Panc = Pancreas (blue), Col = Colon (orange). p-value as indicated. Solid line indicates the mean FC value per group. Error bars: S.E.M.

642 Figure 2

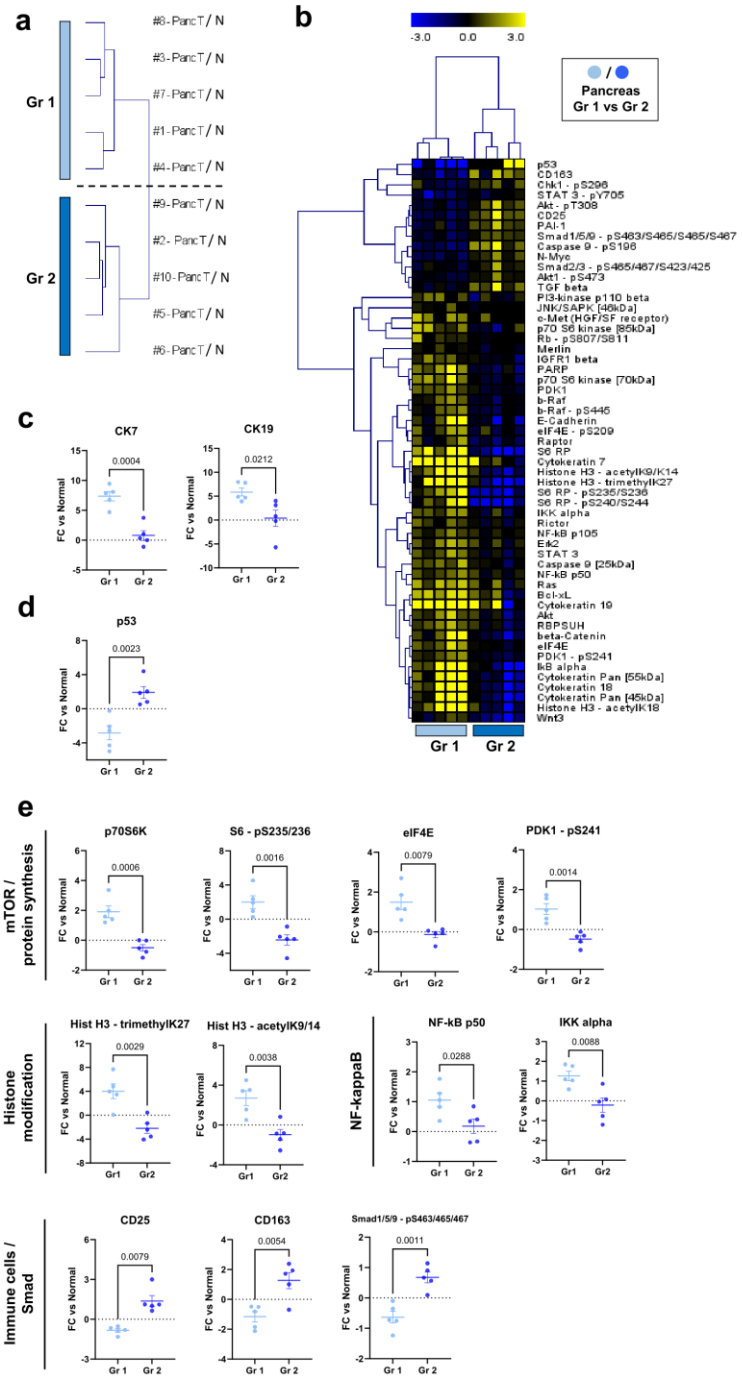

643

644 **Figure 2: Relative expression differences within the pancreas cohort. a:** Hierarchical Cluster analysis
645 of pancreas tumors only (n=10) using relative expression data (Log2 FC tumor/matched normal);
646 Group 1 = Gr1 (light blue), Group 2 = Gr2 (dark blue). **b:** Heatmap and Hierarchical Cluster analysis of
647 analytes significantly different between Gr1 (n=5) and Gr2 (n=5) pancreas tumors; Wilcoxon test, $p <$
648 0.05. **c-e:** Tumor/normal relative DigiWest data (Log2 FCs) for **c:** Cytokeratins 7 and 19, **d:** p53, and **e:**
649 selected analytes of interest with their pathway allocation; either the Mann-Whitney test or unpaired
650 t-test was used depending on data distribution. p-value as indicated. Solid line indicates the mean FC
651 value per group. Error bars: S.E.M.

Figure 3

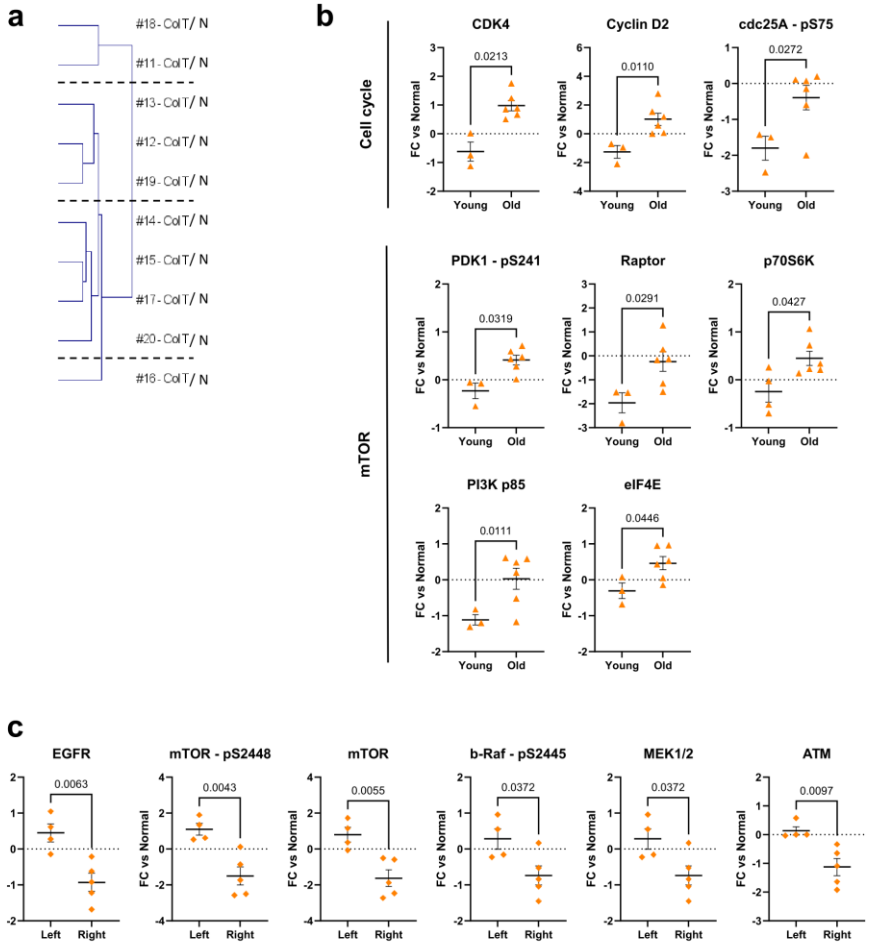

Figure 3: Relative expression differences within the colon cohort. a: Hierarchical Cluster analysis of pancreas tumors only (n=10) using relative expression data (Log2 FC tumor/matched normal). **b-c:** Tumor/normal relative DigiWest data (Log2 FCs) for differentially expressed analytes comparing groups of tumors based on clinical characteristics. **b:** Patient age - young (< 55 years, n=3) versus old (> 55 years, n=6). **c:** Tumor localization - left (n=4) versus right (n=5). Due to differences in group size, Welch´s t-test ($p < 0.05$) was used instead of unpaired t-test. p-value as indicated. Solid line indicates the mean FC value per group. Error bars: S.E.M.

662 Figure 4

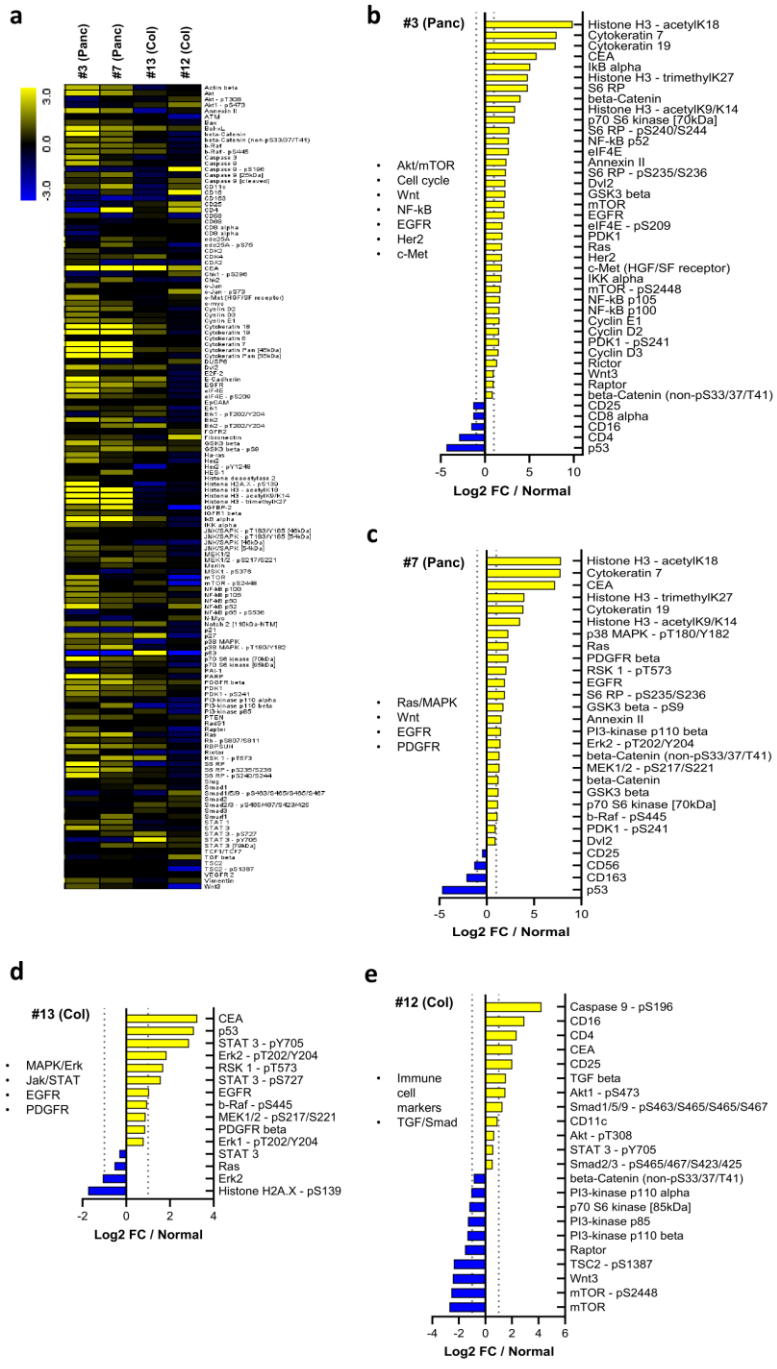

663

664 **Figure 4: Individual pancreas and colon tumor profiles (exemplary). a:** Heatmap showing
665 tumor/normal relative DigiWest data (Log2 FCs) of all analytes for given example cases (#3, #7, #13,
666 #12). **b-e:** Selection of key up- or downregulated analytes versus matched normal tissue for
667 respective example case. Selection was based on markers and key regulatory (pathway) proteins.
668 Individual bulleted lists indicate affected pathways including potential drug targets. Analogue profiles
669 of all other 16 patients are shown in **Suppl. Figs. S8-S23.**

670

671 Figure 5

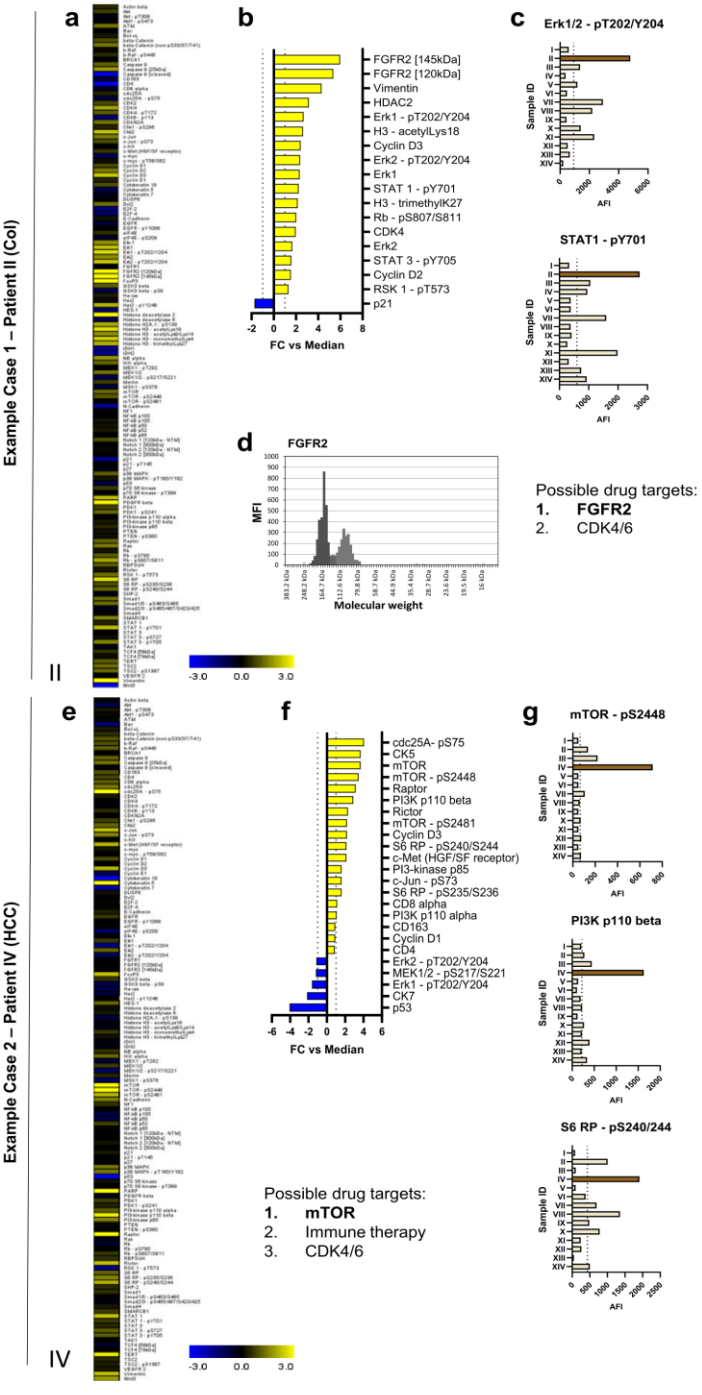

672

673 **Figure 5: Personalized tumor profiles for select prospective MTB cases. a-d:** Case/profile 1 (patient
674 II) – colon carcinoma. **a:** Heatmap of DigiWest expression data (normalized AFI) as Log2 FC in relation
675 to median signal (baseline) across all tumors (I-XIV). **b:** Selection of key analytes shown relative to
676 baseline signal. **c:** Expression data (normalized AFI) for Erk1/2 – pT202/204 and STAT1 – pY701 in all
677 tumors (I-XIV). Sample-specific signal is shown in brown and dashed line indicates median signal
678 across all samples. **d:** DigiWest peak profile of FGFR2. Black peak=145 kDa, grey peak=120 kDa;
679 MFI=median fluorescent intensity. **e-g:** Case/profile 2 (patient IV) – hepatocellular carcinoma. **e:**
680 Heatmap of DigiWest expression data (normalized AFI) as Log2 FC in relation to median signal
681 (baseline) across all tumors (I-XIV). **f:** Selection of key analytes shown relative to baseline signal. **g:**
682 Expression data (normalized AFI) for mTOR – pS2448, PI3K p110 beta and S6 RP – pS240/244 in all
683 tumors (I-XIV). Sample-specific signal is shown in brown and dashed line indicates median signal
684 across all samples. A ranking of potential treatment recommendations based on DigiWest data is
685 given. Most promising drug target printed in bold. Analogue profiles of all other 12 patients are
686 shown in the **Suppl. Figs. S25-S36.**

12. Tables

Table 1

#	Origin	Patient Age (y)	Pre-Therapy	Localization (Colon)	Markers	Key Pathways	Receptors	Others	Pathway identified?
1	Pancreas	74	none	---	CEA+++ CK19+++ CK7+++	**p53 loss/cell cycle++** **Ras/MAPK/Erk++**	**c-Met** **VEGFR** Her2	mTOR-p70S6K-S6	**Yes**
3	Pancreas	72	none	---	CEA+++ CK19+++ CK7+++	**Akt/mTOR++** **p53 loss/cell cycle++** **beta-catenin++**	EGFR Her2 c-Met	Histone modifications NF-kB	**Yes**
4	Pancreas	73	none	---	CEA+++ CK19+++ CK7++ **AXII-**		c-Met	NF-kB Histone modifications protein synthesis+	No
7	Pancreas	69	none	---	CEA+++ CK19+++ CK7+++	**Ras/MAPK/Erk/p38++** Wnt/beta-catenin+	**EGFR** **PDGFR**	p53 loss Histone modifications	**Yes**
8	Pancreas	74	none	---	CEA+ CK19++ CK7+++ **CK5+++**	**Akt/mTOR++**	Her2 EGFR	Histone modifications p53 loss/cell cycle NF-kB	**Yes**
2	Pancreas	67	none	---	CEA+ CK19++ CK7+++	**immune cells++** cell cycle+		NF-kB	**Yes**
5	Pancreas	50	none	---	CEA+++ CK19+			TGF beta/Smad+ Akt - Caspase 9	No
6	Pancreas	84	none	---	CEA+++ **CK19--** **pan-CK--**	**immune cells++**		TGF beta/Smad+ p53++ PIK3CA++	**Yes**
9	Pancreas	59	none	---	CEA+++ CK19+++ CK7+	**Ras/MAPK/Erk+++** **Immune cells++**	PDGFR	PI3K/Akt/mTOR TGF beta/Smad EMT	**Yes**
10	Pancreas	55	none	---	**CEA-** **CK7-**	**Immune cells+**		EMT p53++	(No)
11	Colon	51	5-FU + Radiation	left	CEA+++ **CK19+++** CDX2++	**EMT**		Histone modifications Immune cells+	**Yes**
12	Colon	55	none	right	CEA++	**Immune cells+**		TGF beta/Smad+ Akt - Caspase 9	**Yes**
13	Colon	72	5-FU + Irinonetecan	left	CEA+++	**MAPK/Erk+++** **Jak/STAT+++**	**EGFR** PDGFR		**Yes**
14	Colon	86	none	left	CEA+++ CDX2++	**Akt/mTOR ++**	c-Met	TGF beta/Smad+ p53+++	**Yes**
15	Colon	77	none	right	CEA++	**cell cycle++**	**Her2**		**Yes**
16	Colon*	30	none	right	CEA+++ **CK7++**			**mostly downregulations** Caspase 9 Immune cells	No
17	Colon	77	Radiation	right	CEA+++			**mostly downregulations** Caspase 9	No
18	Colon**	26	Cisplatin / Etoposide / Ifosfamide	right	CEA+++ **CK19+++** **CDX2+++** AXII++	**Ras/MAPK/Erk/p38++** **Akt/mTOR++**	**Her2**	**Histone modifications** Wnt/beta-catenin+ Select immune cells	**Yes**
19	Colon	78	none	right	CEA+++	**Developmental pathways+**		Select immune cells	**Yes**
20	Colon	72	none	left	CEA+++	**Akt/mTOR++** Wnt/beta-catenin++		cell cycle++ p53+++	**Yes**

*MSI-high tumor (Lynch syndrome/HNPCC)
**Hepatoid carcinoma (partial endocrine differentiation)

Σ 15/20 (**75%**)

690 **Table 1: Summary of clinical and DigiWest data of retrospective patient cohort.** For each patient (n =
691 20), relevant available clinical data is shown (left) as well as relevant marker proteins, upregulated key
692 pathways and receptors (right). Yes = coherent pathway activity, No = no clear indication of pathway
693 activity, (No) = sample with inconclusive marker pattern (CEA downregulation). Identifications are
694 based on DigiWest data in relation to respective normal tissue (as Log 2 FC). Most apparent or unique
695 expression signatures/sample are indicated in bold. Blue shadings for pancreatic carcinomas are
696 representative of sub-grouping as identified in **Fig.2.** + = relative upregulation versus matched normal
697 tissue, - = relative downregulation.

698 Table 2
699

#	Tumor	Deregulated key pathways (DigiWest)	Pathway identified?	Possible drug targets (DigiWest)	Key mutations (MTB-identified)	MTB drug recommendation	DigiWest supportive to MTB?
I	**Cholangiocarcinoma**	cell cycle Histone methylation (DNA Damage)	**Yes**	1. CDK4/6 2. IDH1 3. Immune therapy	IDH1 mut Cyclins amp TP53 mut ATM mut	IDH1-inh. (Ivosidenib) FGFR-inh.	**(Yes)**
II	**Colorectal carcinoma**	MAPK/Erk STAT1/STAT3 FGFR2 (Histone modification)	**Yes**	1. FGFR 2. CDK4/6	FGFR2 amp	FGFR-inh. + PD-1/PD-L1	**Yes**
III	**Gallbladder carcinoma**	PI3K/mTOR Her2/VEGFR2/c-Met (MAPK/Erk)	**Yes**	1. mTOR 2. Her2 3. TK (Her2/VEGFR/MET) 4. MEK	BRAF mut CDKN1B/2A del CDK4 amp	MEK+BRAF-inh. PD1/PD-L1	**(Yes)**
IV	**Hepatocellular carcinoma**	PI3K/mTOR Immune cells cell cycle	**Yes**	1. mTOR 2. Immune therapy 3. CDK4/6	TSC2 del	mTOR-inh. PD1/PD-L1 + TKI PD1/PD-L1 + Bevacicumab PD1/PD-L1 + anti-CTLA4	**Yes**
V	**Pancreatic carcinoma**	MAPK/Erk PDGFR beta/Her2 (cell cycle)	**Yes**	1. KRAS 2. PDGFR 3. Her2 4. CDK4/6	CDKN1A del KRAS mut	MEK-inh. + CDK4/6-inh. (PARP-inh.)	**Yes**
VI	**Gastric carcinoma (CUP)**	(Histone acetylation, HDAC6)	No	none	FAT1 mut NF1 del BRAF mut	TK-inh. (Lenvatinib) + PD1/PD-L1	No
VII	**Esophageal carcinoma**	MAPK/Erk Akt/PI3K/mTOR Wnt/beta-Catenin STAT1/STAT3	**Yes**	1. FGFR 2. TK (PDGFR/VEGFR)	FGFR2-PAPSS1 fus BRCA2 mut	FGFR-inh. PARP-inh.	**Yes**
VIII	**Gallbladder carcinoma**	MAPK/Erk NF-kB Histone acetylation, HDAC	**Yes**	1. MEK 2. HDAC	IDH1 mut ARID1A del/mut ATM del/mut BAP1 del/mut	IDH1-inh. PD1/PD-L1	No
IX	**Cholangiocarcinoma (metastasis)**	(IDH1/2, Histone modification)	No	none	FGFR2-SHTN1 fus BAP1 del/mut	FGFR-inh.	No
X	**Pancreatic carcinoma**	MAPK/Erk Wnt/beta-Catenin NF-kB VEGFR2	**Yes**	1. MEK 2. KRAS 3. VEGFR	KRAS mut	MEK-inh. Autophagy-inh.	**Yes**
XI	**Cholangiocarcinoma**	p53 loss/cell cycle MAPK/, Akt, STAT Smad signaling PDGFRB, FGFR1	**Yes**	1. TK (PDGFR/FGFR) 2. CDK4/6 3. TGFBR	IDH2 mut SMAD4 mut ARID1A mut (CDKN2A inv)	IDH2-inh.	No
XII	**Pancreatic carcinoma**	cell cycle PI3K/Akt	**Yes**	1. CDK4/6 2. PI3K 3. mTOR	TP53 mut KRAS mut	MEK-inh. + CDK4/6-inh.	**(Yes)**
XIII	**Pancreatic carcinoma**	cell cycle DNA damage Smad signaling	**Yes**	1. CDK4/6 2. TGFRB	NBN mut KRAS mut SMAD4 mut	none	n/a
XIV	**Rectal carcinoma**	p53 loss/cell cycle PI3K/Akt Her2	**Yes**	1. CDK4/6 2. Her2 3. PI3K	TP53 mut ERBB2 amp EGFR amp	none	n/a
			12/14 cases				**8 / 12 cases**

700

Table 2: Summary of DigiWest and genetic/MTB data from MTB patient cohort. Left: Tumor entity of each included patient (n = 14). **Middle:** Key pathways identified by DigiWest are shown. **Yes** = coherent pathway activity, No = no clear indication of pathway activity. In each case, list of potential drug targets is based solely on DigiWest data. Note: General term "Immune therapy" is used for tumors with notable expression of TIL markers ("hot"); here, any form of immune-related therapy could be considered (e.g. PD1/PD-L1). **Right:** Key mutations as identified by MTB sequencing analysis and MTB treatment recommendation. (mut = mutation, del = deletion, amp = amplification, fus = fusion). Rightmost column: Is DigiWest data confirming potential underlying MTB-identified driver mutations and subsequent drug recommendations? **Yes**= supportive, (**Yes**)= partially supportive, **No**= not supportive. Note: For two cases (XIII and XIV), no MTB drug recommendation was made (n/a).

Personalized signaling pathway analysis of gastrointestinal tumors for patient stratification and drug target evaluation using clinically derived core biopsies

Stahl et al.

Supplementary Information

I. Supplementary Figures

II. Supplementary Tables

I. Supplementary Figures

Suppl. Fig. S1

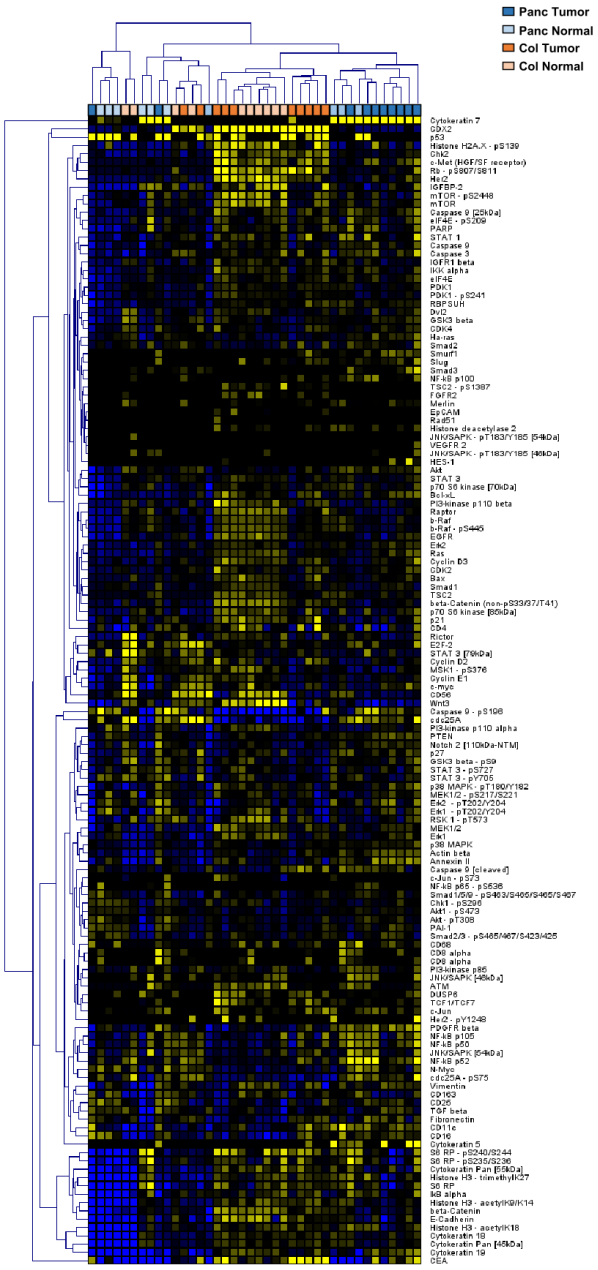

Suppl. Fig. S1: Heatmap and Hierarchical Cluster analysis of DigiWest data set including all retrospectively analyzed tumor and normal (non-tumorous) tissue samples (n = 40). Clustering was performed using Euclidian Distance and complete linkage.

Suppl. Fig. S2

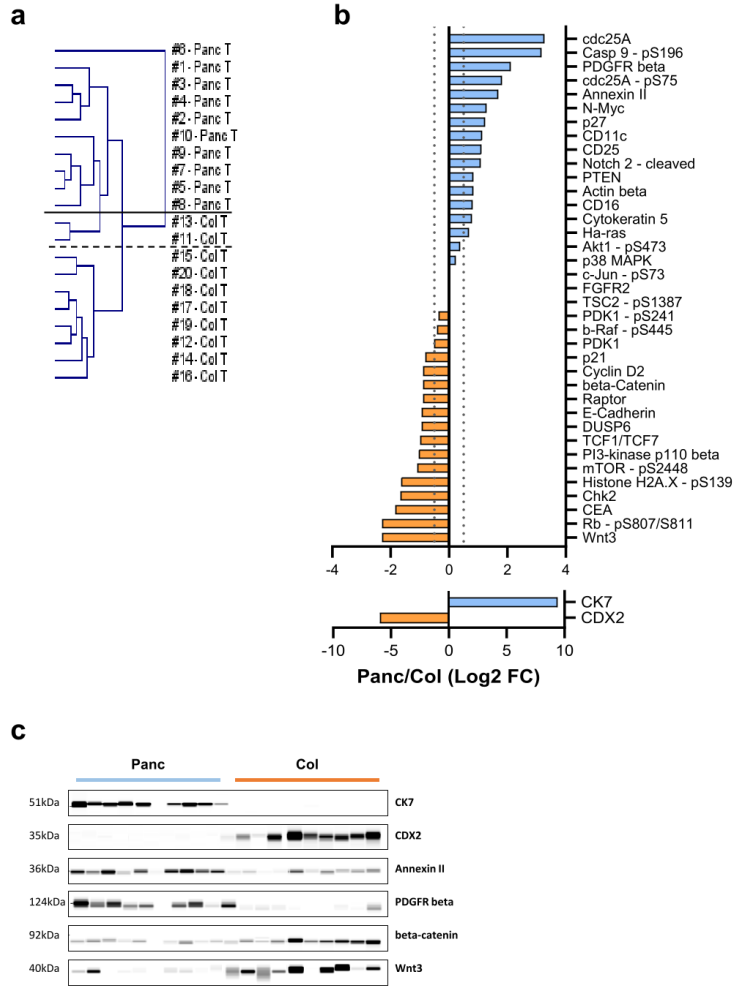

Suppl. Fig. S2: a: Hierarchical Cluster analysis of all pancreas and colon tumor tissues (n = 20). Clustering was performed using Euclidian Distance and complete linkage. Solid line indicates separation based on tissue type; dashed line based on clustering only. **b:** Log2 Fold changes (Median AFI Panc/ Median AFI Col) of all differentially expressed analytes. Analytes with higher expression in pancreas tumors indicated in blue, colon in orange. **c:** Western Blot mimics (grayscale maps generated from DigiWest data) of selected differentially expressed proteins. For graphical representation, background-subtracted raw data from representative pancreas and colon samples were used.

Suppl. Fig. S3

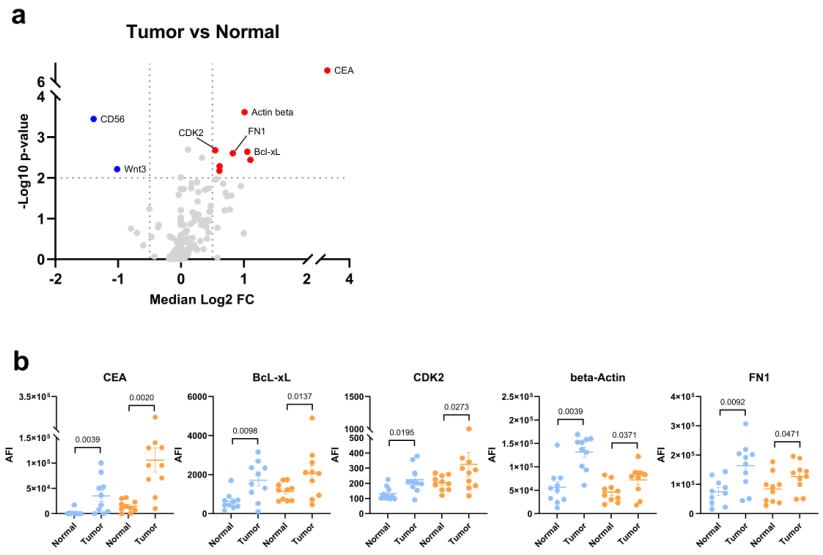

Suppl. Fig. S3: a: Volcano plot of comparison between all tumor (n=20) and their respective normal tissues (n=20); paired t-test, $p < 0.01$. Significantly upregulated proteins are shown in red, downregulated proteins in blue. Analytes with FCs < I0.5I are excluded. **b:** DigiWest data (normalized AFI) for analytes with tumor-associated effects consistent in both tumor types. Separate tumor versus normal comparison for each tumor type (blue = pancreas, orange = colon, tumor - n=10 each, normal – n=10 each); p-value as indicated. Solid line indicates the mean FC value per group. Error bars: S.E.M.

Suppl. Fig. S4

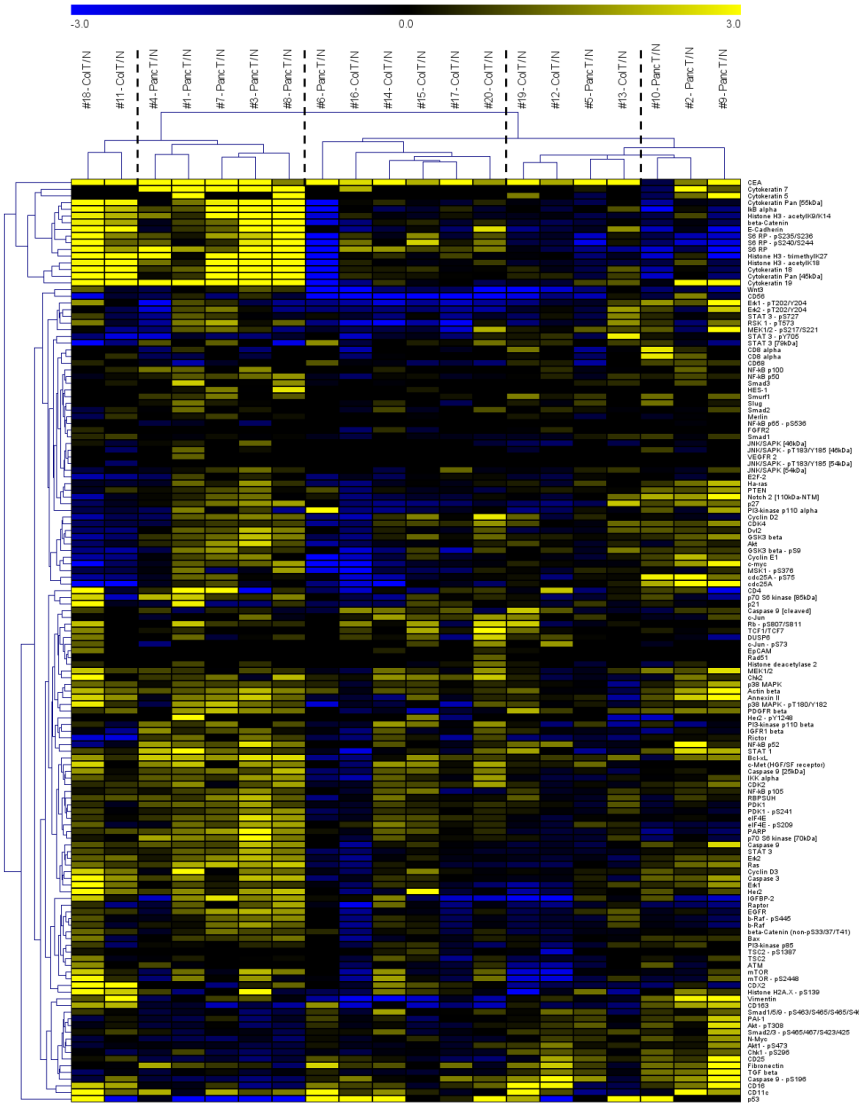

Suppl. Fig. S4: Hierarchical Cluster Analysis of all tumor tissues (n = 20) in relation to their respective, patient-matched normal tissue (T/N as Log2 Fold Changes). Dashed lines separate the observed four sample clusters. Clustering was performed using Euclidian Distance and complete linkage.

Suppl. Fig. S5

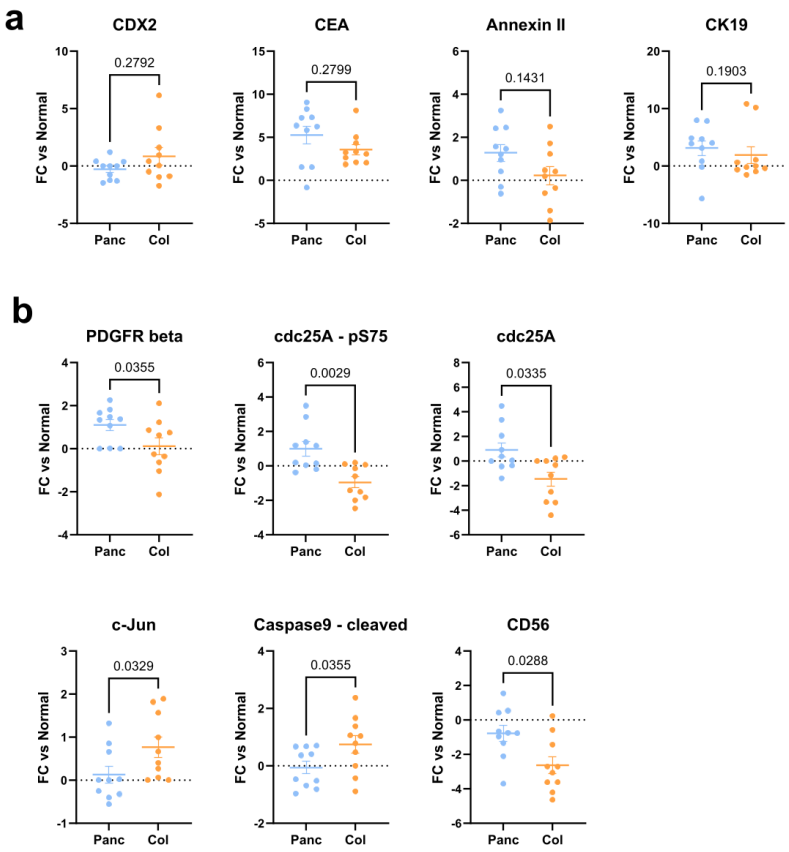

Suppl. Fig. S5: Tumor/normal-matched relative DigiWest data (as Log2 FCs) for additional differentially expressed analytes between tumor types (n = 10 each) based on the comparison in **Fig. 1d**; Mann-Whitney test, $p < 0.05$. **a:** Tissue-specific markers mostly show no differential effects. **b:** Analytes including proteins stemming from tumor suppressor- and oncogenes showing significant differences. Panc = Pancreas (blue), Col = Colon (orange); p-value as indicated. Solid line indicates the mean FC value per group. Error bars: S.E.M.

Suppl. Fig. S6

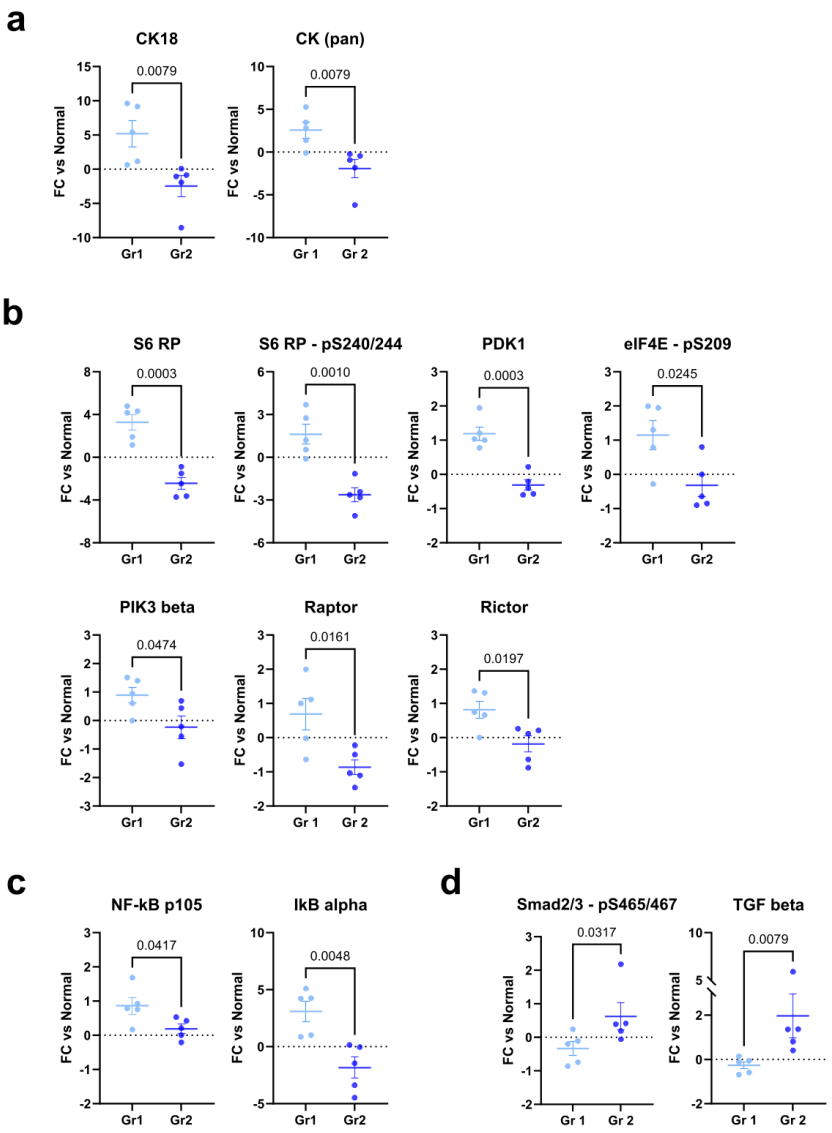

Suppl. Fig. S6: Tumor/normal-matched relative DigiWest data (as Log2 FCs) for additional differentially expressed analytes between Group 1 (light blue, n = 5) and Group 2 (dark blue, n = 5) pancreas tumors based on the comparison from **Fig. 2c-e**; Mann-Whitney test, $p < 0.05$. **a-d:** Analytes of interest sorted according to their pathway/function allocation. **a:** Cytokeratins, **b:** mTOR signaling/protein synthesis, **c:** NF-kappaB signaling, **d:** immune cell markers/Smad signaling. Data shown is a larger collection of relevant analytes from **Fig. 2c-e.** Either the Mann-Whitney test or unpaired t-test was used depending on data distribution; p-value as indicated. Solid line indicates the mean FC value per group. Error bars: S.E.M.

Suppl. Fig. S7

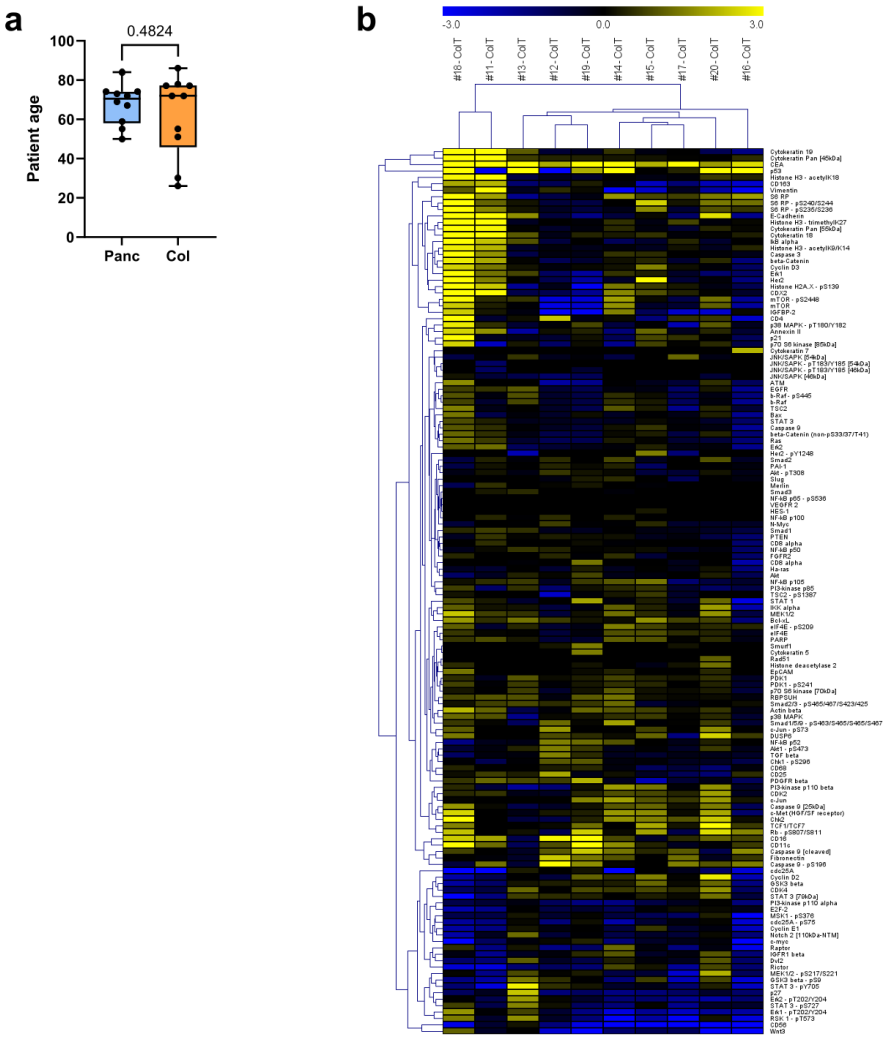

Suppl. Fig. S7: a: Boxplots showing distribution of patient age in pancreas (blue) and colon (orange) CA cohorts (n = 10 each); unpaired t-test. Solid line within the box indicates average patient age/group with whiskers indicating the range (min/max). Individual patient ages are also shown in **Table 1**. **b:** Hierarchical Cluster Analysis of colon tumor tissues (n = 10) in relation to their respective, patient-matched normal tissue (T/N as Log2 Fold Changes). Clustering was performed using Euclidian Distance and complete linkage. Sample tree is also shown in **Fig. 3a**.

Suppl. Fig. S8

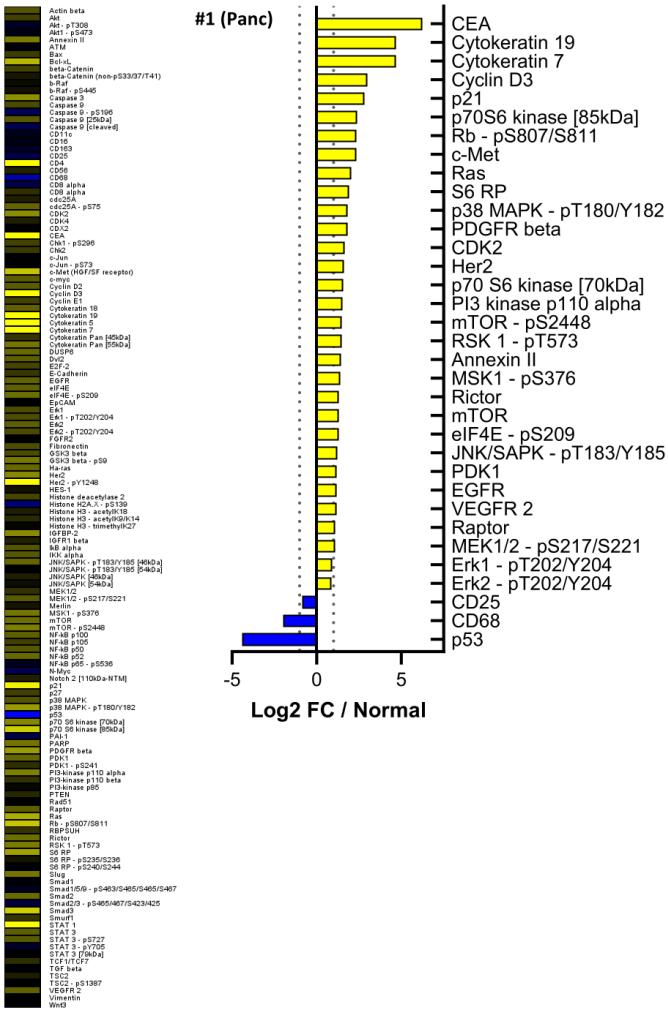

Suppl. Fig. S8: Individual protein profile of pancreas tumor #1. Heatmap showing tumor/normal relative DigiWest data (Log2 FCs) of all analytes (left) and election of key up- or downregulated analytes versus matched normal tissue (right). Selection was based on markers and key regulatory (pathway) proteins.

Suppl. Fig. S9

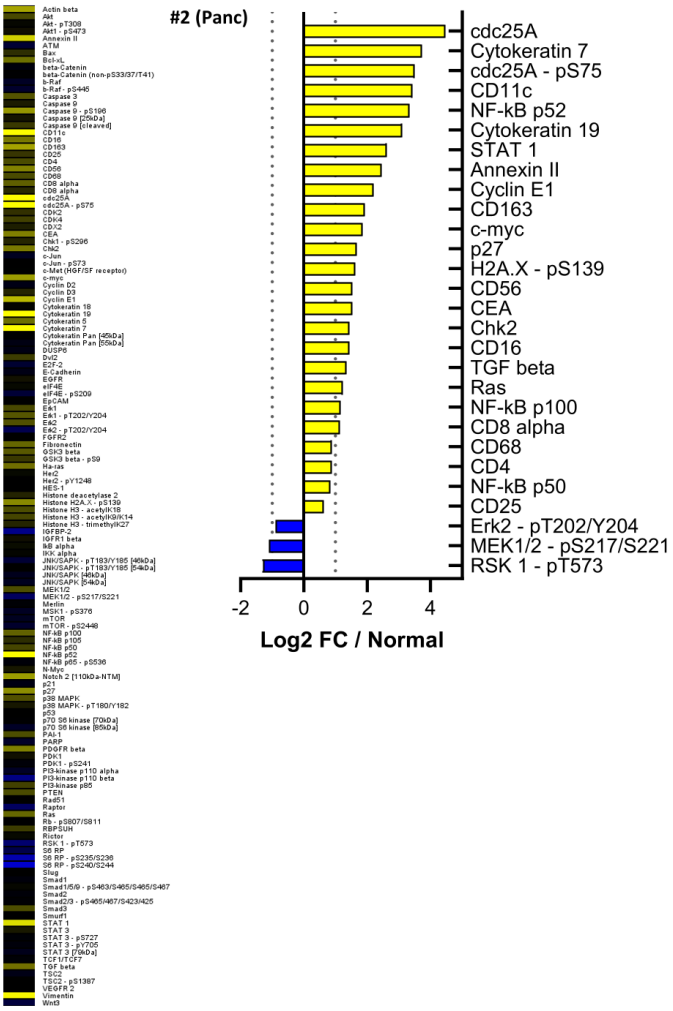

Suppl. Fig. S9: Individual protein profile of pancreas tumor #2. Heatmap showing tumor/normal relative DigiWest data (Log2 FCs) of all analytes (left) and election of key up- or downregulated analytes versus matched normal tissue (right). Selection was based on markers and key regulatory (pathway) proteins.

Suppl. Fig. S10

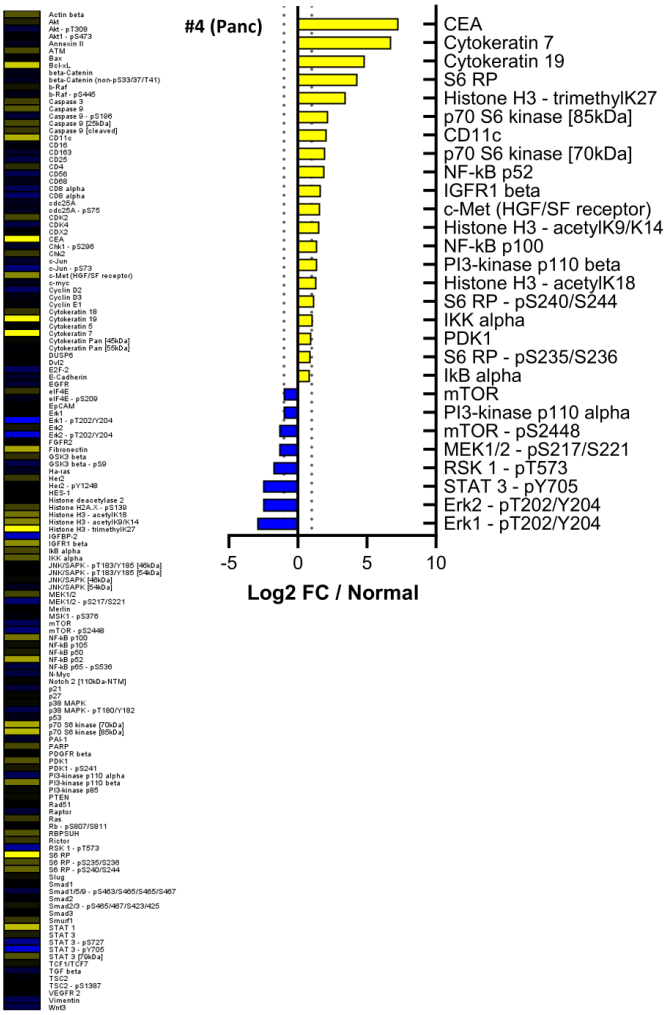

Suppl. Fig. S10: Individual protein profile of pancreas tumor #4. Heatmap showing tumor/normal relative DigiWest data (Log2 FCs) of all analytes (left) and election of key up- or downregulated analytes versus matched normal tissue (right). Selection was based on markers and key regulatory (pathway) proteins.

Suppl. Fig. S11

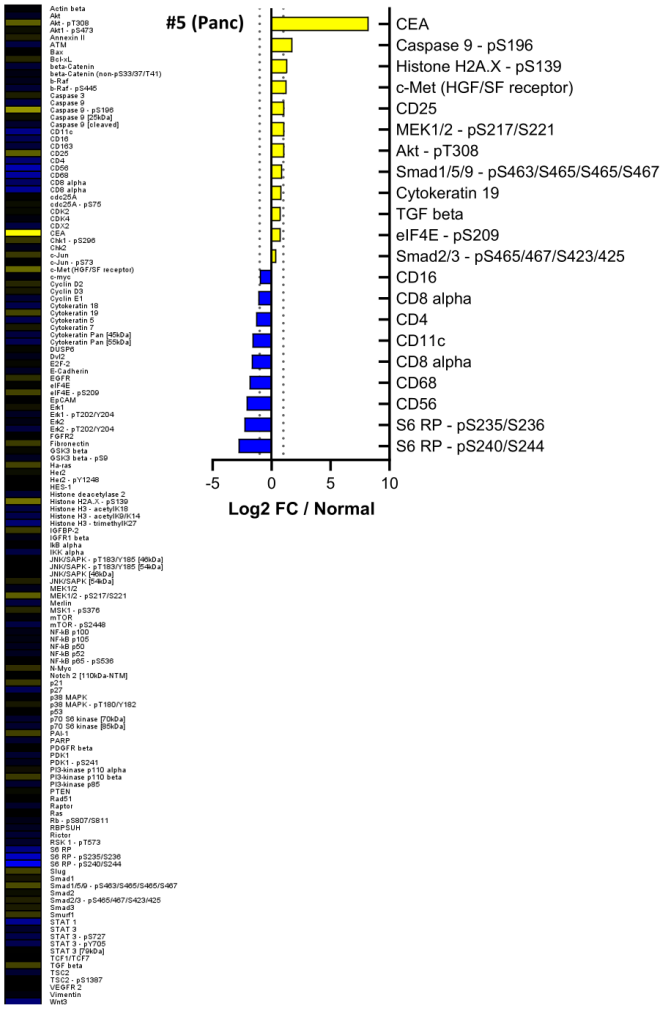

Suppl. Fig. S11: Individual protein profile of pancreas tumor #5. Heatmap showing tumor/normal relative DigiWest data (Log2 FCs) of all analytes (left) and election of key up- or downregulated analytes versus matched normal tissue (right). Selection was based on markers and key regulatory (pathway) proteins.

Suppl. Fig. S12

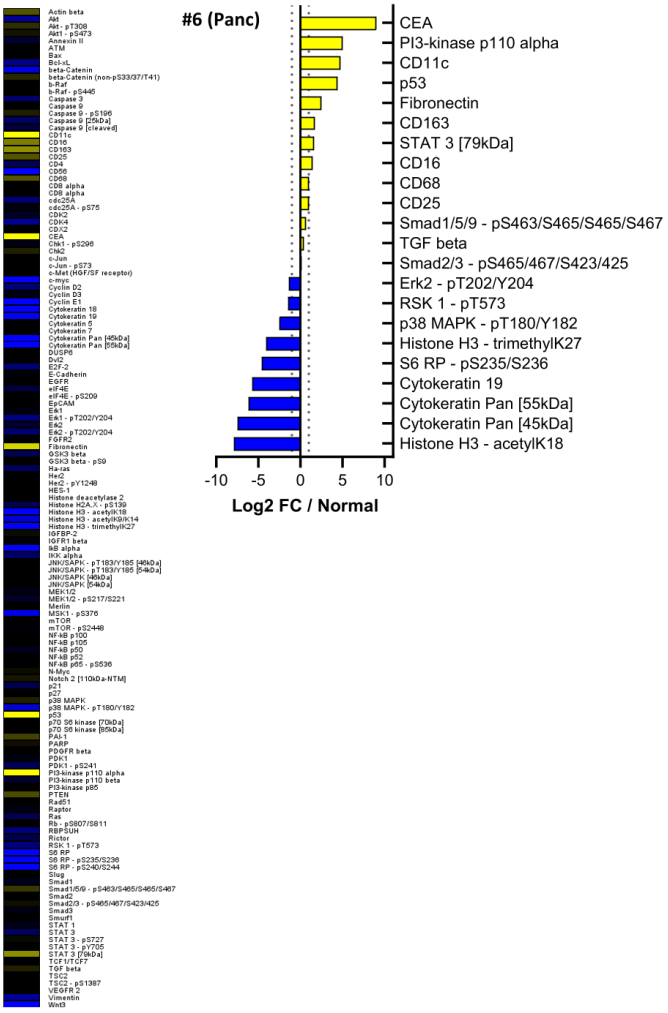

Suppl. Fig. S12: Individual protein profile of pancreas tumor #6. Heatmap showing tumor/normal relative DigiWest data (Log2 FCs) of all analytes (left) and election of key up- or downregulated analytes versus matched normal tissue (right). Selection was based on markers and key regulatory (pathway) proteins.

Suppl. Fig. S13

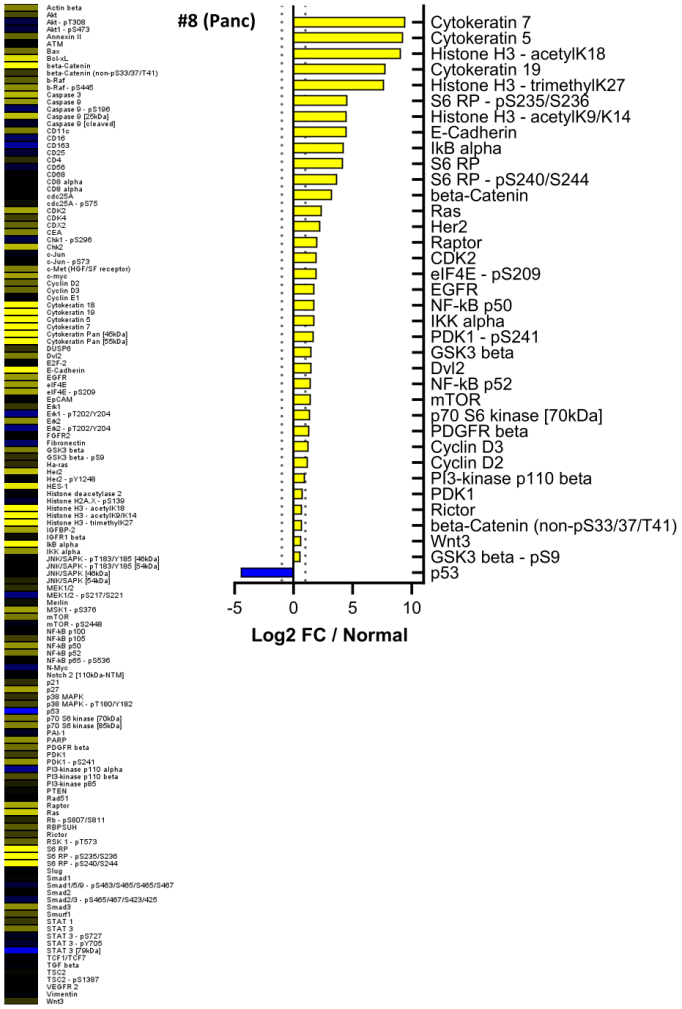

Suppl. Fig. S13: Individual protein profile of pancreas tumor #8. Heatmap showing tumor/normal relative DigiWest data (Log2 FCs) of all analytes (left) and election of key up- or downregulated analytes versus matched normal tissue (right). Selection was based on markers and key regulatory (pathway) proteins.

Suppl. Fig. S14

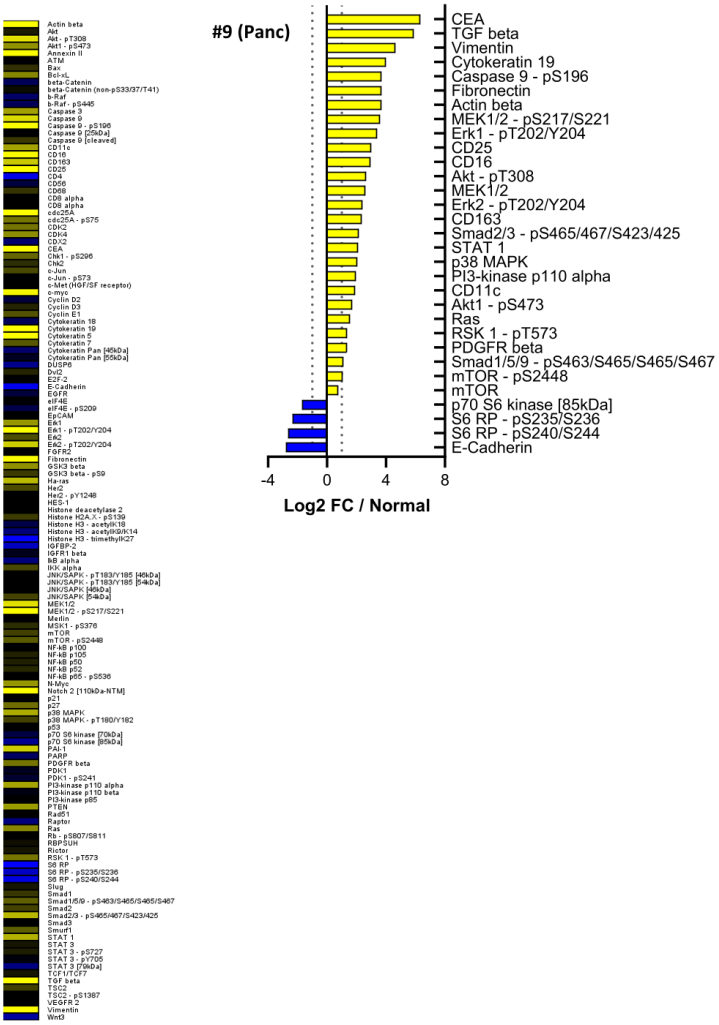

Suppl. Fig. S14: Individual protein profile of pancreas tumor #9. Heatmap showing tumor/normal relative DigiWest data (Log2 FCs) of all analytes (left) and election of key up- or downregulated analytes versus matched normal tissue (right). Selection was based on markers and key regulatory (pathway) proteins.

Suppl. Fig. S15

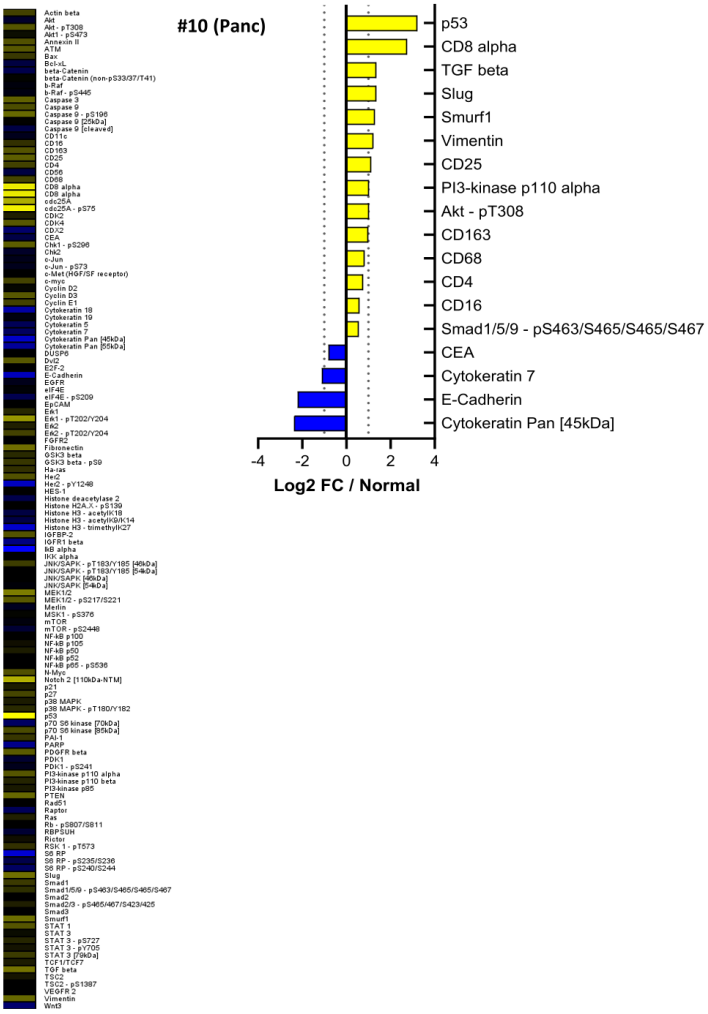

Suppl. Fig. S15: Individual protein profile of pancreas tumor #10. Heatmap showing tumor/normal relative DigiWest data (Log2 FCs) of all analytes (left) and election of key up- or downregulated analytes versus matched normal tissue (right). Selection was based on markers and key regulatory (pathway) proteins.

Suppl. Fig. S16

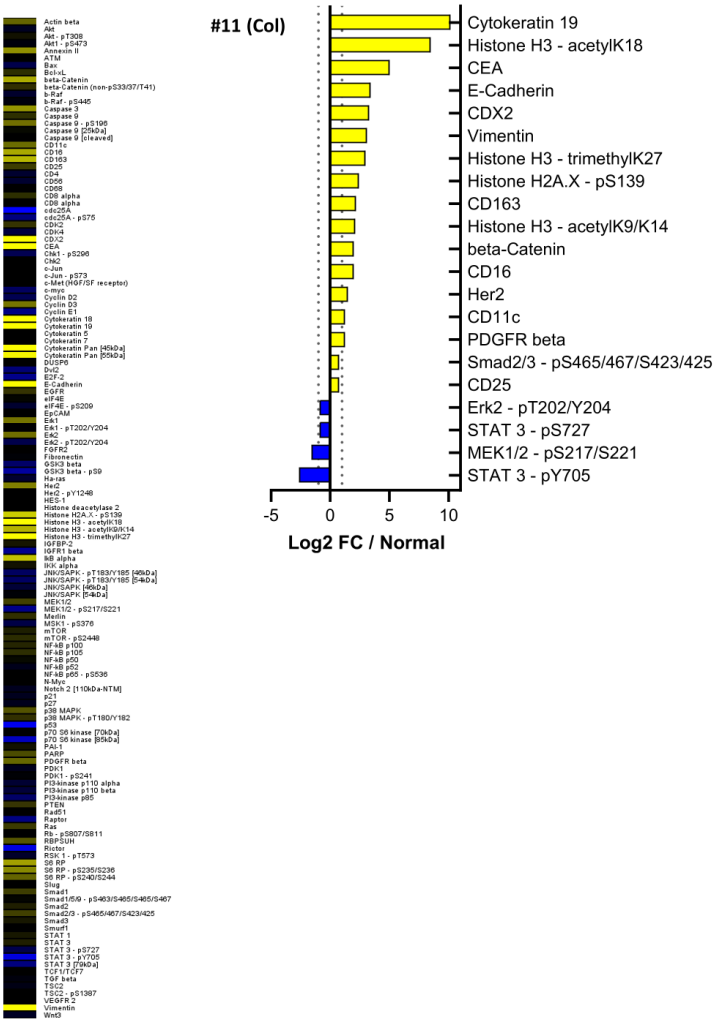

Suppl. Fig. S16: Individual protein profile of colon tumor #11. Heatmap showing tumor/normal relative DigiWest data (Log2 FCs) of all analytes (left) and election of key up- or downregulated analytes versus matched normal tissue (right). Selection was based on markers and key regulatory (pathway) proteins.

Suppl. Fig. S17

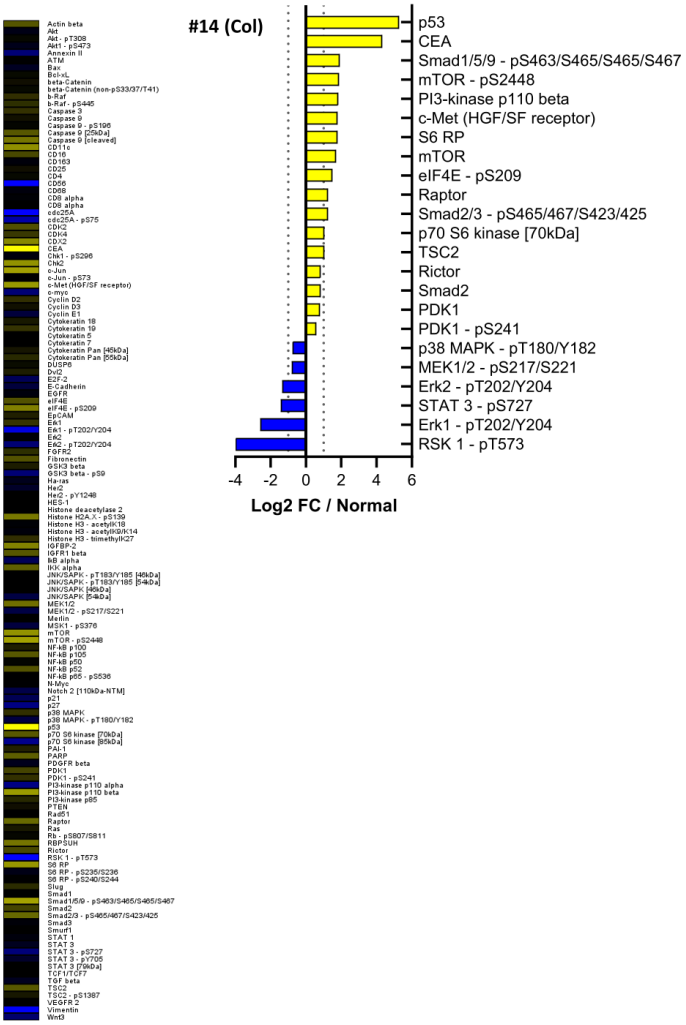

Suppl. Fig. S17: Individual protein profile of colon tumor #14. Heatmap showing tumor/normal relative DigiWest data (Log2 FCs) of all analytes (left) and election of key up- or downregulated analytes versus matched normal tissue (right). Selection was based on markers and key regulatory (pathway) proteins.

Suppl. Fig. S18

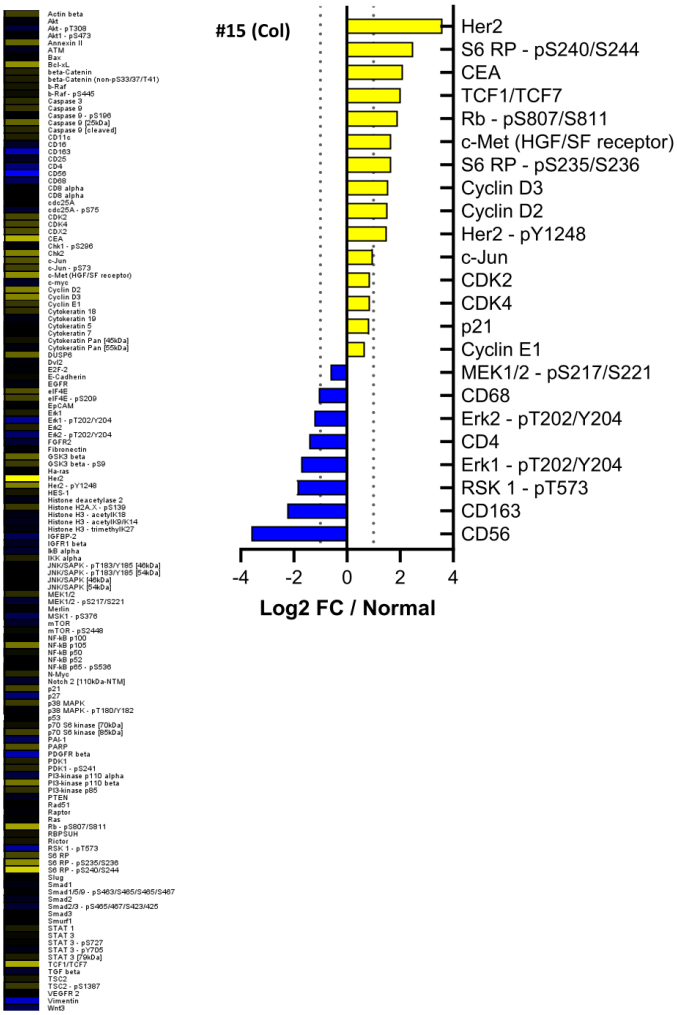

Suppl. Fig. S18: Individual protein profile of colon tumor #15. Heatmap showing tumor/normal relative DigiWest data (Log2 FCs) of all analytes (left) and election of key up- or downregulated analytes versus matched normal tissue (right). Selection was based on markers and key regulatory (pathway) proteins.

Suppl. Fig. S19

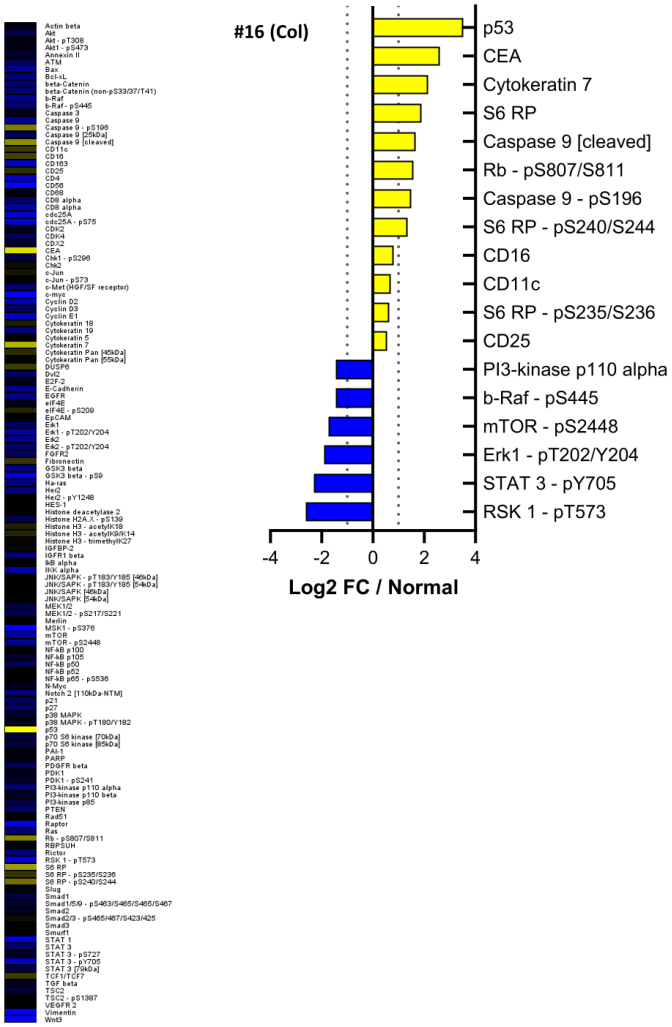

Suppl. Fig. S19: Individual protein profile of colon tumor #16 (**MSI-high tumor**). Heatmap showing tumor/normal relative DigiWest data (Log2 FCs) of all analytes (left) and election of key up- or downregulated analytes versus matched normal tissue (right). Selection was based on markers and key regulatory (pathway) proteins.

Suppl. Fig. S20

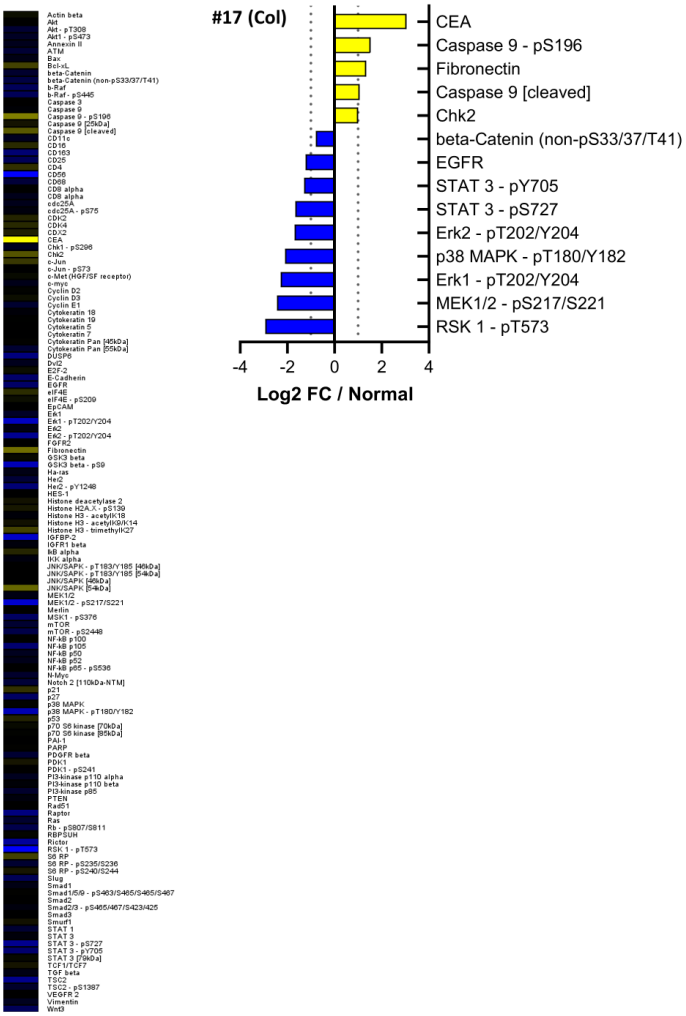

Suppl. Fig. S20: Individual protein profile of colon tumor #17. Heatmap showing tumor/normal relative DigiWest data (Log2 FCs) of all analytes (left) and election of key up- or downregulated analytes versus matched normal tissue (right). Selection was based on markers and key regulatory (pathway) proteins.

Suppl. Fig. S21

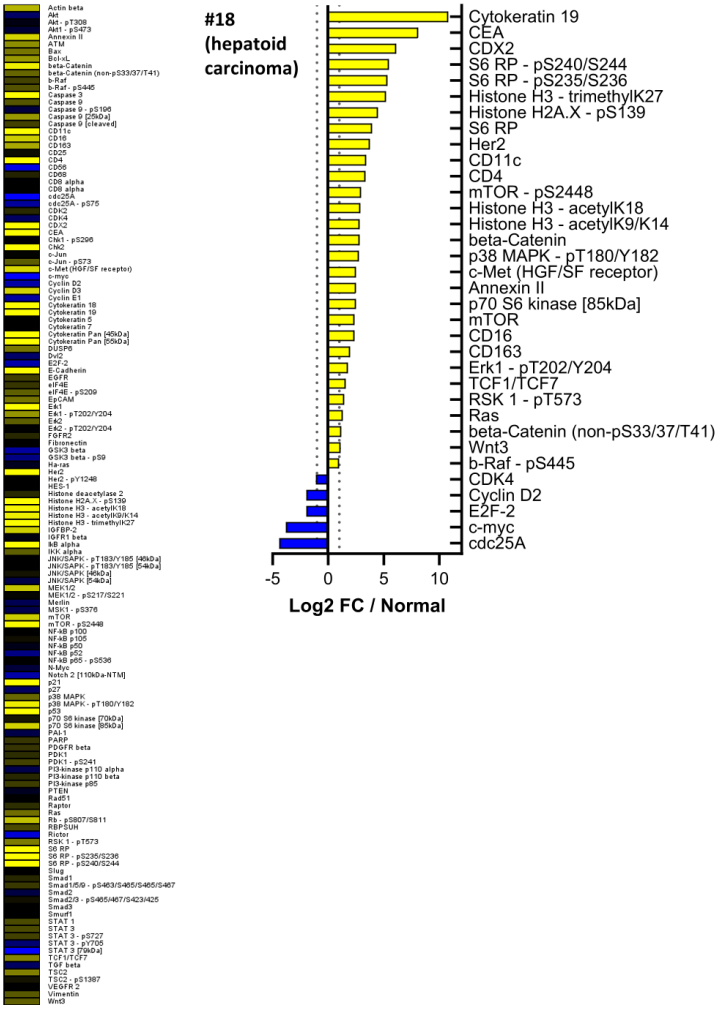

Suppl. Fig. S21: Individual protein profile of colon tumor #18 (**hepatoid carcinoma**). Heatmap showing tumor/normal relative DigiWest data (Log2 FCs) of all analytes (left) and election of key up- or downregulated analytes versus matched normal tissue (right). Selection was based on markers and key regulatory (pathway) proteins.

Suppl. Fig. S22

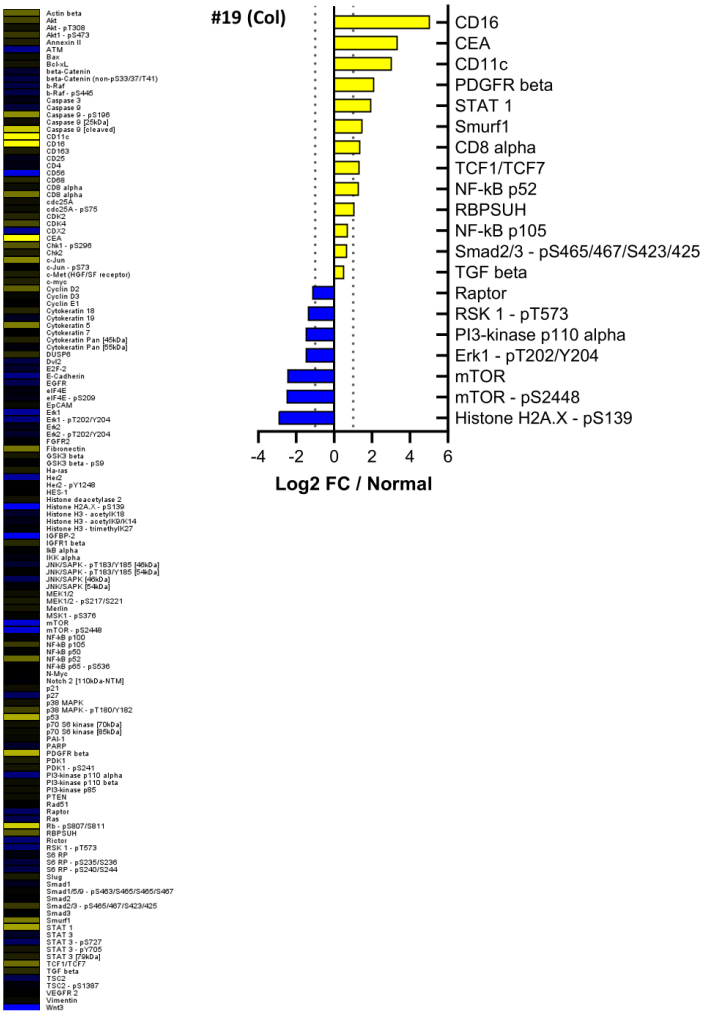

Suppl. Fig. S22: Individual protein profile of colon tumor #19. Heatmap showing tumor/normal relative DigiWest data (Log2 FCs) of all analytes (left) and election of key up- or downregulated analytes versus matched normal tissue (right). Selection was based on markers and key regulatory (pathway) proteins.

Suppl. Fig. S23

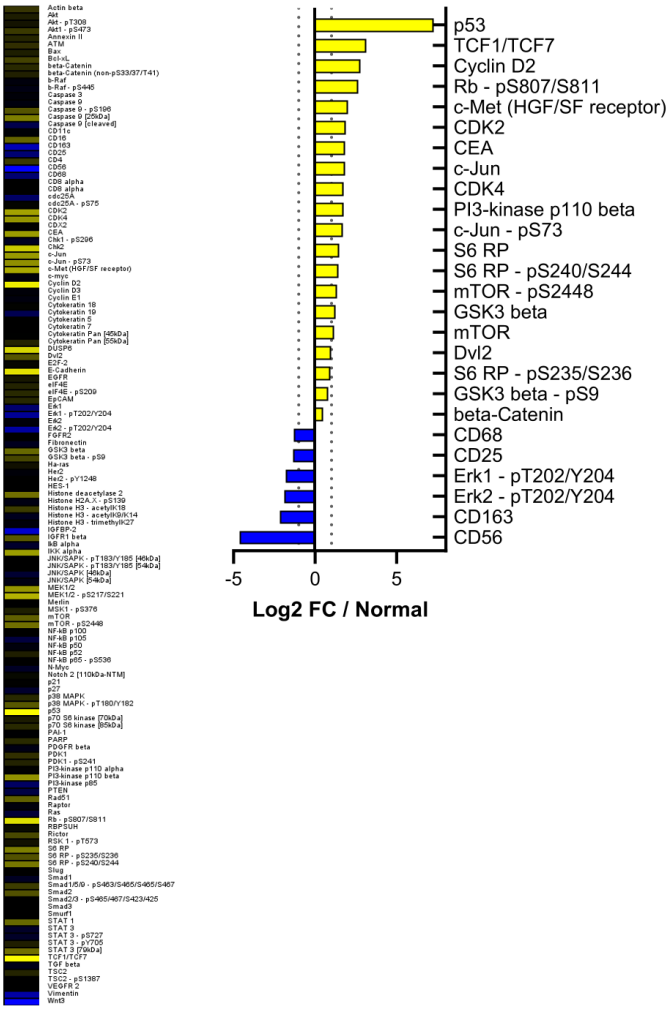

Suppl. Fig. S22: Individual protein profile of colon tumor #19. Heatmap showing tumor/normal relative DigiWest data (Log2 FCs) of all analytes (left) and election of key up- or downregulated analytes versus matched normal tissue (right). Selection was based on markers and key regulatory (pathway) proteins.

Suppl. Fig. S24

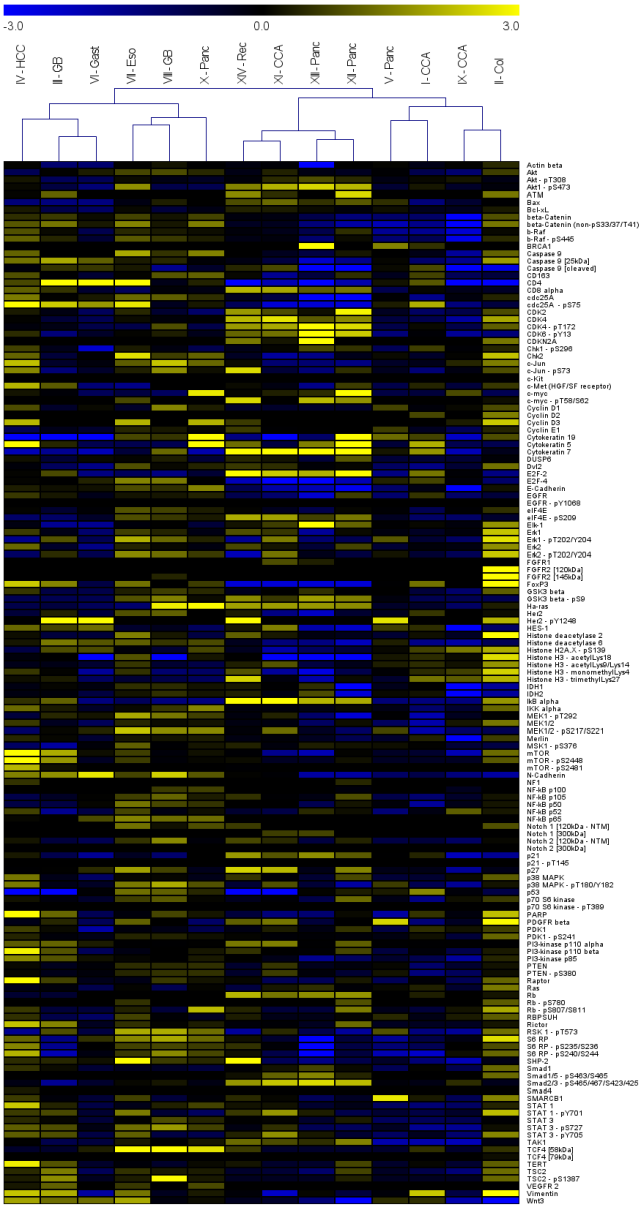

Suppl. Fig. S24: Heatmap and Hierarchical Cluster analysis of DigiWest data set including all non-retrospectively analyzed needle biopsy samples (n = 14). Clustering was performed using Euclidian Distance and complete linkage. HCC = hepatocellular carcinoma, GB = gallbladder carcinoma, Gast = Gastric carcinoma, Eso = esophageal carcinoma, Panc = pancreatic carcinoma, Rec = rectal carcinoma, CCA = cholangiocarcinoma, Col = colon carcinoma.

Suppl. Fig. S25

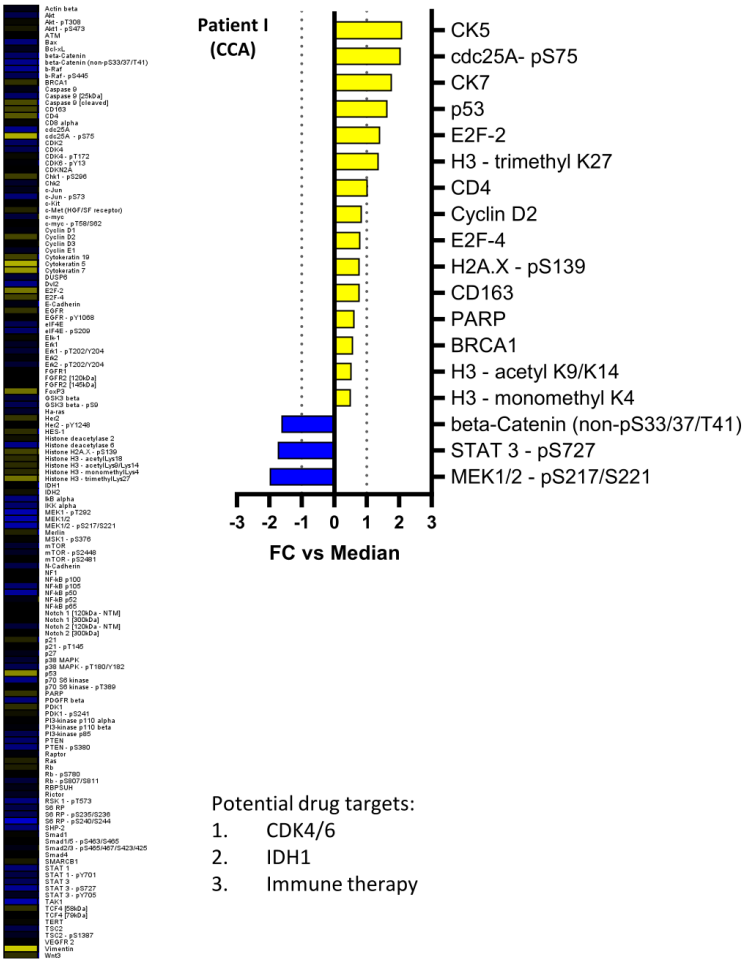

Suppl. Fig. S25: Individual protein profile of patient I (CCA - cholangiocarcinoma). Left: Heatmap of DigiWest expression data (normalized AFI) as Log2 FC in relation to median signal (baseline) across all tumors (I-XIV). Right: Selection of key analytes shown relative to baseline signal. Bottom: Ranking of potential drug targets based on DigiWest data.

Suppl. Fig. S26

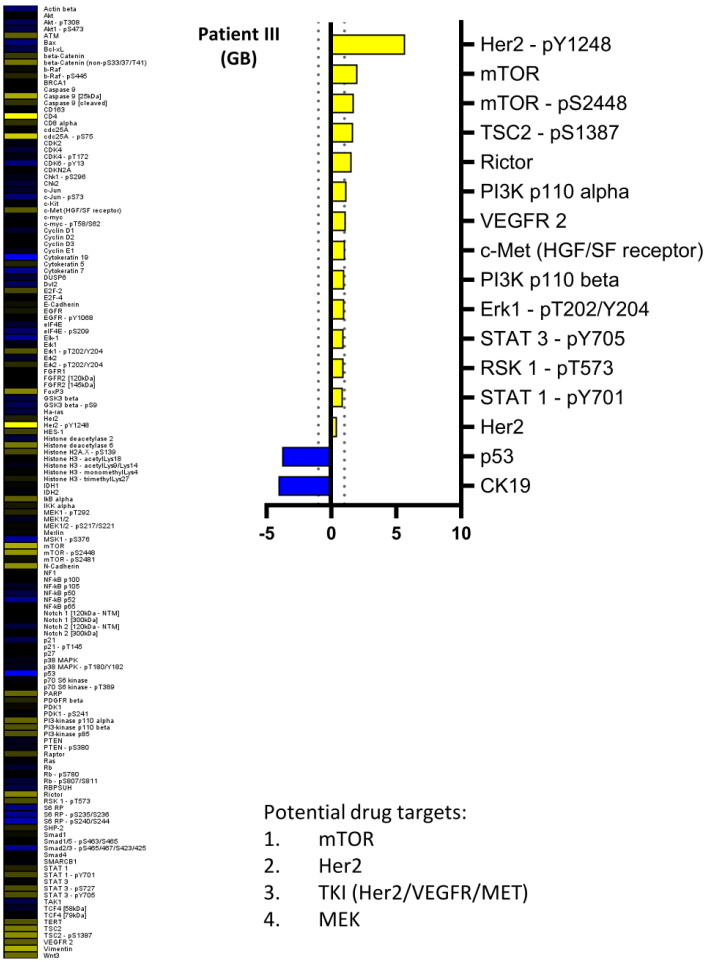

Suppl. Fig. S26: Individual protein profile of patient III (GB – gallbladder carcinoma). Left: Heatmap of DigiWest expression data (normalized AFI) as Log2 FC in relation to median signal (baseline) across all tumors (I-XIV). Right: Selection of key analytes shown relative to baseline signal. Bottom: Ranking of potential drug targets based on DigiWest data.

Suppl. Fig. S27

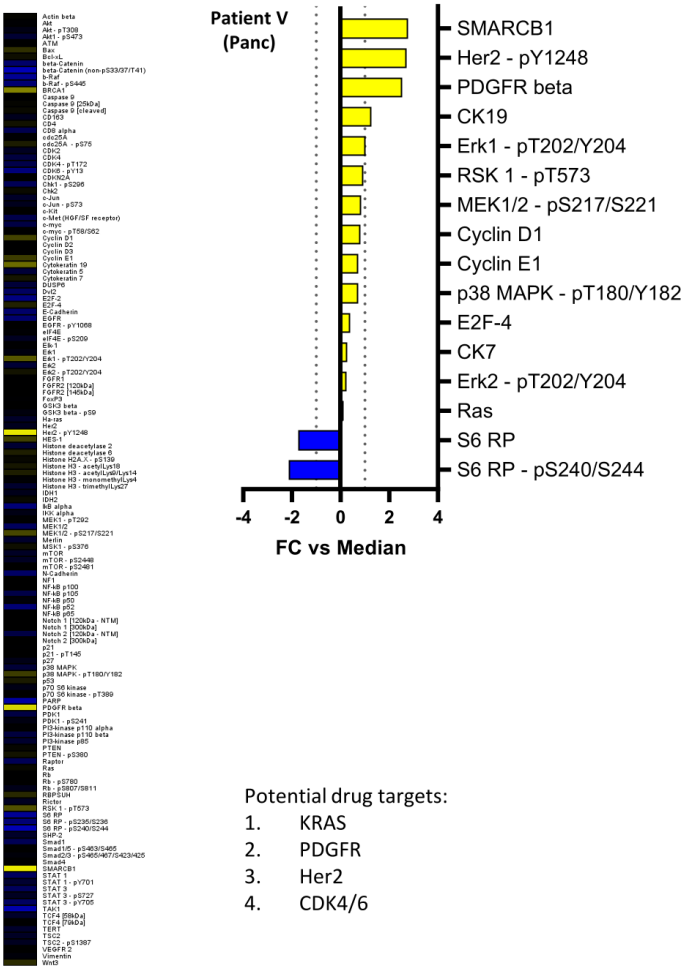

Suppl. Fig. S27: Individual protein profile of patient V (Panc – pancreatic carcinoma). Left: Heatmap of DigiWest expression data (normalized AFI) as Log2 FC in relation to median signal (baseline) across all tumors (I-XIV). Right: Selection of key analytes shown relative to baseline signal. Bottom: Ranking of potential drug targets based on DigiWest data.

Suppl. Fig. S28

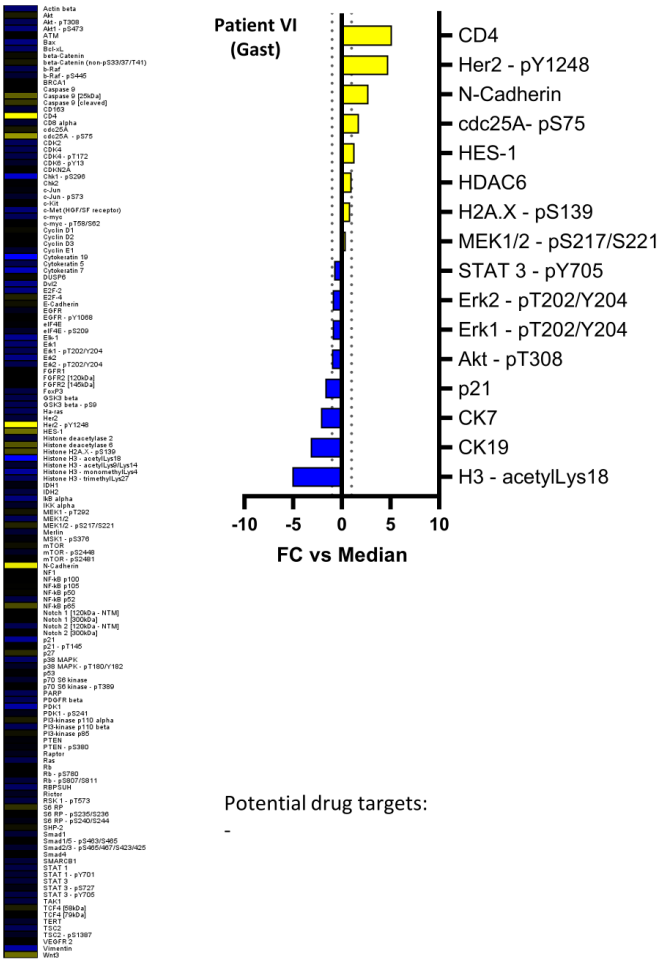

Suppl. Fig. S28: Individual protein profile of patient VI (Gast – gastric carcinoma). Left: Heatmap of DigiWest expression data (normalized AFI) as Log2 FC in relation to median signal (baseline) across all tumors (I-XIV). Right: Selection of key analytes shown relative to baseline signal. Bottom: Ranking of potential drug targets based on DigiWest data.

Suppl. Fig. S29

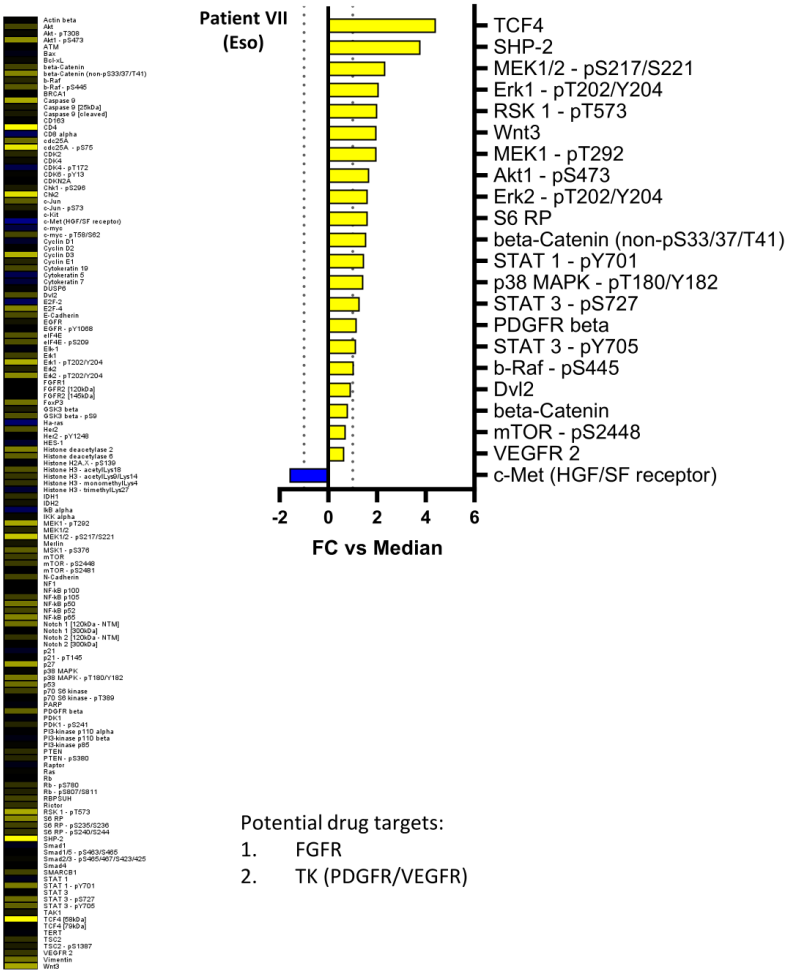

Potential drug targets:

1. FGFR
2. TK (PDGFR/VEGFR)

Suppl. Fig. S29: Individual protein profile of patient VII (Eso – esophageal carcinoma). Left: Heatmap of DigiWest expression data (normalized AFI) as Log2 FC in relation to median signal (baseline) across all tumors (I-XIV). Right: Selection of key analytes shown relative to baseline signal. Bottom: Ranking of potential drug targets based on DigiWest data. Eventual MTB treatment printed in bold.

Suppl. Fig. S30

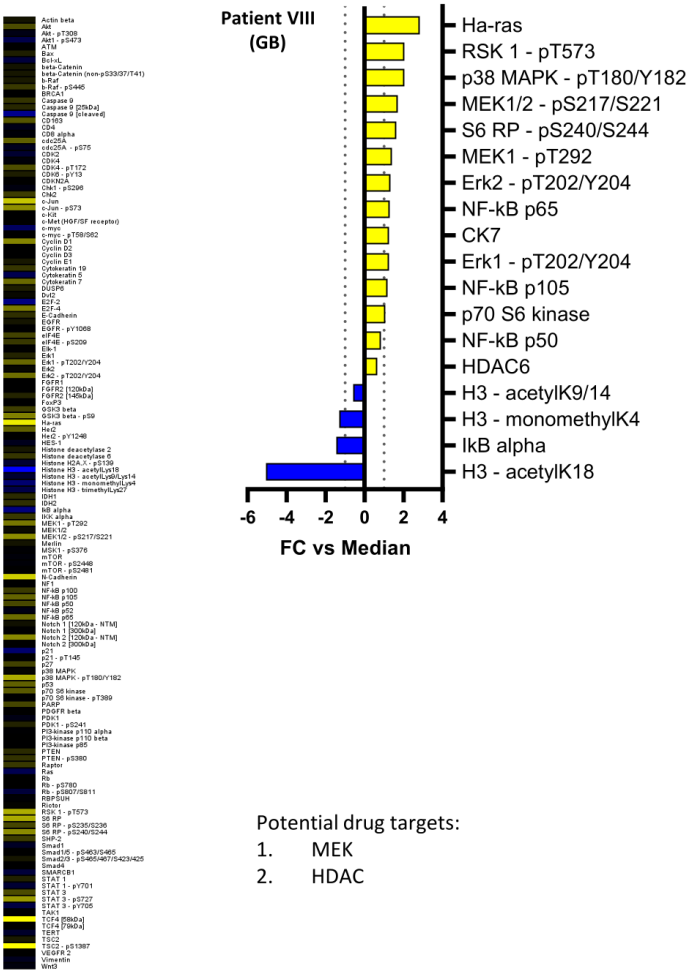

Potential drug targets:

1. MEK
2. HDAC

Suppl. Fig. S30: Individual protein profile of patient VIII (GB – gallbladder carcinoma). Left: Heatmap of DigiWest expression data (normalized AFI) as Log2 FC in relation to median signal (baseline) across all tumors (I-XIV). Right: Selection of key analytes shown relative to baseline signal. Bottom: Ranking of potential drug targets based on DigiWest data.

Suppl. Fig. S31

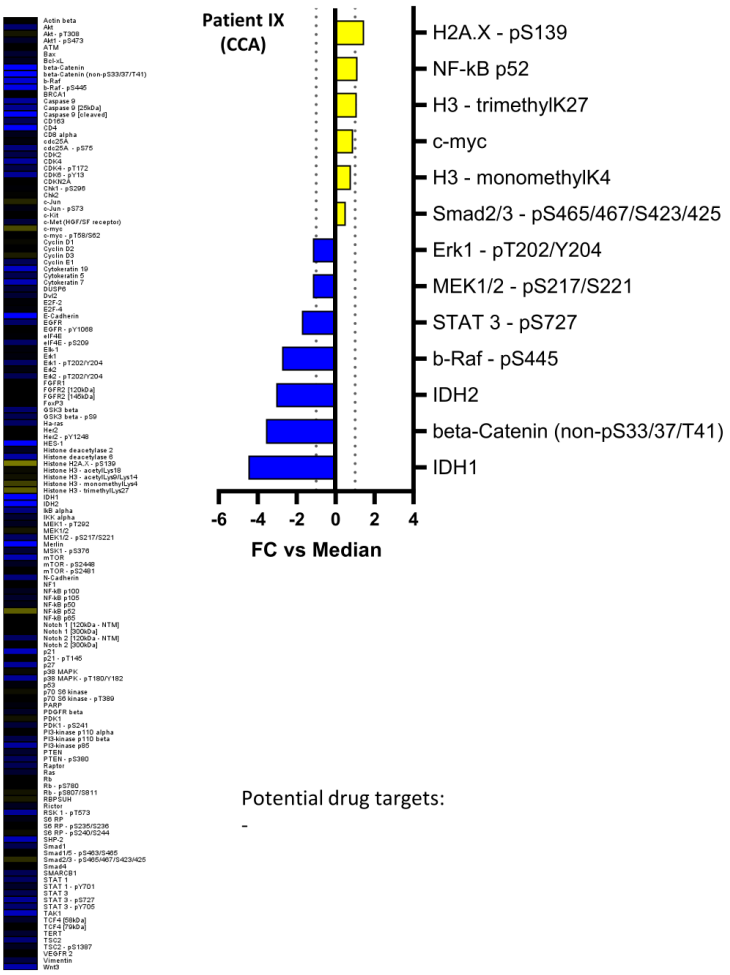

Suppl. Fig. S31: Individual protein profile of patient IX (CCA – cholangiocarcinoma). Left: Heatmap of DigiWest expression data (normalized AFI) as Log2 FC in relation to median signal (baseline) across all tumors (I-XIV). Right: Selection of key analytes shown relative to baseline signal. Bottom: Ranking of potential drug targets based on DigiWest data.

Suppl. Fig. S32

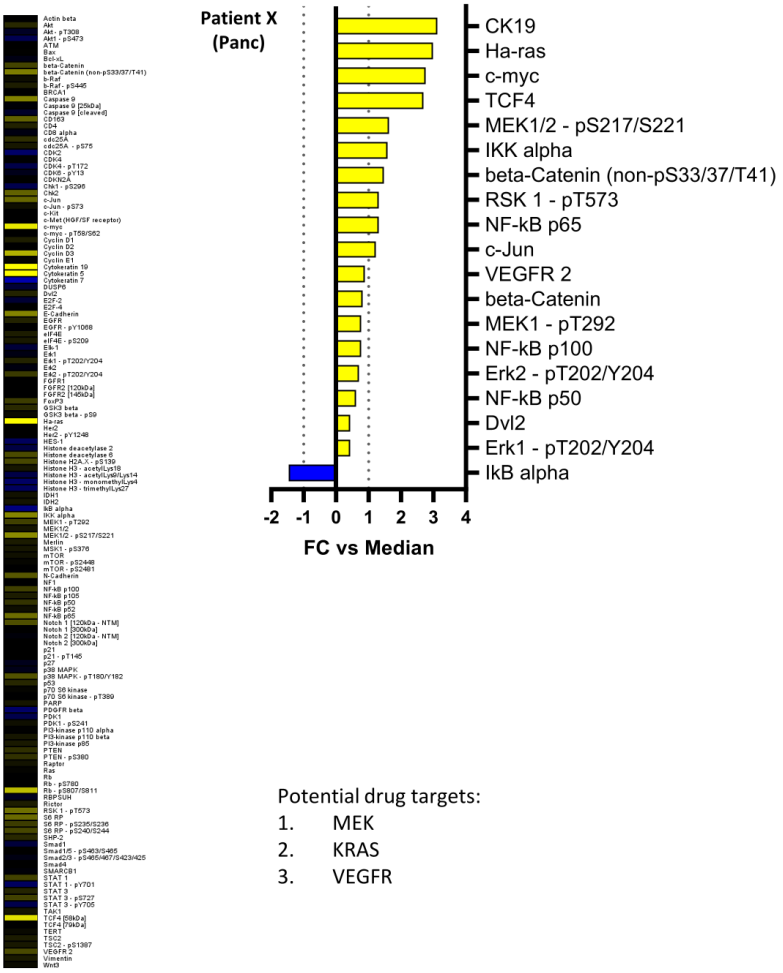

Suppl. Fig. S32: Individual protein profile of patient X (Panc – pancreatic carcinoma). Left: Heatmap of DigiWest expression data (normalized AFI) as Log2 FC in relation to median signal (baseline) across all tumors (I-XIV). Right: Selection of key analytes shown relative to baseline signal. Bottom: Ranking of potential drug targets based on DigiWest data.

Suppl. Fig. S33

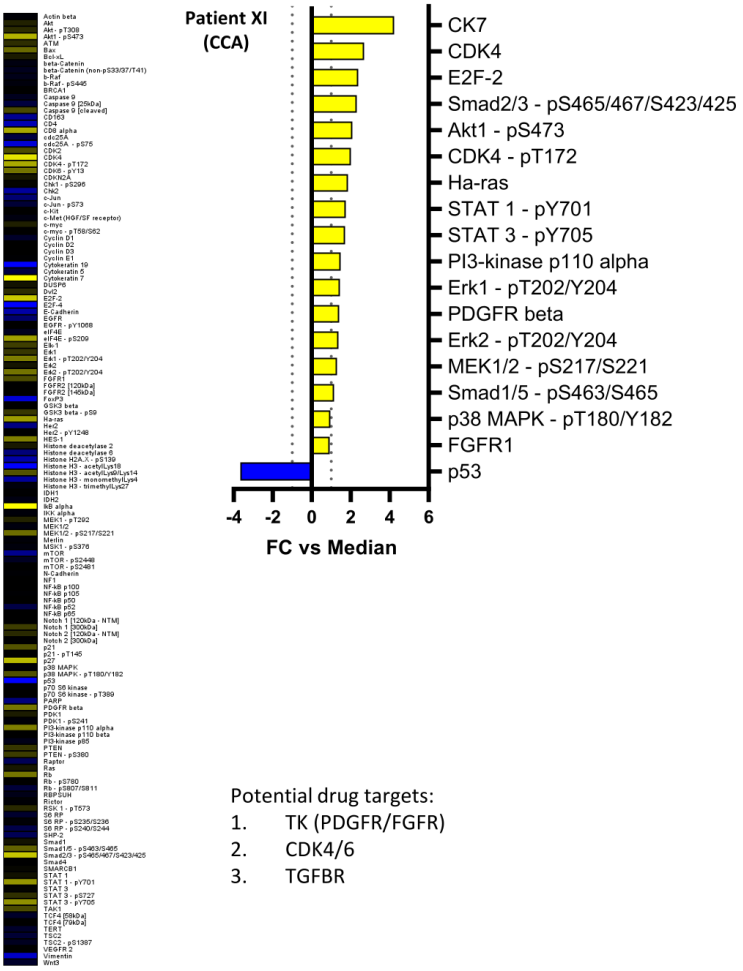

Suppl. Fig. S33: Individual protein profile of patient XI (CCA – cholangiocarcinoma). Left: Heatmap of DigiWest expression data (normalized AFI) as Log2 FC in relation to median signal (baseline) across all tumors (I-XIV). Right: Selection of key analytes shown relative to baseline signal. Bottom: Ranking of potential drug targets based on DigiWest data.

Suppl. Fig. S34

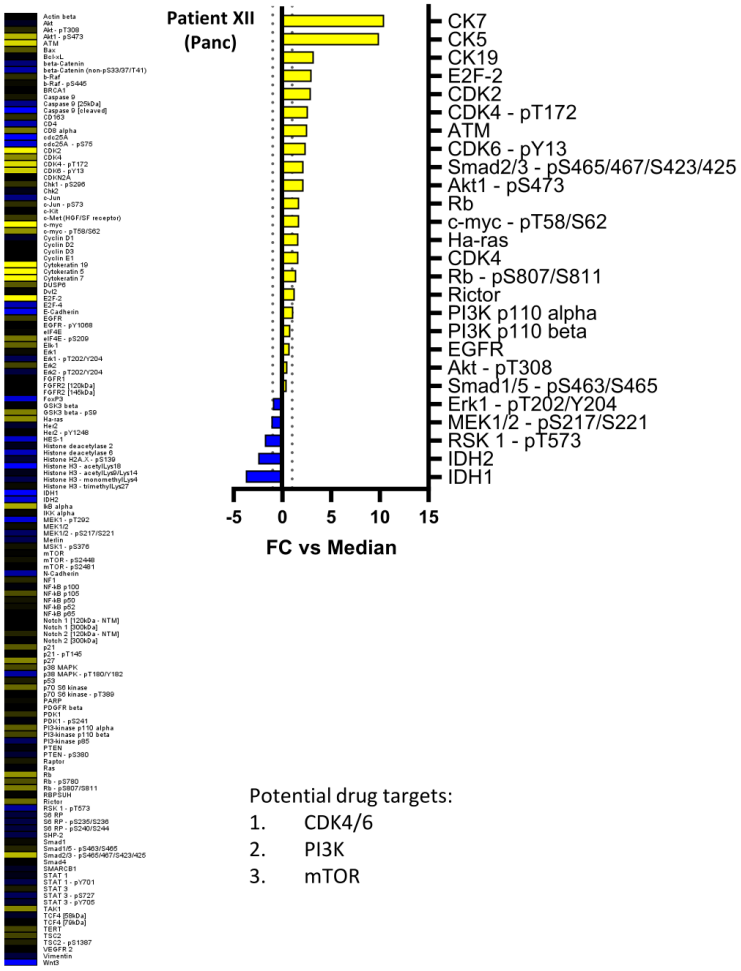

Suppl. Fig. S34: Individual protein profile of patient XII (Panc – pancreatic carcinoma). Left: Heatmap of DigiWest expression data (normalized AFI) as Log2 FC in relation to median signal (baseline) across all tumors (I-XIV). Right: Selection of key analytes shown relative to baseline signal. Bottom: Ranking of potential drug targets based on DigiWest data.

Suppl. Fig. S35

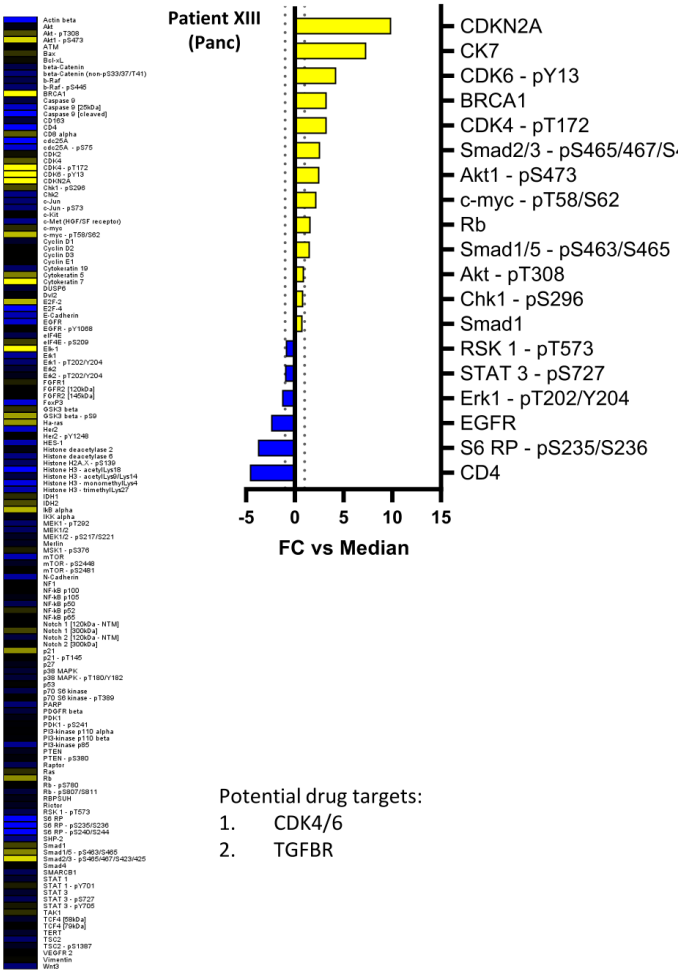

Suppl. Fig. S35: Individual protein profile of patient XIII (Panc – pancreatic carcinoma). Left: Heatmap of DigiWest expression data (normalized AFI) as Log2 FC in relation to median signal (baseline) across all tumors (I-XIV). Right: Selection of key analytes shown relative to baseline signal. Bottom: Ranking of potential drug targets based on DigiWest data.

Suppl. Fig. S36

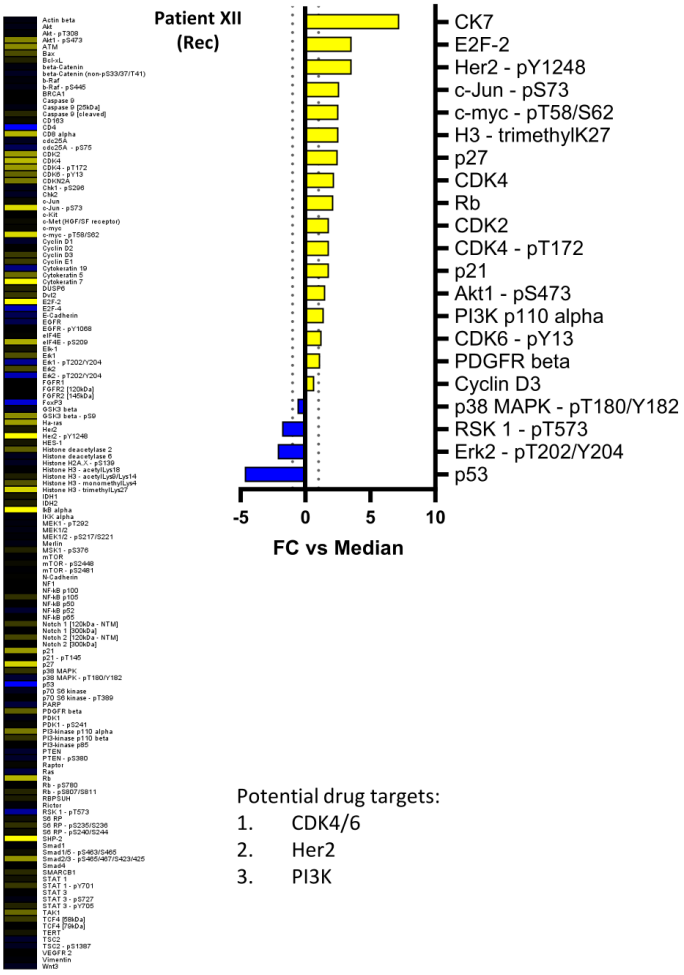

Potential drug targets:

1. CDK4/6
2. Her2
3. PI3K

Suppl. Fig. S36: Individual protein profile of patient XIV (Rec – rectal carcinoma). Left: Heatmap of DigiWest expression data (normalized AFI) as Log2 FC in relation to median signal (baseline) across all tumors (I-XIV). Right: Selection of key analytes shown relative to baseline signal. Bottom: Ranking of potential drug targets based on DigiWest data.

II. Supplementary Tables

Suppl. Table S1

Marker (Analyte)	Gene	Associated Immune Cell Type(s)
CD16	FCGR3A	NK (Natural Killer) Cells, Neutrophils
CD163	CD163	M2 Macrophages
CD4	CD4	T Cells
CD68	CD68	Macrophages
CD8 alpha	CD8A	Cytotoxic T Cells
CD25	IL2RA	Regulatory T Cells (TRegs)
CD11c	ITGAX	Dendritic Cells
CD56	NCAM1	NK (Natural Killer) Cells

Suppl. Table S1: Immune cell markers employed in retrospective DigiWest analysis and their respective associated immune cell types.

Appendix 3

Stahl A., Heider J., Wüst, R., Fallgatter, A. J., Schenke-Layland, K., Volkmer, H., Templin, M. (2024). Patient iPSC-derived neural progenitor cells display aberrant cell cycle control, p53, and DNA damage response protein expression in schizophrenia. *BMC Psychiatry, 24*(1). https://doi.org/10.1186/s12888-024-06127-x

Stahl *et al. BMC Psychiatry* (2024) 24:757
https://doi.org/10.1186/s12888-024-06127-x

BMC Psychiatry

RESEARCH Open Access

Patient iPSC-derived neural progenitor cells display aberrant cell cycle control, p53, and DNA damage response protein expression in schizophrenia

Aaron Stahl[1,2*], Johanna Heider[2], Richard Wüst[3,4], Andreas J. Fallgatter[3,4], Katja Schenke-Layland[1,2], Hansjürgen Volkmer[2] and Markus F. Templin[2*]

Abstract

Background Schizophrenia (SCZ) is a severe psychiatric disorder associated with alterations in early brain development. Details of underlying pathomechanisms remain unclear, despite genome and transcriptome studies providing evidence for aberrant cellular phenotypes and pathway deregulation in developing neuronal cells. However, mechanistic insight at the protein level is limited.

Methods Here, we investigate SCZ-specific protein expression signatures of neuronal progenitor cells (NPC) derived from patient iPSC in comparison to healthy controls using high-throughput Western Blotting (DigiWest) in a targeted proteomics approach.

Results SCZ neural progenitors displayed altered expression and phosphorylation patterns related to Wnt and MAPK signaling, protein synthesis, cell cycle regulation and DNA damage response. Consistent with impaired cell cycle control, SCZ NPCs also showed accumulation in the G2/M cell phase and reduced differentiation capacity. Furthermore, we correlated these findings with elevated p53 expression and phosphorylation levels in SCZ patient-derived cells, indicating a potential implication of p53 in hampering cell cycle progression and efficient neurodevelopment in SCZ.

Conclusions Through targeted proteomics we demonstrate that SCZ NPC display coherent mechanistic alterations in regulation of DNA damage response, cell cycle control and p53 expression. These findings highlight the suitability of iPSC-based approaches for modeling psychiatric disorders and contribute to a better understanding of the disease mechanisms underlying SCZ, particularly during early development.

Keywords Proteomics, DigiWest, IPSC, Neural progenitors, Schizophrenia, Cellular signaling, Cell cycle, p53

*Correspondence:
Aaron Stahl
a.stahl@uni-tuebingen.de
Markus F. Templin
markus.templin@nmi.de
Full list of author information is available at the end of the article

Background

Schizophrenia spectrum disorders (SCZ) are a group of severe neurodevelopmental disorders with a highly heterogeneous clinical presentation of a broad range of symptoms including hallucinations, delusions, emotional blunting and cognitive deficits [1]. Current antipsychotic treatment options for SCZ are purely symptomatic and show only limited efficacy in alleviating negative and cognitive symptoms [2, 3]. Hence, there is an urgent need to develop causal treatments, which has so far been hampered by the still limited knowledge of the molecular mechanisms that are involved in the disease. As SCZ is regarded as a neurodevelopmental disorder, alterations occurring during early brain development are of particular interest. Genome-wide association and exome sequencing studies have linked > 100 risk loci to SCZ but information on the protein level remains limited [4, 5].

Induced pluripotent stem cells (iPSC) have emerged as a valuable source for phenotypic studies of disease-relevant cell types with a patient-specific genetic background. Transcriptomic analysis and shotgun proteomics of iPSC-derived neural progenitor cells (NPC) and neurons have previously helped to gain insight into potential disease-related processes. Most studies investigating the proteome in SCZ employ mass spectrometry approaches [6–8]. Deregulated expression of genes and proteins involved in protein synthesis, cell adhesion, regulation of the cytoskeleton, oxidative stress and neuronal differentiation have been identified in SCZ [8–11]. Additionally, deregulations in key signaling pathways have been described, among which the most prominent changes have been reported for proteins of the Wnt and Akt/glycogen synthase kinase-3 beta (GSK3 beta) signaling pathways in both iPSC and patient studies [10, 12–16]. Postmortem studies have also linked the mitogen-activated protein kinase (MAPK)/ extracellular signal-regulated kinase (ERK) pathway to SCZ [17–19]. Despite the important insights that have been gained by these studies, many important questions regarding the connection between aberrant signaling and cellular (patho)-phenotypes remain unanswered. Moreover, with most studies focusing on the transcriptome level, proteomic studies remain underrepresented in the field. However, they are of great importance given that gene expression changes do not always translate to the protein level. Especially the study of phosphorylated proteins remains difficult using high throughput proteomic approaches but is of great importance for entangling mechanisms surrounding pathway activity. Applying such techniques to relevant neuronal cell types would greatly expand the knowledge of the biological processes at play during the early phases of disease development.

Here, we employ high-throughput Western Blotting (DigiWest) to study protein expression and phosphorylation of 133 proteins in SCZ patient-derived cells on the iPSC and NPC level in a targeted proteomics approach. The DigiWest is a multiplexed Western Blot derivative which transfers the Western Blot onto a bead-based system, thereby greatly increasing throughput while retaining the sensitivity of traditional Western Blotting. In this fashion, expression data from up to 200 proteins and phosphoproteins can be obtained in a targeted manner, allowing extensive analysis of cellular signaling pathways [20]. Applying this method, we aimed to compare differences in protein expression patterns between control (CTR) and SCZ in iPSC and NPC, respectively, to identify potential disease-relevant alterations in cellular signaling.

We report several aberrant SCZ-specific protein signatures, exclusive to NPC, with regards to signaling pathway activity. Most notably, we found proteomic alterations in cell cycle control, DNA-damage response regulation along with impaired differentiation capacity of SCZ NPC. Furthermore, we were able to correlate these alterations to p53 expression and phosphorylation levels in SCZ-derived cells, which provides further mechanistic insights into the early developmental stages of SCZ.

Methods

iPSC line information and maintenance

For detailed information on the three control and four patient-derived iPSC lines used see Additional file 1—Table S1. The CTR1 iPSC line was purchased from Thermo Fisher Scientific (Waltham, MA, USA—#A18945). The CTR2 iPSC line was a gift from the Tumorbiology group at NMI Reutlingen. For clinical patient data, see [21]. iPSC were maintained on plates coated with hESC-qualified Matrigel (Corning, Corning, NY, USA) in mTeSR Plus (STEMCELL Technologies, Vancouver, Canada). For single cell seeding, iPSC were enzymatically passaged using Accutase (Sigma-Aldrich, St. Louis, MO, USA).

NPC generation and maintenance

NPC were generated from iPSC following the embryoid body (EB) protocol of the STEMdiff™ SMADi Neural Induction Kit (STEMCELL Technologies) according to the manufacturer's instructions. The obtained NPC were cultured in STEMdiff™ Neural Progenitor medium (STEMCELL Technologies) on 6-well plates coated with 20% poly-l-ornithine (Sigma-Aldrich) for 2h at room temperature (RT) and 10 µg/ml Laminin (Sigma-Aldrich) at 37 °C overnight. NPC were enzymatically passaged with Accutase. For all experiments, only passage 2 NPC

from three independent rounds of differentiation were used to ensure comparability of results.

DigiWest protein profiling

iPSC were obtained in triplicate and NPC samples from three independent differentiations. DigiWest was performed as published [20] using 12 µg of cellular protein. In brief, the NuPAGE system (Life Technologies) was used for gel electrophoresis and blotting onto PVDF membranes. Proteins were biotinylated on the membrane using NHS-PEG12-Biotin (50 µM) in PBST for 1 h. Sample lanes were cut into 96 strips (0.5 mm each) and placed in one well of a 96-well plate before adding 10 µl elution buffer (8 M urea, 1% Triton-X100 in 100 mM Tris–HCl pH 9.5). Each strip/protein fraction was incubated with 1 distinct Neutravidin-coated MagPlex bead population (Luminex, Austin, TX, USA). Coupling was performed overnight, and non-bound binding sites were blocked with 500 µM deactivated NHS-PEG12-Biotin for 1 h. By pooling all 96 protein-loaded bead populations, the original sample lane was reconstituted.

5 µl aliquots of bead mix were added to 96-well plates containing 50 µl assay buffer (Blocking Reagent for ELISA (Roche) supplemented with 0.2% milk powder, 0.05% Tween-20 and 0.02% sodium azide). Upon discarding of the assay buffer, 30 µl of primary antibody (diluted in assay buffer) was added per well. After overnight incubation at 15 °C, the bead-mixes were washed twice with PBST and species-specific PE-labelled (Phycoerythrin) secondary antibodies (Dianova, Hamburg, Germany) were added for 1 h at 23 °C. Beads were washed twice with PBST before readout on a Luminex FlexMAP 3D instrument.

One hundred thirty-seven primary antibodies (Additional file 2) were selected from a collection of > 1 500 available antibodies, all of which are performance-evaluated and routinely used in DigiWest. Selection was largely based on covering signaling pathways/cellular functions for which associations with SCZ have been described in previous genetic/transcriptomic/proteomic studies as mentioned elsewhere in this manuscript Refs [8–19, 22, 23]. Likewise, to accurately monitor pathway activity during neuronal differentiation, signaling proteins from neurodevelopmental pathways (Wnt [24], Hippo [25], Hedgehog [26], Smad [27] signaling) were additionally selected along with other common signaling and marker proteins. Pathway allocation of analytes was mapped based on the Kyoto Encyclopedia of Genes and Genomes (KEGG) database [28, 29].

For peak integration, an Excel-based analysis tool was used. A total of 148 peaks were identified, with 133 (89.9%) generating reliable signals. Signal intensity was separately normalized to total protein amount on the beads within each differentiation. The software package MeV 4.9.0 was used for heatmap generation and statistical analysis [30]. For heatmaps, fluorescent signals were either median centered across samples for a given analyte (iPSC versus NPC) or centered around the average signal of the three CTR lines within each differentiation (CTR versus SCZ) before Log2 transformation. Raw and normalized DigiWest data can be found in Additional file 3 and 4, respectively.

Immunocytochemistry

For immunocytochemical staining, iPSC or passage-matched NPC were seeded on 96-well µClear™ plates (Greiner, Kremsmünster, Austria). Once 70–80% confluence was reached, cells were fixed with 4% PFA in PBS for 15 min at RT. Cells were washed 3×with PBS and incubated with PBS + 1×BMB blocking reagent (Roche) + 0.1% Triton (Carl Roth, Karlsruhe, Germany) for 30 min at RT. Primary antibodies were diluted in blocking/permeabilization solution and incubated overnight at 4 °C. Afterwards, cells were washed 3×with PBS. Secondary antibodies were incubated in blocking/permeabilization solution for 2h at RT on an orbital shaker and washed with PBS. For nuclear staining, Hoechst 33,258 (Sigma-Aldrich) was diluted in PBS and incubated for 30 min at RT. A complete list of ICC antibodies used in this study can be found in Additional file 1 – Table S2.

Image acquisition and analysis of immunocytochemical staining

Z-Stack images were acquired from four sites per well with the ImageXpress Micro Confocal High-Content Imaging System (Molecular Devices, San Jose, CA, USA). To ensure unbiased image acquisition and analysis, all acquisition parameters for individual antibodies were kept constant within replicates. For image analysis, the software MetaXpress (Molecular Devices) was used. 2D projections were generated and intensity/size thresholding (for nuclear and spot-like staining patterns) was applied to generate a mask covering the fluorescent signal for each marker. Depending on the marker expression pattern (nuclear vs. cytosolic), different parameters were used for analysis. For nuclear stains and stainings in which cells/nuclei were either positive or negative for a marker, the mean stained area was analyzed per image. For stainings, which were present in all cells but varied in intensity between different cells, the mean intensity per image was analyzed. In any case, values from one well were averaged and normalized to Hoechst signal to account for differences in cell density. Data were centered around the mean signal across either all iPSC (Figs. 1C, 2C) or all CTR clones (Figs. 3E, 4H, 6B). Data was obtained from three biological replicates.

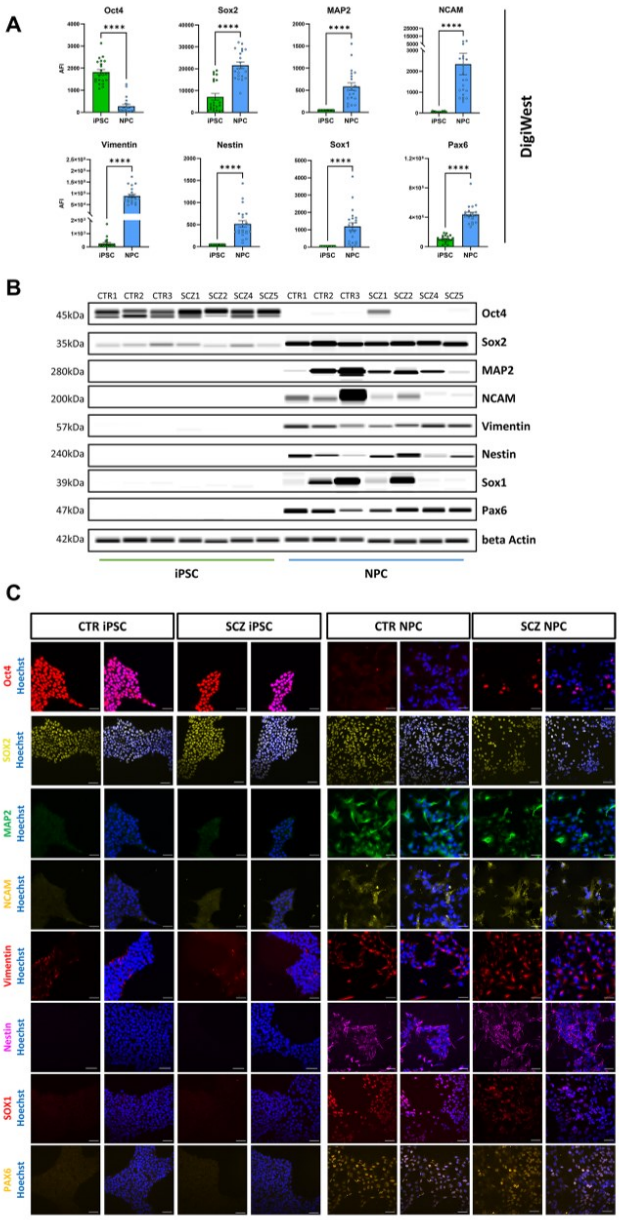

Fig. 1 Marker expression in iPSC and NPC. **A**: DigiWest data (AFI = accumulated fluorescent intensity) of cell-type specific marker proteins in iPSC ($n = 21$) and NPC ($n = 21$); Mann–Whitney test. **B**: Western Blot mimic (gray-scale image) of markers displayed in A (exemplarily shown for one differentiation only). **C:** Example ICC images of marker expression in iPSC (left) and NPC (right) obtained by high-content microscopy. Scale bars: 50 µm. CTR and SCZ cells will be addressed separately at a later stage. $^{*}p < 0.05$, $^{****}p < 0.0001$. Error bars: S.E.M

Flow cytometry cell cycle analysis

Passage-matched NPC were seeded on 12-well plates at an appropriate density to ensure exponential growth until fixation (8.5×10^4/cm^2). The following day, NPC were treated with DMSO or Nocodazole (Sigma-Aldrich, 125nM) for 24h. Afterwards, the cells were detached, counted and 6×10^5 cells per condition fixed with 4% PFA for 15 min at RT. Cells were washed 3×with PBS and treated with 100 µg/ml RNAse A (New England Biolabs, Ipswich, MA, USA) and 0.1% Triton X-100 in TrypLE express (Thermo Fisher) at 37 °C for 30 min for RNA removal and cell permeabilization. For fluorescence-activated cell sorting (FACS), 3×10^5 cells were transferred per well of a 96-well plate and stained with 2 µg/ml propidium iodide (PI) solution (BioLegend, San Diego, CA, USA) in TrypLE express for 30 min at 37 °C. Analysis of PI staining was performed using the FACS Fortessa™ Cell Analyzer (BD Biosciences, Franklin Lakes, NJ, USA). A minimum of 15,000 events was recorded per well, from two wells per condition. Analysis of FACS data was performed using FlowJo 10 (BD Biosciences). The gating strategy is outlined in Additional file 5 – Figure S11A. Cell cycle phases were identified using the build-in univariate cell cycle analysis tool (Dean-Jett-Fox model, [31]).

Cell proliferation assay

Passage-matched NPC were seeded at a density of 2×10^4 cells/well in a 96-well plate in STEMdiff™ Neural Progenitor medium. For 72h, cells were cultivated in the IncuCyte® Live Cell Analysis System (Sartorius, Göttingen, Germany). Whole-well brightfield images were acquired in 4 h intervals with a 10×objective in triplicates for each NPC line. Proliferation was analyzed using the IncuCyte® Basic Analyzer. Confluence was normalized to t=0. Data was obtained from three biological replicates.

Western blot

Size-separation via SDS-PAGE was performed as described above (DigiWest) using 10 µg of protein and blotted onto a Nitrocellulose membrane (VWR). Blocking was performed for 1 h using 5% milk powder (Roth) in TBST. Primary antibodies (identical to those used in DigiWest) were diluted in 1% BSA (Roth) in TBST and incubated overnight at 4 °C. Blots were washed 5×for 5 min in TBST before adding fluorescently labelled secondary antibodies for 1 h (donkey anti-Rabbit IgG (H+L) coupled to IRDye 800CW (LI-COR, Lincoln, NE, USA) and donkey anti-Mouse IgG (H+L) coupled to IRDye 680CW (LI-COR), each at a dilution of 1:10,000 in 5% milk powder in TBST) and detected on a LI-COR instrument. Before analysis, blots were washed 5×for 5 min in TBST and bands were quantified using Image Studio. Uncropped Western Blot images can be found in Additional file 5 – Figure S15.

Neurite outgrowth assay

Passage-matched NPC were seeded into 48-well plates at 1×10^4 cells per well in Neural Progenitor medium. After 24 h, medium was changed to N2-medium (t=0 h), consisting of DMEM/F12+15 mM HEPES, 1×N2-supplement, 1% non-essential amino acids, 1% GlutaMAX, 1.5% glucose solution (all Thermo Fisher), 10 µM SB431542 (Bio-Techne, Minneapolis, MN, USA), 1 µM XAV939 (Sigma-Aldrich), 100 nM LDN193189 (STEMCELL Technologies), 10 ng/ml BDNF (Thermo Fisher). From then on, cells were cultured in the IncuCyte® Live Cell Analysis System (Sartorius) and imaged every 4 h in brightfield mode at 10×magnification. Two wells were imaged per line, and 4 sites per well. After 24 h, a complete medium change with N2 medium was performed and cells were cultured until t=40 h without further medium changes. Using the IncuCyte® NeuroTrack analysis module (Sartorius), neurite length (in mm) per number of cell body clusters was analyzed for each time point. Analysis parameters were defined as follows: cell body clusters with a minimum area of 200 µm, containing cells with a minimum width of 7 µm, were counted. Neurite width was defined as 1 µm. These parameters were analyzed for each of the four sites imaged and then averaged per well. Data was obtained from four biological replicates. Values at t=0 h were set to 1.

(See figure on next page.)

Fig. 2 Expression signatures and pathway upregulation during differentiation. **A**: Heatmap and Hierarchical Cluster analysis of analytes significantly different between iPSC ($n=21$) and NPC ($n=21$) samples (Wilcoxon test, $p<0.001$). **B**: DigiWest data (AFI = accumulated fluorescent intensity) for a subset of proteins with differential expression in iPSC ($n=21$) and NPC ($n=21$). Proteins are grouped according to their pathway allocation; Mann–Whitney test. **C**: Example ICC images of beta-catenin, LEF1 and p21 expression in iPSC (top) and NPC (bottom). Scale bars: 50 µm. **D**: Quantified ICC signals of proteins exemplarily shown in C (iPSC $n=21$, NPC $n=21$) obtained by high-content microscopy. Data are shown relative to mean iPSC signal; Mann–Whitney test. **E–F**: Volcano plot of separate iPSC vs NPC comparison for CTR (**E**—iPSC $n=9$, NPC $n=9$) and SCZ (**F**—iPSC $n=12$, NPC $n=12$) samples (Wilcoxon-Test, $p<0.01$). Significantly upregulated proteins are shown in red, downregulated proteins in blue (analytes with FCs < |1| are excluded). Analytes with a significant interaction effect between cell type and disease allocation ($p<0.05$, 2-Way-ANOVA) are highlighted (also see Additional File 5 – Figure S6 and Additional File 1—Table S3). *$p<0.05$, ***$p<0.001$, ****$p<0.0001$. Error bars: S.E.M

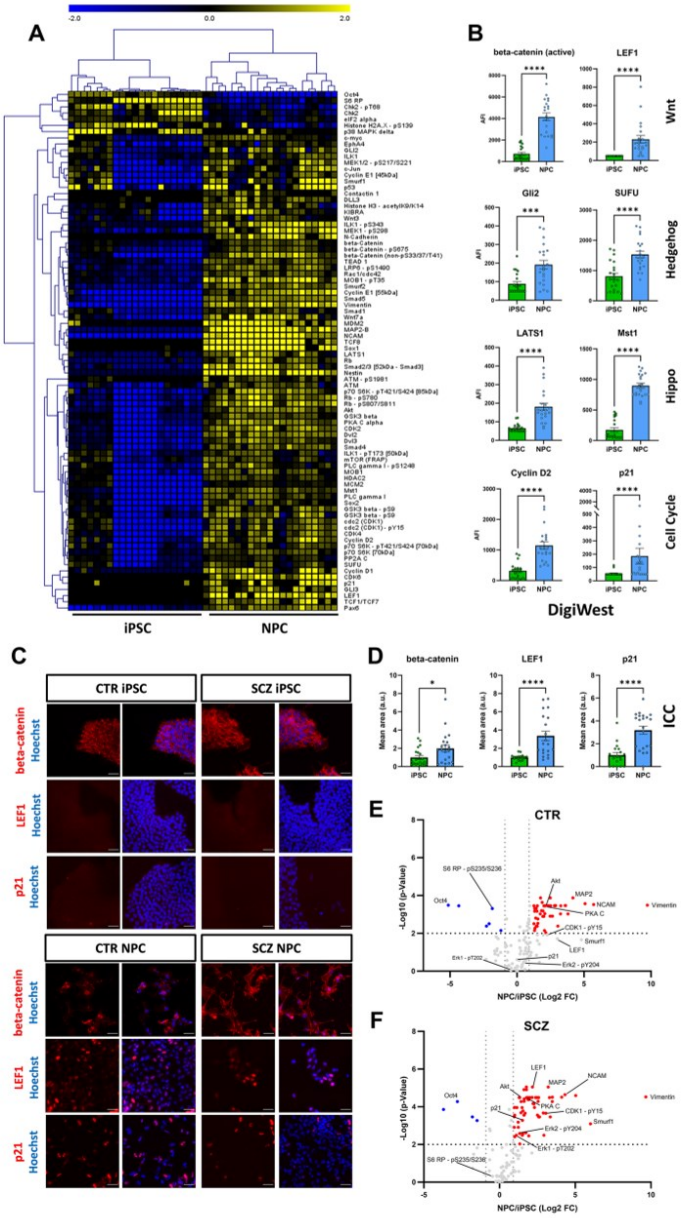

Fig. 2 (See legend on previous page.)

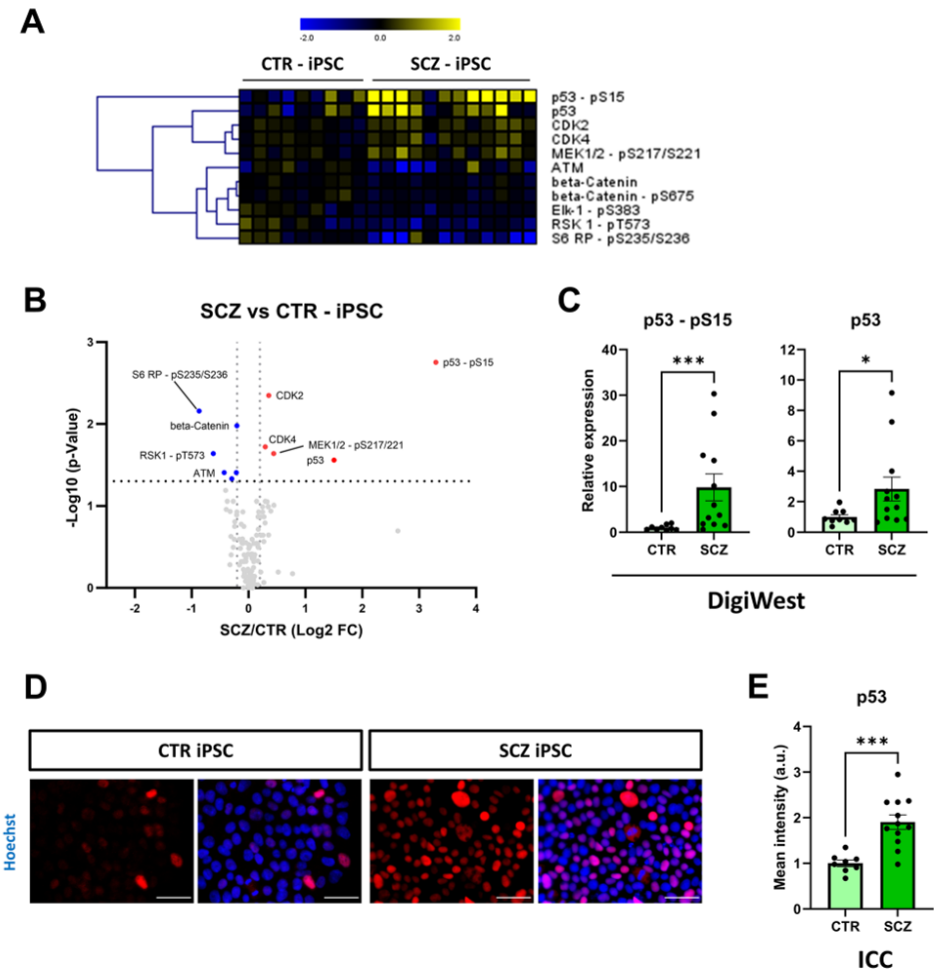

Fig. 3 SCZ-specific alterations in iPSC. **A**: Heatmap with Hierarchical Cluster analysis (HCL) of analytes significantly different (Wilcoxon Test, $p < 0.05$) between CTR ($n = 9$) and SCZ ($n = 12$) iPSC. Log2-transformed data is shown relative to mean signal across CTR lines of the respective differentiation. **B**: Volcano plot of comparison shown in A. **C**: DigiWest data (relative to control mean) of p53 and p53 – pS15 expression comparing CTR ($n = 9$) and SCZ ($n = 12$) iPSC; Mann–Whitney test. **D**: Example images of total p53 ICC staining in iPSC obtained by high-content microscopy. Scale bars: 50 µm. **E**: Quantified ICC signal of total p53 expression (relative to CTR mean) in CTR ($n = 9$) and SCZ ($n = 12$) iPSC (unpaired t-test). $^{*}p < 0.05$, $^{***}p < 0.001$. Error bars: S.E.M

Statistics

Statistical analysis was performed using GraphPad Prism 10 (Graphpad Software). Data was tested for normality using the Shapiro–Wilk Test. Only if both groups were normally distributed, groups were compared via unpaired, two-tailed t-test. If normality was not met, the two-tailed Mann–Whitney-U Test was used. For DigiWest data-based comparisons (used in heatmaps), the Wilcoxon-signed rank test was used. For neurite outgrowth and flow cytometry analysis, data was analyzed with a 2-way ANOVA and Tukey's multiple comparisons test. N numbers and statistical details for each

experiment can be found in the respective figure legend. In all cases, a p-value < 0.05 was considered significant unless stated otherwise.

Results

Characterization of developmental marker expression and signaling pathway activation during NPC differentiation via DigiWest

To characterize the differentiation process from iPSC into NPC, we examined the expression of 133 proteins from three healthy control lines and four SCZ patient lines. This set of proteins was composed of routinely used cell type markers for iPSC and NPC, as well as proteins involved in signaling pathways associated with neurodevelopment and previously linked to SCZ. First, we aimed to investigate the differences between the iPSC and NPC stage independent of disease allocation. Expression signatures of all measured proteins in NPC were consistent between three individual differentiations (Additional file 5 – Figure S1) where NPC of the respective differentiation do not cluster together, demonstrating high reproducibility. When comparing all iPSC (n = 21) and NPC (n = 21) samples, expectedly observed strong changes in the expression of cell-type specific markers. In NPC, DigiWest data shows downregulation of the pluripotency marker Oct4. Sox2 was expressed in both cell types but to a greater extent in NPC. Clear upregulation of neurodevelopmental/NPC-associated markers microtubule-associated protein 2 (MAP2), Vimentin, neural cell adhesion molecule (NCAM), paired-box protein Pax-6 (Pax6), SRY-Box Transcription Factor 1 (Sox1) and Nestin was observed (Fig. 1A, Additional file 5—Figure S2). Although variability in expression levels between individual patient-derived lines does persist, the two cell types are clearly distinguishable when displayed in a Western Blot-like format, as shown in Fig. 1B (Additional file 5 – Figure S3). Expression of these cell type-specific markers was confirmed by immunocytochemical staining (ICC) in both iPSC and NPC (Fig. 1C) with good comparability of DigiWest and ICC as exemplarily shown for four markers (Additional file 5 – Figure S4).

The high-throughput nature of DigiWest allowed us to assess expression of over 130 proteins and phosphoproteins and thus look beyond the expression of traditional cell type markers. We observed further pronounced and consistent expression differences between iPSC and NPC for various other proteins, leaving 61% (81/133) of analytes differentially expressed at a significance level of p < 0.001 (Fig. 2A, Additional file 5 – Figure S2), with the majority becoming strongly upregulated in NPC. These upregulations included key members of signaling pathways involved in neurodevelopment (Fig. 2B), such as Wnt signaling (active and total beta-catenin, Wnt3/7, low-density lipoprotein receptor-related protein 6 (LRP6 – pS1490), GSK3 beta, Dishelleved (Dvl) 2/3, lymphoid enhancer-binding factor 1 (LEF1), transcription factor (TCF) 1/7), Hippo signaling (large tumor suppressor kinase 1 (LATS1), Mob1, macrophage stimulating protein 1 (MST1), TEA domain transcription factor 1 (TEAD), kidney and brain expressed protein (KIBRA)) and Hedgehog signaling (glioma-associated oncogene (GLI)2/3, suppressor of fused protein (SUFU)). Notably, proteins involved in cell cycle regulation (cyclin-dependent kinase (CDK) 1/2/4/6, Cyclin D1/2, p21, Rb) were also strongly elevated in NPC (Fig. 2B). For select proteins we again validated the DigiWest results with ICC. Expression levels of beta-catenin and LEF1, both critical for Wnt signaling, and of the cell cycle modulator p21 were significantly elevated in NPC compared to iPSC (Fig. 2C + D).

When investigating the differentiation process from iPSC to NPC comparing patient and healthy control-derived cells, we mainly observed strong upregulations (CTR: 89.4%, SCZ: 92.4%) and only a handful of downregulations (CTR: 10.6%, SCZ: 7.6%) for both (Additional file 5 – Figure S5). As expected, most changes were shared between CTR and SCZ, given that we already observed highly consistent expression across most samples (see Fig. 2A). Regardless, some select analytes behaved differently in SCZ vs CTR-derived cells during development, as calculated by two-factor-ANOVA (interaction effect p < 0.05). These (e.g. LEF1, Smurf1, p21 or ERK1/2 – pT202/Y204) are highlighted in Fig. 2E/F and are shown in more detail in Additional file 5 – Figure S6/

(See figure on next page.)

Fig. 4 SCZ-specific alterations in NPC. **A**: Heatmap with Hierarchical Cluster analysis (HCL) of analytes significantly different (Wilcoxon Test, p < 0.05) between CTR (n = 9) and SCZ (n = 12) NPC. Log2-transformed data is shown relative to mean signal across CTR lines of the respective differentiation. **B**: Volcano plot of comparison shown in A. **C**: DigiWest data (relative to CTR mean) of Oct4, MAP2, NCAM and Sox1 expression in CTR (n = 9) and SCZ (n = 12) iPSC and NPC, respectively; Mann–Whitney test. **D**: Venn diagram showing the number of analytes differentially regulated between SCZ and CTR in the respective cell type. **E**: DigiWest data (relative to CTR mean) of p53 – pS15 and p53 (total) expression; CTR n = 9, SCZ n = 12, Mann–Whitney test. **F**: Quantified Western Blot signals of p53 – pS15 and p53 (total) expression in NPC (relative to CTR mean). Intensities were normalized to beta-Actin signal; CTR n = 6, SCZ n = 8, Mann–Whitney test. **G**: Western Blot images corresponding to quantification shown in F. **H**: Quantified ICC signal of total p53 expression (relative to CTR mean) in CTR (n = 9) and SCZ (n = 12) NPC (unpaired t-test). **I:** example images of total p53 ICC staining as obtained by high-content microscopy. Scale bars: 50 µm. *p < 0.05, **p < 0.01, ***p < 0.001, ****p < 0.0001. Error bars: S.E.M

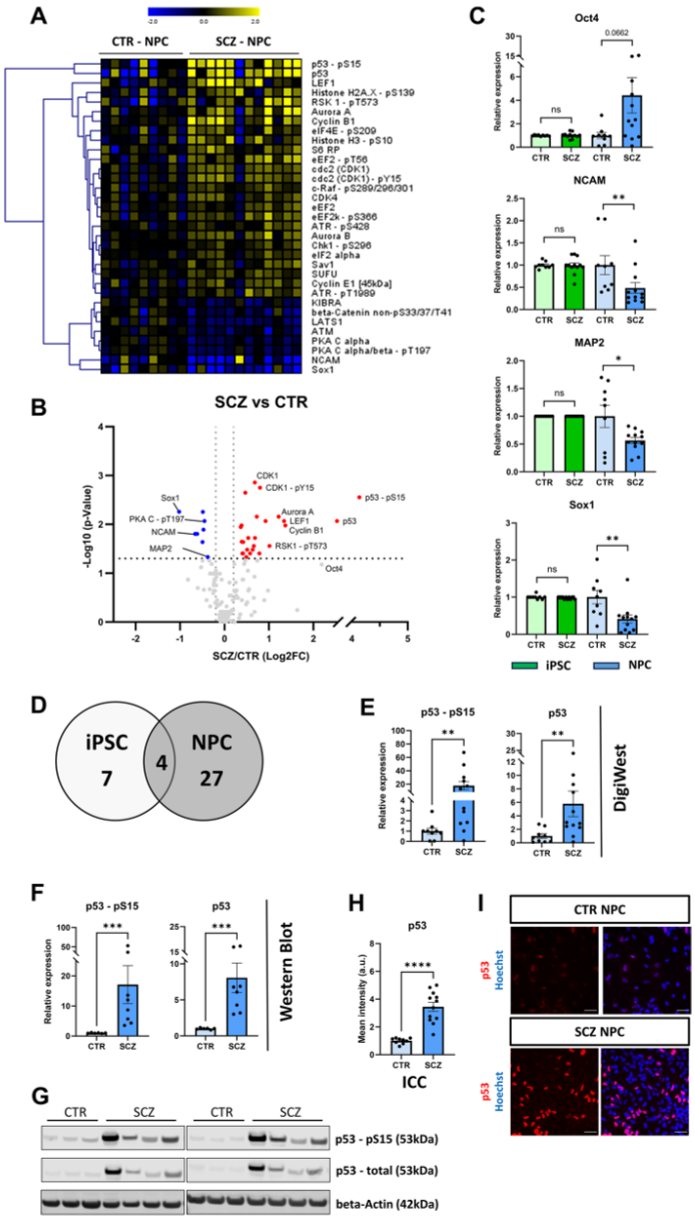

Fig. 4 (See legend on previous page.)

Additional file 1 – Table S3. Overall, these data show that the DigiWest can clearly identify cell-type specific proteomic signatures in differentiated cells thus allowing extensive analysis of cellular signaling during the differentiation process.

SCZ iPSC show only few disease-associated alterations at the protein level

Next, we aimed to investigate disease-specific proteomic signatures at the iPSC and NPC stage, respectively. In iPSC, we found 11 (8%) analytes to be differentially expressed between CTR ($n=9$) and SCZ ($n=12$), with 5 becoming up- and 6 downregulated in SCZ (Fig. 3A + B). By far, the strongest effects in magnitude were observed for p53 phosphorylated at Ser15 (~tenfold upregulation in SCZ), along with total levels of p53 (~twofold upregulation in SCZ) (Fig. 3C). We confirmed upregulation of p53 in SCZ iPSC by ICC (Fig. 3D-E). Other de-regulated proteins showed significant, but less pronounced differences (Additional file 1 – Table S4). These data suggest that, except altered p53 expression and phosphorylation, there are relatively few prominent changes between CTR and SCZ on the iPSC level.

Reduced differentiation capacity of SCZ iPSC into neural progenitor cells

At the NPC stage, we again compared all SCZ ($n=9$) and control ($n=12$) samples and identified 30 analytes (23%) significantly different between the two groups (Fig. 4A + B), three times as many as in iPSC. Of these 30, 23 proteins were upregulated, and 7 were downregulated in SCZ. Crucially, several of the eight cell type-specific markers discussed previously (see Fig. 1) were among the differentially expressed proteins. On average, SCZ NPCs displayed higher levels of Oct4 and decreased levels of MAP2, NCAM and Sox1 compared to CTR NPC, while the other markers were not affected (Fig. 4C, Additional file 5 – Figure S7). Overall, this indicates decreased differentiation efficiency of SCZ NPC. Of note, considerably inter-donor variability was observed within both CTR as well as SCZ groups regarding the expression of these proteins with clones thus contributing to the observed SCZ phenotypes to varying extent (Additional file 5 – Figure S8A-B). To evaluate if decreased differentiation efficiency of SCZ iPSC impacts early neurodevelopmental processes, we tracked neurite outgrowth of NPC for 40 h. Starting 24 h after induction of neuronal differentiation, SCZ NPC showed a reduction of mean neurite length of increasing magnitude over time compared to CTR cultures (Additional file 5 –Figure S9).

Aberrant protein expression and dysregulated signaling pathway activity in SCZ NPC

Of all de-regulated analytes, most analytes (26/30) with differential regulation were exclusive to the NPC stage (Fig. 4D) and will be discussed in detail in Fig. 5, whereas only 4 SCZ-specific effects were conserved from the iPSC stage. Besides minor changes in CDK4 and ataxia-telangiectasia mutated kinase (ATM) expression (Additional file 5 – Figure S10A), these included highly increased levels of phosphorylated p53 (Ser15) and total p53 (Fig. 4E). Noteworthy, the average magnitude of change for these two analytes was twice as high in NPC (20-fold/sixfold) as in iPSC (tenfold/threefold). Similar results were obtained with traditional Western Blotting (Fig. 4F-G). We again confirmed p53 upregulation in NPC via ICC (F ig. 4H-I), also to a greater extent than in iPSC (threefold/1.8-fold). Overall, SCZ-specific alterations of protein expression mostly appear exclusively at the NPC stage, and in the case of p53 dysregulation are more pronounced compared to iPSC.

Furthermore, several of the dysregulated analytes exclusive to NPC were phospho-variants, suggesting deregulated cellular signaling. Accordingly, most of them could be attributed to distinct signaling pathways while others serve as regulators of cellular processes (Fig. 5A-E, Additional file 1 – Table S5). Among them were cell cycle-regulating proteins such as CDK1 – pY15, Cyclin B1 and Aurora Kinase A, as well as Histone H3 – pS10 (a marker for cells undergoing mitosis) all roughly showing a twofold increase in SCZ (Fig. 5A). Total CDK1, Aurora Kinase B and Cyclin E1 (Additional file 5 – Figure S10B) were also upregulated. Notably, they all play a critical role in regulating transition into G2/M phase. Interestingly, the relative inter-donor expression levels of Cyclin B1 and Aurora A, as well as p53 and p53 – pS15 (Additional file 5 – Figure

(See figure on next page.)

Fig. 5 Pathway allocations of SCZ-specific proteins. **A-E**: DigiWest data (relative to CTR mean) of select proteins differentially expressed between CTR ($n=9$) and SCZ ($n=12$) in NPC only (see Fig. 4D), shown in direct comparison with iPSC (CTR $n=9$, SCZ $n=12$). Analytes are grouped based on pathway/cellular function. **A**: Cell cycle regulation, specifically G2/M phase transition, **B**: DNA damage response, **C**: Protein synthesis/translation, **D**: Wnt signaling, **E**: MAPK/Erk signaling. A complete list of all differentially expressed SCZ-specific analytes can be found in Additional file 1—Table S5. Either the Mann–Whitney test or unpaired t-test was used depending on data distribution. $*p<0.05$, $**p<0.01$, $***p<0.001$ or as indicated. Error bars: S.E.M

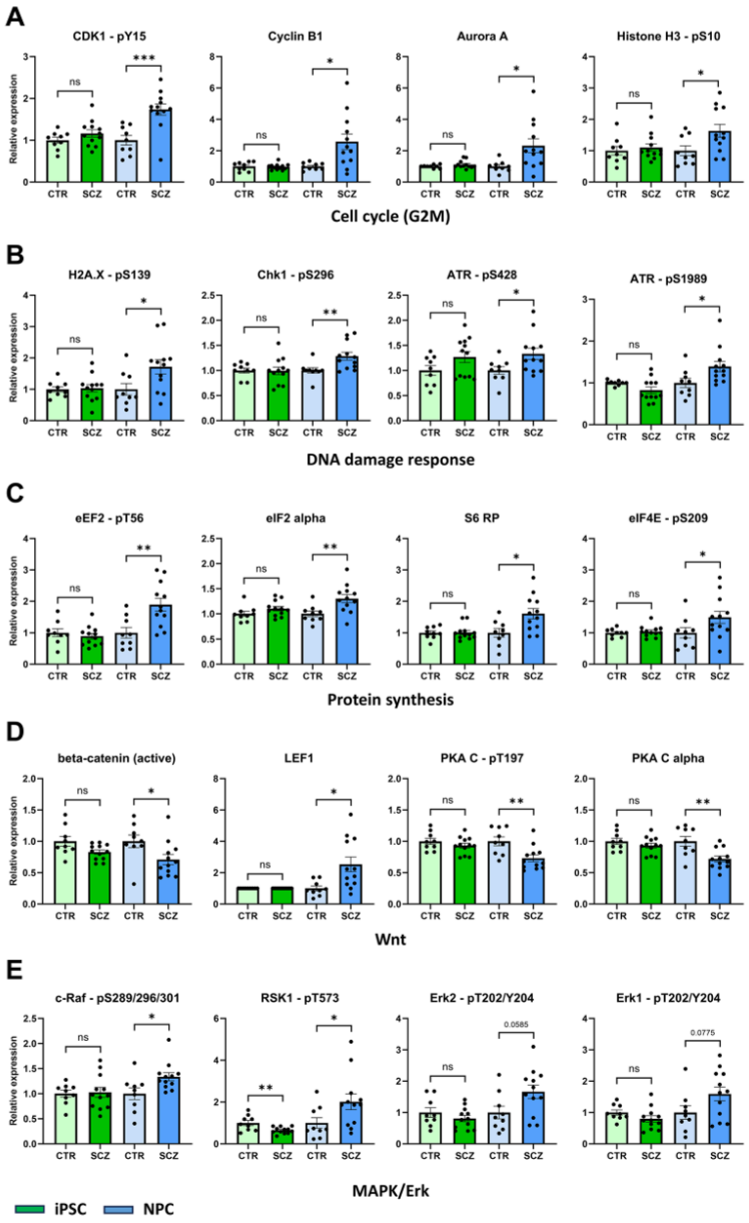

Fig. 5 (See legend on previous page.)

S8C), showed strikingly similar patterns to the relative expression levels of the pluripotency marker Oct4.

Additionally, we observed several alterations in the DNA-Damage-response (DDR) pathway (Fig. 5B). Histone H2A.X (S139), a primary indicator for DNA damage, as well as phosphorylation of crucial DDR proteins Chk1 (S296), and ataxia telangiectasia and Rad3-related kinase (ATR—S428 and ATR – S1989) were elevated in SCZ cells. On the other hand, phospho-ATM (S1981) showed an opposing trend for downregulation (Additional file 5 – Figure S10B).

Upregulation was also observed for several proteins and phospho-variants involved in translation such as eukaryotic elongation factor 2 (eEF2 – pT56), eukaryotic Initiation Factor 2 (eIF2) alpha, the ribosomal protein S6, as well as eukaryotic translation initiation factor 4E (eIF4E) – pS209 (Fig. 5C) along with total eEF2 and eukaryotic elongation factor 2 kinase (eEF2K) – pS366 and (Additional file 5 – Figure S10B). Also, phosphorylation of eukaryotic translation initiation factor 4E-binding protein 1 (4E-BP1, T37/S46, $p = 0.0585$) and the inhibitory site of eIF2 alpha (S51, $p = 0.0601$) showed an up- and downregulatory trend, respectively.

Moreover, we found dysregulations in Wnt signaling (Fig. 5D + Additional file 5 – Figure S10B), such as decreased active beta-catenin (non-pS33/41/45), twofold elevated LEF1, reduced protein kinase A (PKA) C (T197), total PKA C and elevated Casein kinase 1 alpha.

Finally, SCZ NPC also displayed increased phosphorylation of key MAPK proteins (Fig. 5E), namely c-Raf (S289/296/301), Erk2 (T202/Y204), Erk1 (T202/Y204) and Ribosomal S6 kinase (RSK) 1 (T573). Notably, the change of Rsk1 phosphorylation was opposite to iPSC, in which a significant reduction was observed.

Overall, protein expression patterns in NPC derived from SCZ patients suggest cell-type specific dysregulations in translation and protein synthesis, increased DNA Damage and DDR, elevated MAPK/Erk signaling, altered Wnt signaling, and higher expression of proteins governing cell cycle control, specifically those involved in regulating G2/M transition.

SCZ NPC accumulate in G2/M phase of the cell cycle

As upregulation of cell cycle stage-specific mediators have so far not been phenotypically linked with SCZ using iPSC-derived cell types, we aimed to investigate this aspect in more detail. ICC staining for G2/M-associated proteins Aurora A and Cyclin B1 confirmed DigiWest data and revealed an increased expression in SCZ NPC, but not iPSC (Fig. 6A + B). Furthermore, we conducted FACS analysis of propidium iodide staining in NPC to evaluate cell cycle phase distribution. Here, we observed a significantly increased percentage of cells in the G2/M phase for SCZ NPC compared to controls, while S-phase and G0/G1 phase were unaltered (Fig. 6C-D, Additional file 5 – Figure S11B). In addition, CTR and SCZ NPC showed no difference in proliferation rates, thus excluding the possibility that the rise in expression is simply due generally increased cell cycle activity of SCZ NPC (Additional file 5 – Figure S12). We also confirmed elevated Cyclin B1 expression via Western Blotting, with SCZ NPC showing an up-regulatory trend (Additional file 5 – Figure S13).

Expression of differentiation markers and G2/M-phase proteins correlate with p53 levels

To investigate a potential link between p53 expression/phosphorylation and the observed cellular phenotypes, we performed correlation analyses in NPC across all donors among p53 – pS15, p53, differentiation markers as well as G2/M-specific cell cycle regulators (Additional file 5 – Figure S14). As p53 phosphorylation showed the most striking alteration in SCZ NPCs, its correlation analyses are shown in detail. We found a strongly significant positive correlation (Spearman´s $r = 0.9671$) with total p53 levels (Fig. 6E), indicating that p53 phosphorylation is dependent on p53 abundance. Furthermore, we observed a positive correlation with Oct4 ($r = 0.8007$) and negative correlations with MAP2 ($r = -0.6272$) and NCAM ($r = -0.8289$) and Sox1 ($r = -0.6763$), respectively (Fig. 6F), thus establishing a link between p53 and the observed reduced differentiation efficiency. p53 phosphorylation also strongly correlated with G2/M cell cycle proteins Aurora A ($r = 0.8959$) and Cyclin B1 ($r = 0.8614$),

(See figure on next page.)

Fig. 6 Phenotypic cell cycle alterations in SCZ NPC correlate with p53 levels. **A**: Example images of G2/M regulatory proteins Aurora A and Cyclin B1 ICC staining in CTR and SCZ iPSC and NPC obtained by high-content microscopy. Scale bars: 50 µm. **B**: Quantified ICC signal of Aurora A and Cyclin B1 expression (relative to CTR mean) in CTR ($n = 9$) and SCZ ($n = 12$) in iPSC and NPC, respectively (Mann–Whitney test). **C**: Cell phase distribution of CTR and SCZ NPC ($n = 5$–8) in percent; 2-Way ANOVA with Tukey's multiple comparisons test. **D**: Flow-cytometry cell cycle analysis of CTR and SCZ NPC. Nocodazole was used as a positive control. $^{**}p < 0.01$ or as indicated. Error bars: S.E.M. **E–G**: Correlations between p53 – pS15 and **E**: p53 (total), **F**: differentiation markers and **G**: G2/M cell phase regulators. Spearman´s r; $^{**}p < 0.01$, $^{***}p < 0.001$, $^{****}p < 0.0001$. The dashed red line indicates a simple linear regression applied to each XY correlation

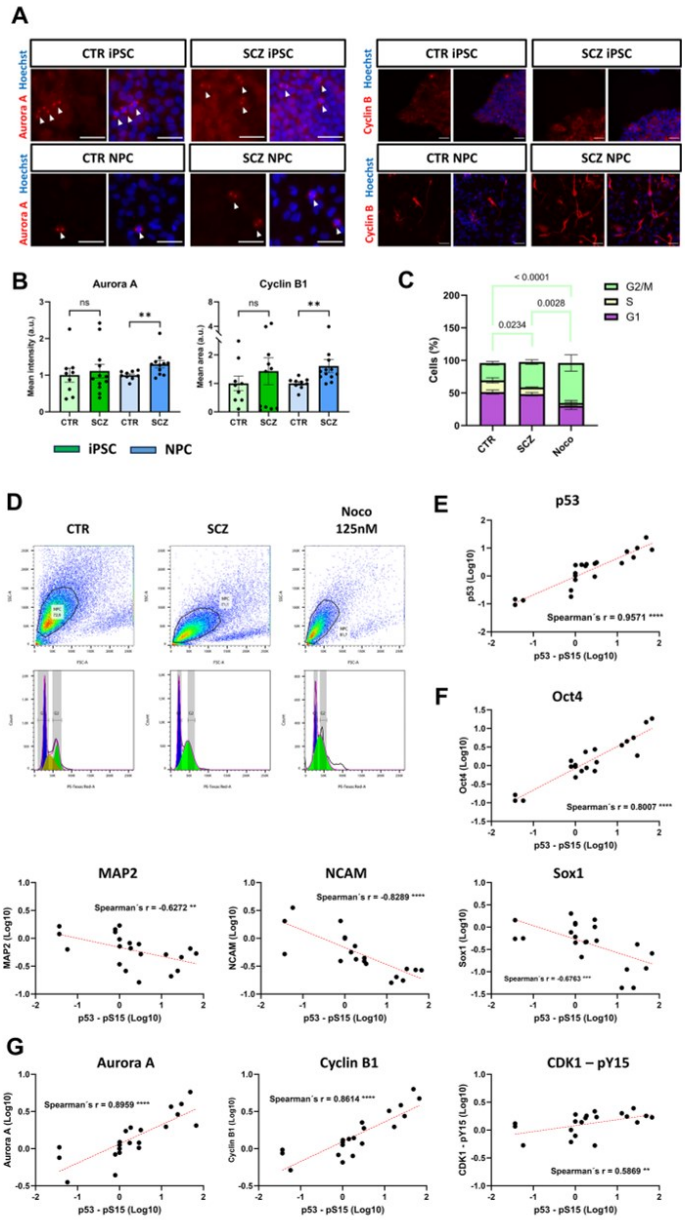

Fig. 6 (See legend on previous page.)

as well as moderately with CDK1 – pY15 ($r=0.5869$, Fig. 6G).

Discussion

Here, we report the first protein profiling analysis focusing on cellular signal transduction to study early neurodevelopmental aberrations in SCZ using iPSC-derived cell types. In a targeted proteomics approach based on the DigiWest technology, we found deregulation of protein expression mainly in NPC derived from patients with SCZ. We demonstrate regulatory alterations in cell cycle control and DNA-damage response along with impaired differentiation capacity. Additionally, we correlatively linked these aberrations to p53 expression and phosphorylation levels in diseased cells. Furthermore, we confirmed previous observations of altered protein synthesis, WNT signaling and MAPK/Erk signaling in SCZ.

The efficient differentiation of iPSC into neuronal cell types is commonly assessed via immunostaining of few selected cell type-specific markers [32]. We demonstrate that DigiWest can recapitulate characteristic pluripotency and neural progenitor marker expression equally well when compared to ICC. We show activation of several key developmental pathways such as Wnt [33], Hedgehog [34], and Hippo [25] signaling, along with changes in cell cycle regulators [35, 36]. Moreover, cells derived from SCZ patients do differ in the expression of select Wnt, MAPK and cell cycle proteins during differentiation. While other studies have also reported decreased neuronal differentiation capacity of SCZ patient-derived iPSC [37, 38], a link to changes in developmental pathway activity underlying these phenotypes has not yet been proposed. Thus overall, DigiWest is a powerful, novel tool for iPSC-based studies as it can highlight disease-associated differences which are not necessarily visible by analysis of differentiation markers alone.

NPCs have frequently been used to recapitulate SCZ pathology in vitro at early neurodevelopmental stages, as it was previously demonstrated that gene expression signatures of iPSC-derived neurons are largely conserved in NPC [9] and that protein signatures of NPC show similarities to patient postmortem brains [11]. In line with this, we mostly observed prevalent changes exclusively in NPC, indicating that most alterations and dysfunctions in pathway regulation occur in differentiated cells, but are not yet present in iPSC. For instance, we provide evidence for regulatory changes of protein synthesis, MAPK signaling and Wnt signaling in SCZ NPC. In support of our findings, several reports using iPSC models of SCZ indicate changes in translation and protein synthesis [6, 8, 11] as well as altered WNT signaling in SCZ NPC [39], neurons [16] and patients [14].

Notably, we did find highly elevated expression levels of p53 and its phosphorylated variant p53-pS15 in SCZ already at the iPSC stage. p53 is a tumor suppressor protein with central roles in regulating cellular responses to genomic alterations and DNA damage along with controlling of the cell cycle and apoptosis. Importantly, p53 is only phosphorylated at Ser15 in response to DNA damage [37, 38]. Furthermore, this phosphorylation event stabilizes p53 levels by reducing interaction of p53 with its negative regulator mouse double minute 2 homolog (MDM2) [40]. p53 is mainly associated with tumorigenesis but also plays a role in brain development, neural stem cell regulation [41], and in several nervous system diseases including SCZ, autism, Parkinson´s disease, Alzheimer´s disease or epilepsy [42]. *TP53* has been identified as a candidate risk gene in SCZ in gene association [43] as well as case–control/family studies [44] have specifically associated genetic variation in *TP53* with SCZ. Further support for an involvement of p53 is given by extensive evidence showing a negative correlation between SCZ and cancer incidence [22, 45, 46].

It has been hypothesized that p53 upregulation in stem cells due to genotoxic stress impairs pluripotency and might lead to unwanted, unspecific differentiation [39]. This aspect could at least in part explain our finding of reduced differentiation efficiency of SCZ iPSC upon neural induction and the resulting lower state of maturity of SCZ NPC, as indicated by higher expression of OCT4 and lower expression of MAP2, NCAM and SOX1. Crucially, for MAP2 and NCAM, transcriptomic profiling of a different set of SCZ patient-derived NPC revealed similar effect [9]. The lower maturation state of SCZ NPC might impact the efficiency of early neurodevelopmental processes, as reflected in a reduction of neurite outgrowth which we and others [9, 47] have observed in SCZ. In accordance with our results, decreased MAP2 expression along with alterations in pathways governing neuronal differentiation have also been reported in SCZ iPSC-derived organoids [23, 48]. Moreover, impaired neuronal differentiation efficiency has been described for 22q11.2 deletion iPSC [38], a CNV associated with SCZ, and patient-derived glutamatergic neurons [37]. It can also be hypothesized that impaired neuronal maturation could influence other key neurodevelopmental processes such as neuronal synapse formation, which is impaired in SCZ [21]. This however needs further investigation. Importantly, the strong up-regulatory trend of p53 was the only notable SCZ-specific alteration present in both iPSC and NPC, highlighting its importance in the context of differentiation.

In addition, our results indicate that SCZ NPC show increased levels of damaged DNA and associated DNA-damage response. While the overarching picture of how

DNA damage is implicated in neurogenesis and SCZ is still incomplete, it has been associated with the disease [49, 50]. For instance, genetic alterations in DNA repair enzymes were linked to SCZ [51] or can induce behavioral changes in mice [52]. A recent transcriptomic study of postmortem SCZ brain tissue also uncovered increased DNA damage repair [53]. Moreover, mass spectrometry analysis of SCZ-derived neural stem cells found alterations in pathways related to mitochondrial function, metabolic activity and DNA repair [54]. Lastly, reactive oxygen species and oxidative stress were shown to be elevated in SCZ NPC [9, 55] and animal models [56]. Thus, our data provide further evidence for a significant implication of DNA damage and repair mechanisms in SCZ pathology. Interestingly, we demonstrate that SCZ NPC display higher levels of G2/M-associated proteins, where cells are checked for DNA damage before cell cycle progression [57]. While we did not observe changes in basal proliferation rate of NPC, our FACS analysis showed a greater proportion of SCZ cells in G2/M phase—it is tempting to speculate that SCZ NPC become stuck in the G2/M phase, potentially leading to delayed cell cycle exit/progression during differentiation. Crucially, p53 can cause G2/M arrest in response to DNA damage [58]. Based on our data, we cannot infer whether cells arrest (and later attempt to recover) or exit the cell cycle temporarily; accordingly, cell cycle arrest has been described as a highly dynamic molecular state [59]. An association of DNA damage and G2/M phase in SCZ has thus far not been reported, although studies have shown alterations in cell cycle control in SCZ models [54, 60, 61] and the relevance of cell phase regulation and progression in neurodevelopment [62]. Most prior studies on SCZ proteomics/transcriptomics/genomics use shotgun approaches, merely reporting SCZ-specific changes on pathway-association level. With DigiWest being a targeted approach, we were able to focus on more detailed mechanisms of pathway activation – also by additionally measuring phosphorylation.

We identified such coherent proteomic changes while confirming previous findings from other omics approaches despite a small cohort size and notable inter-patient variability. Moreover, the four patients had diverse genetic backgrounds and disease manifestations, thus covering various clinical phenotypes, which is helpful in studying multifaceted diseases such as SCZ. Notably, for some of the measured analytes, we detected strong inter-donor variability, likely due to differences in the genetic background of each individual, which was previously shown to be the largest source of variability in a proteomic study on iPSC-derived astrocytes [63]. In addition, there are several other potential sources of inter-donor variability, including donor sex [64] and age, as exonic mutations can accumulate over time [65]. In our dataset, patient line SCZ1 displayed the strongest phenotype for key observations (highest p53 expression, lowest differentiation capacity, highest G2/M proportion), while the SCZ2 patient line showed a more CTR-like phenotype in certain aspects (also see Additional file 5 – Figure S8A). This needs to be kept in mind when interpreting the data as it might reflect the phenotype of certain subgroups of patients only. These limitations could be accounted for in future studies employing a larger number of patients to disentangle the relationship between individual sources of variation and SCZ phenotypes.

Although the aspects discussed above (p53, cell cycle, differentiation efficiency) all have individually been shown to be implicated in SCZ, our correlation data for the first time provide a possible connection between them. It can be speculated that patient-derived progenitor cells acquire DNA damage during early development and deal with it inadequately, causing cell cycle arrest or delay. This could hamper differentiation efficiency, resulting in less mature NPC and eventually neurons, which might contribute to the developmental defects associated with SCZ. In future studies it would be of interest to investigate whether our observed proteomic alterations and association with p53 will be confirmed in larger cohorts to further deepen the understanding of neurodevelopmental failure in SCZ from a mechanistic standpoint.

Conclusion

Using a high-throughput targeted proteomics approach, we uncover aberrant protein expression signatures in SCZ patient-derived NPC. Moreover, diseased cells displayed regulatory changes in cell cycle control along with impaired differentiation capacity. Using our proteomic data, we demonstrate a potential link of these phenotypes to aberrant p53 expression and phosphorylation. We ultimately hypothesize a potential interplay of these disease-specific alterations affecting the differentiation process during early neurodevelopment, which could be mechanistically implicated in the manifestation of developmental alterations occurring in SCZ. Further studies could explore the significance of our findings in larger cohorts using patient-derived neuronal cell types in iPSC-based model systems. Our study not only demonstrates the importance and significance of stem cell-based model systems and protein-based analytics in psychiatric disorders such as SCZ but also highlights our patho-mechanistic findings as accelerators in the search for potential drug targets.

Abbreviations

4E-BP1	Eukaryotic translation initiation factor 4E-binding protein 1
ATM	Ataxia-telangiectasia mutated kinase

ATR	Ataxia telangiectasia and Rad3-related kinase
CDK	Cyclin-dependent kinase
CTR	Control
DDR	DNA damage response
eEF2	Eukaryotic elongation factor 2
eIF2	Eukaryotic initiation factor 2
eIF4E	Eukaryotic translation initiation factor 4E
ERK	Extracellular signal-regulated kinases
FACS	Fluorescence-activated cell sorting
GLI	Glioma-associated oncogene
GSK3 beta	Glycogen synthase kinase-3 beta
ICC	Immunocytochemical staining
iPSC	Induced pluripotent stem cells
KIBRA	Kidney and brain expressed protein
LATS1	Large tumor suppressor kinase 1
LEF1	Lymphoid enhancer-binding factor 1
LRP6	Low-density lipoprotein receptor-related protein 6
MAP2	Microtubule-associated protein 2
MAPK	Mitogen-activated protein kinase
MDM2	Mouse double minute 2 homolog
MST1	Macrophage stimulating protein 1
NCAM	Neural cell adhesion molecule
NPC	Neural progenitor cells
PAX6	Paired-box protein Pax-6
PKA	Protein kinase A
RSK1	Ribosomal S6 kinase 1
RT	Room temperature
SCZ	Schizophrenia
SOX1	SRY-Box Transcription Factor 1
SOX2	SRY-Box Transcription Factor 2
SUFU	Suppressor of fused protein
TCF1/7	Transcription factor 1/7
TEAD1	TEA domain transcription factor 1

Supplementary Information

The online version contains supplementary material available at https://doi.org/10.1186/s12888-024-06127-x.

Additional file 1: Supplementary Tables

Additional file 2: DigiWest Antibodies

Additional file 3: DigiWest Raw Data

Additional file 4: DigiWest Normalized Data

Additional file 5: Supplementary Figures

Acknowledgements
Not applicable.

Authors' contributions
Conceptualization: AS, JH, HV and MFT; methodology: AS, JH; formal analysis: AS and JH; investigation: AS and JH.; data curation: AS and JH; writing—original draft preparation: AS, JH and MFT; writing—review and editing: HV, RW, AJF, KS-L; material support: RW, AJF; clinical evaluation: RW, AJF; supervision: MFT, HV, AJF and KS-L; project administration: MFT and HV.

Funding
Open Access funding enabled and organized by Projekt DEAL. This work received financial support from the State of Baden-Wuerttemberg (Prädiktive Diagnostik von immunassoziierten Erkrankungen für die personalisierte Medizin, grant no. AZ 35–4223.10/8) and from the State Ministry of Baden-Wuerttemberg for Economic Affairs, Labour and Tourism.

Availability of data and materials
All DigiWest-related raw and normalized data generated or analyzed during this study are included within the article (and its supplementary information files). All other datasets (Western Blot, ICC and FACS) used and/or analyzed during the study are available from the corresponding author on reasonable request.

All other datasets (Western Blot, ICC and FACS) used and/or analyzed during the study are available from the corresponding author on reasonable request.

Declarations

Ethics approval and consent to participate
Ethics approval for the use of all patient-derived iPSC lines was granted from the ethics commission at the University Hospital and Medical Faculty of Tübingen University (311/2013BO1).

Consent for publication
Not applicable.

Competing interests
The authors declare no competing interests.

Author details
[1]Institute of Biomedical Engineering, Department for Medical Technologies and Regenerative Medicine, University of Tübingen, Tübingen 72076, Germany. [2]NMI Natural and Medical Sciences Institute at the University of Tübingen, Markwiesenstraße 55, Reutlingen 72770, Germany. [3]Department of Psychiatry, Tübingen Center for Mental Health (TüCMH), University of Tübingen, Tübingen 72076, Germany. [4]German Center for Mental Health (DZPG), Partner Site Tübingen, Tübingen 72076, Germany.

Received: 5 July 2024 Accepted: 30 September 2024
Published online: 31 October 2024

References

1. Tandon R, Gaebel W, Barch DM, Bustillo J, Gur RE, Heckers S, et al. Definition and description of schizophrenia in the DSM-5. Schizophr Res. 2013;150(1):3–10.
2. Carbon M, Correll CU. Thinking and acting beyond the positive: the role of the cognitive and negative symptoms in schizophrenia. CNS Spectr. 2014;19(Suppl 1):38–52 (quiz 35-7, 53).
3. Stepnicki P, Kondej M, Kaczor AA. Current Concepts and Treatments of Schizophrenia. Molecules. 2018;23(8):2087.
4. Singh T, Poterba T, Curtis D, Akil H, Al Eissa M, Barchas JD, et al. Rare coding variants in ten genes confer substantial risk for schizophrenia. Nature. 2022;604(7906):509–16.
5. Trubetskoy V, Pardinas AF, Qi T, Panagiotaropoulou G, Awasthi S, Bigdeli TB, et al. Mapping genomic loci implicates genes and synaptic biology in schizophrenia. Nature. 2022;604(7906):502–8.
6. English JA, Fan Y, Focking M, Lopez LM, Hryniewiecka M, Wynne K, et al. Reduced protein synthesis in schizophrenia patient-derived olfactory cells. Transl Psychiatry. 2015;5(10):e663.
7. Rodrigues JE, Martinho A, Santa C, Madeira N, Coroa M, Santos V, et al. Systematic Review and Meta-Analysis of Mass Spectrometry Proteomics Applied to Human Peripheral Fluids to Assess Potential Biomarkers of Schizophrenia. Int J Mol Sci. 2022;23(9):4917.
8. Topol A, English JA, Flaherty E, Rajarajan P, Hartley BJ, Gupta S, et al. Increased abundance of translation machinery in stem cell-derived neural progenitor cells from four schizophrenia patients. Transl Psychiatry. 2015;5(10):e662.
9. Brennand K, Savas JN, Kim Y, Tran N, Simone A, Hashimoto-Torii K, et al. Phenotypic differences in hiPSC NPCs derived from patients with schizophrenia. Mol Psychiatry. 2015;20(3):361–8.
10. Maschietto M, Tahira AC, Puga R, Lima L, Mariani D, Paulsen Bda S, et al. Co-expression network of neural-differentiation genes shows specific pattern in schizophrenia. BMC Med Genomics. 2015;8:23.
11. Nascimento JM, Saia-Cereda VM, Zuccoli GS, Reis-de-Oliveira G, Carregari VC, Smith BJ, et al. Proteomic signatures of schizophrenia-sourced iPSC-derived neural cells and brain organoids are similar to patients' postmortem brains. Cell Biosci. 2022;12(1):189.
12. Emamian ES, Hall D, Birnbaum MJ, Karayiorgou M, Gogos JA. Convergent evidence for impaired AKT1-GSK3beta signaling in schizophrenia. Nat Genet. 2004;36(2):131–7.

13. Freyberg Z, Ferrando SJ, Javitch JA. Roles of the Akt/GSK-3 and Wnt signaling pathways in schizophrenia and antipsychotic drug action. Am J Psychiatry. 2010;167(4):388–96.
14. Hoseth EZ, Krull F, Dieset I, Morch RH, Hope S, Gardsjord ES, et al. Exploring the Wnt signaling pathway in schizophrenia and bipolar disorder. Transl Psychiatry. 2018;8(1):55.
15. Peng Y, Xu Y, Cui D. Wnt signaling pathway in schizophrenia. CNS Neurol Disord Drug Targets. 2014;13(5):755–64.
16. Brennand KJ, Simone A, Jou J, Gelboin-Burkhart C, Tran N, Sangar S, et al. Modelling schizophrenia using human induced pluripotent stem cells. Nature. 2011;473(7346):221–5.
17. Funk AJ, McCullumsmith RE, Haroutunian V, Meador-Woodruff JH. Abnormal activity of the MAPK- and cAMP-associated signaling pathways in frontal cortical areas in postmortem brain in schizophrenia. Neuropsychopharmacology. 2012;37(4):896–905.
18. Kyosseva SV, Elbein AD, Griffin WS, Mrak RE, Lyon M, Karson CN. Mitogen-activated protein kinases in schizophrenia. Biol Psychiatry. 1999;46(5):689–96.
19. Yuan P, Zhou R, Wang Y, Li X, Li J, Chen G, et al. Altered levels of extracellular signal-regulated kinase signaling proteins in postmortem frontal cortex of individuals with mood disorders and schizophrenia. J Affect Disord. 2010;124(1–2):164–9.
20. Treindl F, Ruprecht B, Beiter Y, Schultz S, Dottinger A, Staebler A, et al. A bead-based western for high-throughput cellular signal transduction analyses. Nat Commun. 2016;7:12852.
21. Breitmeyer R, Vogel S, Heider J, Hartmann SM, Wust R, Keller AL, et al. Regulation of synaptic connectivity in schizophrenia spectrum by mutual neuron-microglia interaction. Commun Biol. 2023;6(1):472.
22. Chou FH, Tsai KY, Su CY, Lee CC. The incidence and relative risk factors for developing cancer among patients with schizophrenia: a nine-year follow-up study. Schizophr Res. 2011;129(2–3):97–103.
23. Notaras M, Lodhi A, Fang H, Greening D, Colak D. The proteomic architecture of schizophrenia iPSC-derived cerebral organoids reveals alterations in GWAS and neuronal development factors. Transl Psychiatry. 2021;11(1):541.
24. Mulligan KA, Cheyette BN. Neurodevelopmental Perspectives on Wnt Signaling in Psychiatry. Mol Neuropsychiatry. 2017;2(4):219–46.
25. Sahu MR, Mondal AC. Neuronal Hippo signaling: From development to diseases. Dev Neurobiol. 2021;81(2):92–109.
26. Gulino A, Di Marcotullio L, Ferretti E, De Smaele E, Screpanti I. Hedgehog signaling pathway in neural development and disease. Psychoneuroendocrinology. 2007;32(Suppl 1):S52–6.
27. Hiew LF, Poon CH, You HZ, Lim LW. TGF-beta/Smad Signalling in Neurogenesis: Implications for Neuropsychiatric Diseases. Cells. 2021;10(6):1382.
28. Kanehisa M, Goto S. KEGG: kyoto encyclopedia of genes and genomes. Nucleic Acids Res. 2000;28(1):27–30.
29. Kanehisa M, Sato Y. KEGG Mapper for inferring cellular functions from protein sequences. Protein Sci. 2020;29(1):28–35.
30. Saeed AI, Sharov V, White J, Li J, Liang W, Bhagabati N, et al. TM4: a free, open-source system for microarray data management and analysis. Biotechniques. 2003;34(2):374–8.
31. Fox MH. A model for the computer analysis of synchronous DNA distributions obtained by flow cytometry. Cytometry. 1980;1(1):71–7.
32. Rust R, Weber RZ, Generali M, Kehl D, Bodenmann C, Uhr D, et al. Xeno-free induced pluripotent stem cell-derived neural progenitor cells for in vivo applications. J Transl Med. 2022;20(1):421.
33. Mulligan KA, Cheyette BNR. Wnt Signaling in Vertebrate Neural Development and Function. J Neuroimmune Pharmacol. 2012;7(4):774–87.
34. Yang C, Qi Y, Sun Z. The Role of Sonic Hedgehog Pathway in the Development of the Central Nervous System and Aging-Related Neurodegenerative Diseases. Front Mol Biosci. 2021;8:711710.
35. Hardwick LJA, Ali FR, Azzarelli R, Philpott A. Cell cycle regulation of proliferation versus differentiation in the central nervous system. Cell Tissue Res. 2015;359(1):187–200.
36. Zaveri L, Dhawan J. Cycling to Meet Fate: Connecting Pluripotency to the Cell Cycle. Front Cell Dev Biol. 2018;6:57.
37. Robicsek O, Karry R, Petit I, Salman-Kesner N, Muller FJ, Klein E, et al. Abnormal neuronal differentiation and mitochondrial dysfunction in hair follicle-derived induced pluripotent stem cells of schizophrenia patients. Mol Psychiatry. 2013;18(10):1067–76.
38. Toyoshima M, Akamatsu W, Okada Y, Ohnishi T, Balan S, Hisano Y, et al. Analysis of induced pluripotent stem cells carrying 22q11.2 deletion. Transl Psychiatry. 2016;6(11):e934.
39. Fu X, Wu S, Li B, Xu Y, Liu J. Functions of p53 in pluripotent stem cells. Protein Cell. 2019;11(1):71–8.
40. Shieh SY, Ikeda M, Taya Y, Prives C. DNA damage-induced phosphorylation of p53 alleviates inhibition by MDM2. Cell. 1997;91(3):325–34.
41. Xiong Y, Zhang Y, Xiong S, Williams-Villalobo AE. A Glance of p53 Functions in Brain Development, Neural Stem Cells, and Brain Cancer. Biology. 2020;9(9):285.
42. Li H, Zhang Z, Li H, Pan X, Wang Y. New Insights into the Roles of p53 in Central Nervous System Diseases. Int J Neuropsychopharmacol. 2023;26(7):465–73.
43. Zhuo C, Wang D, Zhou C, Chen C, Li J, Tian H, et al. Double-Edged Sword of Tumour Suppressor Genes in Schizophrenia. Front Mol Neurosci. 2019;12:1.
44. Ni X, Trakalo J, Valente J, Azevedo MH, Pato MT, Pato CN, et al. Human p53 tumor suppressor gene (TP53) and schizophrenia: case-control and family studies. Neurosci Lett. 2005;388(3):173–8.
45. Ji J, Sundquist K, Ning Y, Kendler KS, Sundquist J, Chen X. Incidence of cancer in patients with schizophrenia and their first-degree relatives: a population-based study in Sweden. Schizophr Bull. 2013;39(3):527–36.
46. Mortensen PB. The incidence of cancer in schizophrenic patients. J Epidemiol Community Health. 1989;43(1):43–7.
47. Grunwald LM, Stock R, Haag K, Buckenmaier S, Eberle MC, Wildgruber D, et al. Comparative characterization of human induced pluripotent stem cells (hiPSC) derived from patients with schizophrenia and autism. Transl Psychiatry. 2019;9(1):179.
48. Notaras M, Lodhi A, Fang H, Greening D, Colak D. The proteomic architecture of schizophrenia iPSC-derived cerebral organoids reveals alterations in GWAS and neuronal development factors. Transl Psychiatry. 2021;11(1):541.
49. Markkanen E, Meyer U, Dianov GL. DNA Damage and Repair in Schizophrenia and Autism: Implications for Cancer Comorbidity and Beyond. Int J Mol Sci. 2016;17(6):856.
50. Catts VS, Catts SV, Jablensky A, Chandler D, Weickert CS, Lavin MF. Evidence of aberrant DNA damage response signalling but normal rates of DNA repair in dividing lymphoblasts from patients with schizophrenia. World J Biol Psychiatry. 2012;13(2):114–25.
51. Sujitha SP, Kumar DT, Doss CGP, Aavula K, Ramesh R, Lakshmanan S, et al. DNA Repair Gene (XRCC1) Polymorphism (Arg399Gln) Associated with Schizophrenia in South Indian Population: A Genotypic and Molecular Dynamics Study. PLoS ONE. 2016;11(1):e0147348.
52. Bjorge MD, Hildrestrand GA, Scheffler K, Suganthan R, Rolseth V, Kusnierczyk A, et al. Synergistic Actions of Ogg1 and Mutyh DNA Glycosylases Modulate Anxiety-like Behavior in Mice. Cell Rep. 2015;13(12):2671–8.
53. Shishido R, Kunii Y, Hino M, Izumi R, Nagaoka A, Hayashi H, et al. Evidence for increased DNA damage repair in the postmortem brain of the high stress-response group of schizophrenia. Front Psychiatry. 2023;14:1183696.
54. Zuccoli GS, Nascimento JM, Moraes-Vieira PM, Rehen SK, Martins-de-Souza D. Mitochondrial, cell cycle control and neuritogenesis alterations in an iPSC-based neurodevelopmental model for schizophrenia. Eur Arch Psychiatry Clin Neurosci. 2023;273(8):1649–64.
55. da Silveira Paulsen B, de Moraes Maciel R, Galina A, Souza da Silveira M, dos Santos Souza C, Drummond H, et al. Altered oxygen metabolism associated to neurogenesis of induced pluripotent stem cells derived from a schizophrenic patient. Cell Transplant. 2012;21(7):1547–59.
56. Cabungcal JH, Counotte DS, Lewis E, Tejeda HA, Piantadosi P, Pollock C, et al. Juvenile antioxidant treatment prevents adult deficits in a developmental model of schizophrenia. Neuron. 2014;83(5):1073–84.
57. Barnum KJ, O'Connell MJ. Cell Cycle Regulation by Checkpoints. In: Noguchi E, Gadaleta MC, editors. Cell Cycle Control: Mechanisms and Protocols. New York: Springer; 2014. p. 29–40.
58. Chen J. The Cell-Cycle Arrest and Apoptotic Functions of p53 in Tumor Initiation and Progression. Cold Spring Harb Perspect Med. 2016;6(3):a026104.
59. Stallaert W, Taylor SR, Kedziora KM, Taylor CD, Sobon HK, Young CL, et al. The molecular architecture of cell cycle arrest. Mol Syst Biol. 2022;18(9):e11087.

60. Fan Y, Abrahamsen G, McGrath JJ, Mackay-Sim A. Altered cell cycle dynamics in schizophrenia. Biol Psychiatry. 2012;71(2):129–35.
61. Okazaki S, Boku S, Otsuka I, Mouri K, Aoyama S, Shiroiwa K, et al. The cell cycle-related genes as biomarkers for schizophrenia. Prog Neuropsychopharmacol Biol Psychiatry. 2016;70:85–91.
62. Cremisi F, Philpott A, Ohnuma S. Cell cycle and cell fate interactions in neural development. Curr Opin Neurobiol. 2003;13(1):26–33.
63. Beekhuis-Hoekstra SD, Watanabe K, Werme J, de Leeuw CA, Paliukhovich I, Li KW, et al. Systematic assessment of variability in the proteome of iPSC derivatives. Stem Cell Res. 2021;56:102512.
64. Waldhorn I, Turetsky T, Steiner D, Gil Y, Benyamini H, Gropp M, et al. Modeling sex differences in humans using isogenic induced pluripotent stem cells. Stem Cell Reports. 2022;17(12):2732–44.
65. Lo Sardo V, Ferguson W, Erikson GA, Topol EJ, Baldwin KK, Torkamani A. Influence of donor age on induced pluripotent stem cells. Nat Biotechnol. 2017;35(1):69–74.

Supplementary Information

The entire Supplementary Information is available at BMC Psychiatry (https://doi.org/10.1186/s12888-024-06127-x).